Instituto Andaluz de Ciencias de la Tierra (CSIC-UGR)
Depto. Mineralogía y Petrología (UGR)

Late Holocene climate variability in the western Mediterranean: an integrated organic and inorganic multiproxy approach

Variabilidad climática en el oeste del Mediterráneo durante el Holoceno Tardío: una aproximación integrada de indicadores orgánicos e inorgánicos

Memoria de Tesis presentada por la Licenciada en Ciencias Ambientales Dña. Vanesa Nieto Moreno para optar al grado de Doctora por la Universidad de Granada.

Esta Tesis Doctoral ha sido dirigida por la Dra. Dña. Francisca Martínez Ruiz, Investigadora Científica del CSIC, del Instituto Andaluz de Ciencias de la Tierra (CSIC-UGR), y el Dr. D. Miguel Ortega Huertas, Catedrático de Universidad, del Departamento de Mineralogía y Petrología de la Universidad de Granada.

Granada, 8 de febrero de 2012

Vº Bº de los Directores

La Doctoranda

Francisca Martínez Ruiz

Miguel Ortega Huertas

Vanesa Nieto Moreno

Late Holocene climate variability in the western Mediterranean: an integrated organic and inorganic multiproxy approach.

Vanesa Nieto Moreno

I.S.B.N.: 978-84-15418-30-6
Depósito Legal: GR-329-2012

Edita e Imprime: Godel Impresiones Digitales

Instituto Andaluz de Ciencias de la Tierra (CSIC-UGR)
Depto. Mineralogía y Petrología (UGR)

Tesis Doctoral

Late Holocene climate variability in the western Mediterranean: an integrated organic and inorganic multiproxy approach

Variabilidad climática en el oeste del Mediterráneo durante el Holoceno Tardío: una aproximación integrada de indicadores orgánicos e inorgánicos

Vanesa Nieto Moreno

Esta Tesis Doctoral ha sido financiada por los proyectos CGL2006-13327-CO4-04/CLI (MEC), CGL2009-07603 (MEC, subprograma BTE), CTM2009-07715 (Secretaría de Estado de Investigación, MICCIN; EU FEDER), 200800050084447 (MARM), el proyecto P09-RNM-05212 (Junta de Andalucía), el programa Training-Through-Research y el Grupo de Investigación RNM 179 de la Junta de Andalucía, así como por la beca del programa I3P concedida por el Consejo Superior de Investigaciones Científicas. Asimismo se agradece al proyecto CSD2006-00041 (TOPOIBERIA). El trabajo de investigación ha sido mayormente desarrollado en el Instituto Andaluz de Ciencias de la Tierra (IACT) del Consejo Superior de Investigaciones Científicas (CSIC), en el Departamento de Mineralogía y Petrología de la Universidad de Granada (UGR), y en el Centro de Instrumentación Científica (CIC), todos ellos sitos en Granada, así como en el Royal Netherlands Institute for Sea Research (NIOZ) en Texel (Holanda).

He sido un hombre de secretos a voces, y a veces, las más, de verdades innecesarias, todo hombre oye lo que le gusta oír, mientras, difícilmente, escucha lo que no le gusta. Todos estamos hechos de verdades a medias.

Manuel Nieto Jiménez (1949-2010)

MÁS DIFÍCIL TODAVÍA

Conseguía casi todo lo que se proponía. Finalmente, abandonó el periodismo y llegó a convertirse en astronauta. Camino de Marte, a cinco millones de kilómetros de la Tierra, aún podía escuchar en su cabeza la voz de aquellos que tantas veces le habían reprochado una notable falta de objetividad.

Dejándose mecer por la ingravidez, sonreía al imaginar la expresión de sus caras antes la evidencia de su ya irrefutable capacidad para juzgar las cosas desde fuera.

Belén Nieto Moreno

DE LA SOPORTABLE LEVEDAD

Sobre la nada ingrávida gravito
perdido el baricentro de mi peso,
proyectil que ha olvidado ya el regreso,
lanzado con desgana al infinito.

Impávido mi mundo deshabito
privado de emociones, sin acceso
a risa o llanto, lágrima ni beso,
silencio sin espacio para el grito.

Hastío y más hastío, interminables,
lento marca el reloj una esperada
sucesión de minutos no evitables.

Y paso así jornada tras jornada,
ascensión y caída equiprobables,
suspendido con nada de la nada.

José Nieto Jiménez (1939-2005)

Table of Contents

Abstract
Resumen

This Thesis provides an integration of molecular and inorganic geochemical proxies for a detailed high resolution paleoenvironmental characterization of the Late Holocene in the westernmost Mediterranean Sea. Marine records from the western Algerian-Balearic and Alboran Sea basins have been used as archives for paleoclimatic and paleoceanographic reconstructions. Age-depth models from these records have been obtained based on ^{14}C dating complemented with the activity depth-profiles of ^{210}Pb. In the western Algerian-Balearic basin, a geochemical approach has been supplemented by multivariable statistical analyses for the identification of detrital input oscillations (fluvial-derived elements and eolian input fluctuations), marine productivity (total organic carbon, Br/Al and organometallic ligands), grain size distribution (sortable silt and quartz content), oxygenation conditions and post-depositional alteration (redox-sensitive elements) during the last 4000 yr. Within this time interval, the Roman Humid Period (RHP) and the Little Ice Age (LIA) are evidenced as humid periods, characterized by higher riverine influence and low Saharan eolian input while drier paleoclimatic conditions are observed during the Late Bronze Age-Iron Age (LBA-IA), the Dark Ages (DA) and the Medieval Climate Anomaly (MCA). Furthermore, more energetic paleocurrent circulation at this time is denoted by faster and well oxygenated bottom waters. The mid-late RHP appeared as the most humid during the Late Holocene, and also enhanced marine productivity is recognized. Variations in solar irradiance are claimed as the major natural forcing process contributing to climate variability in this region during the last 4000 yr, modulated by the North Atlantic Oscillation (NAO) during the MCA and the LIA. In the north-western Alboran Sea basin, two higher resolution records have enabled a comprehensive multiproxy reconstruction of climate responses during the last two millennia through the combination of a wide suite of inorganic and organic geochemical proxies. Hence, sea surface temperatures (SST) (TEX^{H}_{86} and $U^{k'}_{37}$ ratios-derived SST), fluctuations in chemical elements (major and trace elements content), mineral composition of marine sediments (bulk and clay mineralogy) as well as grain size distribution have depicted paleoenvironmental (fluvial and eolian input oscillations and past SST), and paleocenographic (paleocurrent intensity and redox sensitive elements) conditions during the MCA, the LIA, the Industrial Period (IP) and the second half of the twentieth century. Additionally, further information such as paleoproductivity (related to upwelling) and paleohydrological conditions (relative contribution by land plants and provenance of the sedimentary organic matter) have been gathered

from the diol index, the carbon isotopic composition of long straight chain *n*-alkanes and the BIT index. The organic geochemical record reveals a gradual long term decline of SST throughout the last two millennia based on TEX^{H}_{86} and $U^{k'}_{37}$ ratios, with warmer temperatures during the MCA, and the LIA recorded as the coldest period. A sharp and unprecedented SST increase took place during the Industrial Era and the twentieth century. This trend is in agreement with Northern Hemisphere temperature oscillations forced by solar irradiance variations and anthropogenic greenhouse warming during the last 2000 yr. Moreover, during periods of a persistent high NAO state, lower riverine influence and an intensification of the wind-induced upwelling conditions are exposed by the BIT index and the bloom of *Proboscia* diatoms. Concerning hydrological conditions, the isotopic composition of *n*-alkanes disclosed a predominantly fluvial C_3 plant contribution while the low BIT index revealed a dominant marine provenance for the organic matter. The inorganic geochemical record displayed the MCA and the second half of the twentieth century as prevalent dry periods based on decreasing trends of fluvial-derived elements ratios (Si/Zr and K/Zr) and higher Saharan eolian input (Zr/Al and Zr/Rb ratios). Wetter conditions were recognized during the LIA and the IP instead, with a concurrence of wet spells and minor Saharan eolian contribution during periods of lower sunspots activity. Two events of strengthening Atlantic waters flowing into the Mediterranean Sea were registered by a remarkable change in the paleoceanographic record (faster bottom currents and oxygenated bottom waters). An outstanding anthropic contribution during the last centuries is likewise discernable by a progressive raise in heavy metal concentrations since industrial times (Pb, Zn and Cu). This multiproxy climatic assessment, encompassing different records from the westernmost Mediterranean, has depicted a sequence of dry and humid periods with coincident signals for the overlapped periods (LIA and MCA) in the two studied basins that are also coherent with the North Atlantic climatic framework during the Late Holocene, which further support the link between this region and the North Atlantic ocean-atmosphere system.

La presente Tesis Doctoral presenta un estudio multidisciplinar, basado en la integración de indicadores geoquímicos orgánicos e inorgánicos, con objeto de realizar una reconstrucción paleoambiental de muy alta resolución durante el Holoceno Tardío en el oeste del Mediterráneo. Para ello se han seleccionado diversos registros marinos recuperados en las cuencas Argelino-Balear y de Alborán, los cuales han servido como archivos para la reconstrucción de condiciones paleoclimáticas y paleocenaográficas. Los modelos de edad de estos registros se han obtenido a partir de dataciones de ^{14}C y ^{210}Pb en cada uno de los testigos de sedimento estudiados. En el oeste de la cuenca Argelino-Balear, el estudio geoquímico, que se ha completado con análisis estadísticos multivariantes, ha permitido establecer oscilaciones en el aporte detrítico a la cuenca (fluctuaciones de elementos derivados del aporte fluvial y eólico), en la productividad marina (carbono orgánico total, relación Br/Al y ligandos organometálicos), en la distribución del tamaño de grano (contenido en cuarzo y en limo grueso entre 10-63 μm), así como en las condiciones de oxigenación de las aguas profundas y en la alteración diagenética (elementos sensibles a cambios en las condiciones redox) durante los últimos 4000 años. En este intervalo de tiempo, el Periodo Húmedo Íbero-Romano y la Pequeña Edad de Hielo han sido identificados como periodos húmedos, caracterizados por una mayor influencia fluvial y un menor aporte eólico procedente del Sáhara. Sin embargo, durante el intervalo Bronce Final-Edad del Hierro, la Alta Edad Media, y la Anomalía Climática Medieval, se han reconocido condiciones paleoclimáticas más áridas. Además, durante estos últimos intervalos, las condiciones de paleocirculación fueron más energéticas, con flujos de corriente más rápidos y corrientes de fondo con aguas más oxigenadas. El Periodo Húmedo Íbero-Romano Medio y Tardío se ha reconocido como el más húmedo de todo el Holoceno Tardío, cuando, además, se produjo un notable incremento en la productividad marina. La principal causa de variabilidad climática en esta región durante los últimos 4000 años se ha atribuido a cambios en la irradiación solar, modulados a su vez por la Oscilación del Atlántico Norte durante la Anomalía Climática Medieval y la Pequeña Edad de Hielo. En el noroeste de la cuenca de Alborán, dos registros marinos de mayor resolución, han permitido realizar una reconstrucción aún más detallada de las respuestas climáticas durante los últimos dos milenios mediante la combinación de un amplio conjunto de indicadores geoquímicos orgánicos e inorgánicos. Así, la reconstrucción de las paleotemperaturas de las aguas marinas superficiales (los índices TEX^{H}_{86} y $U^{k'}_{37}$), las variaciones en la composición quí-

mica (contenido en elemento mayores y traza) y mineralógica de los sedimentos (mineralogía total y de arcillas) y la distribución de tamaño de grano han permitido determinar las condiciones paleoambientales (paleotemperaturas superficiales del agua del mar, fluctuaciones en el aporte eólico y fluvial) y paleoceanográficas (intensidad de paleocorrientes y elementos sensibles a condiciones redox) durante periodos tales como la Anomalía Climática Medieval, la Pequeña Edad de Hielo, la Era Industrial y la segunda mitad del siglo XX. Adicionalmente, se ha obtenido información de las condiciones de paleoproductividad (en relación a eventos de "upwelling" o surgencia de aguas profundas frías y ricas en nutrientes) y paleohidrológicas (procedencia de la materia orgánica sedimentaria y contribución relativa de plantas terrestres) mediante los índices BIT y diol, y mediante la variación en la composición isotópica de carbono de los *n*-alcanos con número impar de carbonos. El registro orgánico ha revelado un descenso gradual de las temperaturas superficiales marinas a lo largo de los últimos dos milenios en base a los índices TEX^{H}_{86} y $U^{k'}_{37}$, mostrando temperaturas más cálidas durante la Anomalía Climática Medieval y registrando la Pequeña Edad de Hielo como el periodo más frío de los últimos 2000 años. Durante la Era Industrial y la segunda mitad del siglo XX se ha reconocido un notable aumento de las temperaturas, sin precedente en los últimos dos milenios. Estas tendencias se correlacionan, además, con otras reconstrucciones de paleotemperaturas en el Hemisferio Norte, las cuáles han sido atribuidas a variaciones en la irradiación solar durante los últimos dos milenios así como al calentamiento global de origen antropogénico durante los últimos siglos. Además, a partir del índice BIT y el incremento de diatomeas del género *Proboscia*, en épocas con un persistente índice positivo de la Oscilación del Atlántico Norte se ha detectado un menor aporte fluvial y una intensificación del "upwelling". En lo que a condiciones hidrológicas se refiere, la composición isotópica de los alcanos pone de manifiesto una contribución predominantemente fluvial de plantas C_3 durante los últimos 2000 años, mientras el índice BIT indica un origen principalmente marino de la materia orgánica. El registro inorgánico mostrado ha permitido reconstruir la Anomalía Climática Medieval y la segunda mitad del siglo XX como periodos fundamentalmente áridos en base a la disminución en las relaciones de elementos derivados del aporte fluvial (Si/Zr y K/Zr) y a una mayor contribución eólica procedente del Sáhara (razones Zr/Al y Zr/Rb). Durante la Pequeña Edad de Hielo y la Era Industrial se han registrado condiciones más húmedas y con menor aporte eólico sahariano, concurrentes con periodos de

menor actividad solar y manchas solares. Asimismo, se han registrado dos eventos de intensificación de entrada de aguas atlánticas en el Mar Mediterráneo en base a cambios en las condiciones de paleocirculación (mayor velocidad de paleocorrientes y aguas profundas más oxigenadas). Durante los últimos siglos un progresivo incremento en las concentraciones de metales pesados desde tiempos industriales (Pb, Zn y Cu) ha puesto de manifiesto una notable contribución antrópica. En definitiva, este análisis climático basado en la integración de múltiples indicadores geoquímicos y englobando diferentes registros del área más occidental del Mar Mediterráneo, ha permitido establecer una secuencia de fases húmedas y áridas con registros geoquímicos bien correlacionados durante los periodos estudiados en ambas cuencas (la Anomalía Climática Medieval y la Pequeña Edad de Hielo). Igualmente, las respuestas climáticas que se han establecido son coherentes con las oscilaciones climáticas previamente descritas en la región del Atlántico Norte durante el Holoceno Tardío, lo cual corrobora la relación entre el clima de esta región y el sistema océano-atmósfera del Atlántico Norte.

Motivation, objectives and layout

The Earth's climate system encompasses different subsystems: the atmosphere, the lithosphere, the hydrosphere, the biosphere and the cryosphere, which are intimately coupled, so changes in one of the components affect the rest of the system. Additionally, climate responses to external natural forcing (orbital, solar, and volcanic forcing) and internal climate variability (the North Atlantic Oscillation, El Niño Southern Oscillation, and changes in the Atlantic Meridional Overturning Circulation) are further intricated by positive or negative feedbacks as well as non-linear responses. Over most of the Earth's history, climate variability has been forced by natural mechanisms. Nevertheless, since pre-industrial times, human-induced activities (land-use changes and soil degradation, increases of greenhouse concentrations and aerosols, and stratospheric ozone depletion) may have induced additional changes in the climate system, and the exact magnitude of the climate change response to this forcing remains still unknown (e.g., Wanner et al., 2008). Therefore, to further decipher the extent to which anthropogenic activities may have influenced the climate system, and in order to disentangle this effect from natural climate variability, it is needed to improve our knowledge of recent climate fluctuations. In this sense, the Late Holocene is of particular interest to the understanding of the Earth's climate system, since the boundary conditions of the climate did not change dramatically in relation to present time.

Our most immediate climate past has been recorded by direct instrumental measurements of climate variables, which are by far the most reliable climatic data. Nevertheless, they are widespread and sparse until the 1950s (there are just a few records at high resolution from the oceans, the tropics and the Southern Hemisphere) and cover a short time period of the Earth's climate history (available from 1850 onwards). Thus, indirect or "proxy" indicators of climate variability provided by natural archives constitute the basis to unravel climatic information prior to industrial times as they span a much wider geographical coverage from a broad variety of archives and for longer time-scale periods (e.g., Mann et al., 1999). Among natural archives, marine records have been revealed as excellent archives for past climate reconstruction, offering an unique, global and continuous signal of the ocean response to climate change and also providing records of terrestrial and atmospheric processes (e.g., Hillaire-Marcel and Vernal, 2007).

Within this context, this Thesis was projected to contribute towards the advance of understanding the causes of climate variability and predicting vulnerability to potential climate change. It also aims to better identify major patterns of climate variability on centennial and longer time-scales, including natural variations and human-induced changes during the Late Holocene. With this purpose, marine sediment records from the westernmost Mediterranean have been selected. This region is highly sensitive to climate variability due to its latitude, located in a transitional zone between two climate belts, the mid-latitude westerlies system and the subtropical high-pressure belt. Additionally, high sedimentation rates in this region provide very high-resolution for paleoclimate reconstruction. Likewise, previous work focussed on the last deglacial cycle has demonstrated the exceptional suitability of this region for climate variability reconstructions at centennial and millennial scales (e.g., Cacho et al., 1999; Moreno et al., 2002; Sierro et al., 2005; Martrat et al., 2007; Jiménez-Espejo et al., 2008; Combourieu-Nebout et al., 2009; Rogerson et al., 2010). Studied marine records include gravity (305G, 306G) and box cores (384B and 436B) recovered in the Algerian-Balearic basin and in the north-western Alboran Sea basin respectively, during different oceanographic cruises (TTR-14 and TTR-17). After sampling, a robust age-depth model, provided by the activity-depth profiles of ^{210}Pb and ^{137}Cs, together with ^{14}C dates and a suite of different geochemical analyses, has allowed the characterization of climate conditions and the identification of forcing mechanisms and anthropic contributions during the last four millennia.

Accordingly, the two major objectives considered are:

I. Reconstructing climate variability during the Late Holocene in the western Mediterranean by using a multi-proxy approach in order to identify and characterize the main climate and oceanographic oscillations.

II. Unravelling main forcing factors (natural and anthropic) driving climate variability in the westernmost Mediterranean during this time interval.

In order to fulfil these aims, the following specific goals were also established:

1. To acquire well dated high resolution marine records (gravity and box-cores)

by obtaining a robust age-depth model based on the activity profiles of ^{210}Pb and ^{137}Cs, together with ^{14}C dating.

2. To compile and integrate a multi-proxy inorganic geochemical (major and trace elements contents), sedimentological (grain size distribution) and mineralogical record (bulk and clay mineralogy) for the characterization of paleoenvironmental and paleoceanographic responses.

3. To identify the main geochemical families, in terms of their affinity and origin, by a statistical approach (cluster and redundancy analyses) in order to group proxies for detrital input oscillations, marine productivity, oxygenation conditions, paleocurrent intensity and post-depositional alteration. The first eigenvector of the Principal Component Analysis is also tackling main sources and contribution of the different processes controlling sedimentary deposition.

4. To obtain and integrate a multiproxy organic record (TEX^{H}_{86} and $U^{k'}_{37}$ ratios, BIT index, diol index and isotopic composition of *n*-alkanes) for the reconstruction of paleoclimate variability during the last two millennia (sea surface temperatures, terrestrial input fluctuations, upwelling and paleoproductivity conditions).

5. Comparing results with other documentary, instrumental, lacustrine and pollen records from the Iberian Peninsula, as well as other records from the western Mediterranean, the North Atlantic realm, northern Europe, north Africa, Greenland, and the Northern Hemisphere.

6. To assess the potential natural forcing as well as possible anthropic imprints contributing to climate variability in the westernmost Mediterranean.

Following these objectives, this Thesis is arranged in four chapters. The first chapter preludes the theoretical basis for this dissertation, including an overview on natural climate oscillations and the driving mechanisms identified during the Late Holocene at global and regional scales, introducing our case of study, the western Mediterranean region. The used integrated multiproxy approach and the multivariate statistical strategy adopted for the characterization of climate and anthropic imprints in the study area during the Late Holocene are likewise in-

troduced in this section. Then, the results of this study are presented in paper format throughout the consecutive three chapters. The second chapter provides a multiproxy reconstruction of paleocenographic (paleocurrent intensity and redox conditions) and paleoenvironmental conditions (fluvial and eolian input oscillations) as well as underlying forcing mechanisms by fluctuations in chemical (major and trace elements content, total organic carbon), mineral composition (bulk and clay mineralogy) and grain size distribution in two gravity cores from the Algerian-Balearic basin. The third chapter reports a detailed paleoclimatic reconstruction for the last two millennia obtained from two Alboran Sea deep-sea records and based on a wide suite of molecular proxies, which have been used for the first time at such a high resolution in this region. Sea surface temperatures, marine paleoproductivity and paleohydrological conditions have been established for the Medieval Climate Anomaly, the Little Ice Age, the Industrial Era and the twentieth century. The last chapter also focuses on the same records, enabling further advance in the comprehension of climate variability during this time-intervals, and describing wet and arid phases which have been correlated with instrumental and documentary records during the last 500 yr.

A comparison of the obtained results with other instrumental, lacustrine and pollen records from the Iberian Peninsula, marine records from the western Mediterranean, and other evidences from the North Atlantic realm, northern Europe, north Africa, Greenland, and the Northern Hemisphere is also accomplished all over these three chapters. Finally, the main conclusions inferred from this integrated perspective are addressed. Further information such as core pictures, X-ray images, Scanning Electron Microscopy photographs, tables including the smectite composition identified by Transmission Electron Microscopy in analyzed sediments, and related scientific production, is gathered as appendixes.

Chapter I

Despite significant uncertainties and limitations associated with the science of climate change and predicted future climate impacts (e.g., Hillerbrand and Ghil, 2008), there is uniform scientific consensus and growing evidences that the Earth has been warming over the last 50 yr likely due to the rising levels in anthropogenic greenhouse gas concentrations emitted by human activities (fossil fuel burning and land-use changes), and that the increase in global temperatures will continue in the next decades (IPCC, 2007). Scientific programs and organizations of national or international standing such as the U.S. Global Change Research Program (USGCRP) (**http://www.globalchange.gov/**), the National Academy of Sciences (NAS) (**http://www.nasonline.org/**), the National Research Council (NRC) (**http://www.nationalacademies.org/**), the Intergovernmental Panel on Climate Change (IPCC) (**http://www.ipcc.ch/index.htm**), or the National Oceanic and Atmospheric Administration (NOAA) (**http://www.noaa.gov/**) have broadly reported in synthesis assessments and surveys of opinion among climate scientists this scientific agreement (e.g., National Research Council, 2006; Solomon et al., 2007; Karl et al., 2009; Blunden and Baringer, 2011).

According to the 2007 Fourth Assessment Report by the IPCC, global mean surface temperature have increased by 0.76±0.19°C from 1850 to 2005 yr AD, being the twelve last years the warmest in the instrumental record since 1850 yr AD, and the rate of warming over the last 50 yr was almost double than over the last century. Future trends based on projections for the 21st century expect a warming of 0.2ºC per decade for the next two decades with a further warming of about 0.1°C per decade if the concentrations of all greenhouse gases and aerosols would remain constant at the level of the year 2000 (Fig. I.1) (Trenberth et al., 2007).

The atmospheric concentration of CO_2 has steadily increased from a pre-industrial value of about 280 ppm to its present level of about 379 ppm, meanwhile Antarctic ice core records demonstrated that such concentrations did not exceed 300 ppm for the last 650,000 years before the preindustrial era (Fig. I.2) (e.g., Siegenthaler et al., 2005). The unprecedented rising of the anthropogenic carbon dioxide levels are very likely to have caused these increasing global average temperatures, which appears as anomalous in relation to the climate of the last 20,000 years (e.g.,

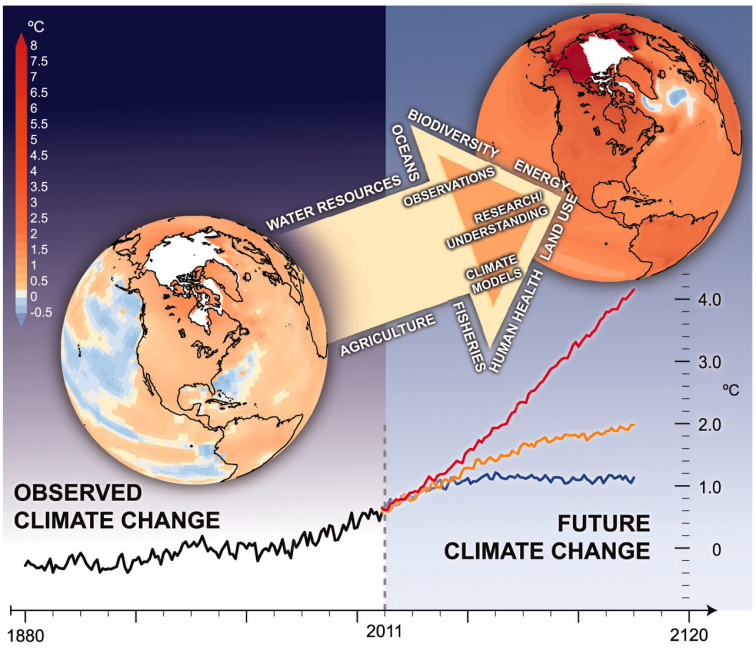

Figure I.1. Climate data from observations (annual mean surface temperature anomalies 2006–2010 yr AD from the 1951–1980 yr AD base period average; the globe at left) and climate model simulations for the future greenhouse gas and aerosol emission scenario (projected surface temperature anomalies; the globe at right) (Overpeck et al., 2011)

Björck, 2011).

Scientific evidences for the global warming of the climate system comprise significant increases in worldwide average land and ocean surface temperatures and surface specific humidity, retreats in ice cover extent, rises in global mean sea level, increased precipitation in eastern parts of North and South America, northern Europe and northern and central Asia and drying in the Sahel, the Mediterranean, southern Africa and parts of southern Asia, more intense and longer droughts and changes in the large-scale atmospheric circulation (increase in intense tropical cyclone activity, more frequent "El Niño", strengthened mid-westerly winds and number of hurricanes in the North Atlantic above normal) (Trenberth et al., 2007).

Even if these changes are detected worldwide, their effects are more visible on areas located on the border of climatic belts, being more sensitive to latitudinal migrations of such belts. Among these regions, the Mediterranean area has been identified as a "hotspot" highly vulnerable region for climate change, with projected altera-

tions and environmental impacts much severe than in other territories in the world such as higher temperatures and droughts, reduced water availability, hydropower potential, summer tourism and crop productivity, and health risks due to frequent heat waves and wildfires (e.g., Bernstein et al., 2007; Lindner et al., 2010). To advance in the assessment of naturally internal variability as well as to provide additional predictability on modelling the climate system in sensitive regions (such as the Mediterranean Sea), separating natural from anthropogenically-forced decadal variability, it is necessary a better understanding of past trends and variability (e.g., Solomon et al., 2010).

Understanding past climate variability is thus essential to increase the knowledge on current climate change and to predict climate responses and potential future climate scenarios. In this regard, the Late Holocene is an important reference period for evaluating the significance of future climate change and impacts, because forcing factors and climate boundary conditions have been similar to that of present day (e.g., Mayewski et al., 2004). Hence, the paleoclimate reconstruction carried out for this time period will significantly contribute to our overall understanding of Earth's climate at regional and global scales.

I.1. Climate variability over the last millennia

The lack of direct measurements of climate variables such as temperatu-

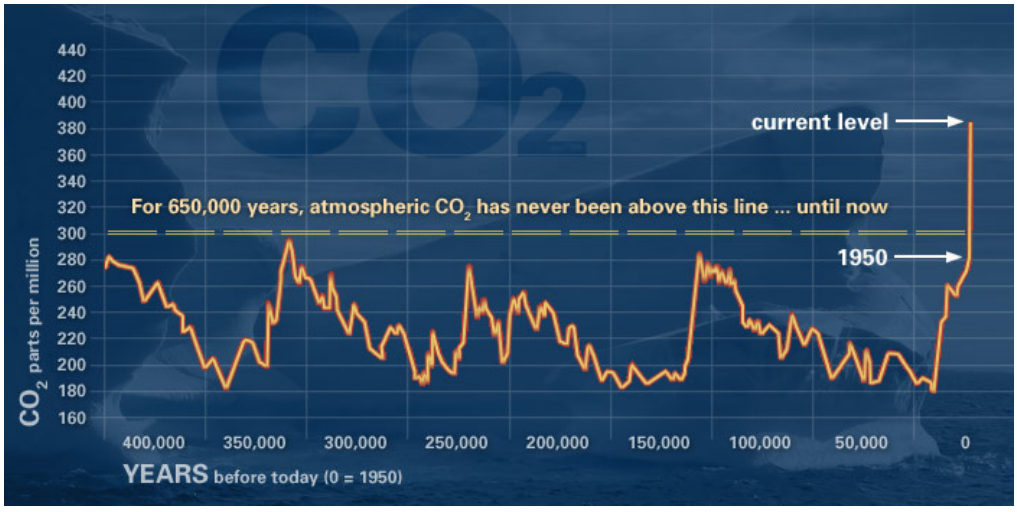

Figure I.2. CO_2 concentrations (ppm) reconstruction for the last 400,000 yr based on ice cores and recent direct measurements (http://www.noaa.gov/)

re and precipitation at centennial and longer time-scales, i.e. beyond the instrumental record, requires of a longer perspective relying on indirect indicators or proxies of past climate variability provided by documentary sources and natural archives (ice cores, tree rings, coral reefs, speleothems, boreholes, marine and lake sediments). A widespread number of multiproxy-based studies over the past few decades have been focussed on the reconstruction of Northern Hemisphere surface temperatures variations spanning the past two millennia in an effort to provide predictive insights into future climate change. Some of these approaches (e.g., Mann et al., 1999; Jones et al., 2001; Moberg et al., 2005) have been included into the 2007 IPCC Fourth Assessment Report and together with the recent compilations by Mann et al. (2008) and Wahl et al. (2010), they concluded and agreed in a "Hockey Stick" common pattern proposed by Mann et al. (1999), which is characterized by an unprecedented increase of the average Northern Hemisphere temperatures during the late twentieth century (as representing the curve of the stick), warmer than any other for at least the past 1300 years (Fig. I.3). The sustained rate of warming over the past century reported from instrumental and proxy records at hemispheric scales has provoked a further effort to track climate variability and its underlying forcing mechanisms during the last millennia (e.g., Bradley et al., 2003; Jones and Mann, 2004; Goosse et al., 2005; Jones et al., 2009; Mann et al., 2009; Trouet et al., 2009, 2011), with a special attention devoted to medieval times due to its potential value as a "natural" analogue in the recent past of the 20st century greenhouse warming (e.g., Seager et al., 2007; Diaz et al., 2011; Graham et al., 2011). The so-called Medieval Warm Period (MWP) was described for the first time by Lamb (1965), based on documentary proxy records in northern Europe, the North Atlantic, southern Greenland and Iceland, as a notable warm period which lasted a few centuries between 900-1200 yr AD, followed by a decline of temperature after 1550 yr AD, the Little Ice Age (LIA; 1500-1850 yr AD), which probably did produce the lowest temperatures and the greatest extensions of ice on land and sea since the last ice age. Subsequently, Hughes and Diaz (1994) highlighted the lack of synchronicity for this warming between different regions, referring such period as anomalous rather than global, based on the available evidence, and thus Stine (1994) re-defined this term as the Medieval Climate Anomaly (MCA) (800-1300 yr AD), considering some other anomalies different from

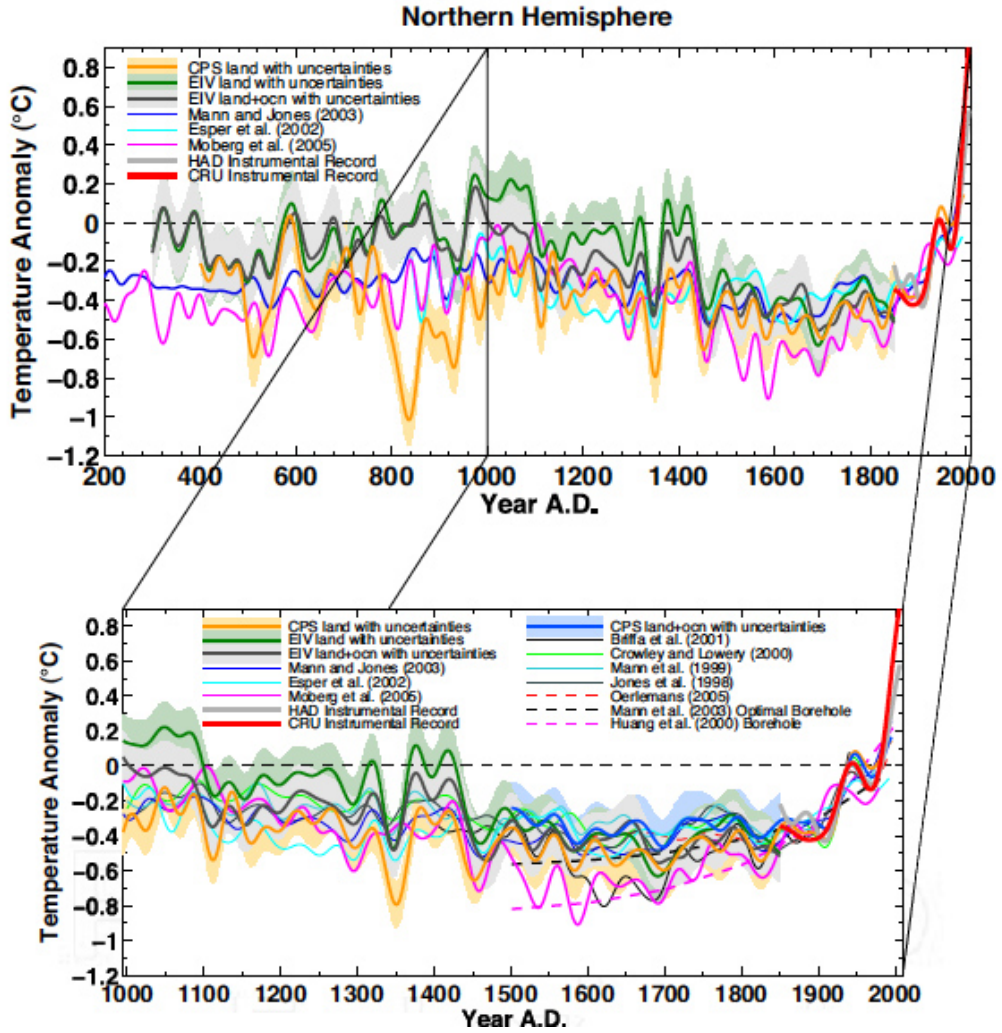

Figure I.3. Hemispheric surface temperature variations reconstructions over the past two millennia and instrumental Northern Hemisphere land surface temperature record (1850–2006 yr AD) (Mann et al., 2008)

temperature, such as multi-centennial droughts in North and South America. Such anomalies have been also evidenced during this time-interval in southern Europe and the Mediterranean region (e.g., Seager et al., 2007).

Solar variability, volcanic activity, and ocean-atmosphere interactions represent plausible forcing mechanisms to explain the MCA-LIA type century-scale climatic anomalies. Recently, Trouet et al. (2009), based on tree-ring and speleothem records as precipitation and drought proxies from Morocco and Scotland respectively

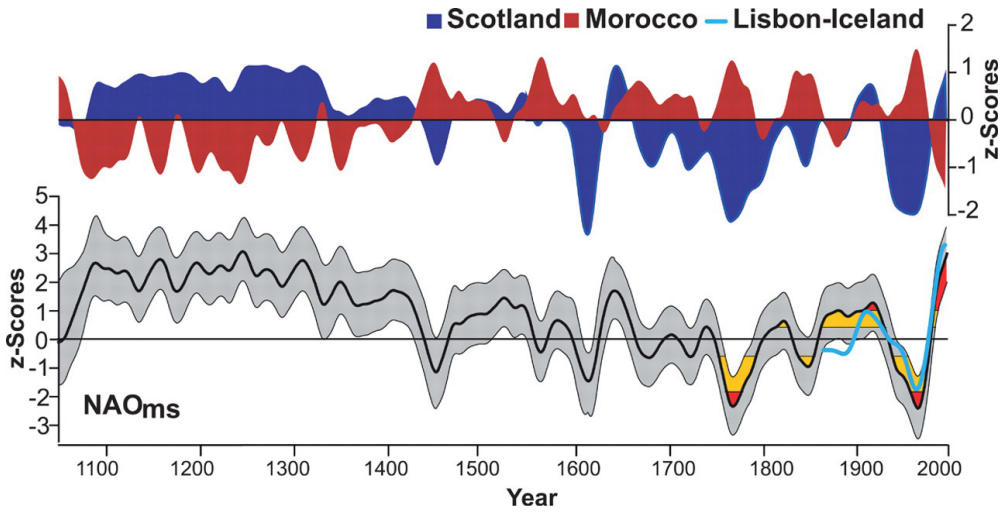

Figure I.4. Proxy-derived long-term NAO reconstruction (Top). Reconstructed winter precipitation for Scotland and Palmer Drought Severity Index for Morocco (Bottom). Winter NAO reconstruction (black curve) is the difference of the Scotland and Morocco records. The grey area is the estimated uncertainty; yellow and red areas are the 10 and 33% highest and lowest values since 1700. The blue line represents the 30-year smoothed Lisbon-Iceland instrumental NAO index series (Trouet et al., 2009)

(Fig. I.4), proposed a persistent positive North Atlantic Oscillation (NAO) during the MCA to explain the see-saw wet (dry) and cold (warm) anomalies in the North Atlantic-European sector (northern Europe vs. southern Europe and northern Africa). Thus, enhanced solar irradiation and/or reduced volcanic activity might have induced changes in the tropical Indo-Pacific sea surface temperatures (SST), which could have resulted in a strengthening of the NAO. Positive NAO-associated stronger westerlies, driving a further northerly storm track towards northern Europe, may have enhanced the Atlantic Meridional Overturning circulation (AMO), the latter arisen salinity and SST anomalies in the tropical Atlantic and a related northward migration of the Intertropical Convergence Zone (ITCZ) as a constructive feedback mechanism, which reinforced La Niña–like conditions in the tropical Indo-Pacific (Fig. I.5). Despite this intense effort, nowadays there is no sufficiently understanding on the precise changes related to regional climate forcing, internal variability, system feedbacks, and the responses of surface climate, land-cover, biosphere and hydrosphere, being this issue included in the current top interests of the scientific community (PAGES news, 2011). For that aim, PAGES developed the "Regional 2k Network"; a set of Working Groups that collect and pro-

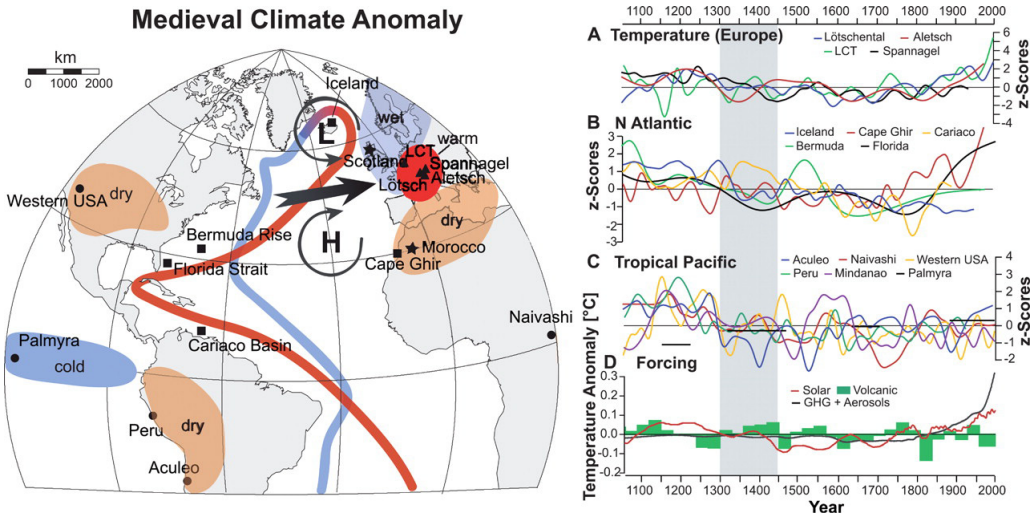

Figure I.5. Large-scale MCA pattern. Geographical location and time series (1050–2000 yr AD) of proxy records of European temperatures [(A), black triangles in the map at left], North Atlantic conditions [(B), black squares], tropical Pacific conditions [(C), black circles], and external forcings (D) (right side). The 1300-to-1450 yr AD MCA-LIA transition period is highlighted in gray. The map indicates inferred climatic conditions and an intensified AMOC during the MCA, as derived from the proxy records. L=Icelandic Low; H=Azores High (left side) (Trouet et al., 2009)

cess the best available time series and spatial reconstructions of important climate system variables for a given region (Newman et al., 2009).

I.2. Mediterranean climate variability during the Late Holocene

The westernmost Mediterranean realm evokes a high scientific interest due to its unique geographical, morphological, historical and climatic characteristics which make the Mediterranean a region undergoing climatic and anthropogenic forcing. It is a marginal and semi-enclose basin isolated from the global ocean system and connected to the Atlantic Ocean through the narrow Strait of Gibraltar (14.5 km wide and less than 300 m deep) and circulation patterns characterized by sub-basin scale gyres due to the irregular seafloor topography and a general thermohaline circulation with associated deep water formation processes (e.g., Lionello et al., 2006). The magnitude of human impacts reached its maximum during the Roman occupation. Over the last two millennia, natural and/or human-set fires, combined with land use changes and a long-term Mid to Late Holocene climate aridification have resulted in high degree of xerophytization (e.g., Carrión et al., 2010; Durrieu de Madron et al., 2011).

From a climatic point of view, the western Mediterranean is located in a transitional zone between two climate belts (Fig. I.6): the westerlies system, which dominates over central and northern parts of Europe, and the subtropical high pressure belt over North Africa or ITCZ. The northern and southern migration of these two belts determines the hydrological regime in this region. In summer, the subtropical high pressure is displaced to the north and most of the Mediterranean experiences intense drought. During winter, the subtropical conditions are displaced southward, and the Mediterranean comes under the influence of the temperate westerlies with associated Atlantic depressions progressing eastward over Europe (e.g., Sumner et al., 2001; Issar, 2003). The precipitation regime in the Mediterranean is controlled by the NAO, which is one of the major patterns of atmospheric circulation variability in the Northern Hemisphere with centres of action in the Icelandic low and the Azores high, and responsible for most of the climatic variability in the North Atlantic (Hurrell, 1995; Trigo et al., 2002). The NAO alternates between a "high-index" pattern, characterized by a well developed and intense Icelandic Low and Azores High, associated with stronger wester-

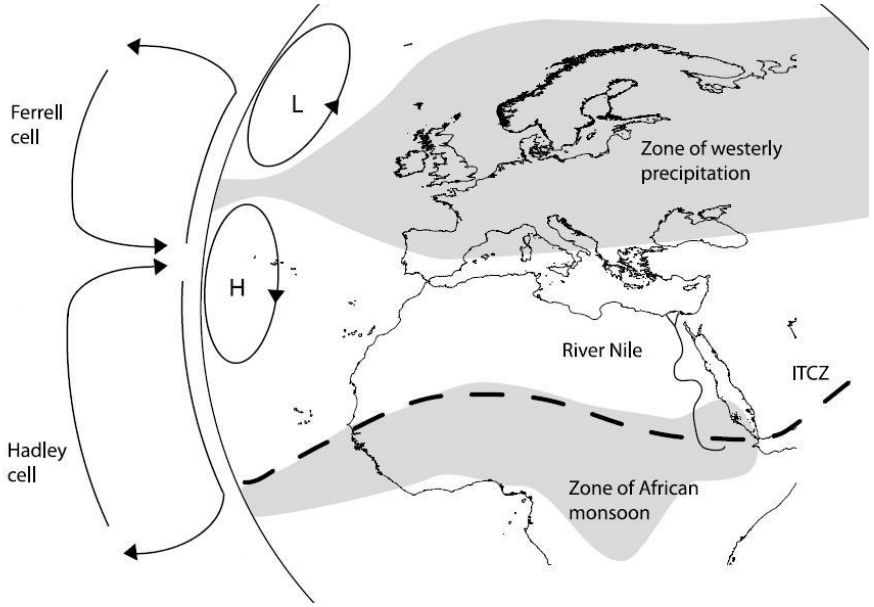

Figure I.6. Climatic context of the Mediterranean region. ITCZ is shown in summer position. Arrows represent wind directions. Shaded areas represent precipitation zones. H=high pressure, L=low pressure (Jilbert et al., 2008)

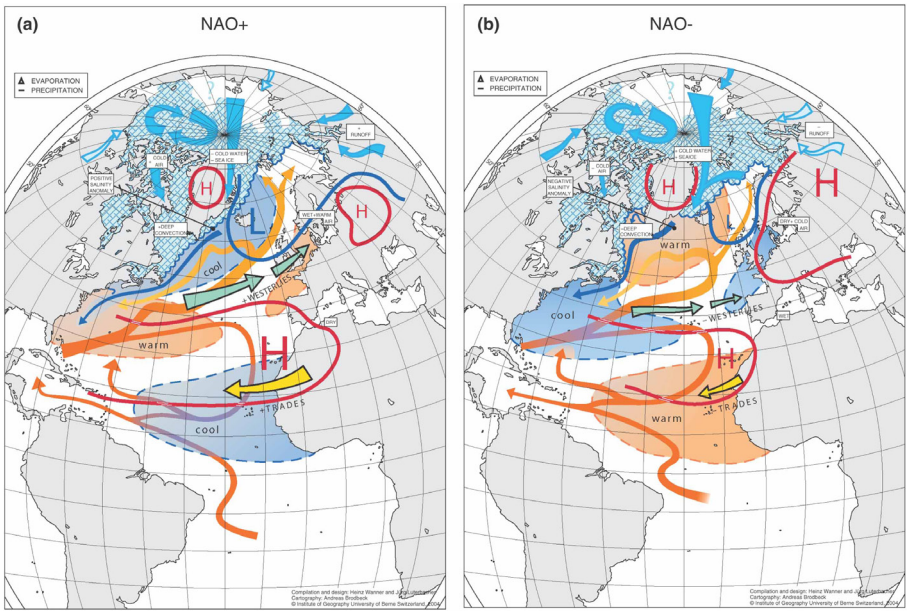

Figure I.7. Graphical representation of the two modes or states of the NAO. Surfaces mark SST and sea-ice extension, arrows show the flow systems in ocean, atmosphere and rivers, blue and red lines indicate near surface sea level pressures and white rectangles describe characteristic climate conditions or important processes. (a) Positive mode, (b) Negative mode (Wanner et al., 2001)

lies (and thus higher precipitation) over the eastern North Atlantic and the European continent, and a "low-index" pattern in which these anomaly cells are rather weak, thus giving place to reduced westerlies over the eastern North Atlantic and increasing precipitation in the western Mediterranean (Wanner et al., 2001; Trigo et al., 2004) (Fig. I.7). It has been proposed that the El Niño Southern Oscillation (ENSO) exerts a positive forcing on the NAO state, with an intensification of the Azores high and drier conditions in southern Europe during the cold phase of the ENSO (la Niña-like conditions) (e.g., Pozo-Vázquez et al., 2005).

The climate over the western Mediterranean has experienced a sequence of humid/dry and warm/cold periods during the Late Holocene. In the Iberian Peninsula, several lake reconstructions based on geochemical and biological analyses and tree-ring data have recorded warmer temperatures, lower lake levels and higher salinities during medieval times (11th to 13th centuries, MCA) and generally more humid conditions during the Roman Imperial epoch and cooler temperatures and wetter conditions between 14th-19th

centuries (LIA) (Moreno et al., 2008; Roberts et al., 2011). In northern Spain, the Estanya lake (in the Pre-Pyrenean range) recorded shallow lake levels and saline conditions during medieval times (870-1300 yr AD), and generally higher water levels from 1300-1850 yr AD. Maximum lake levels occurred during the 19th century, coinciding with higher population and agricultural expansion in the area, whereas declining lake levels associated with warmer climatic conditions are found during the 20th century (Morellón et al., 2011). Tree rings data in the Spanish Pyrenees showed warmer temperatures than average in the 14-15th centuries and an unprecedented warming in the 20th century, when six of the ten warmest decades were found. Colder temperatures are referred to the LIA (~1450-1850 yr AD) (Büntgen et al., 2008). Lake sediments indicated that the warmest winters in the Pyrenees occurred during the MCA and also during the Roman Humid Period (RHP, ~2700-2400 cal. yr BP), and winters were coldest during parts of the LIA (Pla and Catalan, 2005). In central Spain, the Taravilla lake (Guadalajara province) recorded fluctuations in the intensity of paleofloods (Moreno et al., 2008) likewise found in fluvial activity reconstructions from the Tagus river (Benito et al., 2003). In southern Spain, varved-lakes sediments (Zóñar Lake, Córdoba province) evidence the most humid period for the last 4000 yr during the Iberian-Roman ages (2500-1600 cal. yr BP) although it includes an arid interval at 2100-1800 cal. yr BP. Arid conditions are revealed during the MCA and two humid periods are recognized during the LIA (1200-1400 yr AD and at 1600 yr AD) (Martín-Puertas et al., 2008, 2010). Marine and terrestrial pollen records from the western Mediterranean have evidenced forest cover regression episodes during the Late Bronze Age-Iron Age (LBA-IA, ~3600-2600 cal. yr BP), the Dark Ages (DA, ~1600-1150 cal. yr BP) and the MCA (Jalut et al., 2000, 2009; Combourieu-Nebout et al., 2009), and a decrease in river activity has been also noticed during these periods in southern Europe (Magny et al., 2002; Macklin et al., 2006). For the twentieth century, recent works confirm a decrease in rainfall and moisture availability in the Mediterranean basin, with more frequent and severe drought episodes. Changes in atmospheric circulation patterns have been evoked as partially responsible for declining precipitation trends and major drought episodes (e.g., Sousa et al., 2011).

I.3. Inorganic geochemistry as a tool for paleoclimatic reconstructions

The elemental composition of marine sediments provides a wide range of information on sediment sources (terrestrial run-off and dust transport), primary organic production, sedimentary oxygenation and post-depositional changes in the sedimentary record (Calvert and Pedersen, 2007). Among such elements, Rb/Al, Mg/Al, K/Al, Si/Al, Ti/Al and Zr/Al ratios have been broadly used in the western Mediterranean for paleoenvironmental reconstructions (e.g., Moreno et al., 2002; Frigola et al., 2007; Jiménez-Espejo et al., 2008). Aluminum-normalization is commonly applied due to it conservative behaviour in order to discern possible fluctuations (enrichment or depletion of specific elements) in the lithogenic fraction (Van der Weijden, 2002). Rubidium readily substitutes potassium in aluminosilicate minerals, magnesium and potassium are supplied by chlorite and illite+feldspar respectively of fluvial provenance, whereas zircon is enriched in loess and Saharan dust, belonging to mineral phases chemically resistant to weathering and being mainly carried by wind-blown dust (e.g., Wehausen and Brumsack, 1999; Nijenhuis et al., 2001). Silicon makes up most of the major rock-forming minerals, comprising detrital input to the basin as aluminosilicates and quartz since biogenic opal is not efficiently preserved in this area due to enhanced dissolution processes with depth, thus being bound to minerals ranging on a considerably wide particle size (e.g., Kolla et al., 1979). Titanium occurs in accessory Ti-bearing heavy minerals (e.g. rutile, ilmenite or titanite) and some clay minerals, thus having multiple hosts in marine environments (e.g., Calvert and Fontugne, 2001).

Ba/Al and biogenic barite have been previously proposed and used as a proxy of export productivity in the western Mediterranean Sea in relation to episodes of enhanced productivity such as during the Heinrich events (e.g., Moreno et al., 2004; Jiménez-Espejo et al., 2008). Additionally, bromine content and Br/Al ratio may also show a good correlation and are linked to organic matter due to bromine uptake from seawater by phytoplankton (e.g., Ziegler et al., 2008).

Several redox-sensitive trace elements have provided information about changes in bottom water oxygenation conditions in the Alboran Sea record, being useful as paleoredox proxies because its valence can change depending on the prevailing redox conditions (e.g., Moreno et al., 2004; Rogerson et al., 2008). Thus, Cr, Mo, U and V tend to be less soluble under reducing condi-

tions, resulting in enrichments of highly insoluble species of lower valence while Cu, Cd, Ni and Zn form highly insoluble sulphides without undergoing a change in their valence under anoxic conditions (e.g., Calvert and Pedersen, 1993). Although, as mentioned above, U and Cu form highly insoluble sulphides under reducing conditions, authigenic U and Cu also show a good correlation and can be associated to the organic carbon flux, may complex with organic matter and be mainly ubiquitous as organometallic ligands (e.g., McManus et al., 2005).

Other redox-sensitive elements such as Mn and Fe have also supplied additional information on bottom water oxygen conditions in the western and eastern Mediterranean Sea (e.g., Masqué et al., 2003; Gallego-Torres et al., 2007). Mn^{2+} and Fe^{2+} are oxidized to insoluble Mn^{4+} and Fe^{3+} (Fe and Mn oxy-hydroxides) from the water column under oxic conditions, being accumulated as ferric and manganese oxides on the sediment surface. As additional sediment accumulates, thus under sub-oxic conditions, iron and manganese are reduced to soluble Fe^{2+} and Mn^{2+} and diffuses upwards. This remobilization can lead to oxidation and precipitation of Fe and Mn oxy-hydroxides at the redoxcline where a post-depositional oxidation front is encountered when bottom waters are reventilated and penetrates downwards into the sediments while organic matter burns down and the redoxcline further deepens (e.g., Mangini et al., 2001). These oxy-hydroxides usually include considerable amounts of other trace metals, as molybdenum or cobalt, which are also enriched in the post-depositional oxidation front, and they most likely co-precipitate with or are scavenged by Fe and Mn oxy-hydroxides (e.g., Tribovillard et al., 2006).

I.4. Molecular fossils as paleoceanographic proxies

An increasing number of geochemical proxies relying on inorganic and organic fossil remains have been developed during the last few decades (e.g., Eglinton and Eglinton, 2008; Castañeda and Schouten, 2011) (Fig. I.8), and numerous studies are currently applying these proxies to reconstruct paleoenvironmental conditions in marine sedimentary sequences from around the world, including the westernmost Mediterranean region.

The inference of past SST is one of the most significant tools for the reconstruction of climate variability beyond the instrumental record. The main

widely applied inorganic methods are those based on the quantitative composition of planktonic fossil assemblages in relation to modern ones through the calibration of transfer functions (e.g., Imbrie and Kipp, 1971; Hutson, 1980), the oxygen isotopic composition ($\delta^{18}O_{calcite}$) (Shackleton, 1974) and the Mg/Ca ratio of foraminiferal calcite (Elderfield and Ganssen, 2000), which have been extensively implemented in the western Mediterranean during the last deglacial cycle (e.g., Pérez-Folgado et al., 2004; Sierro et al., 2005; Cacho et al., 2006; Serrano et al., 2007; Rogerson et al., 2010). Nevertheless, there are some secondary effects as the isotopic composition, the carbonate ion concentration and the salinity of the seawater from which the carbonate precipitates as well as partial shell dissolution, introducing considerable uncertainty into

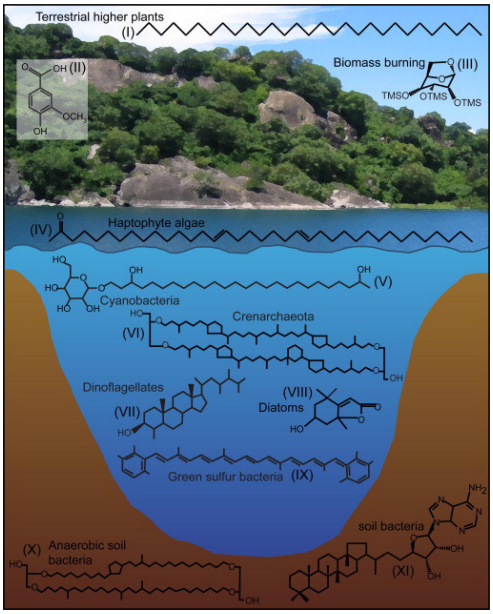

Figure I.8. The biomarker concept. Structures shown include the (I) C_{29} n-alkane (a biomarker for terrestrial higher plants), (II) vanillic acid (a lignin phenol and biomarker for terrestrial higher plants), (III) levoglucosan (a biomarker for biomass burning), (IV) the $C_{37:2}$ methyl alkenone (a biomarker for haptophyte algae), (V) 1-(Ohexose)-3,25-hexacosanediol (a heterocyst glycopid and biomarker for N_2-fixing cyanobacteria), (VI) crenarchaeol (an isoprenoid glycerol dialkyl glycerol tetraether -GDGT- and biomarker for Thaumarchaeota), (VII) dinosterol (a biomarker for dinoflagellates), (VIII) loliolide (the anoxic degradation product of the pigment fucoxanthin, the major carotenoid present in diatoms), (IX) isorenieratene (a pigment produced by green sulphur bacteria that is used as an indicator of stratified conditions in ancient lake sediments), (X) branched GDGT IIb (thought to be produced by anaerobic soil bacteria and a biomarker for soil organic matter), and (XI) adenosylhopnane (an intact bacteriohopanepolyol -BHP- that has been proposed as a biomarker of soil bacteria) (Castañeda and Schouten, 2011)

the use of these proxies as paleothermometers (e.g., Lea, 2003)

The most widely worldwide proxy based on organic fossil remains used in paleoclimatology for SST reconstructions is the $U^{k'}_{37}$ index (Brassell et al., 1986), which quantifies the degree of unsaturation (two, three or four double bonds) of long chain ketones with 37 carbon atoms (alkenones) biosynthesized by haptophyte algae (coccolitophorids, mainly *Emiliana huxlei*) (Fig. I.9). This index has a direct relationship with average annual temperature in order that the degree of unsaturation increase, and so the relative proportion of the three double bonds ketone biosynthesized, as temperature of the water decreases (Prahl and Wakeham, 1987; Müller et al., 1998). This proxy has also been successfully used in the western Mediterranean Sea, showing a good correlation with the $\delta^{18}O$ record from the GISP2 ice core to abrupt events during the last deglacial cycle (Cacho et al., 1999, 2001; Marchal et al., 2002; Martrat et al., 2004, 2007).

Recently, Schouten et al. (2002) proposed a new proxy to reconstruct past SST based on archaeal isoprenoid tetraether membrane lipids, the TEX_{86} index (TetraEther indeX of tetraethers consisting of 86 carbon atoms), which quantifies the relative distribution of cyclopentane moieties in the glycerol diphytanyl glycerol tetraethers (GDGTs) of the membrane lipids of the marine domain Archaea. These organisms are ubiquitous in the marine pelagic environment and biosynthesize GDGTs containing 0-3 cyclopentane moieties and crenarchaeol (which in addition to four cyclopentane moieties has a cyclohexane moiety) together with small quantities of a crenarchaeol regioisomer. The GDGT "crenarchaeol" (GDGT IV), which contains four cyclopentane moieties and a cyclohexane moiety (Fig. I.10), is suggested to be specific to the Thaumarchaeota (formerly Crenarchaeota) (Pitcher et al., 2011). This index correlates well with SST (0-100 m) in order that higher temperatures will result in an increase in the relative amounts of GDGTs with two or more cyclopentane moieties (Wuchter et al., 2004, 2005; Kim et al., 2008). TEX^{H}_{86} has been previously applied in the Alboran Sea basin to evidence SST fluctuations during the penultimate interglacial-glacial cycle (Huguet et al., 2011).

Some other climatic variables, such as terrestrial input and marine productivity, can provide a more comprehensive characterization of modes and processes governing natural climate

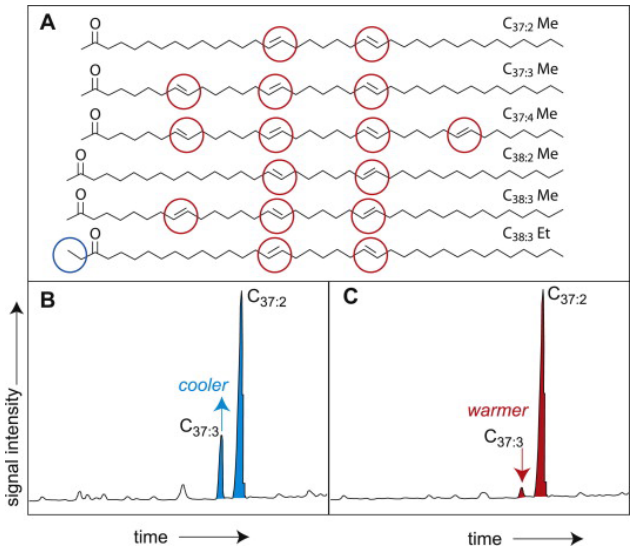

Figure I.9. a) Examples of structures of methyl (Me) and ethyl (Et; circled in blue) long-chain alkenones, b) and c) Illustration of the $U^{k'}_{37}$ SST proxy. As temperature increases, the relative proportion of the $C_{37:3}$ alkenone decreases (Castañeda and Schouten, 2011)

variability. Among these proxies, long straight chain *n*-alkanes, with predominantly odd over even carbon number (C_{25}-C_{31}), are major lipid components of the epicuticular waxes of terrestrial higher plants leaves (Eglinton and Hamilton, 1967). These compounds are transported into the oceans by wind (Schefuß et al., 2003) or fluvial run-off (Castañeda et al., 2007), being deposited and well-preserved in marine sediments (Fig. I.11). Fluctuations in the weighted mean average carbon isotopic composition ($\delta^{13}C_{WMA27\text{-}33}$) of the odd-carbon numbered *n*-alkanes can be used to track possible changes in the source and the relative contribution by plants using a different carbon fixation pathway during photosynthesis thus providing further insights about paleohydrological conditions driving climate variability. C_3 plants are the most ^{13}C depleted and commonly found (around –36‰; trees, most shrubs, cool-season grasses and sedges) whereas C_4 plants (around –21.5‰; warm-season grasses and sedges) are found predominantly in tropical savannahs, temperate grasslands, and semideserts (Collister et al., 1994). Cacho et al. (2000) used the *n*-hexadecanol/*n*-nonadecane index in the Alboran Sea basin to evidence deep water oxygenation conditions during cold events. Additionally, the BIT index (Branched versus Isoprenoid Tetraether index) provides further information regarding the origin of the sedimentary organic matter due to it is a proxy based

on the relative terrestrial input of organic matter into the oceans (Hopmans et al., 2004). This index quantifies the relative contribution of terrestrial branched GDGTs in relation to the marine isoprenoidal crenarchaeol (Weijers et al., 2006) (Fig. I.10). Its value varies between 0 and 1, representing marine and terrestrial organic matter end-members, respectively. Regarding paleoproductivity conditions, Rampen et al. (2008) proposed a novel long chain diol index as an indicator of upwelling conditions which quantifies the relative contribution of 1,14 long chain diols in diatoms from the genus *Proboscia* (Fig. I.12). These diatoms have been previously identified as the main source which biosynthesize these ubiquitous marine lipids (Sinninghe Damsté et al., 2003) and have been previously applied as a productivity proxy during upwelling conditions in sediment trap samples from the Arabian Sea (Rampen et al., 2007).

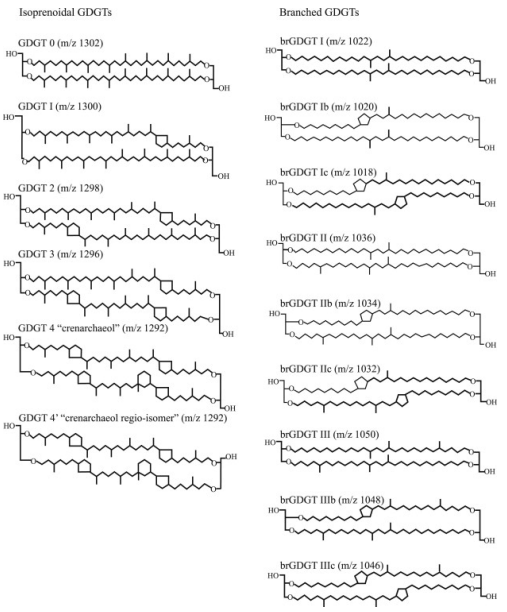

Figure I.10. Structures of the isoprenoid and branched GDGTs used for calculating TEX^{H}_{86}, the BIT index, and MBT/CBT (Castañeda and Schouten, 2011)

I.5. Statistical insights into paleoclimatic proxies

Statistical analyses are useful tools for handling, summarizing and interpreting large geochemical and mineralogical paleoenvironmental data for paleoclimatic reconstructions (e.g., Giralt et al., 2008, 2011; Martín-Puertas et al., 2011; Morellón et al., 2011).

Thus, assuming that the variables have environmental significance, normalized matrix clusters of the geochemical data can be applied in order to split the data set into discrete groups of samples that have environmental similarities in terms of their affinity and provenance source. In this way, additional and more precise knowledge regarding the relationship between the different proxies as well as the environmental information provided can be attained. As an illustrative example, barium has been proposed and extensively used as a paleoproductivity proxy in the Mediterranean Sea

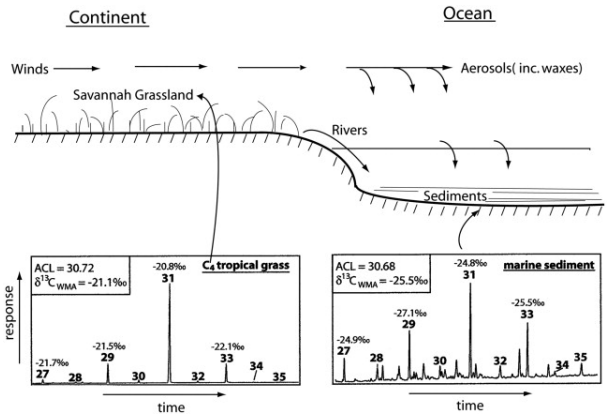

Figure I.11. Plant-wax lipids in ocean sediments. Typical GC traces are shown for the n-alkane fractions [C_{27}–C_{35}] of a C_4 tropical grass and for a marine sediment from the southeast Atlantic. The $\delta^{13}C$ values (in ‰) are marked for each of the prominent odd-carbon-number homologues. The $\delta^{13}C_{WMA}$ (weighted mean average) is also shown for this carbon-number range, together with the Average Chain Length (ACL). The distribution and isotopic compositions in the marine sediment are in accord with a significant input of n-alkanes from the African savannah C_4 grasslands (Eglinton and Eglinton, 2008)

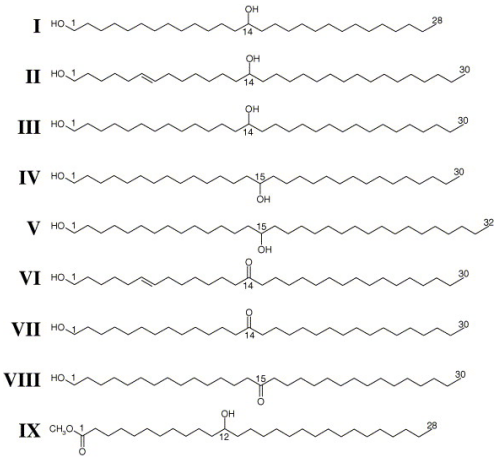

Figure I.12. Structures of (I) C_{28} 1,14-diol, (II) $C_{30:1}$ 1,14-diol, (III) C_{30} 1,14-diol, (IV) C_{30} 1,15-diol, (V) C_{32} 1,15-diol, (VI) $C_{30:1}$ 1,14-keto-ol (tentative), (VII) C_{30} 1,14-keto-ol, (VIII) C_{30} 1,15-keto-ol, (IX) C_{29} 12-hydroxy methyl alkanoate (Rampen et al., 2007)

at time of enhanced productive episodes (e.g. sapropels, Heinrich events). Nevertheless, when no Ba excess is recognized as it is the case for the Late Holocene, statistical analyses show how this element relates to detrital input, being associated with alumino-silicates (see Chapter II, IV and appendixes). Moreover, it is possible to complement this information and to further identify possible provenances of the chemical elements in relation to their associated mineral phases by Redundancy Analyses (RDA). Hence, quartz arises in an intermediate position between detrital proxies of fluvial and eolian provenance, which suggests that it could come from both sources. On the other hand, cluster and RDA analyses bound Si to aluminium, thus revealing clay minerals

as the most important hosts and riverine input as the main supply to the basin during the Late Holocene (see Chapter II and IV).

Similarly, Principal Component Analyses (PCA) allows reducing the dimensionality of the sedimentary dynamic of the basin problem and disentangling the main environmental processes controlling sedimentary deposition. In this way, cores located in close proximity have evidenced different processes influencing sediment deposition (e.g. water oxygenation conditions in core 306G, situated on a small pelagic high; and detrital-productivity oscillations in core 305G, located at the continental slope, see Chapter II). The identification of these processes have also allowed further understanding to explain their respective differences in the geochemical and the sedimentological record such as grain size distribution, redox conditions and post-depositional oxidation fronts. Additionally, the first eigenvector of the PCA in this study has showed that despite local differences concerning paleoceanographic conditions, the dominant climatic signal is coherent in both records, and also contributed in the unravelling of the mechanisms driving natural climate variability in the westernmost Mediterranean. Consequently, this multivariate statistical approach has been successfully applied to the geochemical and mineralogical datasets for the characterization of climate conditions in the western Mediterranean during the Late Holocene.

Chapter II

Tracking climate variability in the western Mediterranean during the Late Holocene: A multiproxy approach

V. Nieto-Moreno, F. Martínez-Ruiz, S. Giralt, F. Jiménez-Espejo, D. Gallego-Torres, M. Rodrigo-Gámiz, J. García-Orellana, M. Ortega-Huertas, and G.J. de Lange

Climate of the Past, 7: 1395-1414 (2011); doi:10.5194/cp-7-1395-2011

Abstract

Climate variability in the western Mediterranean is reconstructed for the last 4000 yr using marine sediments recovered in the west Algerian-Balearic basin, near the Alboran basin. Fluctuations in chemical and mineralogical sediment composition as well as grain size distribution are linked to fluvial-eolian oscillations, changes in redox conditions and paleocurrent intensity. Multivariate analyses allowed us to characterize three main groups of geochemical and mineralogical proxies determining the sedimentary record of this region. These three statistical groups were applied to reconstruct paleoclimate conditions at high resolution during the Late Holocene. An increase in riverine input (fluvial-derived elements —Rb/Al, Ba/Al, REE/Al, Si/Al, Ti/Al, Mg/Al and K/Al ratios), and a decrease in Saharan eolian input (Zr/Al ratio) depict the Roman Humid Period (RHP) and the Little Ice Age (LIA), while drier environmental conditions are recognized during the Late Bronze Age-Iron Age (LBA-IA), the Dark Ages (DA) and the Medieval Climate Anomaly (MCA). Additionally, faster bottom currents and more energetic hydrodynamic conditions for the former periods are evidenced by enhanced sortable silt (10-63 μm) and quartz content, and by better oxygenated bottom waters —as reflected by decreasing redox-sensitive elements (V/Al, Cr/Al, Ni/Al and Zn/Al ratios)—. In contrast, opposite paleoceanographic conditions are distinguished during the latter periods, i.e. the LBA-IA, the DA and the MCA. Although no Ba excess was registered, other paleoproductivity indicators (total organic carbon content, Br/Al ratio, and organometallic ligands such as U and Cu) display the highest values during the RHP, and together with increasing preservation of organic matter, this period exhibiting by far the most intense productivity of the last 4000 yr. Fluctuations in detrital input into the basin as the main process managing deposition —reflected by the first eigenvector defined by the Principal Component Analyses— point to solar irradiance and the North Atlantic Oscillation variability as the main driving mechanisms behind natural climate variability over decadal to centennial time-scales for the last 4000 yr.

II.1. Introduction

Although more attention has been classically devoted to major climate changes during the last deglacial period (Heirich stadial 1, Bølling-Allerød interstadial, and Younger Dryas) (Dansgaard et al., 1993; Magny et al., 2001; Stein et al., 2009), the Holocene is also punctuated by rapid climate variability including polar cooling, aridity, and changes in the intensity of atmospheric circulation (Mayewski et al., 2004; Wanner et al., 2008). These climatic oscillations have been described in Greenland ice cores (e.g., O'Brien et al., 1995; Dawson et al., 2007), and in North Atlantic (e.g., Bond et al., 1997; Bianchi and McCave, 1999), Mediterranean (e.g., Casford et al., 2001; Rohling et al., 2009), Tropical Atlantic (e.g., deMenocal et al., 2000; Rimbu et al., 2004), and Antarctic deep sea cores (e.g., Masson et al., 2000; Bárcena et al., 2002); as well as in lake sediments (Magny, 2004; Jones et al., 2006), peat bogs (e.g., Blackford and Chambers, 1995), speleothems (e.g., McDermott et al., 2001; Mangini et al., 2007), fossil pollen (e.g., Willard et al., 2005; Jalut et al., 2009) and tree rings (e.g., Esper et al., 2002; Moberg et al., 2005). Nevertheless, the overall lack of agreement about the worldwide distribution, precise timing, amplitude or cause of these fluctuations underlines the need for additional regional records to reconstruct climate change (Hughes and Diaz, 1994; Crowley and Lowery, 2000; Broecker, 2001).

At the global scale, natural external forcing —including solar irradiance variations and volcanic activity— have been highlighted as the main driving mechanisms of natural climate variability on centennial to millennial time-scales during the Holocene (van Geel et al., 1999; Crowley, 2000; Bond et al., 2001). At regional scales, patterns of natural internal climate variability such as El Niño-Southern Oscillation (ENSO) and the North Atlantic Oscillation (NAO) are known to vary over decadal to centennial time-scales (Jones et al., 2001; Turney and Palmer, 2007; Trouet et al., 2009). System response to multiple forcing and internal climate variability is further complicated by positive or negative feedbacks and non-linear responses, such as an interruption or weakening of the North Atlantic Deep Water (NADW) production rate during abrupt cold events (Bond et al., 1997; Bianchi et al., 1999). Besides the mechanisms underlying these natural climate fluctuations, Bond et al. (1997) describe several pervasive millennial scale North Atlantic cooling events (ice-rafted debris events) underway

during the Holocene (with a mean pacing of ~1500 yr; nearly the same as the Dansgaard/Oeschger events during the last glaciation), the Little Ice Age (LIA) being the most recent one.

Evidence of abrupt events at the millennial scale during the last glacial-interglacial transition have been previously reported in the westernmost Mediterranean (e.g., Cacho et al., 1999, 2001; Moreno et al., 2002, 2005; Bout-Roumazeilles et al., 2007; Jiménez-Espejo et al., 2007, 2008), revealing that this region is highly sensitive to climate forcing and provides ultra high-resolution records at both centennial and millennial scales. Abrupt decreases of paleo-sea surface temperatures and salinities in the Alboran basin (Cacho et al., 1999; Bárcena et al., 2001; Melki et al., 2009), fresh polar-derived water flowing into the Mediterranean Sea through the Strait of Gibraltar (Sierro et al., 2005; Rogerson et al., 2010), intensification of north-westerly winds towards the Gulf of Lyon and thus enhanced Western Mediterranean Deep Water formation (WMDW) (Voelker et al., 2006; Frigola et al., 2008), continental dryness and reduction of the forest cover extent in the westernmost Mediterranean borderlands (Combourieu-Nebout et al., 2002; Sánchez-Goñi et al., 2002), and higher eolian input from the Saharan region (Moreno et al., 2005; Bout-Roumazeilles et al., 2007) have been correlated with cold spells taking place in the North Atlantic realm (Heinrich and Dansgaard/Oeschger stadials). Such findings support the linkage of this region with the North Atlantic coupled ocean-atmosphere system.

Despite the broad and intensive paleoenvironmental research performed in the western Mediterranean during the last few decades, high resolution marine records of the Late Holocene are comparatively scarce. The last 4000 yr of this time interval are characterized by several climatic fluctuations, the best identified among them being the Late Bronze Age-Iron Age (LBA, 3600-2600 cal. yr BP; Van Geel et al., 1996), the Roman Humid Period (RHP, 2600-1600 cal. yr BP; Issar, 2003), the Dark Ages (DA, 1600-1150 cal. yr BP; Berglund, 2003), the Medieval Climate Anomaly (MCA, 1150-650 cal. yr BP; Lamb, 1965; Hughes et al., 1994) and the LIA (650-150 cal. yr BP; Bradley and Jones, 1993). In this work we integrated data from two different marine records from the western Algerian-Balearic basin. After high resolution analysis, they are compared with records from the Alboran Sea basin. A multiproxy approach was adopted, fea-

turing statistical characterization of the data sets, major and trace element-content fluctuations, grain size distribution, total organic carbon content and mineral composition of marine sediments. This multiproxy approach allowed for the identification and characterization of the main climate oscillations and regional changes over the past 4000 yr, to further advance our understanding of natural climate variability in the westernmost Mediterranean.

II.2. Climatological and oceanographic setting

The Mediterranean climate is characterized by warm-hot dry summers and mild-cold wet winters due to the influence of the subtropical high-pressure belt and the mid-latitude westerly system (e.g., Lionello et al., 2006). During winter the subtropical high reaches its southernmost position, allowing incursions of westerly winds that introduce mid-latitude cyclones from the Atlantic Ocean, resulting in a low intensity precipitation over the Mediterranean region. During summer, the subtropical high-pressure belt remains over this region, restraining precipitation and inducing climate dryness (e.g., Sumner et al., 2001; Bolle, 2003).

At decadal time-scales, the prevailing winter climate variability pattern in the North Atlantic region is the NAO (e.g., Hurrell, 1995; Trigo et al., 2004). The positive phase of the NAO is characterized by stronger than usual westerlies, tracing a pathway across middle latitudes farther to the north, and leading to dry and cold winters in southern Europe, the Mediterranean, and northern Africa, and to warm and wet winters in northern Europe (e.g., Wanner et al., 2001; Trigo et al., 2002). Furthermore, enhanced dust transport from the Saharan region to the Mediterranean Sea has been evidenced during positive NAO phases (Moulin et al., 1997). The negative phase of the NAO is linked to opposite trends.

In terms of oceanographic conditions, the western Mediterranean Sea is characterized by a thermohaline circulation driven by excessive evaporation with respect to precipitation and runoff (e.g., Bethoux, 1979). Hence, the Atlantic jet stream becomes saltier and denser when it flows into the Mediterranean Sea (Modified Atlantic Water, MAW); and two anticyclonic gyres are produced when it progresses eastwards to the Algerian basin (Western and Eastern Alboran Gyres) (e.g., Perkins et al., 1990; Millot, 1999). The MAW is offset by a deep-water outflow (Mediterranean Outflow Water; MOW) consisting

of Levantine Intermediate Water (LIW) and WMDW, respectively originated in the Levantine Mediterranean Sea and in the Gulf of Lyon (Millot, 2008).

II.3. Paleoenvironmental proxies: The mineralogical and geochemical record in the western Mediterranean Sea

The detrital fraction of deep-sea sediments is a reliable proxy for paleoceanographic and paleoenvironmental reconstructions (e.g., Chamley, 1989) because it provides insight regarding the climate conditions prevailing in source areas and the mechanisms involved in the transport of material from land to sea (riverine and eolian input), as well as changes in the oceanic and atmospheric circulation that may trigger its dispersion (e.g., Bout-Roumazeilles et al., 2007; Fagel, 2007).

Previous studies of clay mineral composition in marine sediments from the western Mediterranean signal riverine input from the Iberian margin (e.g., Fabres et al., 2002) and wind-blown transport of particles from the African margin as the main sources of the detrital fraction (e.g., Guerzoni et al., 1997). Illite, chlorite and smectite are fluvial-derived, whereas kaolinite is considered reworked wind-blown particles from western Morocco and northern Algeria (e.g., Bout-Roumazeilles et al., 2007).

Element/Al ratios (such as Rb/Al, REE/Al, Mg/Al, K/Al, Si/Al, Ti/Al and Zr/Al) have also been studied to infer fluctuations in terrestrial run-off, erosional processes and riverine and eolian input to the Alboran basin (e.g., Moreno et al., 2005; Jiménez-Espejo et al., 2008; Martín-Puertas et al., 2010). Aluminum-normalization is commonly used to envisage fluctuations in detrital aluminosilicate source material (e.g., Van der Weijden, 2002). Rare earth elements (REE) are reliable indicators for tracing source provenance, as they are transferred nearly quantitatively in the terrigenous component through erosion and sedimentation (e.g., McLennan, 1989).

Meanwhile, redox-sensitive trace elements (such as V/Al, Cr,/Al, Ni/Al and Zn/Al) provide information about changes in bottom water oxygenation because their solubility depends on their valence, which in turn depends on the prevailing redox conditions (e.g., Martínez-Ruiz et al., 2003; Moreno et al., 2004; Jiménez-Espejo et al., 2007; Rogerson et al., 2008).

Approaches to correlate grain size to paleocurrent intensity refer to the

percentage of sortable silt or coarse silt (SS, 10-63 μm) as a proxy of relative paleocurrent speed (e.g., McCave et al., 1995; McCave and Hall, 2006). This proxy has been successfully applied in the western Iberian margin, showing that high SS values correlate with faster flows and better oxygenated deep waters (e.g., Hall and McCave, 2000). Thus, we have considered silt coarser than 10 μm in the fine fraction as an indicator for paleocurrent speed equivalent to the UP10 index applied by Frigola et al. (2007) and Rogerson et al. (2008) in marine sediments from the western Mediterranean, rather than the sediment fraction susceptible to transport by wind as previously reported by Moreno et al. (2002).

II.4. Materials and methods

Two gravity-cores, 305G (36º23,603'N, 1º22,710'W, 2512 m.b.s.l.) and 306G (36º27,846'N, 1º11,166'W, 2574 m.b.s.l) —recovered during the Training-Through-Research Cruise 14 (TTR-14), Leg 2, in the west Algerian-Balearic basin— were selected for this study (Fig. II.1) (Comas and Ivanov, 2006).

Both cores were sampled in 1 cm thick slices to obtain a high resolution

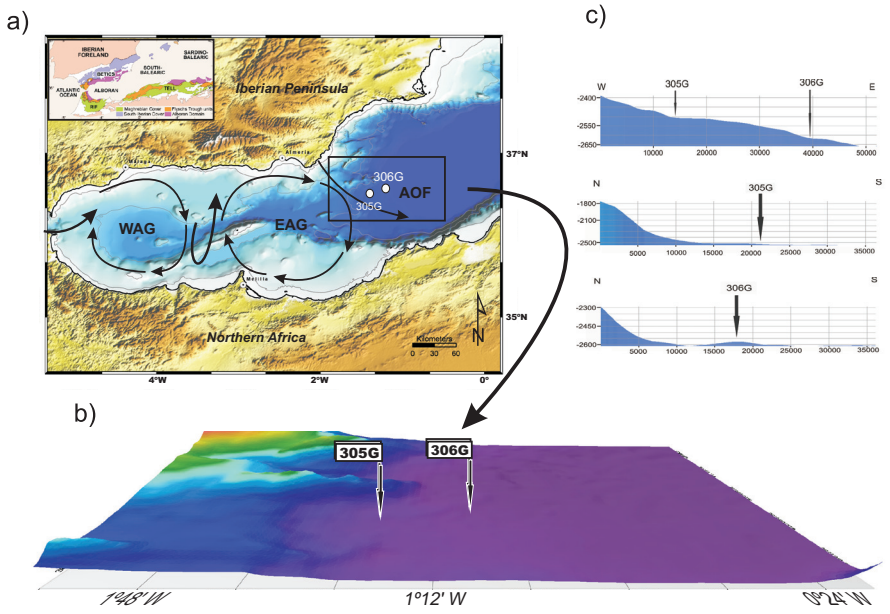

Figure II.1. a) Site setting of the studied cores in the west Algerian-Balearic basin b) bathymetric map and c) topographic profile showing the main physiographic features of the area under study. WAG: Western Alboran gyre, EAG: Eastern Alboran gyre, AOF: Almería-Orán Front

record for the last 4000 yr. Samples were treated to analyze chemical and mineralogical composition using different techniques. Bulk and clay mineral compositions were obtained by X-Ray Diffraction using a PANalytical X'Pert PRO diffractometer with Cu-Kα radiation and automatic slit. Clay fraction separation and sample preparation was performed according to the international recommendations compiled by Kisch (1991). Diffractograms were visually interpreted using Xpowder software (Martin, 2004; http://www.xpowder.com). Peak areas were measured in order to estimate semi-quantitative mineral contents, the estimated error being <5% for bulk mineral composition and 5-10% for clay mineral proportions.

Quantitative geochemical microanalyses every five centimetres for clay mineral characterization were achieved by Transmission Electron Microscopy (HR-TEM; Philips CM-20 provided with and EDAX microanalysis system). Additional morphological analyses of clays, barite and pyrite from selected samples were acquired by Field Emission Scanning Electron Microscopy (FE-SEM; LEO-Carl Zeiss-GEMINI-1530). Barite was separated from eight selected samples with higher Ba content by a sequential leaching procedure (Eagle et al., 2003).

Major elements were measured using Wavelength Dispersive X-Ray Fluorescence Spectrometry (WDXRF; Bruker AXS S4 Pioneer with an Rh anode X-ray tube), using pressed pellets, with an analytical detection limit of 0.1% and an instrumental error <1%. Trace elements were analyzed by Inductively Coupled Plasma-Mass Spectrometry (ICP-MS; Perkin-Elmer Sciex Elan 5000) using Re and Rh as internal standards with an instrumental error of ±2% and ±5% for elemental concentrations of 50 ppm and 5 ppm, respectively (Bea, 1996). Samples were prepared by sequential acid digestion (HNO_3+HF) and measured in triplicate. REE values (La, Ce, Pr, Nd, Sm, Eu, Gd, Tb, Dy, Ho, Er, Tm, Yb, Lu) were normalized with respect to CI chondrite according to McDonough and Sun (1995) with a resolution of five centimetres in both cores.

Total organic carbon (TOC) content was determined using a Horiba EMIA-320V Series Carbon/Sulfur Analyzer. Grounded samples were subjected to acid leaching (HCl) onto glass fiber filters in order to remove inorganic carbon. Treated samples were oxidized by the high-frequency induction furnace method under an oxygen stream,

and CO_2 gases evolved were detected by calibrated infra-red (IR) cells. TOC content was expressed as a percentage of dry weight. The accuracy of the method is 92%, and precision is 0.01%.

A granulometric study was undertaken on the bulk fraction at 2 cm intervals, taking away the coarse fraction (>63 μm) by wet sieving and removing carbonates and organic matter from the remaining silt (2-63 μm) and clay fraction (<2 μm) by treatment with acetic acid (three times during 24 hours each round, using 5 $ml \cdot L^{-1}$ in the first acid attack and then 10 $ml \cdot L^{-1}$ in the other two) and hydrogen peroxide (10%, one week), respectively. Grain size was determined as a cumulative mass percentage using a Micromeritic Sedigraph III 5120, which measures particles ranging from 0.10 to 63 μm. Resolution and accuracy are, respectively, 1 and 0.1 μm. Two split fractions were established for the terrigenous silt: a) fine silt (2-10 μm), cohesive, mainly composed of clay minerals and settled as aggregated material, and b) coarse silt (10-63 μm) or sortable silt (SS), predominantly composed of quartz and feldspar, and with non-cohesive behaviour.

Statistical treatment of analytical data was performed using the statistical software package R (Development Core Team, 2011). Stratigraphically-constrained cluster analyses were applied to identify the main geochemical families and the outliers (isolated samples with anomalous values). The normalized geochemical dataset was also clustered in order to find groups of variables showing similar behaviour. The complete linkage method (or furthest neighbour method) was used for clustering purposes. Redundancy Analyses (RDA) were carried out on the geochemical and the mineralogical data set using the "vegan" package (Oksanen, 2009) to infer the relationship between them, and Principal Component Analyses (PCA) were performed on the geochemical data set to characterize the main underlying gradients governing the sedimentary environment.

II.5. Age-depth model and sedimentation rate

The age-depth model is based on ^{14}C dating complemented with the activity-depth profiles of ^{210}Pb. Five ^{14}C-AMS dates for each core were performed on monospecific planktonic foraminifera (*Globigerina bulloides*) extracted from the >125 μm fraction. Samples were analyzed by Accelerator Mass Spectrometry at the National Centre for Accelerators (CNA Spain) and the Poznan Radiocarbon Laboratory (Poland). Radiocarbon

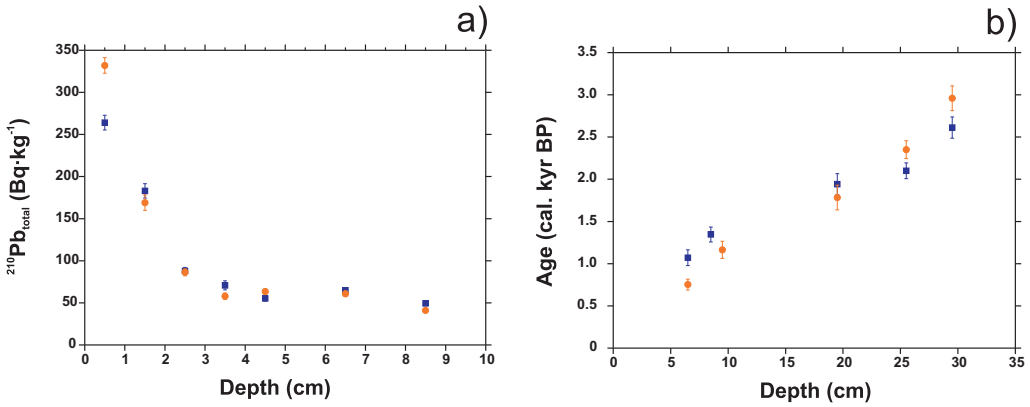

Figure II.2. Activity profiles of $^{210}Pb_{total}$ (Bq·kg^{-1}) for cores 305G (blue squares) and 306G (orange circles) with error bars representing 1σ uncertainties (a) and ^{14}C dates for core 305G (blue squares) and 306G (orange circles) with error bars representing 2σ uncertainties (b)

ages were calibrated to calendar years (cal. BP) using CALIB 6.0 software (Stuiver and Reimer, 1993) and MARINE09 curve (Reimer et al., 2009), assuming a marine reservoir age correction of 400 yr (Table II.1). In order to obtain an age-depth model, a linear interpolation was applied between dates, giving mean sedimentation rates of 10.2 and 10.7 cm·kyr^{-1} for cores 305G and 306G, respectively (Fig. II.2b). Mean sedimentation rates and ^{210}Pb inventories are similar to those reported in other deep Mediterranean areas by previous authors (García-Orellana et al., 2009).

^{210}Pb was determined in the first five

Table II.1. Radiocarbon dates and calibrated ages for cores 305G and 306G. Results are reported with a 2σ uncertainty

Laboratory code	Core	Core depth (cm)	Conventional Radiocarbon Age (B.P)	Calibrated Age (cal. BP)
Poz-37150	305G	6-7	1520±30	1070±93
CNA567	305G	8-9	1795±40	1346±88
CNA304	305G	19-20	2320±45	1942±124
Poz-37151	305G	25-26	2335±30	1956±94
CNA305	305G	29-30	2870±45	2613±126
Poz-37152	306G	6-7	1130±35	690.5±63.5
CNA306	306G	9-10	1610±45	1164±102
CNA307	306G	19-20	2200±60	1784±146
Poz-37153	306G	25-26	2645±35	2350±105
CNA308	306G	29-30	3160±45	2959±146

centimetres of both cores to obtain the most recent maximum sedimentation rates. Determination of ^{210}Pb activities was accomplished through measurement of its daughter nuclide, ^{210}Po, following the methodology described by Sánchez-Cabeza et al. (1998). Briefly, after addition of a given amount of ^{209}Po as the internal tracer, sediment aliquots of 200-300 mg of each sample were totally dissolved in an acid medium using an analytical microwave oven. Polonium isotopes were plated onto pure silver discs in HCl (1N) at 70ºC while stirring for 8h. Polonium emissions were subsequently counted with α-spectrometers equipped with low-background silicon surface barrier detectors for $4 \cdot 10^5$s. Results showed that ^{210}Pb was in excess only in the two first centimetres (Table II.2). Although ^{210}Pb inventories are similar to those reported in the Algerian-Balearic basin (García-Orellana et al., 2009), they are lower than other sediment records from the area (Masqué et al., 2003), suggesting a loss of the surface part of the sediment during the gravity core reco-

Table II.2. Total ^{210}Pb concentrations and ^{210}Pb inventories for cores 305G and 306G. Results are reported with a 1σ uncertainty

Laboratory Code	Core	Core depth (cm)	$^{210}Pb_{total}$ (Bq·kg^{-1})
305G05	305G	0.5	264±9
305G15	305G	1.5	183±9
305G25	305G	2.5	88±4
305G35	305G	3.5	71±5
305G45	305G	4.5	55±3
305G65	305G	6.5	65±3
305G85	305G	8.5	49±3
306G05	306G	0.5	332±9
306G15	306G	1.5	169±9
306G25	306G	2.5	86±4
306G35	306G	3.5	58±4
306G45	306G	4.5	63±3
306G65	306G	6.5	61±3
306G85	306G	8.5	41±2
$^{210}Pb_{base}$	305G		57±8
^{210}Pb (Bq·m^{-2})	305G		1912±106
$^{210}Pb_{base}$	306G		56±10
^{210}Pb (Bq·m^{-2})	306G		2691±84

very. Although some surface sediment loss is expected due to gravity core recovery, the enrichment of ^{210}Pb in the first centimetres observed in both cores suggest that the loss of sediment is not significant, which is in agreement with the age model inferred from ^{14}C-AMS dates (Fig. II.2a).

II.6. Statistical analyses: Grouping proxies for paleoclimatic reconstruction

The identification and characterization of the main processes behind sedimentary deposition in the study area were based on statistical analyses of the mineralogical and geochemical data sets. Normalized matrix clustering of the geochemical data (Figs. II.3a, b) allowed us to identify the main geochemical families showing similar behaviour, and thus a high correlation in terms of their affinity and origin. RDA biplots illustrate the relationships between the chemical elements and their associated mineral phases. Three main groups in accordance with their origin in both sites were defined (Figs. II.3c, d).

The first group comprises fluvial (illite, feldspars, smectite, dolomite, Al, Th, Rb, Ba, REE, Mg, K, Fe, Si and Ti) and eolian (kaolinite, Zr) derived elements/minerals (Figs. II.3a, b, c, d). Fluvial-derived illite, smectite, feldspar and dolomite are opposed to eolian-derived kaolinite. Quartz appears in between detrital proxies of fluvial and eolian provenance, which suggests that it could come from both sources (Kolla et al., 1979) (Figs. II.3c, d). Ba/Al and biogenic barite are widely used as paleoproductivity proxies in relation to episodes of enhanced productivity such as the Heinrich events (Moreno et al., 2004; Jiménez-Espejo et al., 2008). In this case, no Ba excess was registered and Ba is included in the first group. Hence, its association with alumino-silicates points to a detrital origin. Si and Ti have multiple hosts in marine sediments that vary considerably in particle size, ranging from clay to heavy minerals such as quartz or accessory Ti-bearing heavy minerals (Kolla et al., 1979; Calvert and Fontugne, 2001). Cluster and RDA analyses bound both elements to aluminium, thus revealing clay minerals as the most important hosts and riverine input as the main supply to the basin. REE show a high statistical significance with this detrital group in both cases (for cores 305G and 306G, respectively Th: $r=0.89$ and 0.96, $p<0.01$; Ba: $r=0.79$ and 0.96, $p<0.01$) (Figs. II.3a, b), thus also revealing clay minerals as the most important hosts, while Rb is closely linked to K and to clay minerals

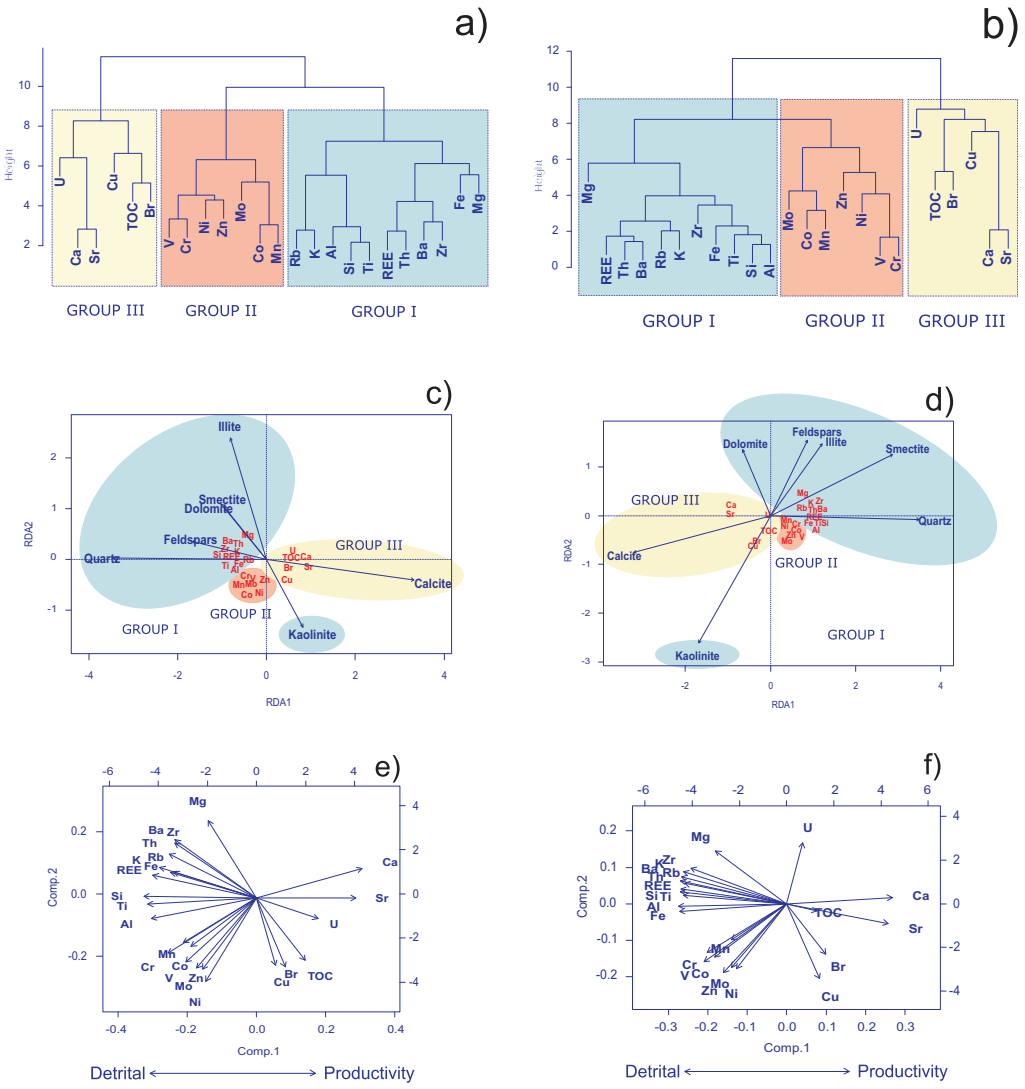

Figure II.3. Statistical treatment of data from both sites. Cluster analyses of the geochemical data for sites 305G (a) and 306G (b), showing three main geochemical families in accordance to their affinity and origin. RDA biplots displaying the relationship between chemical elements and associated mineral phases for sites 305G (c) and 306G (d). Light yellow, orange and blue areas indicate Group I, II or III, respectively. Biplots showing the first and the second eigenvector defined by PCA for sites 305G (e) and 306G (f)

(Horstman, 1957). The second group is composed of redox-sensitive elements including two sub-groups: those which are less soluble under reducing conditions and provide information on water oxygenation conditions (V, Cr, Ni, Zn), and those constituting insoluble oxy-hydroxides under oxic conditions (Mn) and elements easily captured into them (Co, Mo). This second group is asso-

ciated with the detrital one, pointing to alumino-silicates as main hosts. The third group contains paleoproductivity indicators associated with the organic flux, showing the high correlation between Br and marine organic matter, probably due to favoured uptake of bromine from seawater by marine plants (ten Haven et al., 1988; Ziegler et al., 2008). This provides a semiquantitative estimation of sedimentary organic matter. Although U and Cu are often used as redox-sensitive elements, cluster analyses show them to be associated to the cluster containing organic carbon and carbonates.

The first two eigenvectors of PCA account for 70% of the total variance at site 305G and for 73% at site 306G. The first eigenvector represents 47% of the total variance at site 305G and 57% at site 306G, and is mainly controlled by the detrital-productivity groups, whereas the second eigenvector represents 23% of the total variance at site 305G and 16% at site 306G, and is mainly triggered by the water oxygenation conditions (Figs. II.3e, f). This result fits well with the differences in the location of these sites which may have resulted in different processes controlling sediment deposition. Site 305G is located at the continental slope (Figs. II.1b, c) and is thus more affected by bottom currents and in turn, to changes in oxygen conditions. In contrast, site 306G is located in a more distal position in the abyssal plain on a small pelagic high, and is therefore more affected by detrital-marine productivity oscillations.

In light of these results, we applied the geochemical and mineralogical set of identified proxies to reconstruct paleoclimatic and paleoceanographic conditions including detrital input oscillations, marine productivity, oxygenation conditions and grain size distribution as well as post-depositional alteration during the last 4000 yr in the western Mediterranean.

II.7. Results and interpretation of the geochemical and the mineralogical record

II.7.1. Mineral composition and detrital input

The analyzed sediments are predominantly composed of clay minerals (30-70%), calcite (20-45%) and quartz (10-30%), with minor amounts of dolomite and feldspars (<10%). Clay mineral assemblages consist of detrital mica (50-90%), kaolinite+chlorite (5-40%) and smectites (<20%). Additional fibrous clay minerals, such as palygors-

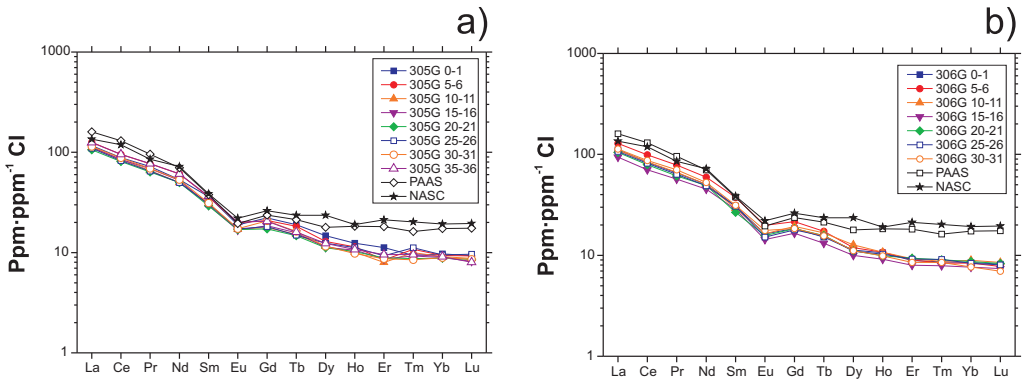

Figure II.4. CI chondrite-normalized REEs patterns (ppm·ppm^{-1} CI) every five centimetres for cores 305G (a) and 306G (b) compared with the standard REE pattern of the NASC and the PAAS (McLennan, 1989)

kite and sepiolite, were identified using Transmission Electron Microscopy and Scanning Electron Microscopy, although their content quantified via X-Ray Diffraction ranges below instrumental error (<5%), for which reason we did not consider them for the present study. These analyses verify that the smectite composition corresponds to Al-rich beidellites, indicating a detrital origin (chemical weathering) and a provenance from soils in the source areas (Martínez-Ruiz et al., 2003).

In both cases, REE values display an uniform pattern parallel to the average upper continental crust composition, with a typical variation consisting of slight L-REE enrichment relative to H-REE depletion and a negative Eu-anomaly, as well as values lower than the North American shale composite (NASC) and the Post-Archean Australian average shale (PAAS) (McLennan, 1989) (Figs. II.4a, b).

At both sites, Rb/Al, REE/Al, Ba/Al, Si/Al, Ti/Al, Mg/Al, and K/Al ratios show a similar general profile with slight differences (Fig. II.5). Both cores exhibit a decreasing trend at 3600-1800, 1600-1300 and 1150-400 cal. yr BP, the trend less evident in the case of Mg/Al and K/Al ratios for core 306G at 3600-2800 cal. yr BP. An increase in these ratios is observed at 1800-1600 and 1300-1150 cal. yr BP and from 400 cal. yr BP to present times. The Zr/Al ratio gives relatively high values at 3600-2600, 1600-1300 and 1150-650 cal. yr BP and low values at 2600-1600 and 650-150 cal. yr BP.

II.7.2. Grain size distribution, oxygen conditions, paleoproductivity indicators and post-depositional alteration

The mean grain size ranges between 1-8 and 0.5-10 μm while the median grain size is <2 and 4 μm at sites 305G and 306G, respectively (Fig. II.6). The grain size distribution therefore consists mainly of clays and fine silts. Clays are most abundant at site 306G and fine silt at site 305G, which fits well with the difference in location mentioned above (Fig. II.1a). Site 306G, more influenced by detrital components, receives the finer fraction of the influx of the terrigenous component; at site 305G, located at the continental slope and more affected by bottom currents, the coarser sediments settle (Figs. II.1b, c). Regarding SS values, a parallel trend is observed at the two sites, the peaks coinciding with increasing trends of the mean and the median distributions, and quartz content. These coarser sediments and higher quartz content occur at 3600-2200 cal. yr BP, and at 1400-400 cal. yr BP, the exception being for core 306G at 3600-2200 cal. yr BP, where finer grain size prevails and lower quartz content is found due to the fact that this site is less influenced by bottom currents.

At site 305G, lower redox-sensitive elements contents (V/Al, Cr/Al, Ni/Al and Zn/Al ratios) (Fig. II.7) coincide with coarser grain size sediment (Fig. II.6) at 3600-2200 and 1400-400 cal. yr BP, and vice versa at 2200-1600 cal. yr BP and from 400 cal. yr BP onwards. Hence, oxygenated bottom waters percolating through the sediment are favoured by coarser grain size. This trend is mirrored by core 306G, excluding the period 3600-2200 cal. yr BP, when high values of redox-sensitive elements are observed, concurring with finer grain size and lower quartz content (Fig. II.6).

TOC values are below 1% at both sites (Fig. II.8). Although the general profile exhibits a progressive down-core decline, both cores display the highest values at 2000-1600 cal. yr BP and at the top of the core. High TOC values also occur at 1150-650 cal. yr BP in core 306G. Br/Al ratio achieves its maximum values during 2000-1600 cal. yr BP and at the top of the core at both sites. Br/Al ratio mainly mirrors the TOC content trend with the exception of the time interval 1150-650 cal. yr BP in core 306G, when a preferential degradation of Br in relation to TOC takes place. U/Th displays a flat pattern at both sites, although this ratio increases at 2000-1600 cal. yr BP when maximum values are reached. The increase concludes around 1150 cal. yr BP at site 306G in contrast. Although Cu/Al ratios display more erratic behaviour, it is possible to discern two Cu/

Al enrichments between 2000 and 1600 cal. yr BP and at the top of both cores as also drawn by U/Th, Br/Al and TOC. Disagreements in these ratios for 1600-1150 cal. yr BP (U/Th in core 305G) and 1150-650 cal. yr BP (TOC in core 306G) are explained in relation to post-depositional conditions.

Both Fe and Mn can precipitate as oxy-hydroxides when bottom waters are reventilated and penetrate downwards into the sediments, thus reflecting post-depositional oxidation fronts while organic matter burns down (deLange et al., 1989). The two sites display a constant post-depositional pattern of Mn/Al except for sudden increases from 5 up to 9 cm depth at site 305G, and from 5 to 9 cm and from 13 to 20 cm depth at site 306G (Fig. II.9), evidencing post-depositional oxidation. Fe/Al enrichments also occur immediately below Mn peaks, at 8 cm depth for site 305G; yet a double peak is seen for site 306G, at 12 and 19 cm depth. Co/Al and Mo/Al are also enriched in the post-depositional oxidation front at both sites, having most likely co-precipitated together with Fe and Mn oxy-hydroxides (Tribovillard et al., 2006) (Fig. II.9). This front is moreover responsible for organic matter oxidation, as supported by the lower values and decreasing trend of TOC at coeval intervals (between 1350 and 600 cal. yr BP in core 305G and from 1750 to 1350 cal. yr BP and 900-450 cal. yr BP in core 306G) (Fig. II.8). Mn and Fe enrichments and early oxidation of organic matter above the redoxcline point to the typical boundary on oxic/suboxic pelagic sediments reported in eastern Mediterranean sapropels and in uppermost hemipelagic sediments in the western Mediterranean (Thomson et al., 1999; Masqué et al., 2003).

The precipitation of Mn is found deeper in core 305G due to the coarser grain size distribution at this site, which allows for a farther downward progression of the oxidation front. Indeed, Masqué et al. (2003) reported post-depositional oxidation fronts ranging from 5.8 cm to as much as 15 cm depth in this sedimentary environment. In core 306G, Br and TOC deposited between 1750 and 1350 cal. yr BP were remobilized due to this post-depositional oxidation front (Figs. II.8, 9), and at 900-450 cal. yr BP there is a preferential loss of Br-containing compounds in relation to TOC as noted by Price et al. (1970) during the early stages of diagenesis. In core 305G, between 1350 and 600 cal. yr BP, the post-depositional oxidation front reaching 9 cm depth may be responsible for remobilization of TOC, Br and U (Figs.

II.8, 9). Elements such as uranium can be remobilized in sediments if oxygen penetrates up to the core depth where authigenic uranium has accumulated (McManus et al., 2005).

II.8. Paleoclimatic and paleoceanographic conditions during the last 4000 yr

II.8.1. Late Bronze Age-Iron Age (LBA-IA) (~3600-2600 cal. yr BP)

Dry conditions are dominant during this period, as indicated by the reduced riverine input from the catchment at both sites (a decreasing trend of fluvial derived-elements) and the relatively high values of the Zr/Al ratio, associated to Saharan eolian input fluctuations (Fig. II.5). This aridification trend coincides with a progressive evolution towards typical Mediterranean climate and aridity, which gradually occurs from the middle Holocene (Wanner et al., 2008), and with one of the major periods of Holocene rapid climate change (RCC) at the hemispheric scale (~3500-2500 cal. yr BP) (Mayewski et al., 2004). During these RCC periods, a southward migration of the Inter-Tropical Convergence Zone (ITCZ) and thus higher intensity of dust export and wind speeds (Weldeab et al., 2003) have been described, which may explain the low latitude aridity associated with this period. Moreover, these arid conditions occurred in the context of a decline in the Northern Hemisphere solar insolation (Steinhilber et al., 2009), cooler air temperatures in Greenland from the middle LBA-IA (Greenland Ice Sheet Project 2 $\delta^{18}O$ record, GISP2 drill site) (Grootes and Stuiver, 1997) and detrital evidences of ice-rafting in the subpolar North Atlantic during the North Atlantic cold and arid event 2 (~2800 cal. yr BP) (Bond et al., 1997, 2001) (Fig. II.10).

Furthermore, dry conditions have been widely described in the western Mediterranean region based on marine and terrestrial pollen records (Jalut et al., 2000, 2009; Combourieu-Nebout et al., 2009). Reduced river activity in southern Europe (Magny et al., 2002; Macklin et al., 2006), cooling events with lower temperatures and faster flows in the Balearic basin (Frigola et al., 2007), and a desiccation phase in a lacustrine record from Southern Spain (Carrión, 2002) are likewise reported for this time frame. Martín-Puertas et al. (2010) recorded a dry period supported by higher Saharan input into the Alboran basin (Zr/Al ratio; core 300G) during this period.

The prevailing paleoceanographic

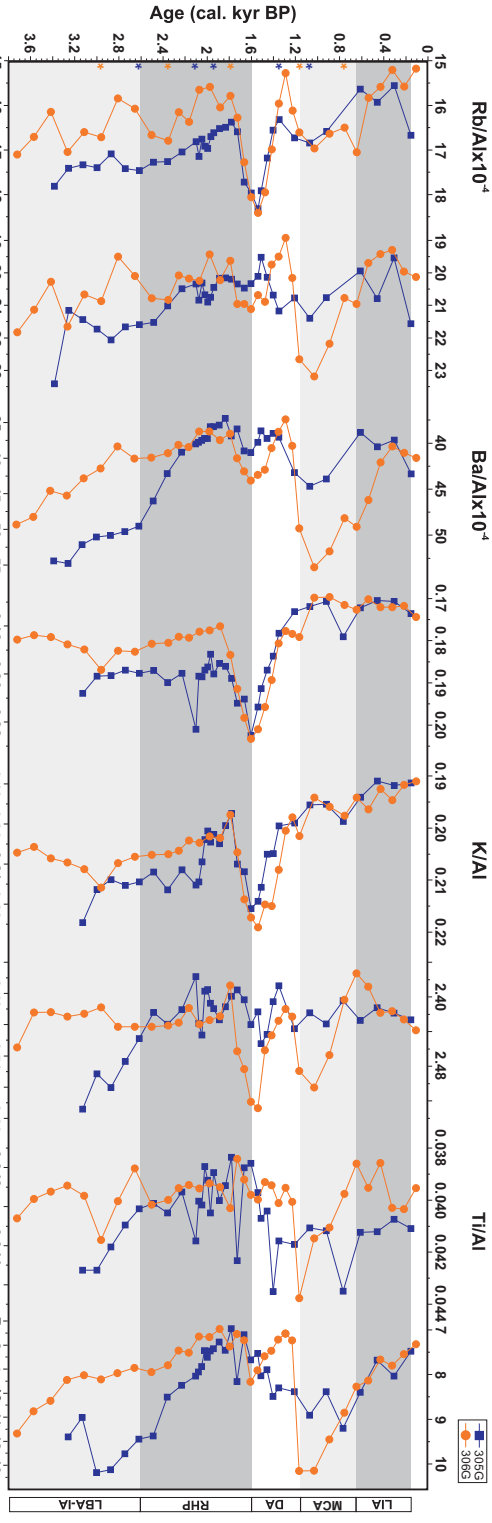

Figure II.5. Age-depth profile of detrital proxies (Rb/Al, REE/Al, Ba/Al and REE/Al·10⁻⁴ ratios, Si/Al, Ti/Al, Mg/Al, and K/Al ratios) for cores 305G (blue squares) and 306G (orange circles). Light grey bars indicate dry periods (MCA: Medieval Climate Anomaly, DA: Dark Ages, LBA-IA: Late Bronze Age-Iron Age), dark grey bars indicate humid periods (LIA: Little Ice Age, RHP: Roman Humid Period). Asterisks indicate the AMS ^{14}C dates

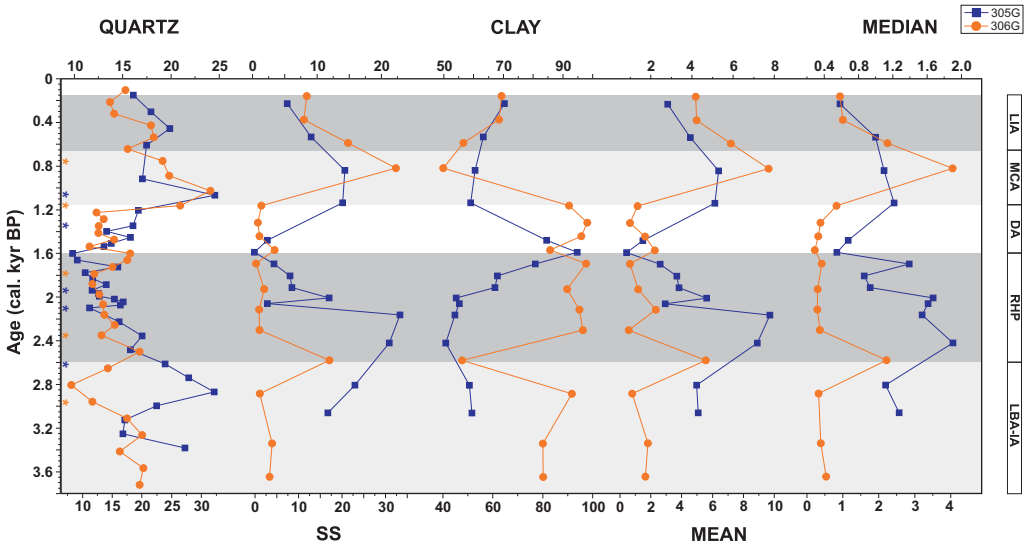

Figure II.6. Age-depth profile of grain size distribution: mean, median, SS (%), clay (%) and quartz content (%) for cores 305G (blue squares) and 306G (orange circles). Light grey bars indicate dry periods (MCA: Medieval Climate Anomaly, DA: Dark Ages, LBA-IA: Late Bronze Age-Iron Age); dark grey bars indicate humid periods (LIA: Little Ice Age, RHP: Roman Humid Period). Asterisks indicate the AMS ^{14}C dates

conditions during this period entail faster flowing and better oxygenated bottom waters, evidenced at site 305G by the deposition of coarser grain size sediments, higher quartz content and lower redox-sensitive trace element values (Figs. II.6, 7). At site 306G, finer grain size, lower quartz content and high values of redox sensitive elements are found. The different locations of exposure would again explain the distinct sedimentary processes (Figs. II.1a, b, c). Low TOC values as well as Cu/Al, Br/Al and U/Th ratios suggest low productivity and, owing to better oxygenated bottom sediments, lower organic matter preservation during this period (Fig. II.8).

II.8.2. The Roman Humid Period (RHP) (~2600-1600 cal. yr BP)

The early and middle RHP (~2600-1800 cal. yr BP) is still marked by dry conditions, signalled by the decrease of fluvial derived-elements (Fig. II.5), although a decreasing trend in Saharan eolian input at both sites (Zr/Al, Fig. II.5) suggests an ongoing establishment of more humid conditions in the western Mediterranean. Other records in this region support this scenario. Accordingly, dry conditions are described for palynological (Jalut et al., 2000, 2009; Combourieu-Nebout et al., 2009), marine (Frigola et al., 2007),

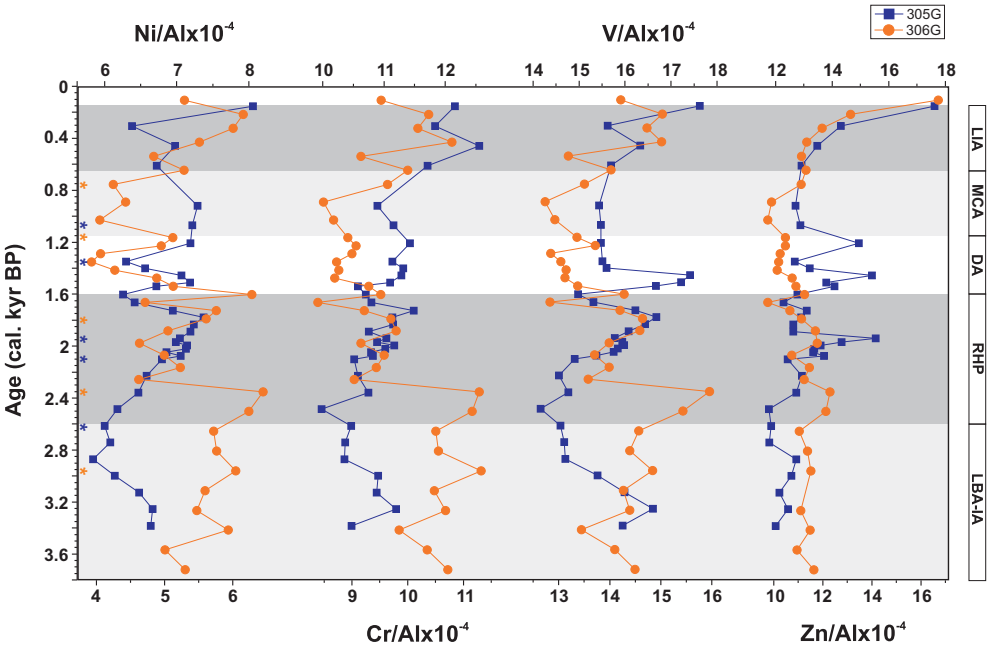

Figure II.7. Age-depth profile of redox proxies (V/Al, Cr/Al, Ni/Al and Zn/Al 10^{-4} ratios) for cores 305G (blue squares) and 306G (orange circles). Light grey bars indicate dry periods (MCA: Medieval Climate Anomaly, DA: Dark Ages, LBA-IA: Late Bronze Age-Iron Age); dark grey bars indicate humid periods (LIA: Little Ice Age, RHP: Roman Humid Period). Asterisks indicate the AMS ^{14}C dates

lacustrine (Carrión, 2002), and fluvial records (Magny et al., 2002; Macklin et al., 2006) in the western Mediterranean.

The most noteworthy event coinciding with this time interval is the sudden rise in fluvial land-derived elements that occurred at the end of the RHP, around 1800 cal. yr BP at both sites (Fig. II.5), thus defining this period as the most humid by far of the last 4000 yr. The Saharan eolian input (Zr/Al ratio) remains low after 1800 cal. yr BP, achieving minimum values during this period and thus supporting the humid conditions (Fig. II.5). This event coincides with higher solar insolation in the Northern Hemisphere (Steinhilber et al., 2009) and generally warm air temperatures in Greenland from the onset of the RHP to 2000 cal. yr BP (Grootes and Stuiver, 1997) that sustain this humid period in the western Mediterrranean (Fig. II.10).

Flooding events in the Iberian Peninsula are also recorded for this time (Macklin et al., 2006). Martín-Puertas et al. (2010) describe wetter conditions sharpening at 1700 cal. yr BP in the Alboran basin (Mg/Al ratio; ODP 976) and a decrease in the eolian input from

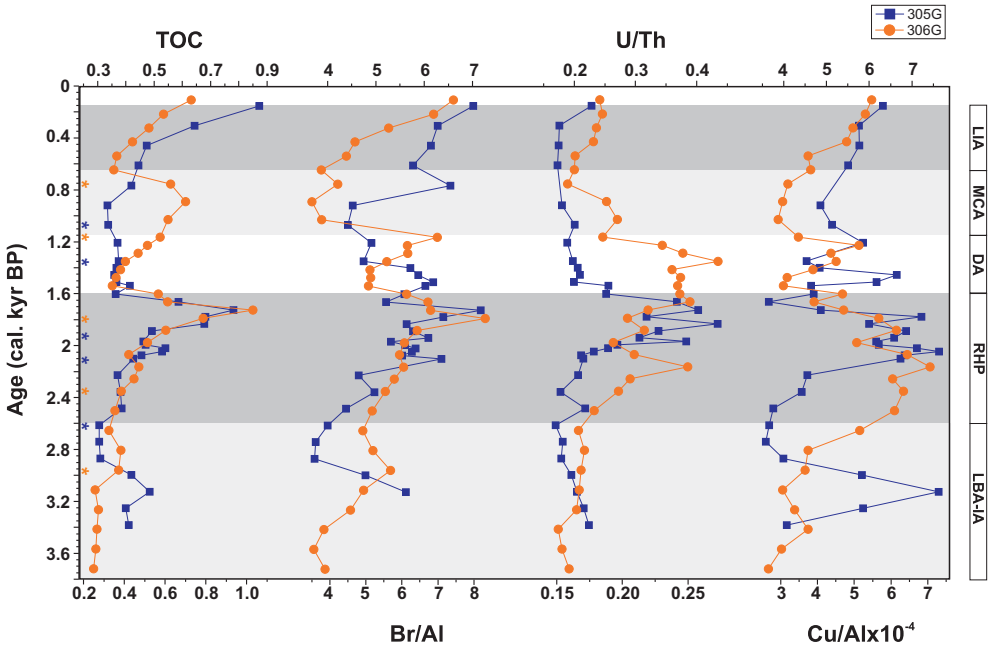

Figure II.8. Age-depth profile of paleo-productivity indicators (Cu/Al·10⁻⁴, TOC, Br/Al and U/Th) for cores 305G (blue squares) and 306G (orange circles). Light grey bars indicate dry periods (MCA: Medieval Climate Anomaly, DA: Dark Ages, LBA-IA: Late Bronze Age-Iron Age); dark grey bars indicate humid periods (LIA: Little Ice Age, RHP: Roman Humid Period). Asterisks indicate the AMS ^{14}C dates

the African margin (Zr/Al ratio; core 300G) to characterize this period as the most humid of the Late Holocene in the southern part of the Iberian Peninsula.

The progressively finer grain size and lower quartz content for this interval (Fig. II.6) indicate slower and less energetic flows, which are supported by slightly increased values of redox sensitive elements (Fig. II.7) suggesting less oxygenated bottom conditions. Furthermore, the sudden increase in TOC values and organometallic ligands (Fig. II.8) reveal increasing organic matter preservation due to these lower oxygen bottom conditions. Thus, the most intense productivity and better preservation of the last 4000 yr is exhibited during this period.

II.8.3. The Dark Ages (DA) (~1600-1150 cal. yr BP)

A progressive dryness peaking around 1300 cal. yr BP at both sites characterizes the DA, which coincides with decreasing solar insolation in the Northern Hemisphere (Steinhilber et al., 2009), another event of ice-rafting in the subpolar North Atlantic (North

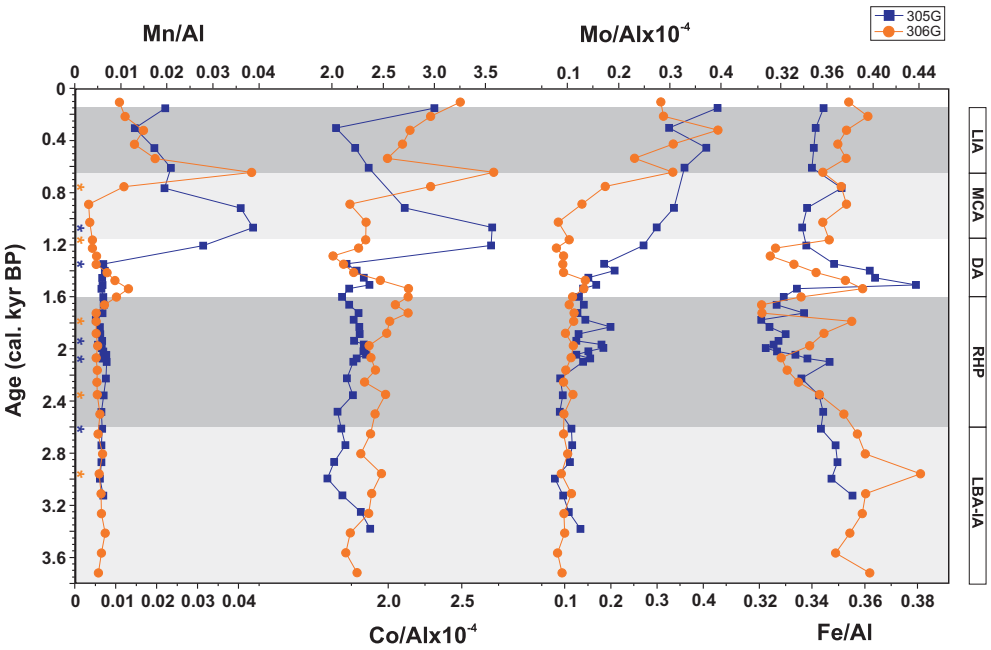

Figure II.9. Age-depth profile of post-depositional proxies (Co/Al and Mo/Al·10⁻⁴, Mn/Al and Fe/Al) for cores 305G (blue squares) and 306G (orange circles). Light grey bars indicate dry periods (MCA: Medieval Climate Anomaly, DA: Dark Ages, LBA-IA: Late Bronze Age-Iron Age); dark grey bars indicate humid periods (LIA: Little Ice Age, RHP: Roman Humid Period). Asterisks indicate the AMS ^{14}C dates

Atlantic cold event 1, ~1400 cal. yr BP) (Bond et al., 1997, 2001), and cooler air temperatures in Greenland (Grootes and Stuiver, 1997). This fact is revealed by a decline in the riverine influence to the basin (Fig. II.5) and a progressive increase in the Saharan eolian input suggested by the Zr/Al ratio from 2000 cal. yr BP until the beginning of the MCA.

Faster bottom currents and more energetic hydrodynamic conditions are evoked by enhanced sortable silt and quartz content (Fig. II.6), and by better oxygenated bottom waters as reflected by decreasing redox-sensitive elements (Fig. II.7). Accordingly, lower TOC values as well as lesser Cu/Al, Br/Al and U/Th ratios are indicative of poor organic matter preservation owing to well-oxygenated bottom sediments (Fig. II.8). In addition, remobilization took place at core 305G due to a post-depositional oxidation front reaching 9 cm depth (Figs. II.8, 9) but not for U/Th at site 306G.

The dryness characterizing the DA is correlated with decreased humidity in the western Mediterranean, evidenced by forest cover regression episodes

(Jalut et al., 2000, 2009; Combourieu-Nebout et al., 2009), a decrease in river activity in southern Europe (Magny et al., 2002; Macklin et al., 2006), cooling events in the Balearic basin (Frigola et al., 2007), and lower lake levels in southern Spain (Carrión, 2002).

II.8.4. The Medieval Climate Anomaly (MCA) (~1150-650 cal. yr BP)

Arid conditions are still predominant in the western Mediterranean during the MCA, as indicated by a decline in the fluvial input into the basin due to a decreasing trend of fluvial-derived elements and higher Zr/Al ratios, which indicate higher Saharan eolian input (Fig. II.5). This arid phase is accentuated during the Medieval solar activity maximum (~850-700 cal. yr BP) (Jirikowic and Damon, 1994) when values of fluvial-derived elements reach a minimum yet Zr/Al ratios are still high. At the hemispheric scale, this time-interval coincides with one period of RCC (~1200-1000 cal. yr BP) due to southward migration of the ITCZ (Mayewski et al., 2004), implying a greater intensity of dust export and wind speeds (Weldeab et al., 2003). Indeed, the highest Saharan eolian input during the last 4000 yr occurred in this phase and in the LBA-IA, both coinciding with periods of RCC.

This phase can be inferred in the Mediterranean borderlands through changes in vegetation (Jalut et al., 2000, 2009; Combourieu-Nebout et al., 2009), and a decrease in river activity in southern Europe (Magny et al., 2002; Macklin et al., 2006). Drier conditions were also registered in marine, lacustrine and pollen records in the Iberian Peninsula during the MCA: lower water levels in lacustrine records, decreased fluvial supply and major Saharan dust particle input in the westernmost Mediterranean as evidenced by marine sediments, and higher xerophytic or heliophytic taxa vegetation documented by pollen records (Moreno et al., 2012; and references therein).

In terms of paleocenographic conditions, faster bottom currents and intense hydrodynamic conditions are suggested by an increase in grain size and quartz content (Fig. II.6). Meanwhile, a decrease in redox-sensitive elements points to better oxygenated bottom waters (Fig. II.7). Though in core 305G, the post-depositional oxidation front reaching 9 cm remobilized TOC, Br and U (Figs. II.8, 9), the oxygenated bottom waters and stronger bottom currents suggest low preservation of organic matter.

Our record furthermore provides

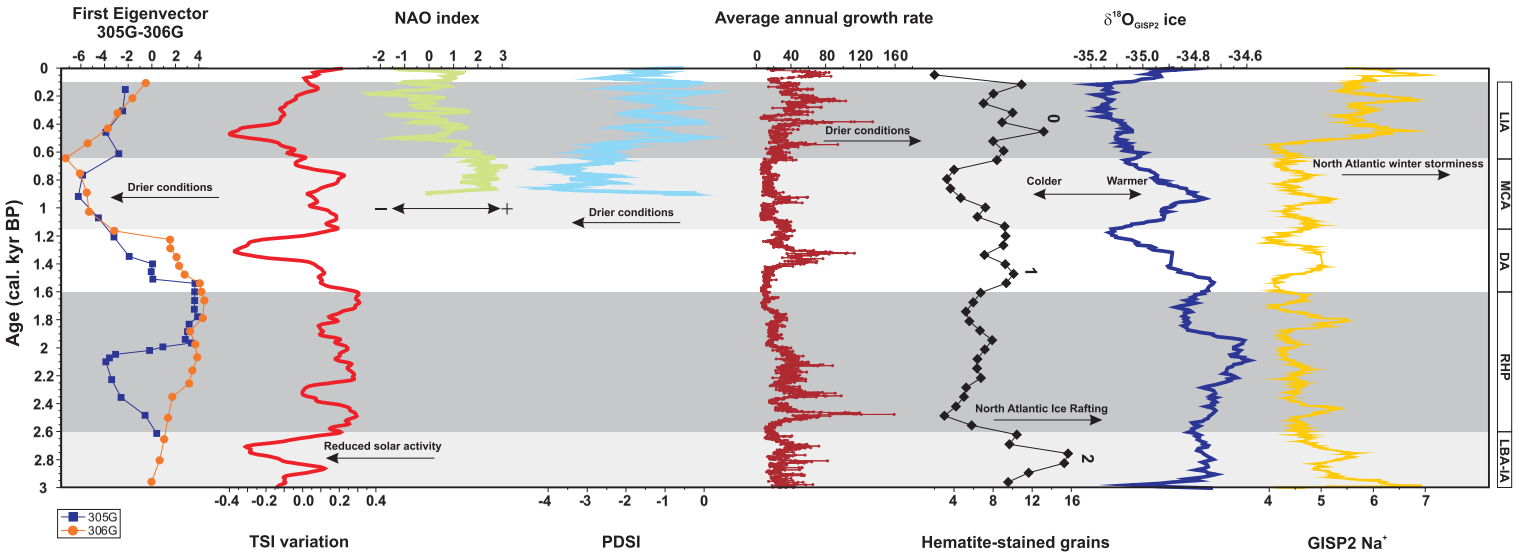

Figure II.10. First eigenvector of cores 305G (blue squares) and 306G (orange circles) compared with the TSI variations (W·m²) during the last 4000 yr (30-point smoothed, red line) (Steinhilber et al., 2009), the NAO index during the last 1000 yr (green line) (Trouet et al., 2009), the Palmer Drought Severity Index (PDSI) based on Cedrus Atlantica ring width from Morocco (North-Western Africa) reflecting aridity changes during the last 1000 yr (10-point smoothed, light blue line) (Esper et al., 2007) and the growth rate variations of stalagmites (microns) from North-Western Scotland reflecting hydrological conditions during the last 4000 yr (brown circles) (Proctor et al., 2000, 2002), the record of increased ice-drifting in the North Atlantic expressed as percentage variations of hematite-stained grains during the last 4000 yr (black diamonds, numbers represent Bond cycles 0-2) (Bond et al., 2001), the high resolution δ¹⁸O record (‰) (30-point smoothed, dark blue line) (Grootes and Stuiver, 1997) from the GISP2 ice core during the last 4000 yr and the sea-salt Na^+ concentration (ppb) (30-point smoothed, yellow line) (Mayewski et al., 1997). Light grey bars indicate dry periods (MCA: Medieval Climate Anomaly, DA: Dark Ages, LBA-IA: Late Bronze Age-Iron Age); dark grey bars indicate humid periods (LIA: Little Ice Age, RHP: Roman Humid Period)

support of dominant positive NAO phases during the MCA over Europe (Trouet et al., 2009). Positive NAO phases in the Mediterranean region are linked to stronger westerlies transporting storms farther to the north and east and resulting in wetter winters over northern Europe —evidenced by stalagmites in north-western Scotland (Proctor et al., 2000, 2002; Baker et al., 2011) and tree ring records from Germany (Büntgen et al., 2010)— along with drier winters over southern Europe and northern Africa, reflected by precipitation data and tree ring records from north-western Africa (Knippertz et al., 2003; Esper et al., 2007) (Fig. II.10). Additionally, enhanced dust transport from the Saharan region to the North Atlantic Ocean and the Mediterranean Sea has been reported during positive NAO phases (Moulin et al., 1997). Certainly, the highest Saharan eolian input and the decreasing trend of fluvial-derived elements occurring during the MCA evidence drier conditions in the westernmost Mediterranean. Furthermore, paleocenographic conditions in this region dominated by oxygenated bottom waters and stronger bottom currents suggest enhanced formation of WMDW likely promoted by stronger westerlies during positive NAO phases.

II.8.5. The Little Ice Age (LIA) (~650-150 cal. yr BP)

The dry conditions recognized during the MCA are maintained during the first half of the LIA until 400 cal. yr BP, as evidenced by a decreasing trend of fluvial-derived elements which reaches even lower values than during the MCA. The Saharan eolian input ratio (Zr/Al ratio) draws a declining trend throughout this period, attaining values as low as during the RHP (Fig. II.5). At the hemispheric scale, this trend correlates with the latest period of significant RCC in the Northern Hemisphere (~600-150 cal. yr BP) (Mayewski et al., 2004), as well the most recent evidence of ice-rafting in the subpolar North Atlantic (North Atlantic cold and arid event 0, ~500 cal. yr BP) (Bond et al., 1997, 2001). Further records in the western Mediterranean mirror these conditions. Thus, Carrión (2002) recorded a desiccation phase in a lacustrine record from Southern Spain, Frigola et al. (2007) described cooling events in the Balearic basin at this time, and Martín-Puertas et al. (2010) also recorded a decrease of riverine input during the first half of the LIA.

After 400 cal. yr BP, a rise in fluvial land-derived elements (Fig. II.5) defines the late LIA. Accordingly, en-

hanced fresh water input, meaning an establishment of wetter conditions in the western Mediterranean, can be envisaged during this time. A slight increase in the riverine input in the Alboran Sea basin is also evidenced in westernmost Mediterranean records during the late LIA (Martín-Puertas et al., 2010); meanwhile higher lake levels and mexophytic vegetation which grows under moderately humid conditions occurred in the Iberian Peninsula (Moreno et al., 2012). Thus, increased fluvial input along with oceanographic oscillations may have also promoted enhanced productivity, as suggested by greater TOC values and organometallic ligands. Indeed, similar increase in productivity is also recognized during the LIA as far as the Sicily Channel, as evidenced by coccolithophore records by Incarbona et al. (2010).

These humid conditions correspond well with a change in the NAO index into a negative mode in the western Mediterranean. Weaker and southward displaced westerlies would bring enhanced precipitation and river discharges to the south of the Iberian Peninsula, as evidenced by our records after 400 cal. yr BP. This displacement may have collapsed the formation of WMDW, as suggested by the less energetic and poorly oxygenated waters, seen in the increasing trend to finer grain size, lower quartz content (Fig. II.6) and higher values of redox sensitive elements (Fig. II.7). Furthermore, our records are compatible with a transition from predominant positive NAO phases to negative ones at 400 cal. yr BP (Fig. II.10).

II.9. Forcing mechanisms driving natural climate variability during the Late Holocene

Solar irradiance variations have been invoked as one of the main forcing mechanisms that drive natural climate variability on centennial to millennial time-scales during the Holocene at the hemispheric scale (van Geel et al., 1999; Crowley, 2000). At millennial scales, times of orbitally-induced declines of solar irradiance in the Northern Hemisphere might have triggered ice-rafted debris discharges into the North Atlantic current (Bond et al., 2001). These abrupt events led to a southward advection of cooler and fresher surface water, thus reducing the North Atlantic Deep Water (NADW) production rate. The weakeness of the global thermohaline circulation could allow these cold pole waters to spread into the Mediterranean Sea through the Strait of Gibraltar. Such events also correlate with an intensification of the

atmospheric circulation over Greenland, producing stronger than normal northerly winds that could promote a strengthening of the WMDW production rate and thus of the Mediterranean thermohaline circulation (O'Brien et al., 1995; van Geel et al., 1999; Bond et al., 2001). These millennial-scale abrupt cooling events occur with a mean pacing of 1500 yrs during the Holocene, similar to the duration of the Dansgaard/Oeschger events that took place during the last deglacial period in the Alboran Sea basin (e.g., Cacho et al., 1999).

Since detrital input is the main process managing deposition at sites 305G and 306G, we have selected the first eigenvector defined by PCA analyses at these sites to compare it with total solar irradiance (TSI) variations ($W \cdot m^{-2}$) over the last 4000 yr (Steinhilber et al., 2009) and the NAO index over the last 1000 yr (Trouet et al., 2009) (Fig. II.10). Thus, positive TSI values are achieved during the RHP and the MCA, whereas negative values are attained during the LBA-IA, the DA and the LIA. Three minimum negative values are reached during the whole record, two of them coinciding with the North Atlantic cold events described by Bond et al. (1997) (1400 and 2800 cal. yr BP) and the other one taking place during the LIA (Fig. II.10). These cold imprints in the TSI variations are mirrored at sites 305G and 306G by decreased fluvial input as discussed above (Fig. II.5).

On the other hand, increasing trends of the first eigenvector in both cores are seen during the RHP (after 2000 cal. yr BP) and the LIA, whereas decreasing ones are achieved during the LBA-IA, early and middle RHP, DA and the MCA (Fig. II.10), respectively evidencing higher and lower riverine input into the basin. High TSI coincides with wet periods such as the RHP (higher riverine input), and low TSI agrees with dry periods, namely the LBA-IA and the DA (lower riverine input). Nevertheless, a lack of correlation throughout the MCA and the LIA in terms of total solar variations suggests some additional forcing affected detrital input in the western Mediterranean.

The MCA has been described as the most recent pre-industrial warm period noted in Europe and over the Northern Hemisphere (Mann et al., 2008, 2009), also characterized by severe and prolonged droughts (Seager et al., 2007). Recently, Trouet et al. (2009) stated strongly-positive NAO phases for the MCA and negatives ones for the LIA as the responsible mechanism of this climate anomalies over the North Atlantic and elsewhere. Thus, the positive

phase of the NAO leads to dry and cold winters in southern Europe, the Mediterranean, northern Africa, northern Canada and Greenland, and warm and wet winters in northern Europe and eastern North America (Wanner et al., 2001; Trigo et al., 2002). As explained above, climate and ocean conditions reconstructed from our records during the MCA and the LIA correspond with a positive and a negative phase of the NAO, thus inducing dry and humid conditions respectively in the western Mediterranean (Fig. II.10). According with our records, wetter (drier) winters are also reflected by tree ring records from north-western Africa during the LIA (MCA) (Esper et al., 2007). Meanwhile, drier (wetter) winters over northern Europe are evidenced by stalagmites in north-western Scotland during the LIA (MCA) (Proctor et al., 2000, 2002) (Fig. II.10). Similarly, other records from different areas support our results. Thus, rising sea-salt Na^+ concentrations from the GISP2 ice core glaciochemical series (Mayewski et al., 1997) have been interpreted as a deepening of the Icelandic low atmospheric pressure, i.e. the deeper the low pressure the stronger the transport of sea-salt Na^+ by winds towards Greenland (Meeker and Mayewski, 2002). The weakening of the Icelandic low would lead more intense winter storminess and enhanced precipitation over the North Atlantic region as described for a negative state of the NAO during the LIA, being preceded by a period of negligible storm activity during the MCA (Fig. II.10). These concentrations coincide with the synchronicity of colder temperatures during the LIA and warmer during the MCA, as recorded by the $\delta^{18}O$ ice GISP2 ice core in Greenland (Grootes and Stuiver, 1997) which is consistent with detrital evidences of an increased ice-drifting event in the North Atlantic during the LIA (Bond et al., 2001) (Fig. II.10).

Hence, our records further support the NAO as a regional mechanism driving natural climate variability together with the TSI in the western Mediterranean during the Late Holocene. In this way, Seager et al (2007) attributed the dry conditions during the MCA in the Mediterranean region to a prevailed positive mode of the NAO and Shindell et al. (2001) pointed out a coupled between low solar insolation and a negative mode of the NAO as responsible of the low temperatures in Europe during the Maunder Minimum at the late LIA. These results also sustain the link of the Mediterranean climate with the North Atlantic climate system driven by atmospheric forcing related to the NAO at centennial and millen-

nial scales during the last 4000 yr.

II.10. Conclusions

Fluctuations in chemical and mineralogical composition as well as grain size distribution in two deep-sea marine records from the western Mediterranean Sea reveal climate oscillations over the past 4000 yr. These records provide further insight into the response of this highly sensitive area to internal climate variability, allowing for the identification and characterization of humid (LIA and RHP) and dry (MCA, DA and LBA-IA) periods. An increase in riverine input (fluvial-derived detrital elements —Rb/Al, Ba/Al, REE/Al, Si/Al, Ti/Al, Mg/Al and K/Al ratios) and a decrease in Saharan eolian input (Zr/Al ratio) characterize the RHP and the LIA. Additionally, weaker bottom currents (lower SS), oxygen-poor bottom waters (high V/Al, Cr/Al, Ni/Al and Zn/Al ratios), and well preserved marine organic matter (TOC content and Br/Al ratio, U and Cu as organometallic ligands) are evidenced, whereas essentially opposite paleoenvironmental and paleoceanographic conditions are recognized during the LBA-IA, the DA and the MCA. Likewise, the highest TOC values achieved during the late RHP, together with increasing preservation of organic matter, point to this time period as by far the most intense productivity of the last 4000 yr. Comparison of the first eigenvector defined by PCA at site 305G and 306G, which represents the detrital input into the basin, with natural external forcing mechanisms of climate variability (such as the TSI and the NAO), would underline the TSI as one of the main mechanisms behind natural climate variability on millennial scales. Further influential sources are the modulation of the NAO, a regional prevailing pattern of winter climate variability in the North Atlantic region, and driving natural climate variability on decadal to centennial scales during the MCA and the LIA in the western Mediterranean.

Chapter III

Climate conditions in the westernmost Mediterranean over the last two millennia: An integrated biomarker approach

V. Nieto-Moreno, F. Martínez-Ruiz, V. Willmott, J. García-Orellana, P. Masqué, and J.S. Sinninghe Damsté

Organic Geochemistry (accepted with corrections)

Abstract

Climate conditions in the westernmost Mediterranean (Alboran Sea basin) over the last two millennia have been reconstructed through the integration of molecular proxies applied for the first time in this region at such high resolution. Two temperature proxies, one based on isoprenoid membrane lipids of marine Thaumarchaeota (the TEX^{H}_{86}-tetraether index of tetraethers consisting of 86 carbons) and the other on alkenones produced by haptophytes ($U^{k'}_{37}$ ratio), were applied to reconstruct sea surface temperatures (SST). Both records reveal a progressive long term decline in SST over the last two millennia and an anomalous rate of warming during the twentieth century, in accord with previously reconstructed temperatures in the Northern Hemisphere due to solar irradiance and anthropogenic forcing during the last two millennia. TEX^{H}_{86}temperatures are higher than those inferred from $U^{k'}_{37}$, probably due to differences in the bloom season of haptophytes and Thaumarchaeota, and reflect summer SST. The Branched versus Isoprenoid Tetraether index (BIT index) indicates a predominant marine provenance for the sedimentary organic matter. The stable carbon isotopic composition of long chain n-alkanes indicates a predominant C_3plant contribution, with no major change in vegetation over the last 2000 yr. The distribution of long chain 1,14-diols (biosynthesized by diatoms of the genus Proboscia) provided insight into upwelling conditions during the last 2000 yr and depicts a correlation with the North Atlantic Oscillation index (NAO index), evidencing enhanced wind induced upwelling during a persistent positive mode of the NAO.

III.1. Introduction

Beyond the instrumental record, the reconstruction of natural climate variability requires reliable proxies for a better understanding of the climate system at longer timescales and a trustworthy prediction of climate change scenarios (Jansen et al., 2007). Sea surface temperature (SST) is one of the most important variables for deciphering further insights into past climate fluctuation. Hence, several geochemical proxies relying on organic fossil remains (or biomarkers) have been developed over the last few decades for paleotemperature reconstructions (e.g. Eglinton and Eglinton, 2008). Biomarkers are sedimentary organic compounds which are biosynthesized by terrestrial or aquatic organisms. In general, they are relatively resistant to degradation and may be preserved in the sedimentary record, being reliable proxies for paleoclimatology.

The first proxy based on biomarkers to infer paleo-SST was the $U^{k'}_{37}$ index (Brassell et al., 1986). It uses long chain ketones with 37 carbons (alkenones) biosynthesized by haptophyte algae and has a direct relationship with average annual SST (Prahl and Wakeham, 1987; Müller et al., 1998). Ten years ago, Schouten et al. (2002) proposed a new proxy for reconstructing past SST, based on archaeal isoprenoid membrane lipids, the TEX_{86} index (TetraEther indeX of tetraethers consisting of 86 carbons), an expression of the number of cyclopentane moieties in the glycerol diphytanyl glycerol tetraethers (GDGTs) of the membrane lipids of marine Crenarchaeota (recently placed into a new phylum of Archaea called Thaumarchaeota; Spang et al., 2010). Thaumarchaeota are prokaryotic single cell microorganisms occurring ubiquitously in the marine environment where they act mainly as nitrifiers (e.g. Wuchter et al., 2006). The TEX_{86} index correlates well with water temperature in the upper water column (0-100 m) and is suitable for reconstructing SST; higher temperatures result in an increase in the relative amount of GDGTs with two or more cyclopentane moieties (Wuchter et al., 2004, 2005; Kim et al., 2008). Recently, a new TEX_{86} calibration was proposed by Kim et al. (2010), which is based on a logarithmic function of TEX_{86} (TEX^{H}_{86}) and predicts more reliable absolute SST, in agreement with estimates based on the $\delta^{18}O$ record of planktonic foraminifera.

Biomarkers may also provide information on variation in terrestrial input from land plants and on marine productivity (e.g. Rosell-Melé and Mcclymont,

2007). Among them, long chain *n*-alkanes are major lipid components of the epicuticular waxes of terrestrial higher plant leaves (Eglinton and Hamilton, 1967). They are transported to the ocean by wind (Schefuß et al., 2003) or fluvial run-off (Castañeda et al., 2007), being deposited and well-preserved in marine sediments. The BIT index (Branched versus Isoprenoid Tetraether index) allows the reconstruction of past fluvial input of soil organic matter (OM) to the marine environment (Hopmans et al., 2004; Weijers et al., 2006). Long chain 1,14-diols, biosynthesized by diatoms in the genus *Proboscia*, are indicators of high primary productivity in the photic zone, such as during upwelling conditions (Sinninghe Damsté et al., 2003). They have been applied as a productivity proxy during upwelling conditions in sediment trap samples from the Arabian Sea (Rampen et al., 2007).

On the basis of these organic proxies, a detailed biomarker study has been performed in the western Mediterranean, a key area for paleoclimate and paleoceanographical reconstruction due to its high sensitivity to climate variability. The western Mediterranean is positioned in a transitional zone between two climate belts (the mid-latitude westerlies system and the subtropical high pressure belt) and linked to the North Atlantic climate system through the Strait of Gibraltar and the influence of the North Atlantic Oscillation (NAO). Studies of the region have mostly addressed SST reconstruction based on alkenones and have focussed on the last deglacial cycle in the westernmost Mediterranean at millennial timescales (Cacho et al., 1999, 2001; Emeis et al., 2000; Marchal et al., 2002; Martrat et al., 2004, 2007). TEX^{H}_{86} has also been applied, together with the $U^{k'}_{37}$, to confirm the abrupt temperature variation during the penultimate interglacial to glacial cycle, where the latter reflected mainly the warmer summer season rather than annual mean SST (ODP 977 site; Huguet et al., 2011). Moreover, the *n*-hexadecanol/*n*-nonadecane index has been applied in the Alboran Sea to record enhanced OM oxidation and well ventilated deep seawater during cold abrupt events (Cacho et al., 2000). All reported records revealed the sensitivity of the region to short term climate change (Dansgaard/Oeschger cycles, Heinrich events and Holocene cold events; Colmenero-Hidalgo et al., 2004), and a possible role of the NAO as a driving mechanism of natural climate variability during the Holocene was suggested (Rimbu et al., 2003; 2004). Nevertheless, although considerable attention has been given to climate variability in the western Mediterranean at millennial

time-scales during the last deglaciation cycles, higher resolution marine records focussed on shorter time scales are comparatively scarce. Recent work on the westernmost Mediterranean has reported climate fluctuation during the last 4000 yr, allowing characterization of dry and humid periods based on variation in chemical and mineralogical composition, as well as grain size distribution (Martín-Puertas et al., 2010; Nieto-Moreno et al., 2011).

Taking into account the significance of both climate sensitivity of the region and the time window for further understanding climate variability and present climate conditions, we focus on the last two millennia, which represent an essential period due its relationship with the present climate and the fact that it is also characterized by significant climate fluctuation, such as the Dark Ages (DA; 350-800 yr AD; Berglund, 2003), the Medieval Climate Anomaly (MCA; 800-1300 yr AD; Lamb, 1965; Hughes and Diaz, 1994) and the Little Ice Age (LIA; 1300-1800 yr AD; Bradley and Jones, 1993). Two marine box cores recovered from the westernmost Mediterranean were sampled at high resolution and TEX^{H}_{86} and the $U^{k'}_{37}$ were used to reconstruct past SST. Furthermore, we complemented the information with other proxies as the BIT index, the diol index and the carbon isotope composition of *n*-alkanes, in order to reconstruct marine paleoproductivity and paleohydrological conditions at time of deposition.

III.2. Material and methods

III.2.1. Sampling

Two box cores, 384B (35º59,161'N, 4º44,976'W, 1022 m.b.s.l.) and 436B (36º12,318'N, 4º18,800'W, 1108 m.b.s.l), recovered from the north-western Alboran Sea basin in 2008 using a KP 1.5 box corer (50 x 50 x 50 cm) during the Training-Through-Research Cruise 17 (Sagas-08 Cruise), Leg 1, on R/V Professor Logachev, were selected (Fig. III.1). Site 384B is situated where the exchange of water between the Mediterranean Sea and the eastern Atlantic through the Strait of Gibraltar takes place. Site 436B is ca. 110 km east of the Strait of Gibraltar and close to the influence of the upwelling cell associated with the northern edge of the Western Alboran Gyre (WAG) (Fig. III.1). This geostrophic front, the so-called Málaga Front, is associated with high biological productivity (Bárcena and Abrantes, 1998). The upwelling is induced by two main mechanisms: the southward drifting of the Atlantic Jet and more important, the wind-driven

upwelling when westerlies blow (Sarhan et al., 2000). At present, SST in the Alboran Sea basin ranges between 13 and 16ºC in winter, 19 and 21ºC in fall, and 23 and 25ºC in summer; the annual average SST ranges between 18 and 20ºC (Santoleri et al., 1994).

Upon retrieval, the cores were subsampled using PVC pipes (50 cm x 11.8 cm) inserted into the sediment. One core from each box core was immediately frozen on board at -18ºC and sampled in 1 cm slices once in the laboratory to provide a high resolution record. The sediments mainly consist of water-saturated brownish mud in the upper part and quite homogeneous greyish clay with foraminifera and some shell fragments in the lower part.

III.2.2. Age-depth model

The model is based on the activity-depth profiles of ^{210}Pb and ^{137}Cs, together with ^{14}C dating. Determination of ^{210}Pb activity was accomplished through the measurement of its daughter nuclide, ^{210}Po, following the methodology described by Sánchez-Cabeza et al. (1998). Samples were dried at 50ºC to constant weight, and dry bulk density and water

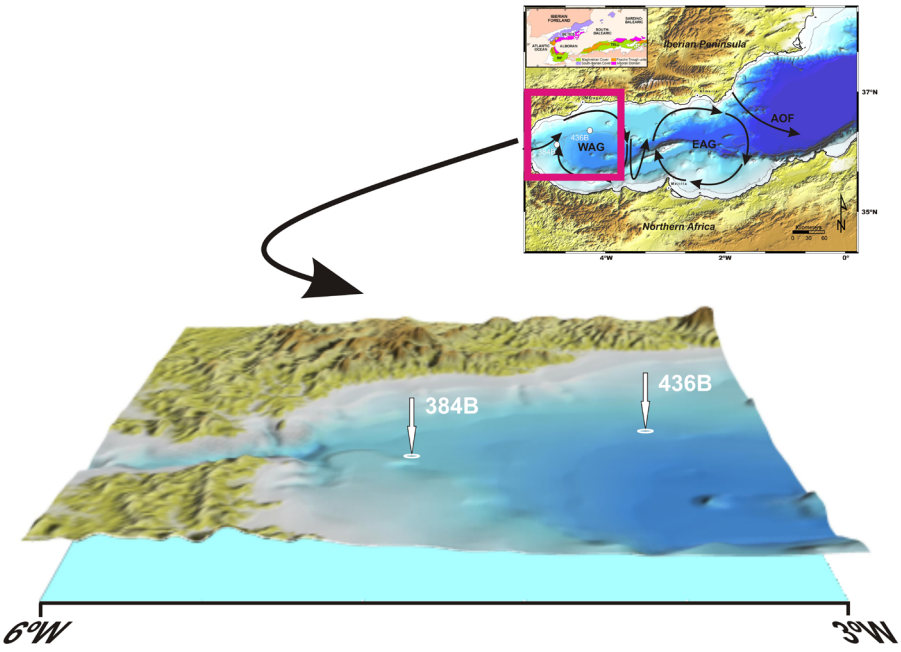

Figure III.1. Location of the studied cores in the Alboran basin (a) and bathymetric map showing the main physiographic features of the area under study (b). WAG: Western Alboran gyre, EAG: Eastern Alboran gyre, AOF: Almería-Orán Front

content were calculated. Briefly, after addition of a given amount of ^{209}Po as internal tracer, aliquots of 200-300 mg of each sample were dissolved in acid by using an analytical microwave oven. Po isotopes were plated onto pure Ag discs in HCl (1N) at 70ºC, while stirring for 8 h. Polonium emission was subsequently counted with α-spectrometers equipped with low-background silicon surface barrier (SSB) detectors for $4 \cdot 10^5$s. ^{226}Ra (via ^{214}Pb through its 351 keV gamma emission line) and ^{137}Cs were determined by way of γ-spectrometry using a high purity well-type Ge detector. Excess ^{210}Pb activity ($^{210}Pb_{xs}$) was determined by subtracting the ^{226}Ra activity (assumed equal to the supported ^{210}Pb activity) from the total ^{210}Pb activity (Figs. III.2a, b).

^{14}C-AMS dates were performed on a monospecific planktonic foramn (*Globigerina bulloides*) extracted from the >125 μm fraction and analyzed by way of accelerator mass spectrometry (Poznan Radiocarbon Laboratory). Radiocarbon ages were calibrated to calendar years (yr AD) using the CALIB 6.0 software (Stuiver and Reimer, 1993) and the MARINE09 curve (Reimer et al., 2009), assuming a marine reservoir age correction of 400 yr. Data are reported with 2σ uncertainty (Fig. III.2c). One post-modern sample was converted to

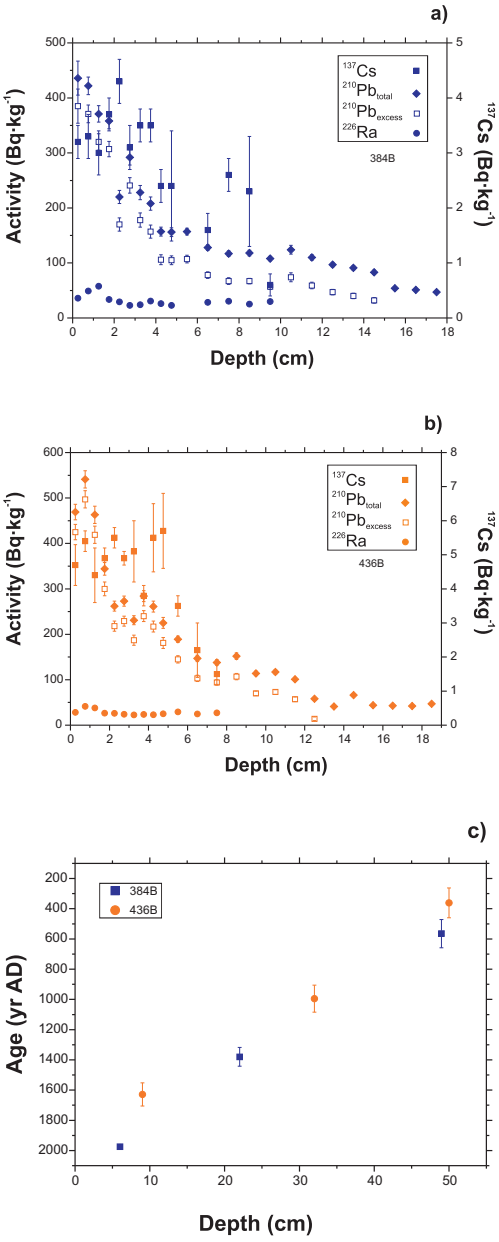

Figure III.2. Activity profiles of $^{210}Pb_{total}$ (diamonds), $^{210}Pb_{excess}$ (open squares), ^{137}Cs (closed squares) and ^{226}Ra (circles) for core 384B (a) and 436B (b) with error bars representing 1σ uncertainties. ^{14}C dates (c) for cores 384B (blue squares) and 436B (orange circles) with error bars representing 2σ uncertainties

yr AD using the CaliBomb software (Reimer et al., 2004) and the calibration dataset of Levin and Kromer (2004), updated by Levin et al. (2008).

III.2.3. Lipid extraction and fractionation

Ca. 5 g of sample (dry mass) was freeze dried and homogenized with an agate mortar and extracted with an accelerated solvent extractor (DIONEX 200) using dichloromethane (DCM) and MeOH (9:1 v/v) at 100ºC and 7.6 x 10^6 Pa. An aliquot of the extract was separated into apolar, ketone and polar fractions using a Pasteur pipette column filled with activated Al_2O_3 and eluted with hexane/DCM (9:1 v/v), hexane/DCM (1:1 v/v) and DCM/MeOH (1:1 v/v), respectively.

III.2.4. TEX^H_{86} and BIT index

An aliquot of the polar fraction containing the GDGTs was dissolved in a high pergormance liquid chromatography (HPLC) grade hexane/isopropanol (99:1 v/v) to a concentration of 2 $mg \cdot ml^{-1}$ and filtered through a 0.45 μm PTFE filter attached to a 1 ml syringe prior to HPLC-MS mass spectrometry (Agilent 1100 with an auto-injector and Chemstation software) according to Hopmans et al. (2000) and Schouten et al. (2007). Detection was achieved using atmospheric pressure chemical ionization (APCI-MS). Identification and quantification of the different GDGTs isomers were carried out via single ion monitoring (SIM, $[M+H]^+$ ions at m/z 1300, 1298, 1296, 1292, 1050, 1036 and 1022, with a dwell time of 234 ms each; Schouten et al., 2007). The TEX_{86} ratio was calculated on the basis of the relative abundance of GDGTs as defined by Schouten et al. (2002) (Eq. 1; roman numbers 1-4' correspond to isoprenoid GDGTs from marine Crenarchaeota with 1-4 cyclopentane rings; 4 is crenarchaeol with four cyclopentane rings and one cyclohexane ring, and 4' is a regio isomer of crenarchaeol):

$$TEX_{86} = GDGT2 + GDGT3 + GDGT4' / GDGT1 + GDGT2 + GDGT3 + GDGT4' \quad (1)$$

The BIT index was calculated from the relative abundance of branched GDGTs and crenarchaeol following Hopmans et al. (2004) (Eq. 2; roman numbers 5-7 correspond to terrestrial branched GDGTs from anaerobic bacteria with 4-6 methyl branches and 4 is crenarchaeol with four cyclopentane rings and one cyclohexane ring):

$$BIT = GDGT5 + GDGT6 + GDGT7 / GDGT5 + GDGT6 + GDGT7 + GDGT4 \quad (2)$$

The TEX^H_{86} (log TEX_{86}) ratio was

converted to SST values according to the empirical formula given by Kim et al. (2010):

$$SST = 68.4 \cdot \log(TEX_{86}) + 38.6 \quad (3)$$

III.2.5. $U^{k'}_{37}$

The ketone fraction was dissolved in ca. 30 µl hexane and injected under conditions described by Schouten et al. (1998, 2000). Samples were measured using a Hewlett Packard 6890 GC instrument provided with an on-column injector and flame ionization detector, equipped with a fused silica column (50 m x 0.32 mm) coated with CP Sil-5 (0.12 µm thickness) and using He as mobile phase. $U^{k'}_{37}$ was calculated from the relative abundance of long chain unsaturated ketones (di- vs. tri-unsaturated C_{37} ketones) following the definition by Prahl and Wakeham (1987):

$$U^{k'}_{37} = [C_{37:2}] / [C_{37:2} + C_{37:3}] \quad (4)$$

$U^{k'}_{37}$ was converted to SST values according to the global calibration of Müller et al. (1998), derived from a global core top calibration which, to a large extent, is based on surface sediments from the Atlantic Ocean (60ºN-60ºS; 0-29ºC) using annual mean temperature at 0 m depth from a climatological database :

$$U^{k'}_{37} = 0.033 \cdot SST + 0.044 \quad (5)$$

The calibration has been applied for the reconstruction of SST in the western Alboran Sea, showing good agreement with average annual mean SST (Cacho et al., 1999, 2002; Martrat et al., 2004, 2007).

III.2.6. Diol index

An aliquot of the polar fraction was chromatographed using a Pasteur pipette column filled with activated Al_2O_3 and DCM/MeOH (90:10 v/v) as solvent, and subsequently silylated by adding 15 µl of BSTFA [N,O-bis (trimethylsilyl)trifluoro-acetamide] and pyridine, and heating the mixture at 60ºC for 20 min. Samples were re-dissolved in ethyl-acetate to a concentration of 2 $mg \cdot ml^{-1}$ and analyzed using a Thermofinnigan TRACE GC instrument equipped with a fused silica column (50 m x 0.32 mm) coated with CP Sil-5 (0.12 µm film thickness), using He as mobile phase and the same GC conditions as above for alkenone analysis (Schouten et al., 1998, 2000). The gas chromatographer was coupled to a Thermofinnigan DSQ quadruple mass spectrometer. Identification and quantification of the different diol isomers was carried out via SIM at m/z 299, 313, 327 and 341 (Versteegh et al., 1997). The diol index was calcula-

ted using the relative abundances of the two dominant *Proboscia* diols (C_{28} and C_{30} 1,14-diol) vs. the C_{30} 1,15-diol (Rampen et al., 2008):

$$\text{Diol index} = [C_{28}\text{1,14-diol} + C_{30}\text{1,14-diol}] / [C_{28}\text{1,14-diol} + C_{30}\text{1,14-diol}] + [C_{30}\text{1,15-diol}] \quad (6)$$

III.2.7. Alkane average chain length and weight average mean $\delta^{13}C$ values

The apolar fraction was separated using a Pasteur pipette column filled with Al_2O_3 impregnated with $AgNO_3$ and using hexane as eluent. The alkane fraction was redissolved in hexane to a concentration of 30 μl. The *n*-alkanes were assigned and quantified using a Hewlett Packard 6890 GC instrument using the same conditions as described above for alkenone analysis. The carbon isotopic composition of the *n*-alkanes was determined using a Thermo Electron DELTA Plus XL isotope ratio monitoring (irm)-GC-MS system. GC conditions were similar to those for GC analysis except that the film thickness of the CP Sil-5 column was 0.4 μm and that a constant flow of He was used at 1.5 $ml \cdot min^{-1}$. Compounds were pyrolyzed at 1450ºC in an empty ceramic tube, which was pre-activated by a CH_4 flow of 0.5 $ml \cdot min^{-1}$ for 5 min as described by Poynter and Eglinton (1990) and Schouten et al. (1998, 2000). CO_2 with a known isotopic composition was used as reference and a mixture of C_{16}-C_{32} *n*-alkanes of known isotopic composition (ranging from −42‰ to −25.6‰ vs. VSMOW) was used to monitor the performance of the system. The stable carbon isotope composition is reported in the δ notation vs. the Vienna PDB standard. The average chain length (ACL) was calculated as the average number of carbons per molecule based on the abundance of the odd numbered *n*-alkanes as follows (Poynter and Eglinton, 1990):

$$ACL = \Sigma(i \cdot Xi) / \Sigma Xi \quad (7)$$

where "Xi" is fraction of total *n*-alkane abundance and "i" ranges from C_{27} to C_{33}. The weighted mean isotopic composition of the odd *n*-alkanes ($\delta^{13}C_{WMA27\text{-}33}$) was determined as follows (Collister et al., 1994):

$$\delta^{13}C_{WMA27\text{-}33} = \Sigma Xi \cdot \delta i \quad (8)$$

where Xi is fraction of total *n*-alkane abundance, δi is individual *n*-alkane δ value and i ranges from C_{27} to C_{33}.

III.3. Results and discussion

III.3.1. Age-depth model and sedimentation rate

$^{210}Pb_{xs}$, ^{226}Ra and ^{137}Cs activity profiles are shown in Fig. III.2. The maximum ^{210}Pb concentration is at the top of each core and decreases down to 12.5 and 14.5 cm depth, respectively. The maximum sedimentation rate obtained using the CF:CS model are 1.49± 0.13 mm·yr^{-1} for 384B and 1.41±0.12 mm·yr^{-1} for 436B. The rates are slightly higher than those derived by Masqué et al. (2003) for cores collected from the same area. The chronological model obtained from these sedimentation rates does not agree with those obtained from ^{137}Cs concentration. In fact, the $^{210}Pb_{xs}$ concentration profile does not show the exponential curve expected from radioactive decay due to the presence of some intervals where $^{210}Pb_{xs}$ activity remains roughly constant. Cores were collected close to the continental margin, and variation in ^{226}Ra concentration is used as a good indicator of change in sediment composition, in agreement with the geochemical results described above, allowing interpretation of the $^{210}Pb_{xs}$ profile as influenced by rapid sedimentation rather than bioturbation (García-Orellana et al., 2006). Applying the CF:CS model to the exponential profile of each core and extracting the most plausible sedimentation rate obtained for both cores, these are 0.69±0.04 mm·yr^{-1} for 384B and 0.85±0.05 mm·yr^{-1} for 436B. These rates agree better with the ^{137}Cs activity profile, with the 1963 yr AD maximum at 4.75 cm and 3.75 cm, respectively, when ^{137}Cs was widely distributed from nuclear weapon testing (Figs. III.2a, b).

^{14}C-derived linear sedimentation rates are 0.30±0.002 and 0.31±0.002 mm·yr^{-1} for 384B and 436B respectively (Fig. III.2c), which are consistent with other sediment records from the area (Masqué et al., 2003). The values are ca. twice those produced from ^{14}C chronology. The differences between ^{210}Pb and ^{14}C age models are well documented and are mainly due to the estimation of sedimentation rate from the ^{210}Pb dating of cores being considered an upper limit (Benninger et al., 1979; Nittrouer et al., 1984). In the case of Alboran Sea, considered a high productivity and margin influenced area, surface mixing layer and bioturbation rate range from 3 to 9 cm and 0.2 to 15 cm^2·yr^{-1} (Masqué et al., 2003), so the discrepancy between both dating methods is justified.

III.3.2. Paleoclimate conditions during the last two millennia (500-1950 yr AD)

III.3.2.1. SST

Variation in reconstructed SST is

relatively small, between 1.3 and 1.5ºC for $U^{k'}_{37}$-based SST, and 1.1 and 2ºC for TEX^{H}_{86}-based SST as range of variation over the last two millennia. SST were estimated for both cores and ranges from 23.2 to 25.2ºC and from 18.5 to 20ºC for TEX^{H}_{86} and $U^{k'}_{37}$, respectively, with average values of 24 and 19ºC. The highest TEX^{H}_{86}-derived SST are reached during the MCA in core 384B and during the DA in core 436B, and the lowest during the LIA in both cores. $U^{k'}_{37}$ based maximum values are reached at the beginning of the MCA in both cores and minimum values are attained during the LIA (Fig. III.3).

Both SST reconstructions show similar overall trends, although TEX^{H}_{86} absolute values are higher than those inferred from $U^{k'}_{37}$ (Fig. III.3). The offset between the TEX^{H}_{86} and $U^{k'}_{37}$ derived SST ranges between 4 and 5ºC. A difference in the bloom season is a plausible explanation for the difference. The downward flux of particles in the

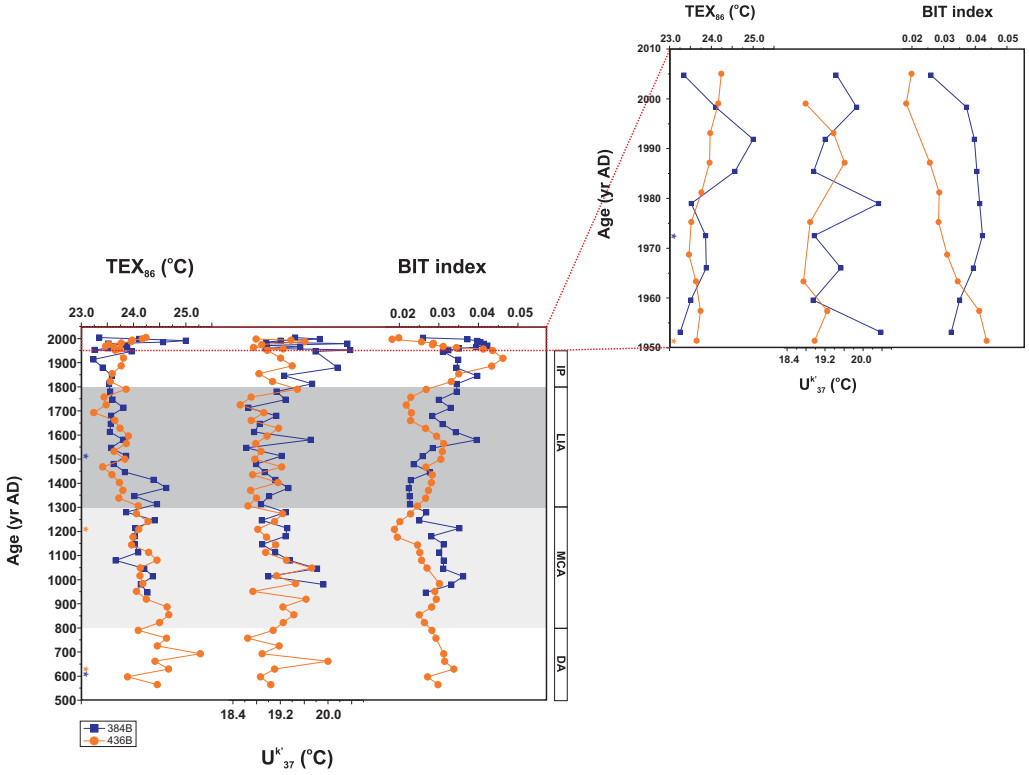

Figure III.3. Reconstructed SST during the last two millennia (200-1950 yr AD) (a) and during the twentieth century (1950-2008 yr AD) (b) for site 384B (blue squares) and site 436B (orange circles): TEX^{H}_{86} and $U^{k'}_{37}$ based SST, and BIT index. Light grey bars indicate dry periods (MCA, Medieval Climate Anomaly); dark grey bars indicate humid periods (LIA, Little Ice Age)

westernmost Mediterranean region is predominantly controlled by fluvial discharge and upwelling-induced primary production at the northern edge of the Western Alboran Gyre (WAG; Fabres et al., 2002). Maximum flux of haptophytes takes place during March and October, before the most productive period (Bárcena et al., 2004). According to García-Gorriz and Carr (1999, 2001), in the present-day Alboran Sea basin, phytoplankton blooms occur predominantly from November to March at SST<17.4ºC whereas the non-bloom period is from May to September with SST>19.5ºC and light is not a growth limiting factor throughout the year. The latter authors also pointed out that transition periods occur in April-May, when thermal stratification starts, and in October-November, coinciding with maximum wind variability and loss of stratification within the basin.

SST estimates based on $U^{k'}_{37}$ (Cacho et al., 1999) and the planktonic foraminifera assemblage methods (Pérez-Folgado et al., 2003), showed that $U^{k'}_{37}$ derived SST correlates with autumn or average annual SST in the Alboran Sea basin during the Holocene (18-20ºC). This is in good agreement with our results that reveal SST of 18.5-20ºC based on $U^{k'}_{37}$ (Fig. III.3).

Although when marine Thaumarchaeota predominantly bloom in the western Mediterranean is unknown, studies at other sites showed that they are generally abundant in surface waters when the majority of the phytoplankton is not blooming (Murray et al., 1998, 1999; Wuchter et al., 2005; Pitcher et al., 2011). This is in agreement with other studies. Castañeda et al. (2010) reported TEX^{H}_{86}-derived SST of ca. 23-25ºC throughout the Holocene in eastern Mediterranean marine records, Leider et al. (2010) pointed out summer SST at the most offshore sites using TEX^{H}_{86} ratios on core tops (0-2 cm) from the Adriatic Sea. Furthermore, in the Alboran Sea basin, Huguet et al. (2011) showed warmer TEX^{H}_{86} SST than estimated from $U^{k'}_{37}$ during MIS7 interglacial in core 977 ODP (21ºC average) and Jiménez-Espejo et al. (2008) found average summer SST of 22 ºC during the Middle Holocene inferred from the modern analogue technique (MAT). Likewise, according to the MEDATLAS/2002 data base (MEDAR Group, 2002), the present average summer and annual SST of the upper water column (0 m) at the studied sites is around 21ºC and 18ºC respectively (Fig. III.4). Hence, we suggest that the TEX^{H}_{86} temperature signal in the western Mediterranean sedimentary record reflects summer SST during the last two

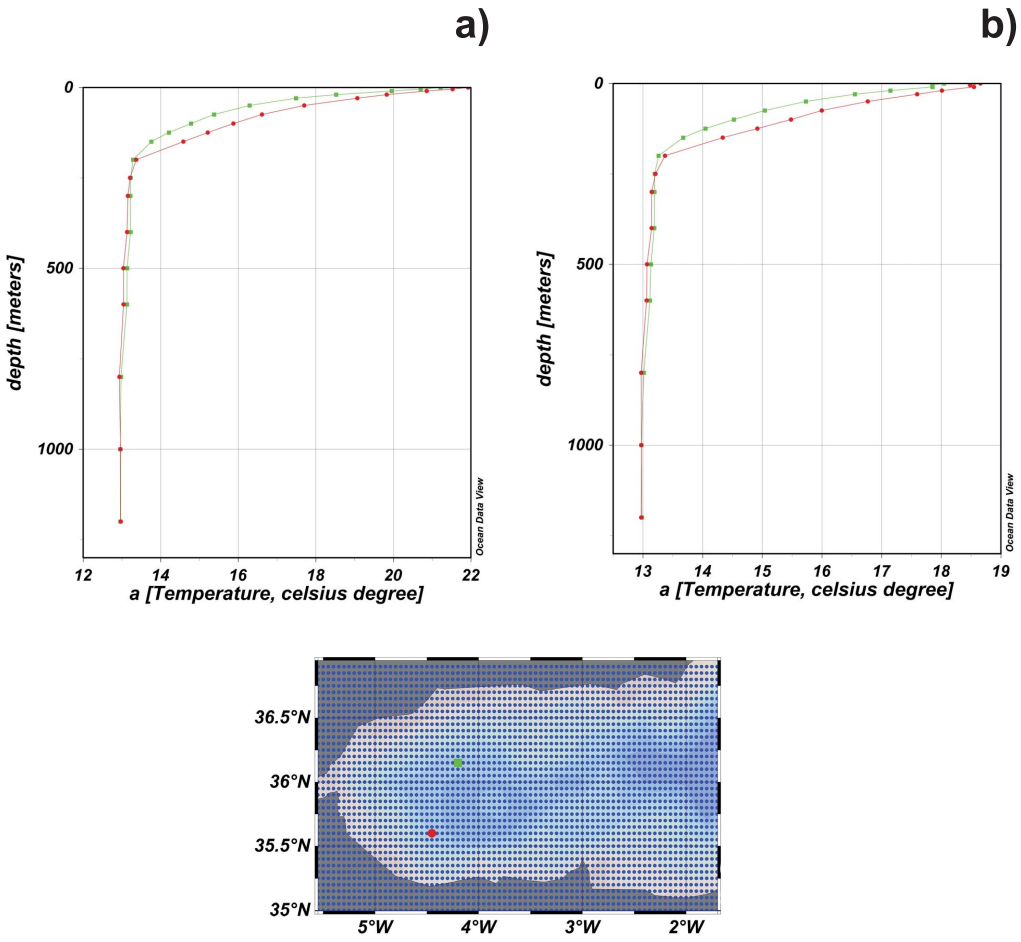

Figure III.4. Present average summer (a) and annual SST (b) of the upper water column (0 m) at the study sites (MEDAR Group, 2002)

millennia. It is unlikely that our TEX^{H}_{86} records are biased by the influence of soil-derived organic matter, the BIT index being always low (Weijers et al., 2006).

In both cores, TEX^{H}_{86} SST progressively dropped from the highest values at the end of the DA (core 436B) and from the beginning of the MCA (core 384B) until the end of the LIA, where minimum values were attained. The pattern is mirrored by $U^{k'}_{37}$ temperatures although the trend is noisy due to the low concentration of alkenones. $U^{k'}_{37}$ SST shows a sharp increase during the Industrial Period (IP; 1800-1950 yr AD), which is not mirrored in TEX^{H}_{86}-derived values where SST only depicts a slight increase.

The MCA has been described as the most recent pre-industrial warm period noted in Europe and over the Northern Hemisphere, warmer than the subsequent LIA, and also with temperatures comparables to those of the twentieth century (Mann et al., 2008, 2009). During the MCA, average temperature values of 24.2 and 19.2ºC were recorded from TEX^{H}_{86} and $U^{k'}_{37}$ respectively in both cores, whereas during the LIA the values are slightly lower: 23.7 and 19ºC for TEX^{H}_{86} and $U^{k'}_{37}$, respectively, in both cores. During the DA, TEX^{H}_{86} SST reached higher values than during the MCA, with a mean temperature of 24.5ºC.

In summary, a progressive long term decline of SST is observed during the last two millennia (Fig. III.3), in accord with the reconstructed cooling due to solar irradiance forcing in Northern Hemisphere series prior to industrialization during the last millennium (Mann et al., 1999; Jones et al., 2001). Both TEX^{H}_{86} and $U^{k'}_{37}$ -based SST estimates reveal the LIA as the coldest period of the last two millennia. Although higher annual mean temperatures have been recorded during the MCA on the basis of $U^{k'}_{37}$, this period does not appear as the warmest of the last 2000 yr prior to the twentieth century, as higher TEX^{H}_{86} SST (summer temperatures) have been recorded previously during the DA. In contrast, annual mean temperatures (based on $U^{k'}_{37}$) provide evidence for the MCA being the warmest pre-industrial period.

III.3.2.2. Terrestrial input fluctuation: Land-ocean correlation

The *n*-alkanes exhibit an unimodal distribution between C_{27} and C_{33}, peaking at C_{31}, and a strong odd/even preference, which indicates a typical origin from the epicuticular wax of terrestrial higher plant leaves (Eglinton and Hamilton, 1967). The ACL does not reveal any considerable fluctuation over the last two millennia, varying between 30.0 and 30.3 (Fig. III.5), suggesting that the higher plant input has not undergone major fluctuation due to climate variability.

The carbon isotopic composition of the odd *n*-alkanes (C_{27} to C_{33}) ranges from -31.2 to -29.6‰ for C_{27}, -32.9 to -31.0‰ for C_{29}, -32.6 to -31.4‰ for C_{31} and -32.5 to -30.4‰ for C_{33} in core 436B, i.e. shows a rather uniform pattern. The $\delta^{13}C$ value of the most abundant *n*-alkanes, C_{29} and C_{31}, runs essentially in parallel, in agreement with their common biosynthetic pathway, and the difference between both trends

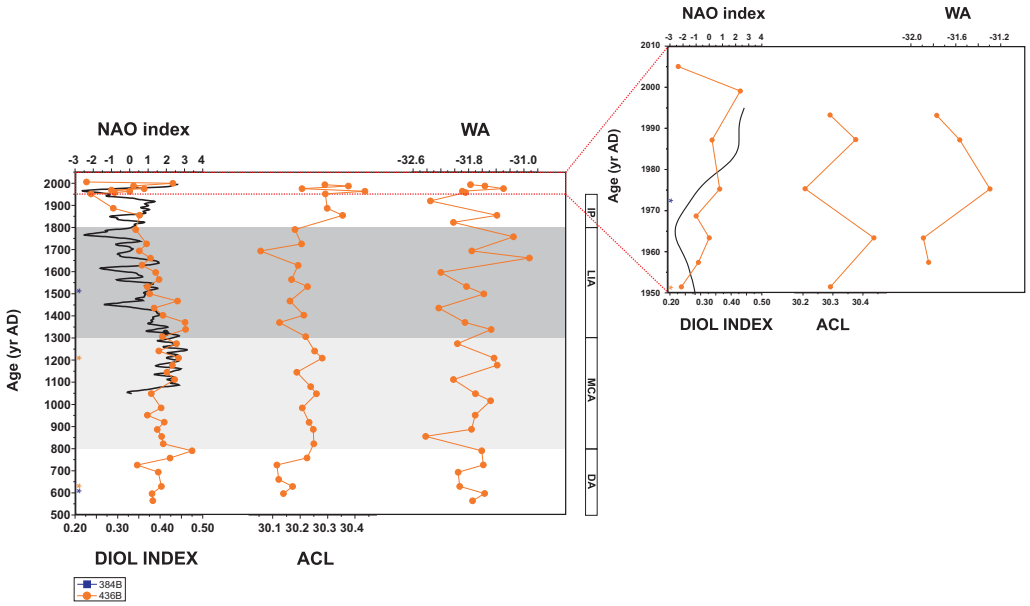

Figure III.5. Fluctuation in soil OM input and paleoproductivity conditions during the last two millenia (200-1950 yr AD) (a) and during the twentieth century (1950-2008 AD) (b) for site 436B: diol index, Average Chain Length (ACL), Weight Average (WA) and TEX^{H}_{86} based SST compared with ACL. Light grey bars indicate dry periods (MCA, Medieval Climate Anomaly); dark grey bars indicate humid periods (LIA, Little Ice Age)

is <1‰, C_{31} being more negative, as observed in other studies (Collister et al., 1994; Bird et al., 1995; Zhao et al., 2000). The $\delta^{13}C_{WMA27-33}$ value can be used to track changes in the source and the relative contribution from plants using a different carbon fixation pathway during photosynthesis (i.e. C_3 vs. C_4 plants) and thus to establish the paleohydrological conditions and vegetation composition through time (e.g. Schefuß et al., 2005). In general, C_3 plants are the most ^{13}C depleted and common, whereas C_4 plants are found predominantly in tropical savannas, temperate grasslands and semi-deserts. C_4 plants have leaf tissue $\delta^{13}C$ values between -10 and -16‰ and C_3 plants between -25 and -30‰. The average $\delta^{13}C$ values of leaf wax derived *n*-alkanes are ^{13}C depleted by ca. 8‰ and 4‰ in C_3 and C_4 plants, respectively (Rieley et al., 1993; Collister et al., 1994). The $\delta^{13}C_{WMA27-33}$ of *n*-alkanes in core 436B fluctuates between -32.4 and -30.9‰ (Fig. III.5). With endmember values of -36‰ and -21‰ for C_3 and C_4 vegetation reported (e.g. Castañeda et al., 2009), this indicates a predominant C_3 plant contribution over the last two millennia.

The BIT index quantifies the relative fluvial input of soil OM in marine environments (Hopmans et al., 2004;

Weijers et al., 2006). Its varies between 0 and 1, representing marine and soil-derived OM end members, respectively. BIT values are low in both cores, ranging from 0.02 to 0.04, with a mean of 0.03 (Fig. III.3). The low values (<0.05 in both cores) suggest only a minor input of riverine derived soil OM into the basin and a mainly marine provenance for the OM. A slightly decreasing trend is observed during the DA and the MCA, with a slightly increasing trend during the LIA in both cores. Higher values occur during the LIA than during the MCA in both cores. The riverine influence is slightly higher during wet periods (higher values during the LIA) than during dry periods (lower values during the MCA).

Regarding the provenance of the *n*-alkanes, the Alboran Sea basin receives riverine and eolian inputs deriving from both the Iberian and the African margin, so both sources might provide plant waxes. On the other hand, a persistent positive mode of the NAO during the MCA and a negative one during the LIA have been described over Europe (Trouet et al., 2009), and enhanced eolian transport of Saharan dust to the Mediterranean Sea has been evidenced during positive NAO phases (Moulin et al., 1997). Indeed, in the western Mediterranean region, an increase in fluvial-derived elements depicts the LIA, while drier environmental conditions are recognized during the MCA (a decrease in fluvial input and enhanced dust transport; Nieto-Moreno et al., 2011). There is no study on disentangling fluvial vs. eolian plant wax *n*-alkane contribution to hemipelagic sediments in the region. Nevertheless, fluvial sediment transport from the northern African margin to this basin seems to be negligible (Fabres et al., 2002) and aeolian transport of dust from the Sahara over the western Mediterranean represents 10–20% of the recent deep sea sedimentation (Guerzoni et al., 1997). Thus, an increase in fluvial input should promote a greater contribution from C_3 plants during wet periods. However, slightly lighter $\delta^{13}C$ values are found during the MCA, when stronger winds, greater eolian input and a decline in fluvial elements are observed. In contrast, partly heavier $\delta^{13}C$ values are evidenced during the LIA when more humid conditions prevailed. Besides, higher BIT values coincide with longer chain length during the LIA, suggesting that fluvial input from the Iberian margin mainly provides plant wax instead of eolian input from the African margin, although this relationship is not altogether clear. Additional studies would be needed to further support this hypothesis.

III.3.2.3. Upwelling and palaeoproductivity indicators

The location of core 436B, close to the influence of the upwelling cell associated with the northern edge of the Western Alboran Gyre (WAG), makes it suitable for studying upwelling conditions in the Alboran Sea using long chain diols. The diol index shows a distinctive trend in the core. The values remain high during the entire DA and the MCA, ranging between 0.35 and 0.5, and then a sharply decreasing trend at the beginning of the LIA starts, reaching the lowest values around 1950 yr AD (diol index 0.2; Fig. III.5). As shown by Rampen et al. (2007) for sediment traps from the Arabian Sea, the diol index may be an useful indicator for high nutrient conditions, since their inferred source, diatoms of the genus *Proboscia*, are often abundant in upwelling regions.

As discussed below, the MCA in the western Mediterranean is characterized by a persistent NAO positive, a decrease in fluvial input and enhanced dust transport from the Saharan region (Nieto-Moreno et al., 2011). In addition, a correlation between the NAO index and westerly wind-induced upwelling has been established for the Alboran Sea (Vargas-Yáñez et al., 2008). This estival wind-induced upwelling might have caused the slightly lower TEX^{H}_{86}-based SST recorded in core 436B vs. 384B throughout the MCA until the beginning of the LIA due to the nutrient-rich upwelled cold water being carried up into the photic zone during the persistent positive NAO phase. In the same way, during the wetter LIA, stratification of the upper water column caused by the input of fluvial-derived nutrients and the turn into a negative mode of the NAO might be responsible of the sharp decrease in this index at this time interval. Thus, the diol index can be used as a proxy to distinguish between high productivity driven by upwelling and high productivity due to enhanced fluvial input.

III.3.3. Significance of climate conditions in the twentieth century (1950-2008 yr AD)

Variation in SST range between 0.5-1.8ºC during the last 60 yr in both cores, close to the range of variation measured for the last two millennia (1.5-2ºC). TEX^{H}_{86} and $U^{k'}_{37}$ ratio-based SST increase from 23.5 to 25ºC and from 18.7 to 20.0ºC respectively, with average values of 23.8 and 19.5ºC, so are of the same order of magnitude as during the last two millennia (23.2 to 25ºC and from

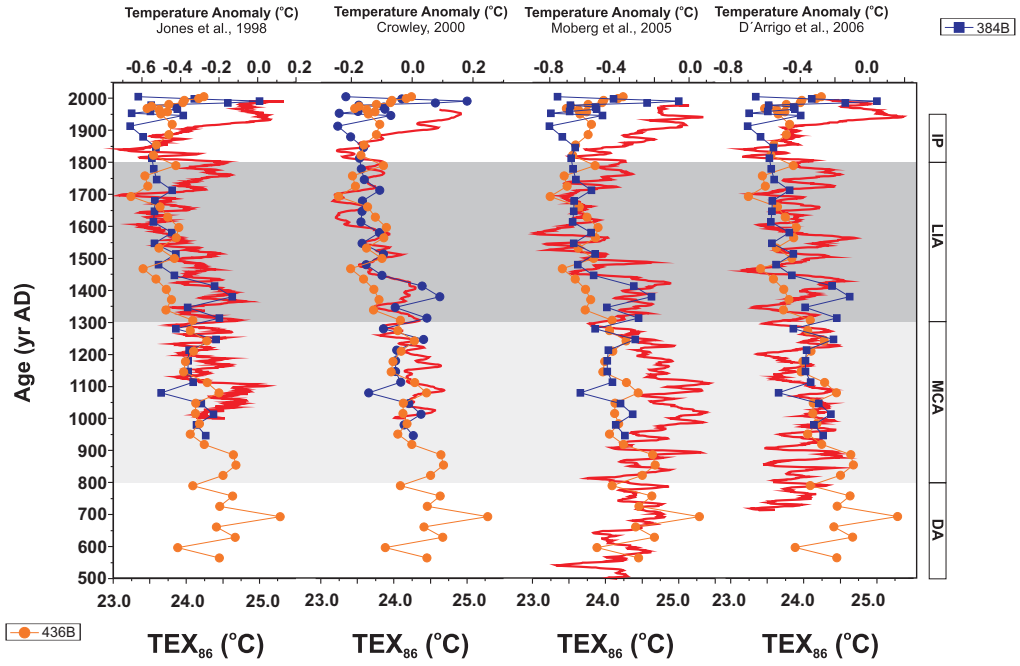

Figure III.6. TEX^{H}_{86}-based SST for site 384B (blue squares) and site 436B (orange circles) compared with high resolution Northern Hemisphere temperature reconstruction extracted from Wahl et al. (2010)

18.5 to 20ºC respectively, with average values of 24 and 19ºC). The highest TEX^{H}_{86} and $U^{k'}_{37}$derived values are reached from 1980 yr AD onwards in both cores and the lowest between 1950 and 1980 yr AD (Fig. III.3). In this way, Tierney et al. (2010) also evidenced an increase of 2ºC on TEX_{86}-derived temperatures for the largest rift lake in East Africa beginning around 1900 yr AD, with the uppermost sample calibrated to 25.7ºC. In our records, SST estimates from the core top are 23.34ºC and 24.24ºC for 384B and 436B respectively.

In general, a progressive and sharp warming took place during the last 60 yr, in accord with previous Northern Hemisphere multi-proxy temperature reconstructions (Rayner et al., 2003; Trenberth et al., 2007; Fig. III.6). Although absolute values of variation and average values during the last two millennia in comparison with the last century are not significantly different, the rate of warming in the twentieth century evidenced from the SST records appears anomalous. This warming is more notably in TEX^{H}_{86}-based SST (summer temperature) than in the $U^{k'}_{37}$-based SST (annual mean temperature). Fig. III.6 show a comparison between TEX^{H}_{86}-based SST for site

384B and 436B and some high resolution Northern Hemisphere temperature reconstruction for the last two millennia extracted from a newly integrated archive (Wahl et al., 2010). TEX^{H}_{86} shows a similar trend as the Northern Hemisphere temperature reconstruction and thus points to a persistent anthropogenic forcing as a result of an increase in greenhouse gasses (Jones et al., 2001; Jansen et al., 2007).

Regarding terrestrial input fluctuation, the carbon isotopic composition of individual *n*-alkanes also shows a rather uniform pattern during the twentieth century for core 436B. Values range from -30.4 to -29.7‰ for C_{27}, -32.7 to -30.1‰ for C_{29}, -32.3 to -31.3‰ for C_{31} and -31.8 to -30.6‰ for C_{33} in core 436B. The $\delta^{13}C_{WMA27-33}$ of *n*-alkanes fluctuates around -31‰ (Fig. III.5), still suggesting a predominantly C_3 plant contribution in this century. The ACL varies between 30.2 and 30.4 (Fig. III.5), revealing no considerable fluctuation in the provenance source of the higher plant input.

The BIT index remains low, ranging from 0.03 to 0.04 for both cores (Fig. III.3), indicating the marine provenance of the OM. A slightly decreasing trend is observed from the onset of the twentieth century to the present. The soil-derived OM input is slightly higher from the 1950s to the 1980s when BIT values are higher.

Concerning marine productivity, the diol index shows a sharp increasing trend in 436B, with values from 0.2 to 0.4, with lower values from the 1950s to he 1980s and higher ones from the 1980s to the present (Fig. III.5). Additionally, the diol index depicts certain correlation with the NAO index, which records a persistent trend to a positive mode during the last 25 yr (Fig. III.5). The lowest values of the diol index suggest the absence of upwelling conditions, which coincides with a more negative mode of the NAO (less intense winds) and higher BIT values (greater input of fluvial-derived nutrients). During the last 30 yr, higher values of the diol index, a persistent positive mode of the NAO and a slightly lower influence of riverine input (BIT index), evoke an intensification of the upwelling conditions in the area under the influence of the WAG.

III.4. Conclusions

A multi-proxy high resolution record based on organic fossil remains in two marine box cores from the Alboran Sea basin was obtained to further advance ideas towards the reconstruction

of natural climate variability during the last two millennia in the westernmost Mediterranean region. A progressive long term decline in SST was observed during the last two millennia and a sharp increase in SST took place during the twentieth century, in accord with existing Northern Hemisphere multi-proxy temperature reconstructions. Both cores showed similar overall trends, although TEX^{H}_{86}-derived absolute values of SST were higher than those inferred from the $U^{k'}_{37}$ ratio, probably due to differences in the bloom season of haptophyte algae and Thaumarchaeota. TEX^{H}_{86} and $U^{k'}_{37}$ ratios-based SST estimates revealed the LIA as the coldest period of the last two millennia. Although higher SST have been recorded during the MCA, the period does not appear to be the warmest period of the 2000 yr prior to the twentieth century, as higher TEX^{H}_{86}-derived temperatures (summer temperatures) have been recorded previously during the DA. In contrast, annual mean SST (based on $U^{k'}_{37}$) indicates the MCA as the warmest pre-industrial period. The TEX^{H}_{86} index, although reflecting summer SST in the western Mediterranean region, seems to be a reliably proxy for long term SST reconstruction since it shows similar trends to other Northern Hemisphere temperature reconstructions, in accord with the solar irradiance and anthropogenic forcing during the last two millennia. BIT values were low in both cores (<0.05), suggesting a low influence of riverine derived soil OM in the basin and a predominant marine provenance for the OM. The riverine influence was slightly higher during wet periods (LIA) than during dry periods (MCA). Carbon isotopic composition of odd *n*-alkanes suggested a predominantly C_3 plant contribution over the last two millennia and fluvial input as the main provenance source of the higher plants. The highest values of the diol index coincided with a more positive mode of the NAO and lower riverine influence (BIT index), and vice versa, suggesting a bloom of *Proboscia* diatoms due to nutrient-rich upwelled cold water carried up into the photic zone. This was caused by an intensification of the wind-induced upwelling conditions during positive NAO phases such as those prevailing during the MCA or during the second half of the twentieth century.

Chapter IV

Climate imprints and underlying causes during the Medieval Climate Anomaly and the Little Ice Age: A novel record from the Alboran Sea basin

V. Nieto-Moreno, F. Martínez-Ruiz, S. Giralt, D. Gallego-Torres, J. García-Orellana, and M. Ortega-Huertas

To be submitted to The Holocene

Abstract

An integrated multiproxy analysis from westernmost Mediterranean deep-sea sediments has provided new insights into natural forcing mechanisms driving climate variability as well as into anthropic imprints in this region during the last two millennia. Two deep-sea marine records, with a robust age model provided by the activity-depth profiles of ^{210}Pb and ^{137}Cs, together with ^{14}C dating, have allowed a detailed reconstruction of paleoenvironmental and paleoceanographic responses during the Medieval Climate Anomaly (MCA), the Little Ice Age (LIA), the Industrial Period (IP) and the twentieth century at very high resolution. Decreasing trends of fluvial-derived elements (Si and K) and a increasing Saharan eolian input (shown by Zr/Al and Zr/Rb ratios) characterized the MCA and the second-half of the twentieth century as prevalent dry periods, while generally wetter conditions are evidenced during the LIA and the IP, in accordance to a positive mode of the North Atlantic Oscillation (NAO). The LIA developed a sequence of successive short and sharpen dry-wet phase alternation, wet spells occurring under lower intensity of solar radiation and low sunspots activity in the Northern Hemisphere. Furthermore, a noteworthy and sharp decrease of redox-sensitive elements (V/Cr and Ni/Co ratios) and coarser sortable silt at 1450 and 1950 yr AD, support more energetic hydrodynamic conditions (oxygenated bottom water conditions and faster bottom currents) at this time, likely promoted by the strengthened of cooler waters flowing into the Mediterranean Sea. Increasing heavy metal concentrations (Pb, Zn and Cu) at 1750 and 1950 yr AD, and relatively constant levels during pre-industrial times, reflected a significant contribution from anthropic sources, which is also recorded by off-shore sediments.

IV.1. Introduction

Paleoclimate reconstructions over the past millennia are critical for improving the current understanding of climate variability and predicting climate responses to future climate change. Studying our immediate climate past also allows exploring natural modes of variability in similar boundary climate conditions than present time. Thus, such studies lead to make trustworthy and accurate predictions of possible climate fluctuations in the near future (Jones et al., 2001, 2009; Bradley et al., 2003). Within the last millennium, the Medieval Climate Anomaly (MCA; 800-1300 yr AD) (Hughes and Diaz, 1994; Stine, 1994), also termed the Medieval Warm Period (MWP) (Lamb, 1965), and the subsequent Little Ice Age (LIA; 1300-1800 yr AD) (Bradley and Jones, 1993), have become of considerable and increasing interest as they represent recent and distinct periods characterized by notable climatic shifts attributable to natural forcing. Hence, further comprehension of the sensitivity of the climate system by internal climate variability and/or natural forcing may help deciphering the extent to which anthropogenic forcing may have influenced the energy balance of the climate system and thus contributed to global warming (Jansen et al., 2007).

Growing evidences for widespread persistent hydrological and temperature anomalies in the Northern Hemisphere defines the MCA as a warm period, contrasting with the subsequent LIA, when cooler conditions were reached (Mann et al., 2008, 2009). The increase in temperatures during the MCA was also accompanied by prolonged droughts in North America, southern Europe and the Mediterranean region (Seager et al., 2007; Graham et al., 2011). During recent years, several attempts have been undertaken with the aim to explain the persistence of these anomalies during the last two millennia as well as during the transition between the MCA and the LIA (Trouet et al., 2011; and references therein). Among them, a conjunction of ocean-atmosphere feedbacks have been invoked as possible forcing mechanisms, encompassing enhanced solar irradiation and/or reduced volcanic activity during the MCA which might have induced changes in the tropical Indo-Pacific zonal sea surface temperatures (SST) (la Niña-like conditions) that resulted in a strengthening of the North Atlantic Oscillation (NAO) in the North Atlantic realm and stronger associated westerlies, which may have enhanced the Atlantic Meridional Overturning Circulation (AMOC), the latter likewise

reinforcing la Niña-like conditions in the tropical Pacific (Seager et al., 2007; Trouet et al., 2009; Graham et al., 2011).

In order to improve the understanding of recent climate variability, appropriate paleoarchives are required. In this regard, the Alboran Sea basin (westernmost Mediterranean) is a key semi-enclosed basin with high sedimentation rates, which provide ultra high-resolution records for paleoclimatic and paleoceanographic reconstructions. Furthermore, it is located between two climate belts (the mid-latitude westerlies system and the subtropical high-pressure belt) and coupled to the North Atlantic ocean-climate system through the Strait of Gibraltar and the influence of the NAO, which makes the area particularly sensitive to climate changes. Although recent approaches have provide new insights about climate variability during the Late Holocene in the westernmost Mediterranean realm, evidencing the exceptional nature and suitability of this region for climate variability reconstructions at centennial and millennial time-scales (e.g., Martín-Puertas et al., 2010; Nieto-Moreno et al., 2011; Moreno et al., 2012), ultra high-resolution marine records covering the last two millennia are absent. We have recently analyzed two ultra high-resolution records obtained from box cores recovered in the north-western Alboran Sea basin, and on the basis of a novel biomarker approach they have shown a progressive long-term decline in SST over the last two millennia. Also, an anomalous rate of warming during the twentieth century has been reported (Nieto-Moreno et al., 2012), which is coherent with previously reconstructed temperatures in the Northern Hemisphere (Wahl et al., 2010). Furthermore, the LIA was evidenced as the coldest period within the last two millennia whereas warmer temperatures were found during the preceeding MCA, as warm as during the second half of the twentieth century (Nieto-Moreno et al., 2012). Further work from the same two high-resolution and well-dated marine box-cores records is presented here, including a multiproxy approach based on major and trace element content, grain size distribution, total organic carbon (TOC) content and mineral composition of the sediments. A statistical assessment of the data set is performed in order to define and characterize the main proxy families later applied for reconstructing paleoclimatic and paleoceanographic fluctuations in the western Mediterranean. This reconstruction has been compared with other Late Holocene records from the westernmost Mediterranean. Fina-

lly, vertical distributions of pollutants are presented with the aim to identify the anthropogenic contribution during industrial times. Sediment quality guidelines (SQG) have been likewise applied to assess the level of heavy metals accumulated by deep-sea sediments in this basin.

IV.2. Materials and methods

IV.2.1. Sampling

Two box-cores were selected for this study (Fig. IV.1); 384B (35º59,161'N, 4º44,976'W, 1022 m.b.s.l.) and 436B (36º12,318'N, 4º18,800'W, 1108 m.b.s.l), recovered in the north-western Alboran Sea basin in 2008 using a KP 1.5 box-corer (50 x 50 x 50 cm) during the Training-Through-Research Cruise 17 (Sagas-08 Cruise), Leg 1, on R/V Professor Logachev. Site 384B is settled in the north-western part of the Alboran Sea basin, close to the Strait of Gibraltar, where the exchange of water between the Mediterranean Sea and the eastern Atlantic takes place. Site 436B is about 110 km east of the latter site, under the influence of the upwelling

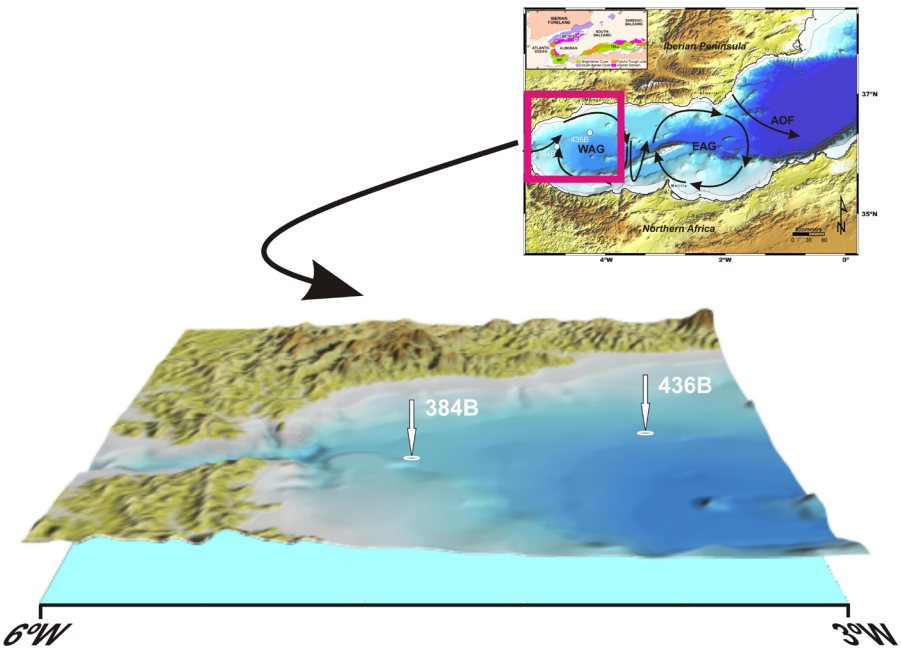

Figure IV.1. Location of the studied cores in the Alboran basin (a) and bathymetric map showing the main physiographic features of the area under study (b). WAG: Western Alboran gyre, EAG: Eastern Alboran gyre, AOF: Almería-Orán Front

cell associated with the northern edge of the Western Alboran Gyre (WAG) (Fig. IV.1).

Upon retrieval, box-cores were directly sub-sampled using PVC pipes (50 cm long and 11.8 cm internal diameter) inserted into the sediment. One of the cores of every box-core was sampled in 1 cm thick slices once in laboratory to obtain a high resolution record. These sediments mainly consist on water-saturated brownish mud in the uppermost centimetres and homogeneous greyish clay with foraminifera and some shell fragments in the lower part.

IV.2.2. Age-depth model

The age-depth model of both cores is based on the activity-depth profiles of ^{210}Pb and ^{137}Cs, plus ^{14}C dating. Determination of ^{210}Pb activities was accomplished through the measurement of its daughter nuclide, ^{210}Po, following the methodology described by Sánchez-Cabeza et al. (1998). Samples were dried at 50ºC until constant weight, and dry bulk density and water content were calculated. Briefly, after addition of a given amount of ^{209}Po as internal tracer, sediment aliquots of 200-300 mg of each sample were totally dissolved in acid medium by using an analytical microwave oven. Polonium

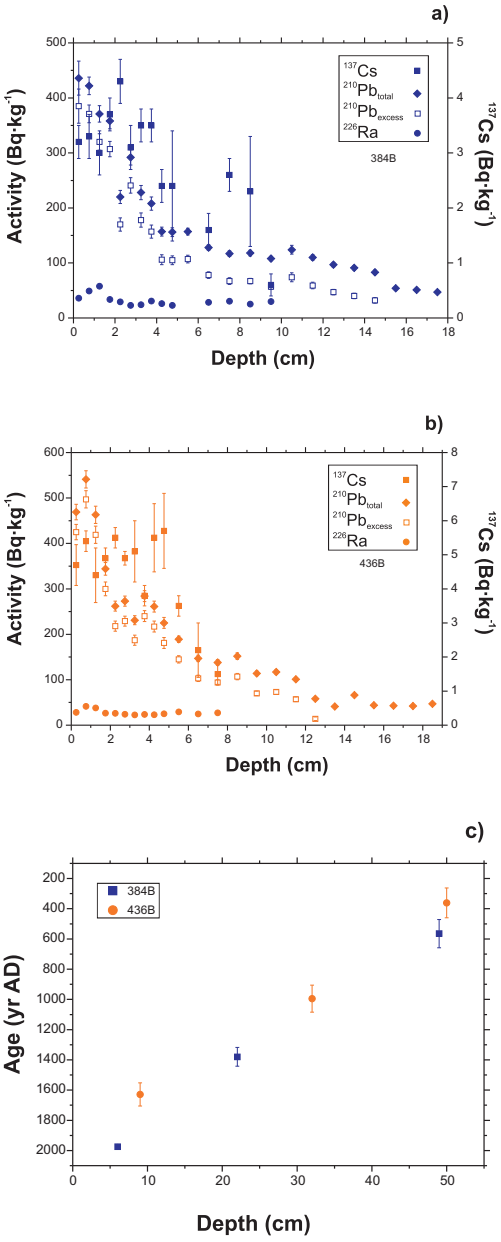

Figure IV.2. Activity profiles of $^{210}Pb_{total}$ (diamonds), $^{210}Pb_{excess}$ (open squares), ^{137}Cs (closed squares) and ^{226}Ra (circles) for core 384B (a) and 436B (b) with error bars representing 1σ uncertainties. ^{14}C dates (c) for cores 384B (blue squares) and 436B (orange circles) with error bars representing 2σ uncertainties

isotopes were plated onto pure silver discs in HCl (1N) at 70ºC while stirring for 8h. Polonium emissions were subsequently counted with α-spectrometers equipped with low-background silicon surface barrier (SSB) detectors for $4 \cdot 10^5$s. ^{226}Ra (via ^{214}Pb through its 351 keV gamma emission line) and ^{137}Cs were determined by γ-spectrometry using a high-purity well-type Ge detector. Excess ^{210}Pb activities ($^{210}Pb_{xs}$) were determined by subtracting the ^{226}Ra activity (assumed equal to the supported ^{210}Pb activity) from the total ^{210}Pb activity (Figs. IV.2a, b).

^{14}C-AMS dates were performed on monospecific planktonic foraminifera (*Globigerina bulloides*) extracted from the >125 μm fraction and analyzed by Accelerator Mass Spectrometry (Poznan Radiocarbon Laboratory). Radiocarbon ages were calibrated to calendar years (yr AD) using the CALIB 6.0 software (Stuiver and Reimer, 1993) and the MARINE09 curve (Reimer et al., 2009), assuming a marine reservoir age correction of 400 yr. Data are reported with a 2σ uncertainty (Fig. IV.2c). One post-modern sample was converted to yr AD using the CaliBomb software (Reimer et al., 2004) and the calibration dataset of Levin and Kromer (2004), updated by Levin et al. (2008).

IV.2.3. Geochemical, mineralogical and sedimentological analyses

Bulk and clay mineral compositions were obtained by X-Ray Diffraction every 1 cm using a PANalytical X'Pert PRO diffractometer with Cu-Kα radiation and automatic slit. Clay fraction separation and sample preparation was performed according to the international recommendations compiled by Kisch (1991). Diffractograms were visually interpreted using Xpowder software (Martin, 2004; http://www.xpowder.com). Peak areas were measured in order to estimate semi-quantitative mineral contents, the estimated error being <5% for bulk mineral composition and 5-10% for clay mineral proportions.

Quantitative geochemical microanalyses every five centimetres for clay mineral characterization were achieved by High-Resolution Transmission Electron Microscopy (HR-TEM) Philips CM-20 provided with and EDAX microanalysis system. Additional morphological analyses of clays, barite and pyrite from selected samples were acquired by Field Emission Scanning Electron Microscopy (FE-SEM) LEO-Carl Zeiss-GEMINI-1530. Barite was separated from selected samples with higher Ba content by a sequential lea-

ching procedure (Eagle et al., 2003).

Major elements were measured using Wavelength Dispersive X-Ray Fluorescence Spectrometry (WDXRF; Bruker AXS S4 Pioneer with an Rh anode X-ray tube), using pressed pellets, with an analytical detection limit of 0.1% and an instrumental error <1%. Trace elements were analyzed by Inductively Coupled Plasma-Mass Spectrometry (ICP-MS; Perkin-Elmer Sciex Elan 5000) using Re and Rh as internal standards with an instrumental error of ±2% and ±5% for elemental concentrations of 50 ppm and 5 ppm, respectively (Bea, 1996). Samples were prepared by sequential acid digestion (HNO_3+HF) and measured in triplicate.

TOC content was determined every 1 cm using a Horiba EMIA-320V Series Carbon/Sulfur Analyzer. Grounded samples were subjected to acid leaching (HCl) onto glass fiber filters in order to remove inorganic carbon. Treated samples were oxidized by the high-frequency induction furnace method under an oxygen stream, and CO_2 gases evolved were detected by calibrated infra-red (IR) cells. TOC content was expressed as a percentage of dry weight. The accuracy of the method is 92%, and precision is 0.01%.

A granulometric study was undertaken on the bulk fraction at 2 cm intervals, removing the coarse fraction (>63 μm) by wet sieving and, carbonates and organic matter from the remaining silt (2-63 μm) and clay fraction (<2 μm) by treatment with acetic acid (three times during 24 hours each round, using 5 $ml \cdot L^{-1}$ in the first acid attack and then 10 $ml \cdot L^{-1}$ in the other two) and hydrogen peroxide (10%, one week), respectively. Grain size was determined as a cumulative mass percentage using a Micromeritic Sedigraph III 5120, which measures particles ranging from 0.10 to 63 μm. Resolution and accuracy are, respectively, 1 and 0.1 μm. Two split fractions were established for the terrigenous silt: a) fine silt (2-10 μm), cohesive, mainly composed of clay minerals and settled as aggregated material, and b) coarse silt (10-63 μm) or sortable silt (SS), predominantly composed of quartz and feldspar, and with non-cohesive behaviour.

Statistical treatment of analytical data was performed using the statistical software package R (Development Core Team, 2011). The normalized geochemical dataset was clustered in order to find groups of variables showing similar behaviour. The complete linkage method (or furthest neighbour method)

was used for clustering purposes. Redundancy Analyses (RDA) were carried out on the geochemical and the mineralogical data set using the "vegan" package (Oksanen, 2009) to infer the relationship between them, and Principal Component Analyses (PCA) were performed on the geochemical data set to characterize the main underlying gradients governing the sedimentary environment. The correlation coefficient of Pearson (r) was calculated on 49 and 53 samples in core 384B and 436B respectively to evaluate the relationship between variables.

IV.3. Age-depth model and sedimentation rate

$^{210}Pb_{excess}$ ($^{210}Pb_{xs}$), ^{226}Ra and ^{137}Cs activity profiles of cores 384B and 436B are shown in Fig. IV.2. In both cores, the maximum ^{210}Pb concentrations are observed at the top of the core and decreases downwards in both cores to 12.5 and 14.5 cm depth, respectively. The maximum sedimentation rates obtained using the CF:CS model are 1.49±0.13 mm·yr^{-1} for core 384B and 1.41±0.12 mm·yr^{-1} for core 436B. These sedimentation rates are slightly higher than those derived by Masqué et al. (2003) in sediment cores collected in the same area. The chronological models obtained from these sedimentation rates do not agree with those obtained from the ^{137}Cs concentrations. In fact, the $^{210}Pb_{xs}$ concentration profile does not show the exponential curve expected from radioactive decay due to the presence of some intervals where $^{210}Pb_{xs}$ activity remains roughly constant. Cores were collected close to the continental margin, and variations in the ^{226}Ra concentration are used as a good indicator of changes in sediment composition in agreement with the geochemical results described above, allowing interpretation of the $^{210}Pb_{xs}$ profile as influenced by rapid sedimentation rather than bioturbation (García-Orellana et al., 2006). The most plausible sedimentation rate applying the CF:CS model to the exponential profile of each core are 0.69±0.04 mm·yr^{-1} for core 384B and 0.85±0.05 mm·yr^{-1} for core 436B. These sedimentation rates agree better with ^{137}Cs activity profile with the 1963 yr AD maximum at 4.75 cm and 3.75 cm, respectively, when ^{137}Cs was widely distributed from nuclear weapons testing (Figs. IV.2a, b).

^{14}C-derived linear sedimentation rates are 0.30±0.002 and 0.31±0.002 mm·yr^{-1} for cores 384B and 436B respectively, which are consistent with other sediment records from the area (Masqué et al., 2003) (Fig. IV.2c). ^{210}Pb values are approximately two times higher than those produced by ^{14}C

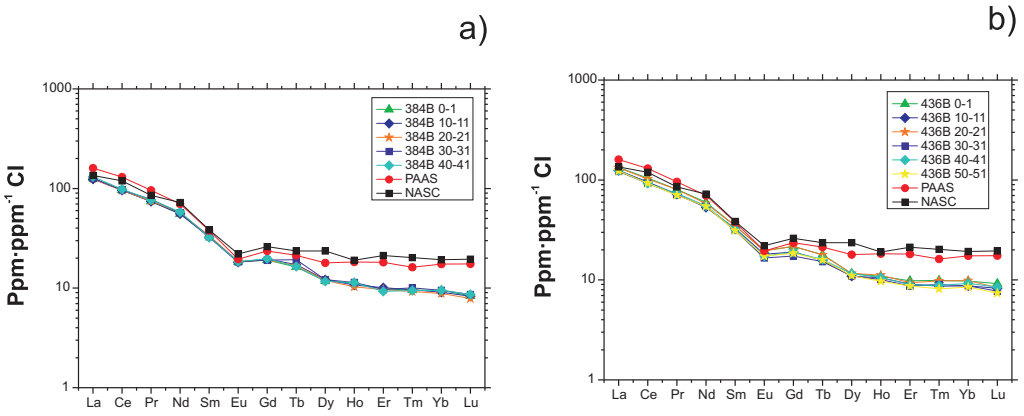

Figure IV.3. CI chondrite-normalized REEs patterns (ppm·ppm^{-1} CI) every ten centimetres for cores 384B (a) and 436B (b) compared with the standard REE pattern of the NASC and the PAAS (McLennan, 1989)

chronology. The differences between ^{210}Pb and ^{14}C-derived age models are well documented; sedimentation rates from the ^{210}Pb dating of sediment cores may be considered as an upper limit (Benninger et al., 1979; Nittrouer et al., 1984). In the case of Alboran Sea, considered a relatively high productivity and margin influenced area, surface mixing layers and bioturbation rates ranges from 3 to 9 cm and from 0.2 to 15 cm^2 ·yr^{-1} (Masqué et al., 2003) and therefore the discrepancy between both dating methods is well justified.

IV.4. Results: Sediment composition, geochemical proxies and heavy metal concentrations

Analysed sediments are predominantly composed of clay minerals (30-70%), calcite (10-30%) and quartz (10-30%), with minor amounts of dolomite and feldspars (<10%). Clay mineral assemblages consist of detrital mica (50-80%), kaolinite (10-25%) and smectites (5-30%). Additional fibrous clay minerals, such as palygorskite and sepiolite, were identified using Transmission Electron Microscopy and Scanning Electron Microscopy, although their content quantified via X-Ray Diffraction ranges below instrumental error (<5%). The same analyses verify that the smectite composition corresponds to Al rich beidellites, indicating a detrital origin (chemical weathering) and a provenance from soils in the Iberia margin (Martínez-Ruiz et al., 2003).

At both sites, REE values display a CI-normalized pattern (McDonough and Sun, 1995) parallel to the average upper continental crust composition with no significant change throughout

the core. This pattern consist of the classic slight L-REE enrichment relative to H-REE depletion and a negative Eu-anomaly, as well as values lower than the North American shale composite (NASC) and the Post-Archean Australian average shale (PAAS) (McLennan, 1989) (Figs. IV.3a, b). Additionally, its inclusion in the detrital group due to its high correlation with clay minerals, points to REE as reliable indicators for tracing source provenance, as they are transferred nearly quantitatively in the terrigenous component through erosion and sedimentation into the Alboran basin.

Rb/Al and REE/Al ratios exhibit a similar profile in both cores (Fig. IV.5). An increase in these ratios is observed at 500-800, 950-1150 and 1800-1950 yr AD and high values are observed at 1550-1800 yr AD. Decreasing trends are recognized at 800-950, 1150-1300, 1300-1550, 1800-1950 yr AD and during the second half of the twentieth century. Zr/Al ratio shows an opposed tendency during those time periods instead. Considering Zr as a typically eolian proxy, enriched in loess and Saharan dust and being mainly carried by wind-blown dust (e.g., Moreno et al., 2002), and Rb as a fundamentally fluvial input indicator, which substitutes potassium in aluminosilicate minerals, we used these elements to calculate detrital elemental ratios such as Si/Zr, K/Zr and Zr/Rb, with the aim of enhancing eolian/fluvial fluctuations signals. Zr/Rb exhibits more clear decreasing (500-800, 1000-1100, 1300-1500, 1590-1650, and 1750-1900 yr AD) and increasing tendencies (800-1000, 1100-1300, 1500-1590, 1650-1750, and 1900-2010 yr AD). As for Si/Zr and K/Zr ratios, opposite trends are observed. Low amplitude changes presented by Rb/Al and REE/Al during the second half of the twentieth century are clearly evidenced by Si/Zr and K/Zr ratios.

The first eigenvector obtained from both records (Fig. IV.5) represent detrital input into the basin. In order to acquire a more reliable and accurate result, Br and TOC were removed from the calculation of this vector, due to the non-allocthonus origin of these elements as previously revealed by the Branched versus Isoprenoid Tetraether index (BIT index), which indicated a predominant marine provenance for the sedimentary organic matter (Nieto-Moreno et al., 2012), and because organic matter is easily affected by diagenetic oxidation. Both records display a sustained raise, revealing a progressive detrital input during the whole analyzed time interval, being more sharpened in core 436B between 1300-1800 yr AD.

The mean grain size is <6 μm while the median grain size is <3 μm at both sites (Fig. IV.6). Hence, the grain size distribution consists mostly of clays (50-75%) and fine silts (30-40%) with minor proportions of coarse silt (<15%). Clays are the most abundant grain size at site 384B and fine silt at site 436B. SS values display a similar trend on both sites, with coarser sediments at 700-850 yr AD, 1300-1800 yr AD and 1960-2000 yr AD. These peaks coincide with increasing trends of the median distribution (Fig. IV.6).

Elemental ratios used to infer redox conditions in Mediterranean sapropels from the eastern Mediterranean, such as V/Cr and Ni/Co ratios (e.g., Gallego-Torres et al., 2007) were also calculated (see Fig. IV.7). Although no significant change is observed in these ratios at site 384B, there is a drastic decrease on the record from site 436B between 1470 and 1850 yr AD and 1960 yr AD onwards (Fig. IV.7).

TOC values vary between 0.7-1% at the two sites, displaying a progressive down-core decline (Fig. IV.8) punctuated by relative maxima around 1725, 1650, 1460, 1240, and 900 yr AD in both cores. Br/Al ratio mainly mirrors the TOC content trend, supporting the high correlation between Br and marine organic matter (Figs. IV.4, 8) and providing a semiquantitative estimation of sedimentary organic matter (Ziegler et al., 2008). Sr and Ca follow a sustained decrease during the last 2000 yr (Fig. IV.8), in accordance with the opposed tendency of the detrital input shown by the first eigenvector (Fig. IV.5). Mg/Al ratio is reflecting the same progression throughout core 436B (Fig. IV.8) whereas on site 384B, Mg behaves differently between 1300-1800 yr AD when it shows a raising trend coinciding with the detrital component (Fig. IV.5).

Mn, Co and Mo are only enriched in the upper 2 cm of the section, presenting constantly low values throughout the rest of the core (Fig. IV.9). Increased concentrations of Cu, Zn and Pb are recorded in the upper 15 cm of both cores (Table IV.3), while relatively constant concentrations are found downcore (Fig. IV.11). A progressive raise of these ratios from 1750 yr AD and a steep increase from 1950 yr AD to present times is observed, when maximum values are reached, although describing a slight decrease at 1975-1990 yr AD. Maximum concentrations of these elements are recorded in the upper 2 cm in both cores, coinciding with Mn enrichments (Figs. IV.9, 11).

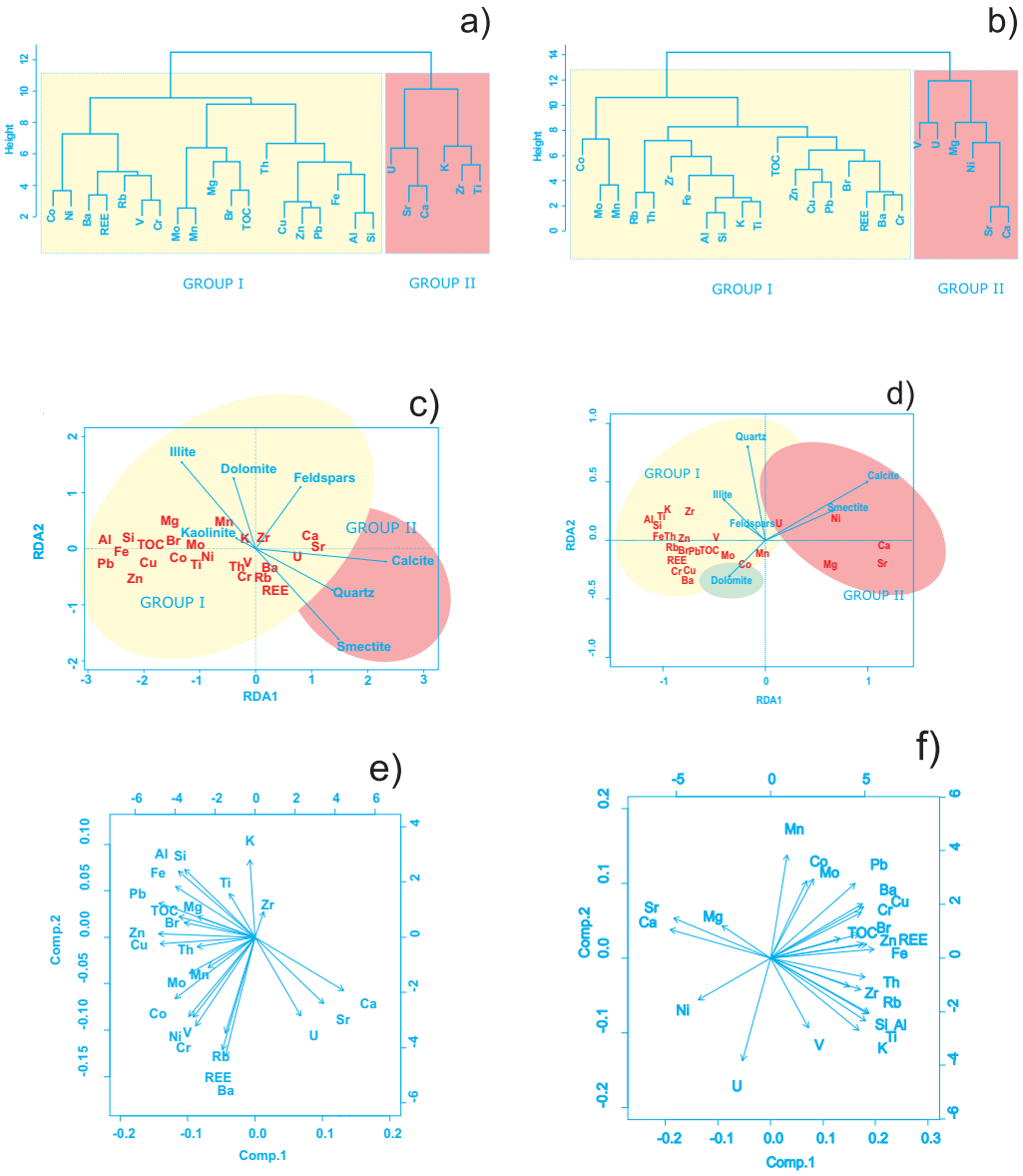

Figure IV.4. Statistical treatment of data from both sites. Cluster analyses of the geochemical data for sites 384B (a) and 436B (b), and RDA biplots for sites 384B (c) and 436B (d). Light yellow and red areas indicate Group I and II, respectively. Biplots showing the first and the second eigenvector defined by PCA for sites 384B (e) and 436B (f)

IV.5. Statistical analyses and interpretation; an insight into paleoclimatic reconstruction

A multivariate statistical strategy has been applied to the mineralogical and geochemical data sets in order to disentangle the main contribution of the different processes controlling se-

Table IV.1. Pearson's correlation coefficients between major and trace elements, REE and TOC for core 384B

	Rb	Sr	Ba	V	Cr	Co	Ni	Cu	Zn	Mo	U	Th	REE	Zr	Al	Fe	Ca	Mg	K	Mn	Si	Ti	Pb	Br	TOC
Rb	1																								
Sr	0.15	1																							
Ba	**0.72**	0.18	1																						
V	0.79	-0.19	0.7	1																					
Cr	0.73	-0.21	0.77	**0.88**	1																				
Co	0.34	-0.32	0.51	0.56	0.65	1																			
Ni	0.48	-0.11	0.57	**0.72**	**0.73**	0.83	1																		
Cu	0.35	-0.59	0.27	0.65	0.55	0.71	0.65	1																	
Zn	0.26	-0.67	0.28	0.55	0.5	0.69	0.56	**0.89**	1																
Mo	0.02	-0.24	0.26	0.22	0.32	**0.88**	0.59	0.51	0.54	1															
U	0.28	0.49	0.33	0.22	0.13	-0.23	0.06	-0.36	-0.43	-0.29	1														
Th	0.32	-0.07	0.11	0.42	0.27	0.35	0.46	0.63	0.58	0.28	-0.1	1													
REE	**0.78**	0.12	**0.86**	0.76	0.78	0.42	0.55	0.33	0.31	0.18	0.47	0.34	1												
Zr	0.02	0.02	-0.11	0.06	0.03	-0.12	0.02	-0.12	-0.12	-0.18	0.09	0.02	-0.12	1											
Al	0.08	-0.72	-0.13	0.36	0.24	0.25	0.21	**0.7**	**0.7**	0.16	-0.47	0.45	0.01	0.06	1										
Fe	0.03	-0.69	-0.03	0.34	0.31	0.43	0.4	0.7	0.77	0.28	-0.44	0.49	0.03	0.32	0.73	1									
Ca	-0.05	**0.8**	0.06	-0.32	-0.27	-0.46	-0.29	-0.82	-0.84	-0.36	0.6	-0.48	-0.01	0.16	-0.85	-0.77	1								
Mg	-0.09	-0.32	0.05	0.11	0.09	0.35	0.17	0.45	0.47	0.49	-0.38	0.21	0.04	-0.37	0.49	0.22	-0.49	1							
K	0.03	-0.25	-0.3	0.09	-0.07	-0.42	-0.27	0.04	0.01	-0.51	-0.05	0.12	-0.16	0.47	0.57	0.38	-0.22	-0.04	1						
Mn	-0.04	-0.19	0.18	0.08	0.17	**0.74**	0.4	0.32	0.32	**0.92**	-0.25	0.01	0.05	-0.2	0.05	0.06	-0.22	0.49	-0.51	1					
Si	0.05	-0.64	-0.13	0.35	0.23	0.18	0.21	0.64	0.62	0.07	-0.36	0.44	0.01	0.22	0.94	0.78	-0.75	0.45	0.67	-0.05	1				
Ti	0.13	-0.28	-0.13	0.22	0.18	-0.01	0.07	0.19	0.21	-0.13	-0.02	0.24	0.01	**0.65**	**0.46**	0.58	-0.21	-0.17	0.64	-0.21	0.59	1			
Pb	0.11	-0.8	0.06	0.43	0.4	0.62	0.45	**0.9**	**0.92**	0.5	-0.61	0.5	0.09	-0.13	**0.81**	0.79	-0.94	0.5	0.12	0.33	0.7	0.22	1		
Br	-0.15	-0.47	0.13	0.1	0.14	0.58	0.31	**0.54**	**0.64**	0.7	-0.47	0.22	0	-0.26	0.33	0.49	-0.62	0.63	-0.26	0.64	0.29	-0.13	**0.65**	1	
TOC	0.03	-0.49	0.09	0.17	0.21	0.59	0.3	**0.57**	**0.67**	0.67	-0.56	0.25	0	-0.2	0.47	0.51	-0.66	0.62	-0.09	0.61	0.38	0.07	**0.7**	**0.83**	1

dimentary deposition in the study area. Normalized matrix clustering of the geochemical data and RDA biplots between the geochemical and mineralogical datasets allowed us to identify the main geochemical families and to establish the origin and their relationships with the associated mineral phases, respectively. PCA and Pearson's correlation coefficients have been applied to characterize the major processes controlling the sedimentary regime and the relationship between the variables, respectively (Figs. IV.4a, b, c, d).

Two main groups were defined in both cores in accordance with their provenance based on cluster analyses (Fig. IV.4 a, b). The first group mainly comprises elements/minerals of typical detrital origin, both fluvial and eolian, as well as other elements of exogenous

Table IV.2. Pearson's correlation coefficients between major and trace elements, REE and TOC for core 436B

	Rb	Sr	Ba	V	Cr	Co	Ni	Cu	Zn	Mo	U	Th	REE	Zr	Al	Fe	Ca	Mg	K	Mn	Si	Ti	Pb	TOC	Br
Rb	1																								
Sr	-0.66	1																							
Ba	**0.69**	-0.57	1																						
V	0.58	-0.35	0.06	1																					
Cr	0.71	-0.56	0.92	0	1																				
Co	0.38	-0.08	0.39	0.46	0.31	1																			
Ni	-0.4	**0.52**	-0.76	0.41	-0.84	0.11	1																		
Cu	0.68	-0.62	0.89	0.27	0.83	0.52	-0.57	1																	
Zn	0.66	-0.75	0.68	0.36	0.6	0.31	-0.43	0.78	1																
Mo	0.19	-0.28	0.32	0.11	0.26	**0.51**	-0.21	0.38	0.41	1															
U	0.05	0.15	-0.4	0.29	-0.33	-0.37	0.32	-0.38	-0.31	-0.18	1														
Th	0.91	-0.71	0.74	0.47	0.73	0.31	-0.48	0.72	0.74	0.28	0.01	1													
REE	**0.86**	-0.65	**0.91**	0.2	0.92	0.31	-0.74	0.82	0.66	0.24	-0.16	0.89	1												
Zr	0.51	-0.61	0.51	0.22	0.52	0.08	-0.45	0.49	0.53	0.26	-0.04	0.53	0.53	1											
Al	0.75	-0.93	0.56	0.47	0.56	0.15	-0.44	0.59	0.7	0.25	-0.05	0.76	0.67	0.66	1										
Fe	0.65	-0.84	0.76	0.24	0.73	0.3	-0.63	0.75	0.77	0.43	-0.38	0.7	0.74	0.74	0.84	1									
Ca	-0.75	**0.96**	-0.65	-0.37	-0.65	-0.19	**0.55**	-0.68	-0.75	-0.34	0.16	-0.77	-0.74	-0.56	-0.94	-0.86	1								
Mg	-0.31	**0.51**	-0.27	-0.16	-0.27	-0.02	0.28	-0.29	-0.35	-0.05	0.03	-0.27	-0.32	-0.42	-0.38	-0.44	**0.45**	1							
K	0.67	-0.84	0.45	0.46	0.46	0.07	-0.36	0.47	0.59	0.17	0.03	0.67	0.57	0.73	0.94	0.81	-0.82	-0.38	1						
Mn	-0.06	-0.02	0.18	-0.13	0.14	**0.49**	-0.13	0.2	0.18	0.87	-0.26	0.03	0.07	0.12	-0.02	0.24	-0.06	0.03	-0.08	1					
Si	0.74	-0.91	0.59	0.43	0.59	0.1	-0.49	0.61	0.71	0.21	-0.08	0.78	0.7	0.71	0.98	0.86	-0.91	-0.39	0.94	-0.04	1				
Ti	0.72	-0.87	0.54	0.42	0.56	0.06	-0.48	0.54	0.65	0.22	0.04	0.73	0.68	**0.8**	**0.93**	0.85	-0.85	-0.47	0.95	-0.01	0.95	1			
Pb	0.5	-0.59	0.77	0.14	0.7	0.55	-0.5	**0.85**	**0.77**	0.47	-0.64	0.58	0.63	0.43	0.53	0.77	-0.63	-0.23	0.42	0.33	0.54	0.44	1		
TOC	0.34	-0.52	0.55	0.08	0.59	0.15	-0.5	**0.61**	**0.58**	0.1	-0.41	0.4	0.51	0.45	0.47	0.66	-0.49	-0.33	0.44	-0.06	0.51	0.49	0.59	1	
Br	0.56	-0.67	0.73	0.14	0.71	0.19	-0.64	**0.74**	**0.68**	0.48	-0.14	0.66	0.7	0.61	0.63	0.76	-0.7	-0.26	0.56	0.27	0.63	0.66	0.65	0.46	1

provenance (Pb, Zn, Cu). The second group includes elements deposited by processes occurred within the basin, mainly related to paleoproductivity (Ca, Sr). In both cores, Ba show a high statistical significance with Rb and REE (Tables IV.1, 2), thus pointing to a detrital origin and absence of Ba excess. Although Ba/Al ratio has been widely used as a paleoproductivity proxy in relation to episodes of enhanced productivity such as the Heinrich events (Moreno et al., 2004; Jiménez-Espejo et al., 2007), on this time range no Ba excess related to biogenic barite was registered. Pb, Zn and Cu are only present in considerable concentration in recent sediments, and are interpreted to be mainly sourced by industrial activity (see below). Significant exceptions must be interpreted in relation to the oceanographic setting and geographic location of each site. Redox-sensitive elements (V, Cr, Ni, Co, Mo, and Mn) provide information on bottom water oxygenation conditions (Martínez-Ruiz et al., 2003; Moreno et al., 2004; Rogerson et al., 2008). Taking into account the oceanographic setting (intense water masses mixing and strong currents) remarkable changes in redox conditions are unlikely. Thus, elements such as V, Cr or Ni suffer only minor changes (Fig. IV.7) and can only precipitate adsorbed onto clay minerals, as evidenced by the high correlation between them and REE or Rb (Tables IV.1, 2). U-fixation, another redox indicator, only occurs under suboxic conditions, hardly reachable on this environment, and thus U is linked to Ca and Sr rather than related to carbonate precipitation (e.g., Mecee and Benninger, 2002). On the other hand, Mn constitutes insoluble oxy-hydroxides under oxic conditions, often including Co and Mo in their lattice (Tribovillard et al., 2006). A second exception is TOC, which instead of grouping with productivity proxies, appears highly correlated to fluvial-derived elements (Tables IV.1, 2). The high correlation between Br and marine organic matter is due to favored uptake of bromine from seawater by marine plants (ten Haven et al., 1988; Ziegler et al., 2008) (Tables IV.1, 2). Ti has been widely interpreted as an eolian proxy (e.g., Wehausen and Brumsack, 1999). In our dataset Ti shows good correlation with Zr and a moderate correlation with Al (Tables IV.1, 2; Figs. IV.4a, b), indicating a predominant eolian component with minor fluvial origin. K also show a good correlation with Zr and Ti in core 384B (Table IV.1, Fig. IV.4a), thus pointing to an eolian contribution. Finally, Mg also shows a mixed behaviour, being partly associated with carbonates in the form of dolomite and Mg-rich calcite, and partly related

to smectites and chlorites (Table IV.2, Fig. IV.4b).

Similarly, RDA biplots display two main groups of chemical elements and associated mineral phases (Figs. IV.4c, d). Group I encompasses detrital mineral phases of fluvial (illite, dolomite, feldspars) and eolian (kaolinite) origin associated with the chemical elements previously included in this group, and Group II include mineral phases related to productivity (calcite). In core 436B, dolomite appears between both groups, suggesting the existence of both authigenic and fluvial-derived dolomite. Smectite, although its composition indicated a detrital origin as stated before, it is included in the second group, probably due to a relationship between bacterial bloom and nutrient supply via detrital input in both cores.

The first two eigenvectors of PCA account for 60% of the total variance at site 384B and for 67% at site 436B. The first eigenvector represents 40% of the total variance at site 384B and 55% at site 436B, and is mainly controlled by the detrital-productivity group, whereas the second eigenvector represents 20% of the total variance at site 384B and 12% at site 436B, and it is mainly triggered by those elements associated to detrital-productivity processes (Figs. IV.4e, f). This result agrees with the differences in the location of these sites, which may have resulted in different processes controlling sediment deposition. Site 436B is located close to the influence of fluvial discharge from the Iberian margin and thus more affected by detrital input (Fig. IV.1). In contrast, site 384B is located in a comparatively more distal position offshore.

IV.6. Paleoclimate and paleoceanographic conditions

Considering the statistical discrimination of elements and its interpretation in terms of their origin, we address a reconstruction of the paleoclimatic and paleoceanographic conditions during the last two millennia in the westernmost Mediterranean using this geochemical and mineralogical dataset as proxies for detrital input oscillations, marine productivity, oxygenation conditions and grain size distribution as well as post-depositional alteration.

IV.6.1. Grain size distribution, oxygen conditions, and post-depositional alteration

Grain size distribution presents slight differences between the two sites, being site 436B dominated by coarser sediment (fine silts), which is likely due

to the different location of these cores in the basin. Site 436B is more influenced by the eastward shift of the Atlantic jet stream while progressing into the Mediterranean Sea, arising two anticyclonic gyres (Western and Eastern Alboran Gyres) (Millot, 1999) with a high biological productivity associated at the northern and eastern edge of both gyres (Sarhan et al., 2000) (Fig. IV.1). This paleocurrent configuration as well as closer location to the margin may have promoted slightly coarser sediments settle at site 436B.

This oceanographic pattern also affects bottom water currents and thus ventilation and redox-sensitive elements fixation. As mentioned above, V, Cr and Ni precipitation is very low, thus suggesting that sedimentation occurred under oxygenated bottom waters conditions. A remarkable change in bottom water circulation is evident at site 436B (1470-1850 yr AD). Lower V/Cr and Ni/Co ratios indicate more intense circulation, supported by coarser grain size (Fig. IV.6). This intensification is attributed to enhanced Atlantic jet stream incoming into the Mediterranean Sea due to a weakened North Atlantic Deep Water (NADW) production reported for this period (as much as 10% weaker) (Trouet et al., 2011 and references therein). Cold spells and reduced NADW were previously invoked to explain fresh polar-derived waters reaching the Alboran basin (Sierro et al., 2005; Rogerson et al., 2010), thus we claim a similar mechanism.

Both sites exhibit uniform Mn/Al profiles except for the surficial increases in the first two centimetres depth (Fig. IV.9) derived from oxidation. Mn enrichments above the redoxcline point to the typical boundary on oxic/suboxic pelagic sediments reported in uppermost hemipelagic sediments in the western Alboran Sea (e.g., Masqué et al., 2003). Co/Al and Mo/Al are also enriched in the post-depositional oxidation front at both sites, having most likely co-precipitated together with Fe and Mn oxy-hydroxides (Fig. IV.9).

IV.6.2. Paleoclimatic and paleoceanographic evolution during the last two millennia

The combination of the geochemical signal produced by eolian/fluvial input together with sedimentological and geochemical reconstruction of paleoceanographic conditions allows a description of climate evolution in the region for the last two millennia.

The oldest part of our record and up to 800 yr AD is supporting pro-

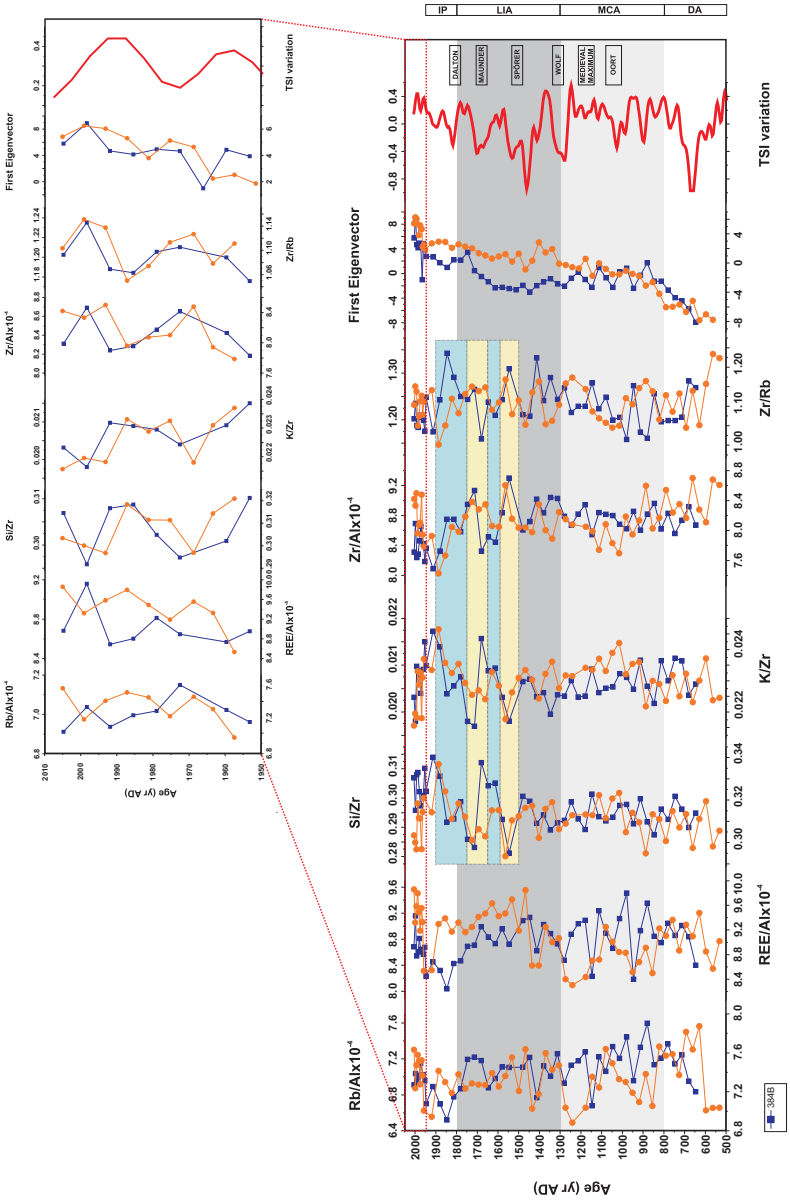

Figure IV.5. Age-depth profile of detrital proxies (Rb/Al, REE/Al: 10^{-4} ratios, Si/Zr, Zr/K, Zr/Al and Zr/Rb ratios) for cores 384B (blue squares) and 436B (orange circles). First eigenvector of cores 384B (blue squares) and 436B (orange circles) compared with the TSI variations ($W \cdot m^{-2}$) during the last 2000 yr (30-point smoothed, red line) (Steinhilber et al., 2009). Light grey bars indicate dry periods (MCA: Medieval Climate Anomaly), dark grey bars indicate humid periods (LIA: Little Ice Age), DA = Dark Ages, IP = Industrial Period. Blue and yellow bars indicate wet and dry periods in Andalusia (South of the Iberian Peninsula) as inferred from rainfall series reconstructions (Rodrigo et al., 1999). Periods of decreased (Oort, Wolf, Spörer, Maunder and Dalton Minimum) and increased (Medieval Maximum) sunspots activity are also indicated at the right side of the figure

gressive wetter conditions at both sites, evidenced by the increase of typical fluvial derived-elements such as Rb/Al and REE/Al ratios, relatively high and constant values of Si/Zr and K/Zr ratios, and an concomitant decrease of the Zr/Al and Zr/Rb ratios, associated to Saharan eolian input oscillations (Fig. IV.5). The first eigenvector also show a raise of the detrital input into the basin at both sites, coming from the driest conditions attained in the whole record at ~600 yr AD (Fig. IV.5). The deposition of finer grain size sediments (low SS values) and high redox-sensitive elements values (V/Al, V/Cr and Ni/Co) indicate relatively low energetic flows and less oxygenated bottom waters (Figs. IV.6, 7). Accordingly, TOC content and Br/Al ratios remains relatively high and without any substantial fluctuation (Fig. IV.8), thus indicating organic matter preservation due to slower oxygen replenishment in bottom waters and higher detrital input into the basin (Figs. IV.5 and 7).

Following this humid period, prevalent dryness is suggested by declining trends of fluvial input into the basin. Minimum values in ratios of fluvial-derived elements are reached in both cores (Si/Zr and K/Zr ratios) around 900 yr AD, and Saharan eolian input (Zr/Al and Zr/Rb ratios) is high between 800-1000 and 1100-1300 yr AD (Fig. IV.5). A pulse of higher fluvial activity (Rb/Al peak) is observed between 1100 and 1000 yr AD. Lower Saharan eolian input is also showed (Zr ratios) during this intermediate wetter period (Fig. IV.5). The first eigenvector describes a moderate and steady trend throughout this time interval, although drawing higher detrital input into the basin in relation to the previous phase (Fig. IV.5). No significant change in paleocenographic conditions is observed and a moderate hydrodynamic situation is still outlasting in the western Mediterranean as suggested by an essentially fine grain size (continuously low SS values) (Fig. IV.6) and concentration of redox-sensitive elements (V/Cr and Ni/Co; Fig. IV.7). Respectively, organic matter is partially preserved (no significant fluctuations of TOC content and Br/Al ratios) (Fig. IV.8), as expected under these conditions of moderate bottom currents.

Progressively wetter conditions govern from 1350 to 1450 yr AD (approx.), thereby, higher riverine input into the basin is manifested by a rise in fluvial-derived elements (Fig. IV.5). A concomitant decrease of the Zr/Al and Zr/Rb ratios also takes place, which indicates lower Saharan eolian input (Fig. IV.5). This is followed by another brief

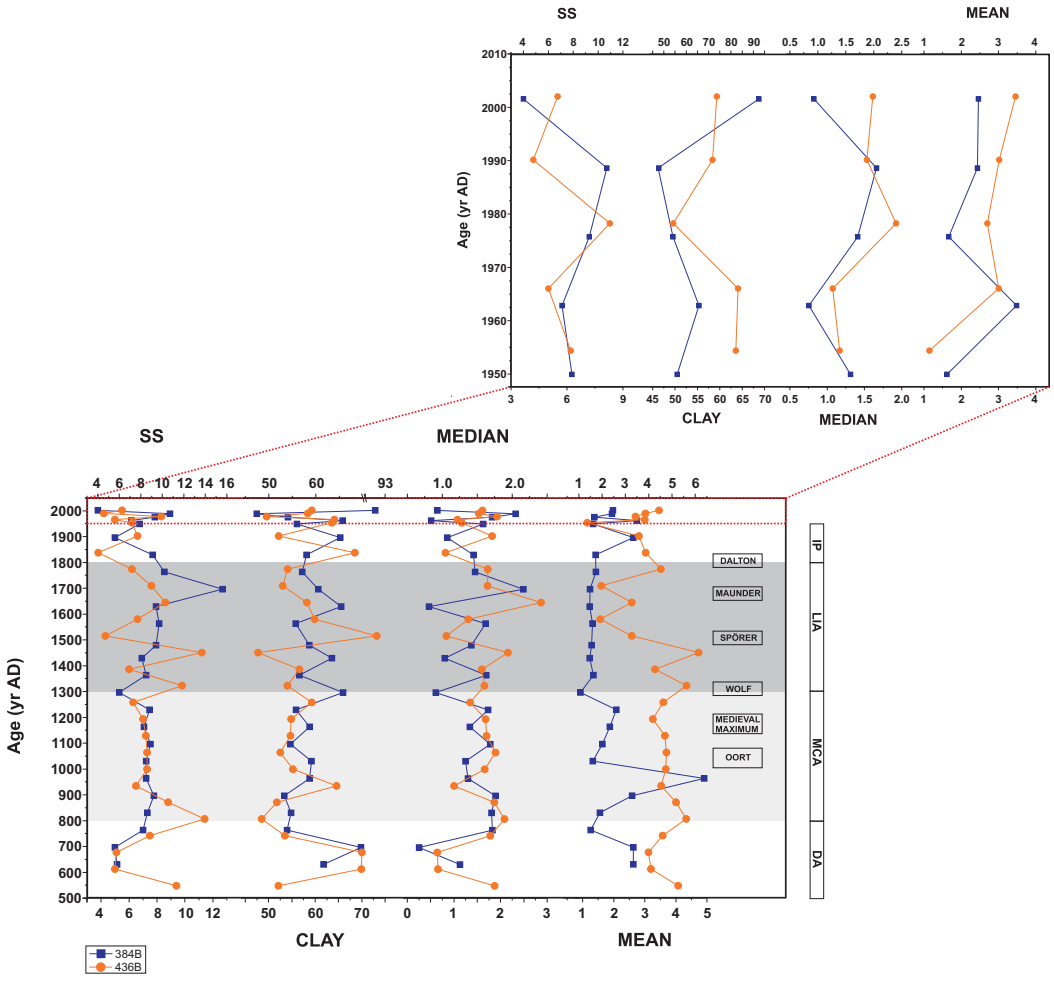

Figure IV.6. Age-depth profile of grain size distribution: SS (%), clay (%), median and mean (μm) for cores 384B (blue squares) and 436B (orange circles). Light grey bars indicate dry periods (MCA: Medieval Climate Anomaly), dark grey bars indicate humid periods (LIA: Little Ice Age), DA = Dark Ages, IP = Industrial Period. Periods of decreased (Oort, Wolf, Spörer, Maunder and Dalton Minimum) and increased (Medieval Maximum) sunspots activity are also indicated at the right side of the figure

period of dryness and higher eolian supply, returning to humid conditions around 1575 yr AD. The first eigenvector delineate a continuous increase of the detrital input all over this time interval in both cores, also suggesting wetter conditions during this time interval (Fig. IV.5). In core 436B, outstanding wetter conditions are noticeable, probably due to the proximity of this core to the Iberian margin (Fig. IV.1), which is more affected by fluvial discharge as stated before (Fig. IV.4).

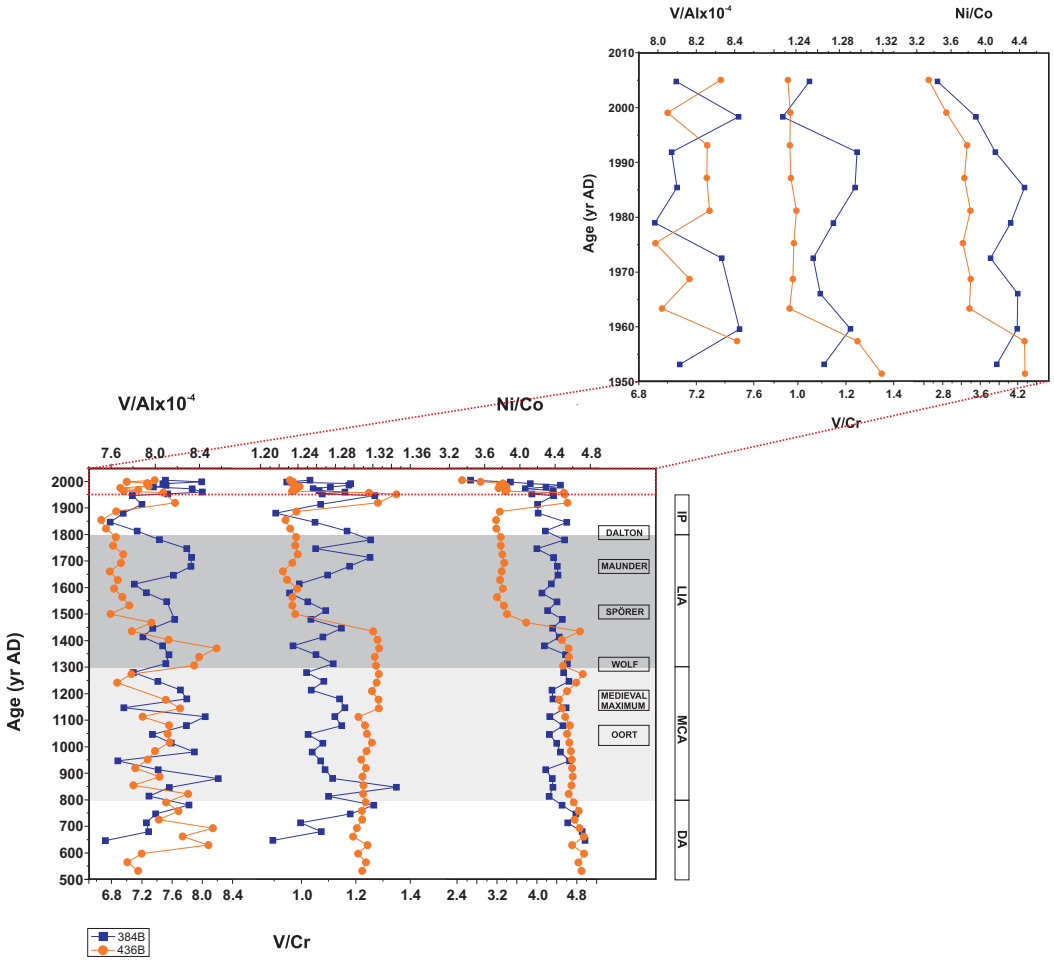

Figure IV.7. Age-depth profile of redox proxies (V/Al·10⁻⁴, V/Cr and Ni/Co ratios) for cores 384B (blue squares) and 436B (orange circles). Light grey bars indicate dry periods (MCA: Medieval Climate Anomaly), dark grey bars indicate humid periods (LIA: Little Ice Age), DA = Dark Ages, IP = Industrial Period. Periods of decreased (Oort, Wolf, Spörer, Maunder and Dalton Minimum) and increased (Medieval Maximum) sunspots activity are also indicated at the right side of the figure

In connection with this framework, a noteworthy change in paleoceanograhic conditions takes place at ~1450 yr AD, lasting until 1900 yr AD. A sudden decrease of redox-sensitive elements in core 436B (V/Cr and Ni/Co ratios) together with higher SS values in both cores indicates more energetic bottom currents after 1450 yr AD (Figs. IV.6, 7). As explained on the previous section, this phase of higher hydrodynamic condition coincides with a period of decreased NADW formation, allowing the entrance in the Mediterra-

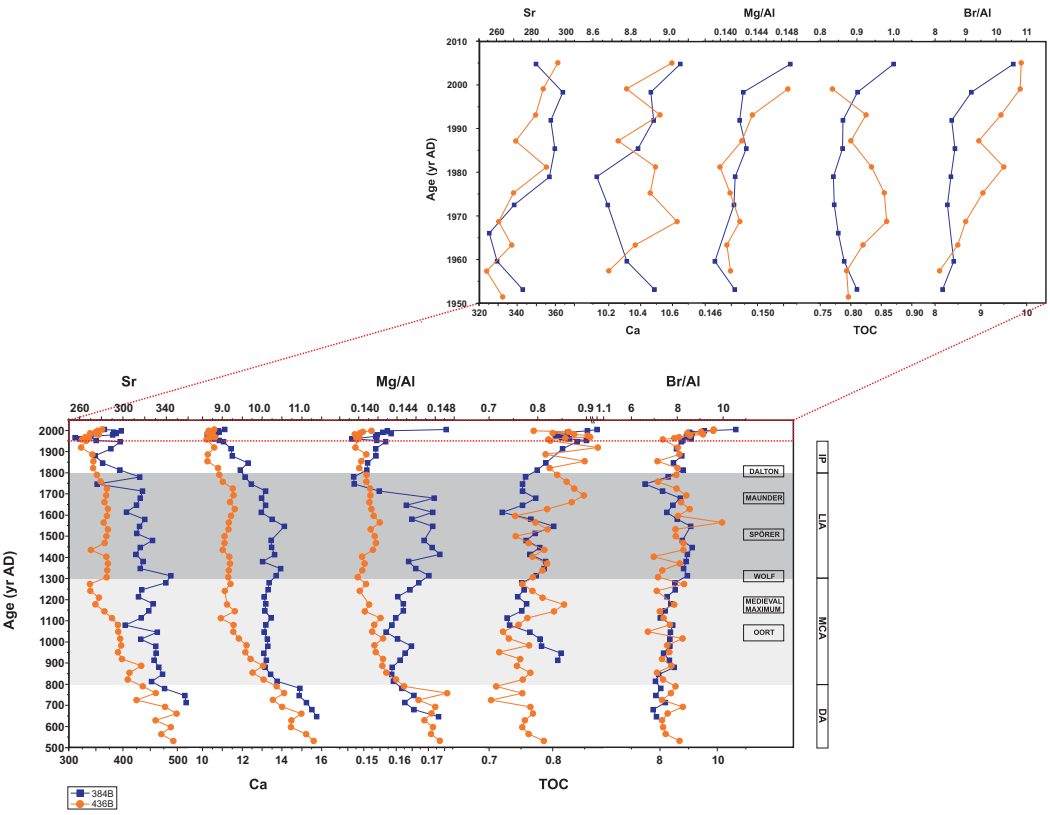

Figure IV.8. Age-depth profile of paleo-productivity proxies (Sr, Ca, TOC content, Mg/Al and Br/Al ratios) for cores 384B (blue squares) and 436B (orange circles). Light grey bars indicate dry periods (MCA: Medieval Climate Anomaly), dark grey bars indicate humid periods (LIA: Little Ice Age), DA = Dark Ages, IP = Industrial Period. Periods of decreased (Oort, Wolf, Spörer, Maunder and Dalton Minimum) and increased (Medieval Maximum) sunspots activity are also indicated at the right side of the figure

nean of cold polar-derived waters. This current produces an anticyclonic gyre while progressing eastwards into the Mediterranean Sea (the Western Alboran Gyre) whose intensification might favors both the upwelling activity and the ventilation of Western Mediterranean Deep Water (WMDW) (Naranjo et al., 2011).

The period between 1550 yr AD and the beginning of the industrial period is characterized by progressively wetter conditions punctuated by sudden increases of fluvial derived-elements occurring at ~1500, 1700 and 1800 yr AD, parallel to the Saharan eolian input decline (Zr/Al and Zr/Rb ratios) in both cores. TOC values and Br/Al ratios depict roughly higher values than previous periods in both records (Fig. IV.8), and three small but clear increa-

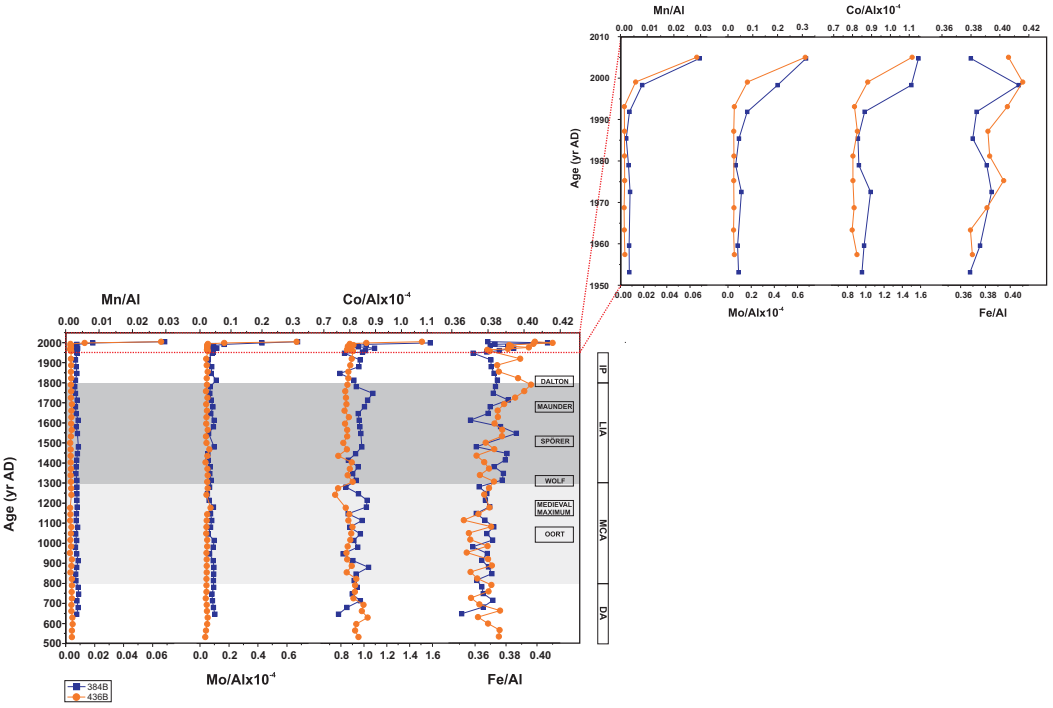

Figure IV.9. Age-depth profile of post-depositional proxies (Co/Al and Mo/Al·10⁻⁴, Mn/Al and Fe/Al ratios) for cores 384B (blue squares) and 436B (orange circles). Light grey bars indicate dry periods (MCA: Medieval Climate Anomaly), dark grey bars indicate humid periods (LIA: Little Ice Age), DA = Dark Ages, IP = Industrial Period. Periods of decreased (Oort, Wolf, Spörer, Maunder and Dalton Minimum) and increased (Medieval Maximum) sunspots activity are also indicated at the right side of the figure

ses broadly coincide with the increase in fluvial derived material that promoted higher organic productivity (Fig. IV.5). The first eigenvector delineate a strengthened increase of the detrital input all over this time interval in both cores.

The increasing wetter conditions are prolonged over the recent Industrial Era as reflected by raising trends of fluvial-derived elements (more evident for Si/Zr and K/Zr ratios). A long-lasting decline of the Saharan eolian input (Zr/Al and Zr/Rb ratios) is also observed in both records (Fig. IV.5, blue bar). Therefore, even wetter conditions are attained during this period, as also evidenced by the first eigenvector of both cores, which shows higher detrital input into the basin (Fig. IV.5). Core 436B, located closer to the Iberian margin (Fig. IV.1) and under a strengthened influence of fluvial discharge (Fig. IV.4), displays higher detrital input (Fig. IV.5). A return into a moderate hydrodynamic situation, consisting of slower bottom currents and less oxygenated

bottom water conditions, is pointed out by low SS values (essentially finer grain size distribution) (Fig. IV.6) and the slightly more efficient precipitation of redox-sensitive elements in core 436B (V/Cr and Ni/Co; Fig. IV.7). An increasing trend of TOC content and no significant fluctuations of Br/Al ratios in both cores (Fig. IV.8), due to higher detrital input and lower oxygenation conditions support this scenario.

The recent-most record, second half of the twentieth century (Figs. IV.5 to 9, and 10, enlarged box) is characterized by a steadily decreasing humidity (as clearly evidenced by fluvial-derived elements Si/Zr and K/Zr ratios) and enhanced Saharan eolian input (Zr/Al and Zr/Rb ratios) (Fig. IV.5). Higher detrital input is also evidenced by the first eigenvector of both cores instead, which could be related to harmful agricultural practices since industrial times. TOC and Br/Al ratios show the highest values and thus high productivity at recent times (Fig. IV.8).

Our records also exhibit a sudden decrease of redox-sensitive elements in core 436B, pointing to a fluctuation into better oxygenated bottom waters (Fig. IV.7), which is supported by raising SS values indicating a sudden re-invigoration of bottom waters currents (Fig. IV.6). The time scale of this observation and the lack of conclusive observations on NADW prevent obtaining a solid interpretation.

IV.6.3. Regional reconstruction and hemispheric scale connections

After the detailed reconstruction obtained from our dataset, we incorporate our results to the knowledge of climate evolution on other regions in the Northern Hemisphere in order to unravel the underlying mechanisms controlling the climate on the western Mediterranean region.

Prevailing humid conditions during the first part of our record characterize the period nominated as the Dark Ages (DA) (~500-800 yr AD). This recovering from previous drier conditions coincides with a minimum in solar insolation in the Northern Hemisphere (~650 yr AD) (Steinhilber et al., 2009), a predominant cooling of air temperatures in Greenland (Grootes and Stuiver, 1997) and a cold and dry period in the subpolar North Atlantic revealed by detrital evidences of ice-rafting (~550 yr AD; North Atlantic Cold event 1) (Bond et al., 1997, 2001) (Fig. IV.10). Thus, this cold phase in subpolar region manifests as increasing wetness in the studied area, as exposed

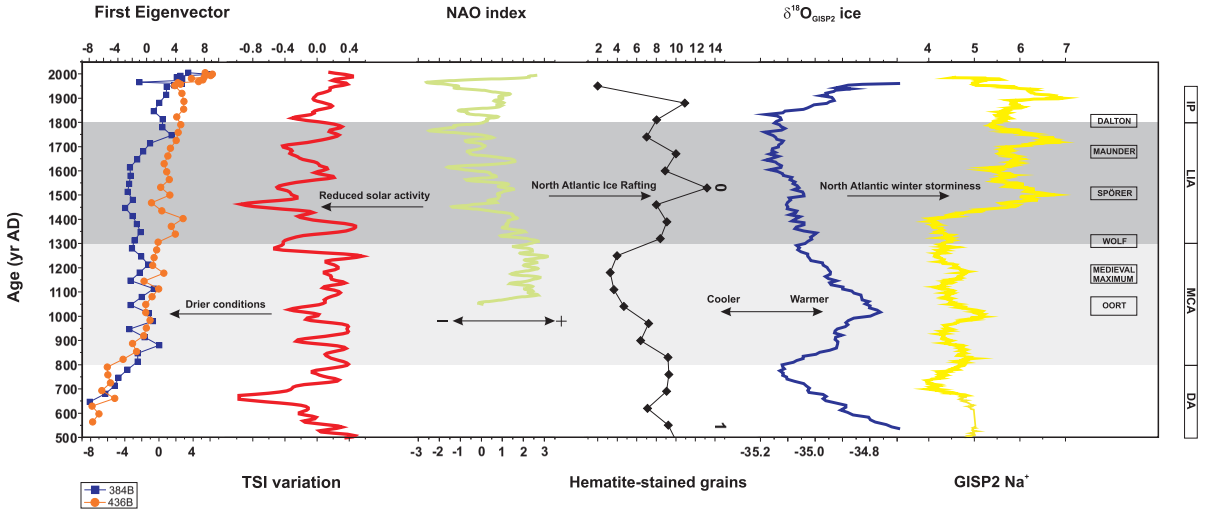

Figure IV.10. First eigenvector of cores 384B (blue squares) and 436B (orange circles) compared with the TSI variations ($W \cdot m^{-2}$) during the last 2000 yr (30-point smoothed, red line) (Steinhilber et al., 2009), the NAO index during the last 1000 yr (green line) (Trouet et al., 2009), the record of increased ice-drifting in the North Atlantic expressed as percentage variations of hematite-stained grains during the last 2000 yr (black diamonds, numbers represent Bond cycles 0-1) (Bond et al., 1997, 2001), the high resolution $\delta^{18}O$ record (‰) (30-point smoothed, dark blue line) (Grootes and Stuiver, 1997) from the GISP2 ice core during the last 2000 yr and the sea-salt Na^+ concentration (ppb) (30-point smoothed, yellow line) (Mayewski et al., 1997). Light grey bars indicate dry periods (MCA: Medieval Climate Anomaly), dark grey bars indicate humid periods (LIA: Little Ice Age), DA = Dark Ages, IP = Industrial Period. Periods of decreased (Oort, Wolf, Spörer, Maunder and Dalton Minimum) and increased (Medieval Maximum) sunspots activity are also indicated at the right side of the figure

on other records (see Nieto-Moreno et al., 2011; and references therein).

The period encompassing from 800 to 1300 yr AD (approx.), the Medieval Climate Anomaly (MCA) (~800-1300 yr AD), depicted as the most recent pre-industrial warm and dry period noted in Europe, which developed under the influence of a persistent positive phase of the NAO (Trouet et al., 2009). The results were prolonged droughts (Seager et al., 2007) and temperatures such as those reached during the twentieth century (Mann et al., 2009). The sedimentary record on the west Alboran Sea clearly images dryer conditions, mainly evidenced by enhanced eolian input (high Zr content) and rapid decrease in fluvial derived elements. The initial arid phase coincides with the Medieval solar activity maximum (~1100-1250 yr AD) (Jirikowic and Damon, 1994). However, within this MCA large arid period, a humid phase is recognized between 1000-1100 yr AD, coinciding with a minimum in solar radiation and sunspots activity in the Northern Hemisphere (Oort minimum, ~1010-1080 yr AD) (Usoskin et al., 2003) (Fig. IV.10). Following this wet pulse, prevailing dry conditions which continue up to 1300 yr AD (approx.) are found, according to the present record and Nieto-Moreno et al. (2011). This is not a local signal, since parallel to these events, very low levels of sea-salt Na^+ concentrations from the GISP2 ice core (Mayewski et al., 1997) show a strengthening of the Icelandic low pressure center restricting the transport of sea-salt Na^+ by winds towards Greenland (Meeker and Mayewski, 2002), inducing dryness, and warmer air temperatures are registered in the region (Grootes and Stuiver, 1997) (Fig. IV.10), as expected for a positive NAO mode (Wanner et al., 2001).

At the end of the MCA and the transition into the Little Ice Age (LIA), the two studied cores record a period of increase in riverine input (~1300 yr AD) that also corresponds with a minimum in solar radiation and sunspots activity in the Northern Hemisphere (Wolf minimum, ~1282-1342 yr AD) (Usoskin et al., 2003). In fact, the LIA is characterized in the Mediterranean region by a series of brief and intense wet periods within an otherwise dry period (Rodrigo et al., 1999), and this is equally interpreted on the present study. Higher riverine input and decreased eolian supply occurred during periods of minimal solar activity, (Spörer, ~1460-1550 yr AD; Maunder minimum, ~1645-1715 yr AD, according to Usoskin et al., 2003). Sharp increases in TOC coincides with Wolf, Spörer and Maunder Minimum, probably due to

the higher riverine input into the basin during these periods of weaker sunspots activity. Thus, as a general rule we can state that wet climate developed under minima solar activity.

The LIA (~1300-1800 yr AD) was interpreted above as progressively more humid transition punctuated by short dry periods. Martín-Puertas et al, (2010) and Nieto-Moreno et al. (2011) also recorded an increase of the riverine input for this period. Moreno et al, (2012) report higher lake levels and mexophytic vegetation, which typically thrive in moderately humid conditions, occurring in the south of the Iberian Peninsula during the LIA. It is also worth mentioning that our records also display a noticeable correlation with rainfall reconstructions during the last 500 yr from the south of the Iberian Peninsula based on original documentary sources calibrated with modern precipitation data. These results present the LIA as a period of dry-wet phase alternation. Prevailing wet anomalies in Andalusia took place at 1590-1650 yr AD whereas the driest periods occurred at 1500-1590 yr AD and 1650-1750 yr AD, being 1540 and 1750 yr AD the driest years during the LIA (Rodrigo et al., 1999). Our records fit well with this reconstruction, showing increasing trends of fluvial-derived elements (Si/Zr and K/Zr ratios) and lower Saharan eolian input (Zr/Al and Zr/Rb ratios) coinciding with those wet periods in Andalusia and vice versa for dry phases (Fig. IV.5). The wettest period which took place in Andalusia during the LIA matches with the highest values of fluvial provenance indicators at this time (1590-1650 yr AD; yellow and blue bars in Fig. IV.5). Regardless of humidity conditions, SST in these sites, both TEX^{H}_{86} and $U^{k'}_{37}$ proxies reveal the LIA as the coldest period of the last two millennia (Nieto-Moreno et al., 2012).

These prevalent wetter and colder climatic conditions are consistent with the atmospheric-oceanic situation hypothesized by Trouet et al. (2009) in southern Europe and north Africa, with more low pressure tracking into this region and leading to increased precipitation during negatives phases of the NAO (Fig. IV.10). The lowest values in European winter temperatures of the past millennium have been also recorded at the late LIA (Mann et al., 2009), thus providing evidences that reduced solar forcing, as occurred during the Maunder minimum, caused a shift toward a low NAO index state, which results in a strong cooling in the North Atlantic and adjacent regions (Shindell et al., 2001). According to this hypothesis, Grootes and Stuiver (1997)

reported cooler conditions in Greenland, Mayewski et al. (1997) recorded a sharp change in Na^+ ions contents in GISP2 ice core at ~1450 yr AD deciphered as a deepening of the Icelandic low, leading to a stronger transport of sea-salt Na^+ towards Greenland and enhanced storm activity over the North Atlantic region (Meeker and Mayewski, 2002), and Bond et al. (1997, 2001) indicated an increase in ice-rafted debris and hence iceberg transports at mid-latitude during this period (~1470 yr AD; North Atlantic Cold event 0) (Fig. IV.10).

These humid conditions continued during most of the Industrial Period and into the early 20th century, according to the interpretation above. For this period, the first series of instrumental climate data are recorded and thus our interpretation becomes more accurate and robust at the same time. In agreement with our record, humid conditions governed the southern Iberian region based on instrumental precipitation series at 1750-1950 yr AD (Rodrigo et al., 1999) and coincide with the most recent phase of minimum sunspots and solar activity in the Northern Hemisphere (Dalton minimum, ~1790-1830 yr AD) (Usoskin et al., 2003) (Fig. IV.5). A negative mode of the NAO is still persistent during this time interval (Trouet et al., 2009), proved by North Atlantic wide evidences; rising sea-salt Na^+ concentrations from the GISP2 ice core in Greenland (Mayewski et al., 1997) show increasing winter storminess in the North Atlantic realm (Meeker and Mayewski, 2002), enhanced ice-rafted debris in the subpolar North Atlantic (Bond et al., 1997; 2001) and cold air temperatures in Greenland during the first half of the IP, becoming gradually warmer from 1850 yr AD on (Grootes and Stuiver, 1997) (Fig. IV.10), all agree with our reconstruction.

The second half of the 20th century is marked by a general decrease in fluvial derived material, even though intense agricultural activity and deforestation should have induced the opposite, thus stressing the interpretation of diminished precipitation and drier climate on the region. A general decreasing trend on instrumental precipitation series in Andalusia from 1960 onwards (Rodrigo et al., 1999) and elsewhere in the Iberian Peninsula (Rodrigo and Trigo, 2007; Gallego et al., 2011) has been also found during the last century. The recent long wintertime dry conditions over Greenland, southern Europe and the Mediterranean, has been related to the persistent and exceptionally positive mode of the NAO since the early

1980s (the highest positive values of the NAO index recorded since 1864 yr AD) (Hurrell, 1995; Rodó et al., 1997), and increasing solar irradiation in the Northern Hemisphere is claimed as natural forcing factors of climate variability (Steinhilber et al., 2009) (Fig. 10). This positive phase of the NAO (Trouet et al., 2009) (Fig. IV.10), which manifests a higher than normal Icelandic low pressure and stronger than average westerlies tracking storminess in a more northerly pathway across middle latitudes, leads to dry winters in southern Europe, the Mediterranean, northern Africa, northern Canada and Greenland, and wet winters in northern Europe and eastern North America (Wanner et al., 2001; Trigo et al., 2002). Indeed, decreasing sea-salt Na^+ concentrations from the GISP2 glaciochemical series also evidence a strengthened low pressure center which blocked the transport of sea-salt Na^+ by winds towards Greenland (Mayewski et al., 1997) and thus producing dryness in Greenland and in the North Atlantic region (Meeker and Mayewski, 2002) (Fig. IV.10). Nevertheless, in order to explain the anomalous and unprecedented warmer temperatures registered in Greenland (Grootes and Stuiver, 1997) (Fig. IV.10), in the Northern Hemisphere (Wahl et al., 2010), as well as in our western Mediterranean records (Nieto-Moreno et al., 2012) during the second half of the twentieth century, some other additional external forcing mechanisms, such as the increasing in CO_2 concentrations and other anthropogenic greenhouse gases due to emissions from human activities, might be claimed and also taken into account.

IV.6.4. Evolution of metal concentrations in the westernmost Mediterranean during the last century: Impact of the anthropic contribution

In a preliminary attempt to identify atmospherically-derived pollution, we have assessed the origin and evolution of metal concentrations during the last two millennia in deep-sea sediments from the westernmost Mediterranean. Thus, the significant correlation between trace metals as Pb, Zn and Cu with respect to Al in both cores, suggest a coupling to clay minerals and a possible riverine provenance (Fig. IV.4a, b, e, f). The moderate correlation with TOC and Br might be responsible for the higher values of Cu in core 436B between 1300-1800 yr AD, arising from the ability of this element to constitute organometallic ligands (Fig. IV.4b). Thus, we have used aluminium-normalization in order to avoid dilution effects by the carbonate fraction and to assess the potential enrichment of these

trace metals relative to aluminosilicates as the fine-grained fraction where these metals are mainly accumulated in the sediments (Calvert and Pedersen, 1993). Normalized concentrations of heavy and trace elements (Pb/Al, Zn/Al and Cu/Al) display a concomitant flat pattern at the deepest parts and surficial concentrations in both cores (Fig. IV.11), thus suggesting a common provenance source which in deep-sea sediments of the western Mediterranean may result from anthropogenic input, bioturbation and/or mixing processes, or diagenetic co-precipitation together with Fe and Mn oxy-hydroxides (Fernex et al., 1992). Mn/Al ratios exhibit a flat profile except for the uppermost two centimeters depth (Fig. IV.9), not coincident with other heavy metal profiles, ^{210}Pb concentrations are observed at the top of the core and are found down to 12.5 and 14.5 cm depth in core 384B and 436B respectively (Figs. IV.2a, b). Background concentrations of the same metals are reached further downwards, so mixing processes are not responsible of these surficial enrichments. Thus, an anthropogenic origin is the most plausible explanation for the significant contribution of these heavy metals into pelagic sediments.

The increasingly raise of Pb/Al, Zn/Al and Cu/Al ratios in both cores starting at 1750 yr AD concurred with the beginning of the Industrial Revolution, likely due to dominant regional and/or local sources (i.e. from mining, burning of fossil fuels and primary and secondary non-ferrous metal smelters as consequence of industrial development). Thus, metal concentrations in deeper levels (before 1750 yr AD) might be considered as the natural background, i.e. as uncontaminated sediments settled during pre-industrial times. Then, the sharpen raise at 1950 yr AD coincided with the use of alkyl-leaded additives in gasoline until the implementation of anti-pollution policies in the early 1970s which decreased emissions over Europe (Heimbürger et al., 2010). Indeed our records registered a slight decrease at 1975-1990 yr AD on these heavy metals (Fig. IV.11). Maximum concentrations at the upper 2 cm might be due to diagenetic co-precipitation of these elements together with Fe and Mn oxy-hydroxides.

Additionally, to evaluate the possible adverse effects associated with high metal concentrations we have also compared metal concentrations with one of the most broadly and internationally recognized SQL: a) the "Effects Range-Low" (ERL; indicative of concentrations below which adverse effects rarely occur) and the "Effects

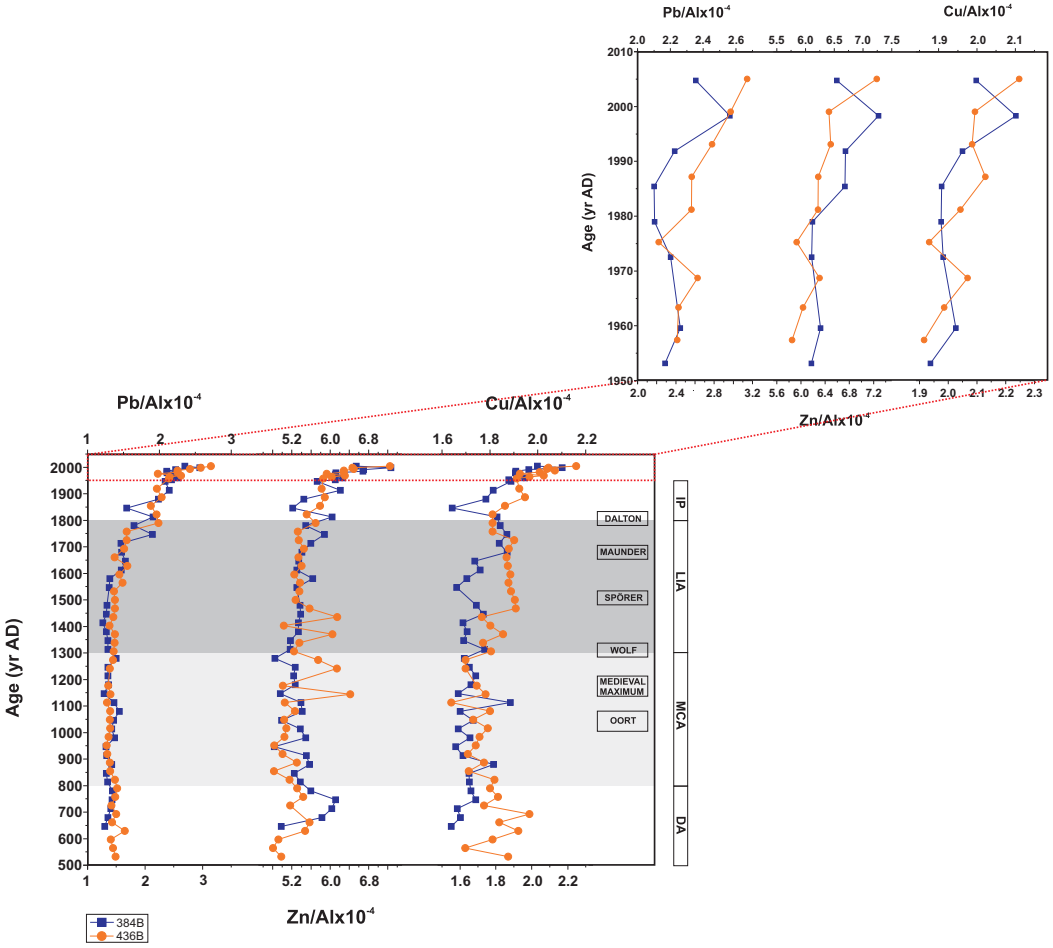

Figure IV.11. Age-depth profile of anthropogenically-derived heavy metals (Pb/Al, Zn/Al and Cu/Al·10⁴) for cores 384B (blue squares) and 436B (orange circles). Light grey bars indicate dry periods (MCA: Medieval Climate Anomaly), dark grey bars indicate humid periods (LIA: Little Ice Age), DA = Dark Ages, IP = Industrial Period. Periods of decreased (Oort, Wolf, Spörer, Maunder and Dalton Minimum) and increased (Medieval Maximum) sunspots activity are also indicated at the right side of the figure.

Range-Median" (ERM; representative of concentrations above which effects frequently occur) developed by the National Oceanic and Atmospheric Administration (NOAA, 1999) based on a wide database compiled from studies carried in saltwater (Long et al., 1995) (Tables IV.3, 4). They were intended as informative (non regulatory) guidelines for the interpretation of chemical data from analyzed sediments, which are associated with adverse effects such as toxicity and to compare the degree of identified contamination among different regions. Thus, Pb, Zn and Cu maximum concentrations remained below the ERL guidelines in both cores, although Cu and Pb concentrations are

in the same order of magnitude and quite close to ERL values in the upper 15 cm of both cores (from 1750 yr AD onwards) (Tables IV.3, 4). Zn concentrations are much lower than the recommended concentrations for acceptable sediment quality in the upper 15 cm (Tables IV.3, 4) .

IV.7. Conclusions

A high-resolution multi-proxy approach from two well-dated deep-sea marine records from the Alboran sea basin has served to decipher natural climate variability and to unravel the forcing mechanisms driving climate change during the last two millennia, as well as to evidence potential anthropic imprints in this basin. According to this approach, prevalent arid conditions depicted the MCA and the second half of the twentieth century as supported by decreasing trends of riverine influence (Si/Zr and K/Zr ratios) and enhanced Saharan eolian input (Zr/Al and Zr/Rb ratios). The LIA appeared as a succession of short and sharpen dry-wet phase alternation, which correlated with rainfall reconstructions from the south of the Iberian Peninsula during the last 500 yr. Raising trends of fluvial-derived elements and a long-lasting decline of the Saharan eolian input documented the IP as a humid period, which is in agreement with instrumental precipitation series in the south of the Iberian Peninsula. The second half of the twentieth century is outlined by a steadily dryness, as also recognized from instrumental meteorological data in the Iberian Peninsula from 1960 yr AD until present day-time. During the last two millennia the higher riverine input and minor Saharan eolian contribution concurred within periods of lower intensity of solar radiation and low sunspots activity in the Northern Hemisphere and vice versa. Our climatic records also evidence correlation with other Late Holocene marine records from the westernmost Mediterranean and with lacustrine and pollen records from the south of the Iberian Peninsula, as well as with Greenland air temperatures and North Atlantic cold events. This support the link between the climate on this region and the North Atlantic realm, driven by the atmospheric forcing related to the NAO. The first eigenvector of PCA at both studied records describes higher detrital input during the LIA in relation to the previous MCA as expected for a positive (previously negative) mode of the NAO. Paleoceanographic fluctuations have also been evidenced at 1450 and 1950 yr AD by a sharpened decrease of redox-sensitive elements (V/Cr and Ni/Co ratios) and coarser sortable silt,

which suggest re-ventilation of bottom waters and faster bottom currents as well as a plausible strengthened cold spell of the Atlantic jet stream into the Alboran Sea. A notable anthropic contribution has been documented at 1750 and 1950 yr AD onwards by the increase in the content of heavy metals (Pb, Zn and Cu).

Table IV.3. Trace metal concentrations in both cores 384B and 436B

Core	Core Depth (cm)	Cu (ppm)	Zn (ppm)	Pb (ppm)	Core	Core Depth (cm)	Cu (ppm)	Zn (ppm)	Pb (ppm)
384B	0.5	31.97	104.75	37.68	436B	0.5	32.91	101.60	46.72
384B	1.5	33.85	117.08	41.27	436B	1.5	33.34	103.84	44.47
384B	2.5	32.14	109.68	36.47	436B	2.5	34.24	101.06	41.26
384B	3.5	31.09	108.94	34.25	436B	3.5	32.89	101.14	41.27
384B	4.5	31.32	100.52	34.57	436B	4.5	30.79	94.40	35.35
384B	5.5	30.93	98.82	35.62	436B	5.5	32.92	100.43	41.83
384B	6.5	27.44	92.00	32.49	436B	6.5	32.25	97.96	39.42
384B	7.5	31.86	102.56	37.01	436B	7.5	30.75	93.94	38.77
384B	8.5	30.75	99.93	35.48	436B	8.5	31.13	94.88	34.15
384B	9.5	31.14	94.48	34.30	436B	9.5	30.66	92.52	35.02
384B	10.5	29.60	101.31	34.90	436B	10.5	31.18	93.50	36.37
384B	11.5	28.93	88.33	32.19	436B	11.5	29.70	92.92	33.72
384B	12.5	27.02	85.90	25.42	436B	12.5	28.34	87.60	34.97
384B	13.5	29.71	98.09	31.05	436B	13.5	27.67	88.44	34.69
384B	14.5	30.06	89.56	26.85	436B	14.5	28.30	84.53	26.67
384B	15.5	30.32	95.33	30.82	436B	15.5	29.95	84.12	26.44
384B	16.5	28.98	88.24	23.10	436B	16.5	29.37	85.53	25.67
384B	17.5	29.25	84.47	23.02	436B	17.5	28.95	83.07	22.92
384B	18.5	27.34	84.14	24.04	436B	18.5	28.71	83.11	26.04
384B	19.5	27.49	82.85	22.93	436B	19.5	29.21	81.54	24.10
384B	20.5	26.42	87.32	20.31	436B	20.5	28.69	82.36	24.65
384B	21.5	25.55	81.52	20.00	436B	21.5	29.12	82.79	22.53
384B	22.5	25.78	82.15	19.73	436B	22.5	29.64	82.07	22.93
384B	23.5	27.14	83.56	19.76	436B	23.5	29.47	85.91	22.73
384B	24.5	27.24	82.77	19.36	436B	24.5	26.75	95.52	22.51
384B	25.5	26.38	83.45	18.99	436B	25.5	27.97	79.54	21.88
384B	26.7	26.62	83.29	19.66	436B	26.7	29.44	96.71	23.65
384B	27.5	26.54	81.22	20.12	436B	27.5	27.60	85.54	23.50

Table IV.3. Trace metal concentrations in both cores 384B and 436B. Continuation

Core	Core Depth (cm)	Cu (ppm)	Zn (ppm)	Pb (ppm)	Core	Core Depth (cm)	Cu (ppm)	Zn (ppm)	Pb (ppm)
384B	28.5	27.56	80.05	19.89	436B	28.5	28.16	83.30	23.08
384B	29.5	26.76	76.58	22.10	436B	29.5	25.82	90.94	22.85
384B	30.5	27.08	83.29	20.27	436B	30.5	25.83	97.23	22.01
384B	31.5	27.64	83.17	20.34	436B	31.5	26.89	76.22	26.94
384B	32.5	26.94	82.44	20.20	436B	32.5	26.50	78.49	21.26
384B	33.5	26.55	78.90	19.60	436B	33.5	27.47	101.17	22.08
384B	34.5	29.88	85.39	21.63	436B	34.5	24.25	78.97	20.90
384B	35.5	26.42	85.44	22.74	436B	35.5	27.33	81.40	21.55
384B	36.5	26.94	77.58	21.23	436B	36.5	26.08	78.43	21.63
384B	37.5	26.49	85.39	21.25	436B	37.5	27.36	79.26	21.74
384B	38.5	27.28	87.23	21.86	436B	38.5	26.31	77.68	21.02
384B	39.5	26.19	76.41	19.86	436B	39.5	26.76	76.61	21.12
384B	40.5	26.87	87.59	20.16	436B	40.5	25.65	78.13	20.95
384B	41.5	28.82	88.37	21.20	436B	41.5	26.43	80.84	21.17
384B	42.5	27.15	83.18	19.98	436B	42.5	25.48	74.52	21.51
384B	43.5	27.26	85.50	20.33	436B	43.5	26.78	76.96	22.01
384B	44.5	26.70	86.84	20.90	436B	44.5	25.66	77.10	22.00
384B	45.5	26.84	94.27	20.66	436B	45.5	25.74	77.21	21.03
384B	46.5	25.32	91.85	20.13	436B	46.5	24.92	74.17	20.33
384B	47.5	25.57	88.86	19.59	436B	47.5	28.22	75.79	21.24
384B	48.5	24.93	75.79	18.85	436B	48.5	25.31	77.42	19.85
					436B	49.5	27.21	77.42	23.29
					436B	50.5	25.04	69.11	19.72
					436B	51.5	23.28	68.63	20.59
					436B	52.5	26.04	69.37	20.74

Table IV.4. Trace metal concentrations in cores 384B and 436B (summary) compared with sediment quality guidelines values (SQG)

Core	Metal	Minimum Concentration	Maximum Concentration	Surface Concentration	ERL	ERM
384B	Cu	24.93	33.85	31.97	34	270
384B	Zn	75.79	117.08	104.75	150	410
384B	Pb	18.85	41.27	37.68	46.7	218
436B	Cu	23.28	34.24	32.91	34	270
436B	Zn	68.63	103.84	101.60	150	410
436B	Pb	19.72	46.72	46.72	46.7	218

Summary and Conclusions
Epílogo y Conclusiones

High resolution organic and inorganic analyses on well-dated gravity and box cores from the western Algerian-Balearic and Alboran Sea basins, have allowed the characterization of climate variability and climate responses (paleoceanographic and paleoenvironmental conditions) as well as underlying natural forcing factors and anthropic contribution during the Late Holocene, also revealing the reliability and sensibility of the studied region for such reconstruction.

In the western Algerian-Balearic basin:

- An increase in riverine influence (fluvial-derived element ratios such as Rb/Al, Ba/Al, REE/Al, Si/Al, Ti/Al, Mg/Al and K/Al ratios) and low Saharan eolian input (Zr/Al ratio) have revealed the Roman Humid Period (RHP) and the Little Ice Age (LIA) as humid periods in contrast with the Late Bronze Age-Iron Age (LBA-IA), Dark Ages (DA) and MCA (Medieval Climate Anomaly), when drier conditions were observed.

- The former humid periods showed less energetic paleoceanographic conditions, as evidenced by weaker bottom currents (lower sortable silt and quartz content), poor oxygen bottom currents (high V/Al, Cr/Al, Ni/Al and Zn/Al ratios) and well-preserved marine organic matter (total organic carbon -TOC- content, Br/Al ratio, U and Cu as organometallic ligands). Opposite trends were found during the LBA-IA, DA and MCA.

- The RHP is pointed out as the most humid and intense productivity period during the last 4000 yr, due to the highest TOC and riverine influence achieved during this time.

- Solar irradiance variability is claimed as the major natural forcing factor during the Late Holocene, modulated by the North Atlantic Oscillation (NAO) during the MCA and the LIA, as drawn by oscillations in the first eigenvector of the Principal Component Analyses (PCA), which represents the detrital input into the basin as the main process controlling the sedimentary regime.

- These dry(wet) conditions during the MCA(LIA), coexisting with faster(slower) bottom currents and poor(well) oxygenated bottom waters, correspond well with a

transition from a predominant positive NAO state to a negative one. Weaker and southward displaced westerlies would bring enhanced precipitation to the Mediterranean during the LIA, which may have collapsed the formation of Western Mediterranean Deep Water (WMDW) in the Gulf of Lyon.

In the western Alboran Sea basin:

- The MCA and the second half of the twentieth century were characterized by dry conditions such as a decline in riverine influence (decreasing trends of fluvial-derived elements ratios, Si/Zr and K/Zr) and higher Saharan eolian input (Zr/Al and Zr/Rb ratios). Wetter conditions were observed during the LIA and the Industrial Period (IP) instead.

- A progressive decline of sea surface temperatures (SST) is recorded during the last 2000 yr, with warmer temperatures during the MCA and colder during the LIA, followed by an unprecedented raise during the second half of the twentieth century. This is consistent with other Northern Hemisphere temperature reconstructions forced by natural solar irradiance variations and anthropogenic greenhouse warming.

- TEX^{H}_{86}-derived absolute values of SST are higher than those estimated from the $U^{k'}_{37}$ ratios, probably reflecting summer SST due to differences in the seasonality of haptophyte algae and Thaumarchaeota, which is in agreement with other studies in the western and eastern Mediterranean.

- The carbon isotopic composition of *n*-alkanes revealed a predominantly riverine C_3 plant contribution during the last two millennia.

- Prevalent low BIT values (<0.5) revealed a dominant marine provenance for the sedimentary organic matter.

- High diol index values coincided with periods of a persistent positive NAO index and lower riverine influence (BIT index). Thus, high NAO states such as those prevailing during the MCA and the second half of the twentieth century might have provoked a bloom of *Proboscia* diatoms due to an intensification of the

wind-induced upwelling conditions.

- The LIA is depicted by a sequence of short and sharp dry/wet phases coinciding with higher/lower intensity of solar radiation and sunspots activity in the Northern Hemisphere.

- A noteworthy change in paleoceanographic conditions (sharp decrease in V/Cr and Ni/Co ratios, enhanced sortable silt) has been recorded at 1450 yr AD, lasting until 1900 yr AD. Thus, faster and well oxygenated bottom currents might be the result of strengthened cooler waters flowing into the Mediterranean Sea during the LIA as a consequence of reduced North Atlantic Deep Water (NADW) formation in the North Atlantic realm as described in the Alboran Sea basin during previous cold phases pacing during the last deglacial period.

- The notable increment in the sedimentary concentration of heavy metals (Pb, Zn, and Cu) from 1750 yr AD onwards claims for an anthropic fingerprint.

From these established conditions, we can conclude, in general terms, that dry/warm and wet/cold conditions during the MCA and the LIA respectively, seems to be promoted by solar irradiance variations and the modulation of the NAO in the westernmost Mediterranean. Additional natural forcing mechanisms, such as a possible weakening of the NADW rate production might have been also involved, as recorded by our records at 1450 yr AD. The persistent positive mode of the NAO during the MCA and the major Saharan eolian input into the basin recorded during this time-interval, might have also induced an intensification of the wind-induced upwelling conditions in the Alboran Sea basin (bloom of *Proboscia* diatoms). Anthropic contribution is also evidenced in this region by the unprecedented temperatures achieved during the second half of the twentieth century as well as increasing concentration of pollutants elements since the beginning of the Industrial Era. Furthermore, obtained results correlate with other instrumental, lacustrine and pollen records from the Iberian Peninsula, marine records from the western Mediterranean, and other evidences from the North Atlantic realm, northern Europe, north Africa, Greenland, and the Northern Hemisphere.

The used multivariate statistical approach has also been proved as feasible for paleoenvironmental reconstructions, allowing the reduction of dimensionality in the geochemical dataset, highlighting the relationship between the different proxies and the environmental information they are providing, and disentangling the main environmental processes controlling sedimentary deposition as well as the major forcing mechanisms attributable to climate variability.

El análisis de alta resolución de indicadores orgánicos e inorgánicos en sedimentos del oeste de las cuencas Argelino-Balear y de Alborán ha permitido la reconstrucción de la variabilidad climática y de las condiciones paleoambientales y paleoceanográficas durante el Holoceno Tardío. Este análisis ha servido igualmente para la caracterización de la respuesta de los distintos componentes del sistema climático a dicha variabilidad y de los mecanismos subyacentes de forzamiento natural y antrópico, poniendo también de manifiesto la idoneidad y sensibilidad del área de estudio para este tipo de reconstrucciones paleoclimáticas:

En el oeste de la cuenca Argelino-Balear:

- Durante el Periodo Húmedo Íbero-Romano y la Pequeña Edad de Hielo se ha puesto de manifiesto una mayor influencia fluvial (relaciones de elementos típicamente derivados del aporte fluvial; Rb/Al, Ba/Al, REE/Al, Si/Al, Ti/Al, Mg/Al y K/Al) y una menor contribución eólica proveniente del Sáhara (razón Zr/Al), identificándose así como periodos húmedos. Sin embargo, durante el periodo correspondiente al Bronce Final-Edad del Hierro, la Alta Edad Media y la Anomalía Climática Medieval, se han identificado condiciones paleoclimáticas más áridas.

- Estos periodos húmedos se han caracterizado por condiciones de paleocirculación menos energéticas, tal y como indica la existencia de corrientes de fondo más lentas (menor contenido en limo grueso y en cuarzo), aguas profundas poco oxigenadas (valores elevados de las razones V/Al, Cr/Al, Ni/Al and Zn/Al) y una mejor preservación de la materia orgánica (contenido en carbono orgánico total, razón Br/Al, y ligandos organometálicos como el U y el Cu). Por el contrario, se han registrado condiciones opuestas durante el Bronce Final-Edad del Hierro, la Alta Edad Media, y la Anomalía Climática Medieval (periodos identificados como áridos).

- El Periodo Húmedo Íbero-Romano se ha reconocido como el más húmedo y el de más intensa productividad de los últimos 4000 años, como indican valores más elevados del contenido en carbono orgánico total y un mayor aporte fluvial.

- El comportamiento del primer vector propio del análisis de componentes principales, el cual representa la entrada detrítica en la cuenca como principal pro-

ceso dominante del régimen sedimentario, apunta al forzamiento natural generado como consecuencia de cambios en la irradiancia solar como principal factor de forzamiento climático durante el Holoceno Tardío, junto con la modulación de la Oscilación del Atlántico Norte en periodos como la Anomalía Climática Medieval y la Pequeña Edad de Hielo.

- Las condiciones áridas y húmedas durante la Anomalía Climática Medieval y Pequeña Edad de Hielo respectivamente, coexistiendo con corrientes de fondo más intensas y aguas de fondo bien oxigenadas en el primer caso y menos intensas con aguas poco oxigenadas en el segundo, se corresponden con una transición desde una fase predominantemente positiva de la Oscilación del Atlántico Norte a una negativa. Los vientos del oeste, debilitados y desplazados hacia el sur, provocarían un aumento de la precipitación en la región Mediterránea durante la Pequeña Edad de Hielo, lo cual podría haber producido el colapso en la formación de aguas profundas del oeste del Mediterráneo en el Golfo de León.

En el noroeste de la cuenca de Alborán:

- Durante la Anomalía Climática Medieval y la segunda mitad del siglo XX se han establecido condiciones áridas, de acuerdo con el declive en el aporte fluvial (tendencias decrecientes de las relaciones de elementos típicamente fluviales, Si/Zr y K/Zr) y un mayor aporte eólico procedente del Sáhara (relaciones Zr/Al y Zr/Rb). Durante la Pequeña Edad de Hielo y la Era Industrial se han establecido, por el contrario, condiciones más húmedas.

- Se ha puesto de manifiesto el progresivo descenso en las temperaturas de las aguas superficiales durante los últimos 2000 años, con temperaturas más cálidas durante la Anomalía Climática Medieval y más frías durante la Pequeña Edad de Hielo, seguidas por un incremento de las mismas durante la segunda mitad del siglo XX, sin precedente durante los últimos dos milenios. Estos registros son, además, coherentes con otras reconstrucciones de temperaturas en el Hemisferio Norte, que muestran oscilaciones derivadas de variaciones en la irradiación solar durante los últimos dos milenios y del calentamiento global de origen antropogénico durante los últimos siglos.

- Los valores absolutos de temperaturas superficiales de aguas oceánicas derivados del índice TEX^{H}_{86} probablemente reflejan temperaturas de verano debido a las diferencias estacionales en el florecimiento de algas Haptophyta y arqueas Thaumarchaeota. Estas diferencias se han puesto también de manifiesto en otros estudios del oeste y del este del Mediterráneo.

- La composición isotópica de carbono de los alcanos ha permitido establecer una contribución predominante de plantas tipo C_3 a lo largo de los últimos dos milenios.

- Los valores tan reducidos del índice BIT (<0.5) han demostrado la procedencia fundamentalmente marina de la materia orgánica.

- Los elevados valores del índice "diol" se corresponden con periodos de fase positiva de la Oscilación del Atlántico Norte y con un menor aporte fluvial (índice BIT). De este modo, fases positivas de la Oscilación del Atlántico Norte como la que tuvo lugar durante la Anomalía Climática Medieval y la segunda mitad del siglo XX podrían haber dado lugar a un florecimiento de diatomeas del género *Proboscia* como consecuencia de una intensificación de las condiciones de "upwelling" debido al efecto del viento (surgencia de aguas profundas más frías y ricas en nutrientes).

- La Pequeña Edad de Hielo se ha registrado como una secuencia de breves pero marcadas fases áridas/húmedas coincidentes con mayor/menor intensidad de irradiación solar y manchas solares en el Hemisferio Norte.

- Un notable cambio en las condiciones paleoceanográficas (descenso significativo en las relaciones V/Cr y Ni/Co, así como un mayor contenido en limo grueso), ha sido registrado en el año 1450 de nuestra era, perdurando hasta el año 1900. Las corrientes de fondo más rápidas y con aguas mejor oxigenadas podrían ser, por tanto, el resultado de una intensificación de la entrada de aguas atlánticas más frías en el Mar Mediterráneo que derivaría de un colapso en la formación de aguas profundas en el Atlántico Norte, tal y como se ha descrito previamente en la cuenca del Mar de Alborán durante eventos fríos de la última deglaciación.

- El importante incremento en la concentración de metales pesados desde el año 1750 registrado en los sedimentos más recientes (Pb, Zn y Cu) sugiere un origen antrópico.

A partir de las condiciones climáticas establecidas, se puede concluir que, en términos generales, las condiciones áridas/cálidas y húmedas/frías que acaecieron durante la Anomalía Climática Medieval y la Pequeña Edad de Hielo respectivamente, derivan de variaciones en la irradiación solar y la modulación de la Oscilación del Atlántico Norte en la región más occidental del Mediterráneo. Otros mecanismos adicionales de forzamiento climático natural, como un posible debilitamiento de la formación de aguas profundas en el Atlántico Norte podrían haber estado asimismo implicados, tal y como se registra en los testigos estudiados para el año 1450. Una persistente fase positiva de la Oscilación del Atlántico Norte durante la Anomalía Climática Medieval, así como la mayor contribución eólica procedente del Sáhara, podrían haber inducido también una intensificación en las condiciones de "upwelling" por efecto del viento en la cuenca del mar de Alborán (florecimiento de diatomeas del género *Proboscia*). La contribución antrópica se ha puesto de manifiesto en esta región por las elevadas temperaturas sin precedente alcanzadas durante la segunda mitad del siglo XX, así como por una mayor concentración de elementos contaminantes desde el comienzo de la Era Industrial. Los resultados obtenidos se correlacionan, además, con otros registros instrumentales, lacustres y polínicos de la Península Ibérica, con registros marinos del oeste del Mediterráneo y con otros registros de la región Norte Atlántica, del norte de Europa, del norte de África, Groenlandia y del Hemisferio Norte.

El análisis estadístico multivariable realizado ha resultado igualmente una herramienta idónea para este tipo de reconstrucciones paleoambientales, permitiendo la reducción de la dimensionalidad del conjunto de datos geoquímicos, dando relevancia a las relaciones entre los diferentes indicadores y a la información ambiental que los mismos proporcionan. Ha puesto, además, de manifiesto los principales procesos ambientales que rigen el depósito sedimentario, así como los mecanismos implicados en la variabilidad climática.

Ackowledgements
Agradecimientos

Me gustaría expresar mi más profunda y sincera gratitud a todos aquellos que han contribuido de un modo u otro a la elaboración de este trabajo, y sin los cuáles no hubiera sido posible.

En primer lugar y como principales promotores de este trabajo, a mis directores Francisca Martínez Ruiz y Miguel Ortega Huertas. Muchas gracias Paqui por acogerme en tu grupo, por darme un voto de confianza a ciegas, y por guiarme durante todo este largo camino. Por tu preocupación en la distancia, por tu cariño y amables palabras en la adversidad, por tus consejos, y por estar siempre al otro lado del teléfono a cualquier hora y cualquier día; dispuesta a ayudar, a escuchar, y a dar lo mejor de ti con una sonrisa. También quiero expresar mi agradecimiento a Miguel, por encontrar un hueco para mí, apoyarme, confiar en mí y ofrecer soporte a este trabajo, y sobre todo por tu empeño y preocupación por terminar con final feliz este capítulo de mi vida.

Otro especial agradecimiento va dirigido al apoyo institucional del Instituto Andaluz de Ciencias de la Tierra (CSIC) y del departamento de Mineralogía y Petrología de la Universidad de Granada, así como a todo el personal integrante de los mismos. En concreto, al director Alberto y al personal de administración del Instituto, Alfonso, Fernando, Elena, Isabel Abril, Ana, Cristina, Amparo, Inma, Eva,… Con vuestra inestimable ayuda cualquier trámite ha sido mucho más llevadero y siempre acompañado de una sonrisa (y un ratito de charla). Siempre me encantó visitaros. A las secretarias más bonitas de la Universidad de Granada, Inés y Sandra, con las que siempre se puede contar dentro y fuera de su despacho. Al personal técnico del Instituto y del Departamento, Elisa, Diana, Rubén, Carmen, Luisa, Leti, Miguel, César, Manolo, Edu, Jesús y Sonia (otra niña bonita junto con las secretarias). Por toda vuestra infinita ayuda en el laboratorio y en los "system error, operation failed", por todas las cervezas que compartimos, las tapas, las casas rurales, las paellas, las comidas navideñas, las fiestas, y porque sois unos compañeros de lo mejorcito que hay. Espero que nos queden muchos eventos más que compartir. Otro especial agradecimiento a los técnicos más entrañables, Emi, Isabel y Juan Santamarina, y a todo el personal del CIC: Maria del Mar, Alicia, Olga y Bendi,... ¡Mis favoritas! ¡Como podéis ser tan primorosas! No puedo olvidarme del personal investigador, comenzando por la línea de Geociencias Marinas del Instituto con Menchu, Paco Lobo, Óscar y Carlota (muchas gracias por vuestras

palabras de ánimo en los pasillos), y continuando con el Departamento de Mineralogía con Daniel, Fernando Nieto, Giuseppe, y Carolina entre otros (siempre apreciaré vuestras cálidas y cordiales palabras).

También merecen una especial mención los que han sido mis tutores durante mis estancias en el extranjero. Michael Böttcher, el cual hizo mi estancia en Alemania una de las más divertidas y peculiares donde las haya habido, y porque allá donde te haya encontrado en Europa siempre has tenido una especial saludo y atención para mí. Tatsuhiko Sakamoto, que fue un pilar imprescindible en Japón y el cuál me hizo descubrir y disfrutar su país y sus costumbres, y sobre todo por su empeño en hacerme sentir como en casa en el confín del mundo. Jaap S. Sinninghe Damsté y Stefan Schouten, con los que tuve el honor de trabajar en Holanda y con los que aprendí una nueva ciencia para mí, la geoquímica orgánica, la cual además de contribuir a esta tesis, me sigue fascinando personal y profesionalmente. A todos aquellos que me ofrecisteis vuestra ayuda y vuestra amistad durante esas estancias, un enorme gracias. Cornelia, Kim, Verónica, Jort, Marcel, Sabine, Ellen, Iijima, Saburo, Saiko, Akiko, Steph, Alex, Chieko, Aníbal,… y en especial por supuesto a Thorsten (fuapo!).

Como co-autores y grandes colaboradores, de los que he aprendido mucho y sin los que este trabajo no habría sido posible, Santi, Jordi, Pere y Gert. Un beso enorme y gracias por estar ahí y dedicarme vuestro tiempo y paciencia.

No quiero dejar en el tintero a mis profesores de Geología de la Universidad de Jaén, si los que esta etapa de tesis no hubiese existido, y en especial a Juan, Chari y Juanma. Muchas gracias por inculcarme vuestra pasión por la Geología, por sentiros orgullosos de mí y sobre todo por hacerme consciente de ello cada vez que os encuentro. Gracias por acordaros de mí y tratarme con cariño y con tanto apoyo como siempre lo hacéis. África, a ti te incluyo como profesora de Geología y de la vida; sabes que te quiero bicho.

Y aquí vienen los imprescindibles, los compañeros de fatigas. Comenzando por el departamento de Mineralogía (Anna, Pedrito, Ana Luque, Julia, Iñaki, Eduardo, Maja) y Petrología (Juan, Idael, Sandra, Jose Alberto), pasando por Estratigrafía y Paleontología (Rute, Pili), y llegando hasta Geodinámica (Pedro, Silvia, Chema,

Vicente, Carlos, Enric) para terminar en Armilla en el nuevo Instituto (Francis, Claudio, Giordana), todos habéis sido una gran y segunda familia durante estos años, de puertas adentro y de cañas afuera. Por supuesto, mis dos despachos 29 (¡el número mágico!). Tanto en la Universidad, Vero y su bonita prole (cuántas horas de lupa compartimos, amore), Marta (y su siempre dulce hacer), Carmen (¡Carmela!¡Qué habríamos hecho sin ti!), Zoltan (y muchos cafés con cigarrito), Amel (mi princesita), y Erwin (¡rubio!¡por favor!); como en el Instituto (los little ponies, Nieves, Rita, Carmina, Luis y Meri). De mi nueva etapa en el Instituto merecen también un beso enorme Chiara y Willy, por su canto y su música, y por todos los ánimos, el apoyo y el cariño que me han ofrecido y me siguen ofreciendo todos los días, y porque siempre habéis tenido un ¿Cómo estás? ¿Qué tal vas? Acompañado de un chute de ánimo. Gracias, sois unos primores. También a Antonio Acosta, por tenerme siempre en consideración, por apoyarme y creer en mí aunque todo estuviera torcido y pintara fatal, y por animarme siempre a seguir mi camino. Muchas gracias por caminar conmigo también todos estos años. De mi estancia anterior en la Estación Experimental del Zaidín quiero dedicar un agradecimiento especial a Paco y Arsenio. Muchas gracias por todo lo que me ayudasteis y por todo lo que aprendí de vosotros en aquel entonces, en el laboratorio y fuera de él, y por la amistad que aún conservo con vosotros, aún en la distancia.

Y para mis más queridos compañeros y por encima de todo amigos, los que más han cuidado de mí (y de mi salud mental) todo este tiempo, unas palabrillas exclusivas para cada uno. Aitor, qué te voy a decir yo que tú no sepas (y si no quiero decirlo va a dar igual porque me vas a pillar de todas formas). Siempre has estado ahí para lo peor y lo mejor, para decirnos todo sin decir nada, para acudir en cualquier momento sin dilación, para gritarnos y querernos al mismo tiempo. Porque no hay nadie con quien necesite decir tan pocas palabras para expresarlo todo y que sepa que siempre tendrá un hueco para mí en caso necesario. Sabes que por lo que a mí respecta, todo es ídem. Juanillo, cariño, hemos llorado y hemos reído juntos, hemos viajado, hemos desvariado y hemos gritado. Gracias por ser tú, tal y como eres, con tus despistes, tus locuras, tus qué sé yo de aquella manera, tus al tiro, y tus yaaa. David, jomío, que esto termine es un alivio más grande para ti que para mí. Muchas gracias por aguantarme, escucharme, regañarme, ayudarme, por "conducirme malamente", por "Porcuna Summer School", por "Culodelmunden", por un barco de nombre extranjero y por mucho "rocanró del güeno". Y sobre todo,

muchas gracias por no dejarme nunca caer en la tentación… de abandonar. Alpi, mi pisciano antipenicilínico, el marinero con más amaneceres en Alborán y el más salao. Gracias por tus mapas, tus programas, tu socorrida ayuda en los peores momentos, tu entrega, por dar todo lo que estuviera en tu mano y más, tus mensajes, tus llamadas, tu risa (me encanta), tu humor, por hacerme sonreir todos los días, tus si no fuera por mí sería por otro, por los bucles infinitos (véase los 150 proverbios en inglés del pródigo refranero español), por ser el hombre que más cerca del altar me ha llevado, y por dejarme robar un trocito de tu vida para encajarlo en la mía. Pa, mi peque, has sido para mí la mejor compañera de futbolín y parchís, la hermana fumadora y bebedora de coca-colas no light, la madre que te quiere, se preocupa y te aconseja desde la experiencia pero que te regaña como la que más, y la amiga que siempre está ahí y que te acoge sin condiciones, más aún cuanto más grande es el batacazo. Gracias por estar ahí también en el peor momento de todos, hacer de tu casa la mía para que todo esto fuera posible, y por darme un abrazo y un beso todas las noches y todas las mañanas. Todos habéis visto lo peor y lo mejor (debe haber algo) de mí, y sabéis que os quiero, y que habéis sido lo mejor que he tenido en todos estos años y qué podré tener nunca.

Y a los que son ajenos a mi vida profesional pero nunca a la personal, y que habéis formado parte de ella en algún momento o desde siempre, también quiero agradeceros el simple hecho de que hayáis estado ahí. Muchas gracias Jean, Yago, Pablo, Benjamín y Lola por todos esos lunes de english chat aderezados con tapa y bien regados con cerveza. Así da gusto (y casi resaca) comenzar la semana. Gracias también a Patrick (¡ratón!), Marga y Marta por ser los mejores compañeros de piso que he tenido; vuestro apoyo, comprensión, y risas han sido fundamentales este último año. Gracias David por tu arte, tu sapiencia, las charlas de cine, novela, y fotografía (y por darme cuenta de todo lo que me falta por saber al respecto) y sobre todo, por tu amistad. Gracias Sara por ser la brujilla que me ha acompañado durante tantos años (anda que no, lo que llevamos encima ya), y porque sean muchos más. Gracias Mari Carmen por tus dulces palabras siempre. Diegui, por salvar el día con una peli y una copa (o dos). David, si estás por ahí, espero que lo sigas un tiempo más. Me ha encantado recuperarte después de 8 años sin mi mitad y que sea justo ahora.

Selenita, a ti te dedico una líneas exclusivas, para que te rías como un loco y

un melón, y para agradecerte de corazón que me incitaras a iniciar esta locura. Muchas gracias por construir un nuevo mundo para nosotros y hacer de mí una mejor personita.

Y por último, y no menos importante, mi familia. Mis padres, Antonio y Mari Cruz, todo esto va dedicado a vosotros. Gracias por vuestra paciencia y cariño, por escucharme, por todo lo que me habéis ayudado y por estar ahí. A mis hermanos Antonio y Belén, por tenerme siempre mimada y dedicarme especial ayuda. Y a los "cuñaos", Nono y Fátima, que de un modo u otro han compartido conmigo esta experiencia y han dejado su granito de arena en ella, ya sea en forma de portada (¡gracias cuñao!), de lector externo de cd's para poder instalar el programa de maquetación de la tesis (¡gracias cuñá!), o simplemente con un poco de charla. A Pablo también, un enorme gracias por amenizar nuestros días durante 3 años ya, y un enorme lo siento por no haber podido dedicarte como "tita" todo el tiempo que te merecías (prometo enmendarlo en el futuro próximo y no estar más fines de semana castigada en la silla y mirando a la pantalla, como te dije una vez). Una mención especial para aquellos que ya no están pero que permanecen, y que se marcharon en el trascurso de esta etapa. Un beso enorme, sé que os hubiera gustado estar ahí, pero de alguna forma para mí lo seguís estando.

Para finalizar, una disculpa para los que hayan podido quedar en el olvido durante la nocturnidad de la redacción, que no en mi mente. Perdonad las prisas de última hora y sobre todo, que al querer agradecer tanto, y a tantos, cada uno de los trocitos de esta etapa, no haya podido abarcar la totalidad del gran conjunto que he tenido la suerte de tener cerca durante estos años de duro trabajo.

References

Baker, A., Wilson, R., Fairchild, I. J., Franke, J., Spötl, C., Mattey, D., Trouet, V., and Fuller, L. (2011), High resolution $\delta^{18}O$ and $\delta^{13}C$ records from an annually laminated Scottish stalagmite and relationship with last millennium climate, *Global and Planetary Change*, 79, 303-311.

Bárcena, M. A., and Abrantes, F. (1998), Evidence of a high-productivity area off the coast of Málaga from studies of diatoms in surface sediments, *Marine Micropaleontology*, 35(1-2), 91-103.

Bárcena, M. A., Cacho, I., Abrantes, F., Sierro, F. J., Grimalt, J. O., and Flores, J. A. (2001), Paleoproductivity variations related to climatic conditions in the Alboran Sea (western Mediterranean) during the last glacial-interglacial transition: the diatom record, *Palaeogeography, Palaeoclimatology, Palaeoecology*, 167(3-4), 337-357.

Bárcena, M. A., Isla, E., Plaza, A., Flores, J. A., Sierro, F. J., Masqué, P., Sánchez-Cabeza, J. A., and Palanques, A. (2002), Bioaccumulation record and paleoclimatic significance in the Western Bransfield Strait. The last 2000 years, *Deep Sea Research (Part II, Topical Studies in Oceanography)*, 49(4-5), 935-950.

Bárcena, M. A., Flores, J. A., Sierro, F. J., Pérez-Folgado, M., Fabres, J., Calafat, A., and Canals, M. (2004), Planktonic response to main oceanographic changes in the Alboran Sea (Western Mediterranean) as documented in sediment traps and surface sediments, *Marine Micropaleontology*, 53(3-4), 423-445.

Bea, F. (1996), Residence of REE, Y, Th and U in granites and crustal protoliths; implications for the chemistry of crustal melts, *Journal of Petrology*, 37(3), 521-552.

Benito, G., Díez-Herrero, A., and Fernández De Villalta, M. (2003), Magnitude and frequency of flooding in the Tagus basin (Central Spain) over the last millennium, *Climatic Change*, 58(1-2), 171-192.

Benninger, L. K., Aller, R. C., Cochran, J. K., and Turekian, K. K. (1979), Effects of biological sediment mixing on the ^{210}Pb chronology and trace metal distribution in a Long Island Sound sediment core, *Earth and Planetary Science Letters*, 43(2), 241-259.

Berglund, B. E. (2003), Human impact and climate changes--synchronous events and a causal link?, *Quaternary International*, 105(1), 7-12.

Bernstein, L., Bosch, P., Canziani, O., Chen, Z., Christ, R., Davidson, O., Hare, W., Huq, S., Karoly, D., Kattsov, V., Kundzewicz, Z., Liu, J., Lohmann, U., Manning, M., Matsuno, T., Menne, B., Metz, B., Mirza, M., Nicholls, N., Nurse, L., Pachauri, R., Palutikof, J., Parry, M., Qin, D., Ravindranath, N., Reisinger, A., Ren, J., Riahi, K., Rosenzweig, C., Rusticucci, M., Schneider, S., Sokona, Y., Solomon, S., Stott, P., Stouffer, R., Sugiyama, T., Swart, R., Tirpak, D., Vogel, C., and Yohe, G. (2007), *Climate Change 2007: Synthesis Report. Contribution of Working Groups I, II and III to the Fourth Assessment Report of the Intergovernmental Panel on Climate Change,* 104 pp., Geneva, Switzerland.

Bethoux, J. P. (1979), Budgets of the Mediterranean Sea: their dependance on the local climate and on the characteristics of the Atlantic waters, *Oceanologica Acta*, 2(2), 157-163.

Bianchi, G. G., and McCave, I. N. (1999),

Holocene periodicity in North Atlantic climate and deep-ocean flow south of Iceland, *Nature*, 397(6719), 515-517.

Bird, M. I., Summons, R. E., Gagan, M. K., Roksandic, Z., Dowling, L., Head, J., Keith Fifield, L., Cresswell, R. G., and Johnson, D. P. (1995), Terrestrial vegetation change inferred from *n*-alkane $\delta^{13}C$ analysis in the marine environment, *Geochimica et Cosmochimica Acta*, 59(13), 2853-2857.

Björck (2011), Current global warming appears anomalous in relation to the climate of the last 20,000 years, *Climate Research*, 48(1), 5-11.

Blackford, J. J., and Chambers, F. M. (1995), Proxy climate record for the last 1000 years from Irish blanket peat and a possible link to solar variability, *Earth and Planetary Science Letters*, 133(1-2), 145-150.

Blunden, J., Arndt, D. S., and Baringer, M. O. (2011), State of the Climate in 2010, *Bulletin of the American Meteorological Society*, 92(6), S1-S266.

Bolle, H. J. (2003), Climate, climate variability and impacts in the Mediterranean area: an overview, in *Mediterranean Climate: variability and trends*, edited by H. J. Bolle, pp. 5-86, Springer, New York.

Bond, G., Showers, W., Cheseby, M., Lotti, R., Almasi, P., deMenocal, P., Priore, P., Cullen, H., Hajdas, I., and Bonani, G. (1997), A pervasive millennial-scale cycle in North Atlantic Holocene and Glacial climates, *Science*, 278(5341), 1257-1266.

Bond, G., Kromer, B., Beer, J., Muscheler, R., Evans, M. N., Showers, W., Hoffmann, S., Lotti-Bond, R., Hajdas, I., and Bonani, G. (2001), Persistent solar influence on North Atlantic climate during the Holocene, *Science*, 294(5549), 2130-2136.

Bout-Roumazeilles, V., Combourieu-Nebout, N., Peyron, O., Cortijo, E., Landais, A., and Masson-Delmotte, V. (2007), Connection between South Mediterranean climate and North African atmospheric circulation during the last 50,000 yr BP North Atlantic cold events, *Quaternary Science Reviews*, 26(25-28), 3197-3215.

Bradley, R. S., and Jones, P. D. (1993), 'Little Ice Age' summer temperature variations: their nature and relevance to recent global warming trends, *The Holocene*, 3(4), 367-376.

Bradley, R. S., Briffa, K. R., Cole, J., Hughes, M. K., and Osborn, T. J. (2003), The climate of the last millenium, in *Paleoclimate, Global Change and the Future*, edited by K.D. Alverson, R. S. Bradley and T. F. Pedersen, Springer-Verlag, New York.

Brassell, S. C., Eglinton, G., Marlowe, I. T., Pflaumann, U., and Sarnthein, M. (1986), Molecular stratigraphy: a new tool for climatic assessment, *Nature*, 320(6058), 129-133.

Broecker, W. S. (2001), Was the Medieval Warm Period global?, *Science*, 291(5508), 1497-1499.

Büntgen, U., Frank, D., Grudd, H., and Esper, J. (2008), Long-term summer temperature variations in the Pyrenees, *Climate Dynamics*, 31(6), 615-631.

Büntgen, U., Trouet, V., Frank, D., Leuschner, H. H., Friedrichs, D., Luterbacher, J., and Esper, J. (2010), Tree-ring indicators of German summer drought over the last millennium, *Quaternary Science Reviews*, 29(7-8), 1005-1016.

Cacho, I., Grimalt, J. O., Pelejero, C., Canals, M., Sierro, F. J., Flores, J. A., and Shackleton, N. (1999), Dansgaard-Oeschger and Heinrich Event imprints in Alboran Sea paleotemperatures, *Paleoceanography*, 14(6), 698-705.

Cacho, I., Grimalt, J. O., Sierro, F. J., Shackleton, N., and Canals, M. (2000), Evidence for enhanced Mediterranean thermohaline circulation during rapid climatic coolings, *Earth and Planetary Science Letters*, 183(3-4), 417-429.

Cacho, I., Grimalt, J. O., Canals, M., Sbaffi, L., Shackleton, N. J., Schönfeld, J., and Zahn, R. (2001), Variability of the western Mediterranean Sea surface temperature during the last 25,000 years and its connection with the Northern Hemisphere climatic changes, *Paleoceanography*, 16(1), 40-52.

Cacho, I., Grimalt, J. O., and Canals, M. (2002), Response of the Western Mediterranean Sea to rapid climatic variability during the last 50,000 years: a molecular biomarker approach, *Journal of Marine Systems*, 33-34, 253-272.

Cacho, I., Shackleton, N., Elderfield, H., Sierro, F. J., and Grimalt, J. O. (2006), Glacial rapid variability in deep-water temperature and $\delta^{18}O$ from the Western Mediterranean Sea, *Quaternary Science Reviews*, 25(23-24), 3294-3311.

Calvert, S. E., and Pedersen, T. F. (1993), Geochemistry of recent oxic and anoxic marine-sediments implications for the geological record, *Marine Geology*, 113(1-2), 67-88.

Calvert, S. E., and Fontugne, M. R. (2001), On the late Pleistocene-Holocene sapropel record of climatic and oceanographic variability in the eastern Mediterranean, *Paleoceanography*, 16(1), 78-94.

Calvert, S. E., and Pedersen, T. F. (2007), Elemental proxies for palaeoclimatic and palaeoceanographic variability in marine sediments: interpretation and application, in *Proxies in Late Cenozoic Paleoceanography*, edited by C. Hillaire-Marcel and A. D. Vernal, Elsevier, Amsterdam.

Carrión, J. S. (2002), Patterns and processes of Late Quaternary environmental change in a montane region of southwestern Europe, *Quaternary Science Reviews*, 21(18-19), 2047-2066.

Carrión, J. S., Fernández, S., Jiménez-Moreno, G., Fauquette, S., Gil-Romera, G., González-Sampériz, P., and Finlayson, C. (2010), The historical origins of aridity and vegetation degradation in southeastern Spain, J*ournal of Arid Environments*, 74(7), 731-736.

Casford, J. S. L., Abu-Zied, R., Rohling, E. J., Cooke, S., Boessenkool, K. P., Brinkhuis, H., De Vries, C., Wefer, G., Geraga, M., Papatheodorou, G., Croudace, I., Thomson, J., and Lykousis, V. (2001), Mediterranean climate variability during the Holocene, *Mediterranean Marine Science*, 2(1), 45-55.

Castañeda, I. S., Werne, J. P., and Johnson, T. C. (2007), Wet and arid phases in the southeast African tropics since the Last Glacial Maximum, *Geology*, 35(9), 823-826.

Castañeda, I. S., Werne, J. P., Johnson, T. C., and Filley, T. R. (2009), Late Quaternary vegetation history of southeast Africa: The molecular isotopic record from Lake Malawi, *Palaeogeography, Palaeoclimatology, Palaeoecology*, 275(1-4), 100-112.

Castañeda, I. S., Schefuß, E., Pätzold, J., Sinninghe Damsté, J. S., Weldeab, S., and Schouten, S. (2010), Millennial-scale sea surface temperature changes in the eastern Mediterranean (Nile River Delta region) over the last 27,000 years, *Paleoceanography*, 25(1), PA1208.

Castañeda, I. S., and Schouten, S. (2011), A review of molecular organic proxies for examining modern and ancient lacustrine environments, *Quaternary Science Reviews*, 30(21-22), 2851-2891.

Cerling, T. E., Wang, Y., and Quade, J. (1993), Expansion of C_4 ecosystems as an indicator of global ecological change in the Late Miocene, *Nature*, 361(6410), 344-345.

Colmenero-Hidalgo, E., Flores, J. A., Sierro, F. J., Bárcena, M. A., Löwemark, L., Schönfeld, J., and Grimalt, J. O. (2004), Ocean surface water response to short-term climate changes revealed by coccolithophores from the Gulf of Cadiz (NE Atlantic) and Alboran Sea (W Mediterranean), *Palaeogeography, Palaeoclimatology, Palaeoecology*, 205(3-4), 317-336.

Collister, J. W., Rieley, G., Stern, B., Eglinton, G., and Fry, B. (1994), Compound-specific $\delta^{13}C$ analyses of leaf lipids from plants with differing carbon dioxide metabolisms, *Organic Geochemistry*, 21(6-7), 619-627.

Comas, M. C., and Ivanov, M. K. (2006), Eastern Alboran margin: the transition between the Alboran and the Balearic-Algerian basins, in *Interdisciplinary geoscience studies of the Gulf of Cadiz and Western Mediterranean basins*, edited by N. H. Kenyon, M. K. Ivanov, A. M. Akhmetzhanov and E. V. Kozlova, pp. 48-61, IOC Technical Series Nº. 70, UNESCO.

Combourieu-Nebout, N., Turon, J. L., Zahn, R., Capotondi, L., Londeix, L., and Pahnke, K. (2002), Enhanced aridity and atmospheric high-pressure stability over the western Mediterranean during the North Atlantic cold events of the past 50 k.y, *Geology*, 30(10), 863-866.

Combourieu-Nebout, N., Peyron, O., Dormoy, I., Desprat, S., Beaudouin, C., Kotthoff, U., and Marret, F. (2009), Rapid climatic variability in the west Mediterranean during the last 25,000 years from high resolution pollen data, *Climate of the Past*, 5(3), 503-521.

Crowley, T. J. (2000), Causes of climate change over the past 1000 years, *Science*, 289(5477), 270-277.

Crowley, T. J., and Lowery, T. S. (2000), How warm was the Medieval Warm Period?, *AMBIO: A Journal of the Human Environment*, 29(1), 51-54.

Chamley, H. (1989), *Clay Sedimentology*, Springer-Verlag, Berlin.

Dansgaard, W., Johnsen, S. J., Clausen, H. B., Dahl-Jensen, D., Gundestrup, N. S., Hammer, C. U., Hvidberg, C. S., Steffensen, J. P., Sveinbjornsdottir, A. E., Jouzel, J., and Bond, G. (1993), Evidence for general instability of past climate from a 250-kyr ice-core

record, *Nature*, 364(6434), 218-220.

Dawson, A. G., Hickey, K., Mayewski, P. A., and Nesje, A. (2007), Greenland (GISP2) ice core and historical indicators of complex North Atlantic climate changes during the fourteenth century, *Holocene*, 17(4), 427-434.

De Lange, G. J., Middelburg, J. J., and Pruysers, P. A. (1989), Middle and Late Quaternary depositional sequences and cycles in the eastern Mediterranean, *Sedimentology*, 36(1), 151-156.

deMenocal, P., Ortiz, J., Guilderson, T., Adkins, J., Sarnthein, M., Baker, L., and Yarusinsky, M. (2000), Abrupt onset and termination of the African Humid Period: rapid climate responses to gradual insolation forcing, *Quaternary Science Reviews*, 19(1-5), 347-361.

Development Core Team, R. (2011), *R: A language and environment for statistical computing*, edited, R Foundation for Statistical Computing, Vienna, Austria.

Diaz, H. F., Trigo, R., Hughes, M. K., Mann, M. E., Xoplaki, E., and Barriopedro, D. (2011), Spatial and temporal characteristics of climate in Medieval times revisited, *Bulletin of the American Meteorological Society*, 92(11), 1487-1500.

Durrieu de Madron, X., Guieu, C., Sempéré, R., Conan, P., Cossa, D., D'Ortenzio, F., Estournel, C., Gazeau, F., Rabouille, C., Stemmann, L., Bonnet, S., Diaz, F., Koubbi, P., Radakovitch, O., Babin, M., Baklouti, M., Bancon-Montigny, C., Belviso, S., Bensoussan, N., Bonsang, B., Bouloubassi, I., Brunet, C., Cadiou, J. F., Carlotti, F., Chami, M., Charmasson, S., Charrière, B., Dachs, J., Doxaran, D., Dutay, J. C., Elbaz-Poulichet, F., Eléaume, M., Eyrolles, F., Fernandez, C., Fowler, S., Francour, P., Gaertner, J. C., Galzin, R., Gasparini, S., Ghiglione, J. F., Gonzalez, J. L., Goyet, C., Guidi, L., Guizien, K., Heimbürger, L. E., Jacquet, S. H. M., Jeffrey, W. H., Joux, F., Le Hir, P., Leblanc, K., Lefèvre, D., Lejeusne, C., Lemé, R., Loÿe-Pilot, M. D., Mallet, M., Méjanelle, L., Mélin, F., Mellon, C., Mérigot, B., Merle, P. L., Migon, C., Miller, W. L., Mortier, L., Mostajir, B., Mousseau, L., Moutin, T., Para, J., Pérez, T., Petrenko, A., Poggiale, J. C., Prieur, L., Pujo-Pay, M., Pulido, V., Raimbault, P., Rees, A. P., Ridame, C., Rontani, J. F., Ruiz Pino, D., Sicre, M. A., Taillandier, V., Tamburini, C., Tanaka, T., Taupier-Letage, I., Tedetti, M., Testor, P., Thébault, H., Thouvenin, B., Touratier, F., Tronczynski, J., Ulses, C., Van Wambeke, F., Vantrepotte, V., Vaz, S., and Verney, R. (2011), Marine ecosystems' responses to climatic and anthropogenic forcings in the Mediterranean, *Progress In Oceanography*, 91(2), 97-166.

Eagle, M., Paytan, A., Arrigo, K. R., van Dijken, G., and Murray, R. W. (2003), A comparison between excess barium and barite as indicators of carbon export, *Paleoceanography*, 18(1), 1021.

Eglinton, G., and Hamilton, R. J. (1967), Leaf epicuticular waxes, *Science*, 156(3780), 1322-1335.

Eglinton, T. I., and Eglinton, G. (2008), Molecular proxies for paleoclimatology, *Earth and Planetary Science Letters*, 275(1-2), 1-16.

Elderfield, H., and Ganssen, G. (2000), Past temperature and $\delta^{18}O$ of surface ocean waters inferred from foraminiferal Mg/Ca ratios, *Nature*, 405(6785), 442-445.

Emeis, K.-C., Struck, U., Schulz, H.-M., Rosenberg, R., Bernasconi, S., Erlenkeuser, H., Sakamoto, T., and Martinez-Ruiz, F. (2000), Temperature and salinity variations of Mediterranean Sea surface waters over the last 16,000 years from records of planktonic stable oxygen isotopes and alkenone unsaturation ratios, *Palaeogeography, Palaeoclimatology, Palaeoecology*, 158(3-4), 259-280.

Esper, J., Cook, E. R., and Schweingruber, F. H. (2002), Low-frequency signals in long tree-ring chronologies for reconstructing past temperature variability, *Science*, 295(5563), 2250-2253.

Esper, J., Frank, D., Büntgen, U., Verstege, A., Luterbacher, J., and Xoplaki, E. (2007), Long-term drought severity variations in Morocco, *Geophysical Research Letters*, 34(17), L17702.

Fabres, J., Calafat, A., Sánchez-Vidal, A., Canals, M., and Heussner, S. (2002), Composition and spatio-temporal variability of particle fluxes in the Western Alboran Gyre, Mediterranean Sea, *Journal of Marine Systems*, 33-34, 431-456.

Fagel, N. (2007), Marine clay minerals, deep circulation and climate, in *Paleoceanography of the Late Cenozoic*, edited by C. Hillaire-Marcel and A. D. Vernal, pp. 139-184, Elsevier, Amsterdam.

Fernex, F., Février, G., Bénaïm, J., and Arnoux, A. (1992), Copper, lead and zinc trapping in Mediterranean deep-sea sediments: probable coprecipitation with Mn and Fe, *Chemical Geology*, 98(3-4), 293-306.

Frigola, J., Moreno, A., Cacho, I., Canals, M., Sierro, F. J., Flores, J. A., Grimalt, J. O., Hodell, D. A., and Curtis, J. H. (2007), Holocene climate variability in the western Mediterranean region from a deepwater sediment record, *Paleoceanography*, 22, PA2209.

Frigola, J., Moreno, A., Cacho, I., Canals, M., Sierro, F. J., Flores, J. A., and Grimalt, J. O. (2008), Evidence of abrupt changes in Western Mediterranean Deep Water circulation during the last 50 kyr: A high-resolution marine record from the Balearic Sea, *Quaternary International*, 181(1), 88-104.

Gallego-Torres, D., Martínez-Ruiz, F., Paytan, A., Jiménez-Espejo, F. J., and Ortega-Huertas, M. (2007), Pliocene-Holocene evolution of depositional conditions in the eastern Mediterranean: Role of anoxia vs. productivity at time of sapropel deposition, *Palaeogeography, Palaeoclimatology, Palaeoecology*, 246(2-4), 424-439.

Gallego, M. C., Trigo, R. M., Vaquero, J. M., Brunet, M., García, J. A., Sigró, J., and Valente, M. A. (2011), Trends in frequency indices of daily precipitation over the Iberian Peninsula during the last century, *Journal of Geophysical Research*, 116(D2), D02109.

García-Gorriz, E., and Carr, M.-E. (1999), The climatological annual cycle of satellite-derived phytoplankton pigments in the Alboran Sea, *Geophysical Research Letters*, 26(19), 2985-2988.

García-Gorriz, E., and Carr, M.-E. (2001), Physical control of phytoplankton distributions in the Alboran Sea: A numerical and satellite

approach, *Journal of Geophysical Research*, 106(C8), 16795-16805.

García-Orellana, J., Gracia, E., Vizcaino, A., Masqué, P., Olid, C., Martínez-Ruiz, F., Piñero, E., Sánchez-Cabeza, J.-A., and Dañobeitia, J. (2006), Identifying instrumental and historical earthquake records in the SW Iberian margin using ^{210}Pb turbidite chronology, *Geophysical Research Letters*, 33(24), L24601.

García-Orellana, J., Pates, J. M., Masqué, P., Bruach, J. M., and Sánchez-Cabeza, J. A. (2009), Distribution of artificial radionuclides in deep sediments of the Mediterranean Sea, *Science of the Total Environment*, 407(2), 887-898.

Giralt, S., Moreno, A., Bao, R., Sáez, A., Prego, R., Valero-Garcés, B. L., Pueyo, J. J., González-Sampériz, P., and Taberner, C. (2008), A statistical approach to disentangle environmental forcings in a lacustrine record: The Lago Chungará case (Chilean Altiplano), *Journal of Paleolimnology*, 40(1), 195-215.

Giralt, S., Rico-Herrero, M. T., Vega, J. C., and Valero-Garcés, B. L. (2011), Quantitative climate reconstruction linking meteorological, limnological and XRF core scanner datasets: The Lake Sanabria case study, NW Spain, *Journal of Paleolimnology*, 46(3), 487-502.

Goosse, H., Renssen, H., Timmermann, A., and Bradley, R. S. (2005), Internal and forced climate variability during the last millennium: A model-data comparison using ensemble simulations, *Quaternary Science Reviews*, 24(12-13), 1345-1360.

Graham, N., Ammann, C., Fleitmann, D., Cobb, K., and Luterbacher, J. (2011), Support for global climate reorganization during the "Medieval Climate Anomaly", *Climate Dynamics*, 37(5), 1217-1245.

Grootes, P. M., and Stuiver, M. (1997), Oxygen 18/16 variability in Greenland snow and ice with 10-3-to 105-year time resolution, *Journal of Geophysical Research*, 102(C12), 26455-26470.

Guerzoni, S., Molinaroli, E., and Chester, R. (1997), Saharan dust inputs to the western Mediterranean Sea: depositional patterns, geochemistry and sedimentological implications, *Deep Sea Research Part II: Topical Studies in Oceanography*, 44(3-4), 631-654.

Hall, I. R., and McCave, I. N. (2000), Palaeocurrent reconstruction, sediment and thorium focussing on the Iberian margin over the last 140 ka, *Earth and Planetary Science Letters*, 178(1-2), 151-164.

Heimbürger, L.-E., Migon, C., Dufour, A., Chiffoleau, J.-F., and Cossa, D. (2010), Trace metal concentrations in the North-western Mediterranean atmospheric aerosol between 1986 and 2008: Seasonal patterns and decadal trends, *Science of the Total Environment*, 408(13), 2629-2638.

Hillaire-Marcel, C., and Vernal, A. D. (2007), *Proxies in Late Cenozoic paleoceanography*, Elsevier, Amsterdam, The Netherlands.

Hillerbrand, R., and Ghil, M. (2008), Anthropogenic climate change: Scientific uncertainties and moral dilemmas, *Physica D: Nonlinear Phenomena*, 237(14-17), 2132-2138.

Hopmans, E. C., Schouten, S., Pancost, R.

D., van der Meer, M. T., and Sinninghe Damsté, J. S. (2000), Analysis of intact tetraether lipids in archaeal cell material and sediments by high performance liquid chromatography/atmospheric pressure chemical ionization mass spectrometry, *Rapid Communications in Mass Spectrometry*, 14(7), 585-589.

Hopmans, E. C., Weijers, J. W. H., Schefuß, E., Herfort, L., Sinninghe Damsté, J. S., and Schouten, S. (2004), A novel proxy for terrestrial organic matter in sediments based on branched and isoprenoid tetraether lipids, *Earth and Planetary Science Letters*, 224(1-2), 107-116.

Horstman, E. L. (1957), The distribution of lithium, rubidium and caesium in igneous and sedimentary rocks, *Geochimica et Cosmochimica Acta*, 12(1-2), 1-28.

Hughes, M. K., and Diaz, H. F. (1994), Was there a 'Medieval Warm Period', and if so, where and when?, *Climatic Change*, 26(2), 109-142.

Huguet, C., Martrat, B., Grimalt, J. O., Sinninghe Damsté, J. S., and Schouten, S. (2011), Coherent millennial-scale patterns in $U_{37}^{k'}$ and TEX_{86}^{H} temperature records during the penultimate interglacial-to-glacial cycle in the western Mediterranean, *Paleoceanography*, 26(2), PA2218.

Hurrell, J. W. (1995), Decadal trends in the North Atlantic Oscillation: Regional temperatures and precipitation, *Science*, 269(5224), 676-679.

Hutson, W. H. (1980), The Agulhas Current during the Late Pleistocene: Analysis of modern faunal analogs, *Science*, 207(4426), 64-66.

Imbrie, J., and Kipp, N. G. (1971), A new micropaleontological method for quantitative paleoclimatology: Application to a late Pleistocene caribbean core, in *The Late Cenozoic Glacial Ages*, edited by K. K. Turekian, pp. 71-181, Yale University Press, New Haven, CT.

Incarbona, A., Ziveri, P., Di Stefano, E., Lirer, F., Mortyn, G., Patti, B., Pelosi, N., Sprovieri, M., Tranchida, G., Vallefuoco, M., Albertazzi, S., Bellucci, L. G., Bonanno, A., Bonomo, S., Censi, P., Ferraro, L., Giuliani, S., Mazzola, S., and Sprovieri, R. (2010), The impact of the Little Ice Age on coccolithophores in the central Mediterranean Sea, *Climate of the Past*, 6, 795-805.

IPCC (2007), Summary for Policymakers, in *Climate Change 2007: The Physical Science Basis. Contribution of Working Group I to the Fourth Assessment Report of the Intergovernmental Panel on Climate Change*, edited by D. Q. S. Solomon, M. Manning, Z. Chen, M. Marquis, K.B. Averyt, M.Tignor and H.L. Miller, Cambridge University Press, Cambridge, United Kingdom and New York, NY, USA.

Issar, A. (2003), *Climate Changes during The Holocene and their Impact on Hydrological Systems*, Cambridge University Press, Cambridge, UK.

Jalut, G., Esteban Amat, A., Bonnet, L., Gauquelin, T., and Fontugne, M. (2000), Holocene climatic changes in the Western Mediterranean, from south-east France to south-east Spain, *Palaeogeography, Palaeoclimatology, Palaeoecology*, 160(3-4), 255-290.

Jalut, G., Dedoubat, J. J., Fontugne, M., and Otto, T. (2009), Holocene circum-Mediterranean vegetation changes: Climate forcing and

human impact, *Quaternary International*, 200(1-2), 4-18.

Jansen, E., Overpeck, J., Briffa, K. R., Duplessy, J. C., Joos, F., Masson-Delmotte, V., Olago, D., Otto-Bliesner, B., Peltier, W. R., Rahmstorf, S., Ramesh, R., Raynaud, D., Rind, D., Solomina, O., Villalba, R., and Zhang, D. (2007), Palaeoclimate, in *Climate Change 2007: The Physical Science Basis. Contribution of Working Group I to the Fourth Assessment Report of the Intergovernmental Panel on Climate Change*, edited by S. Solomon, D. Qin, M. Manning, Z. Chen, M. Marquis, K.B. Averyt, M. Tignor and H.L. Miller, Cambridge University Press, Cambridge, United Kingdom and New York, NY, USA.

Jilbert, T., deLange, G. J., and Reichart, G.-J. (2008), Laminated sediments as archives of short timescale climate change and palaeoceanography of the Mediterranean. *Doctoral Thesis*, Utrecht University.

Jiménez-Espejo, F. J., Martínez-Ruiz, F., Sakamoto, T., Iijima, K., Gallego-Torres, D., and Harada, N. (2007), Paleoenvironmental changes in the western Mediterranean since the last glacial maximum: High resolution multiproxy record from the Algero-Balearic basin, *Palaeogeography, Palaeoclimatology, Palaeoecology*, 246(2-4), 292-306.

Jiménez-Espejo, F. J., Martínez-Ruiz, F., Rogerson, M., González-Donoso, J. M., Romero, O. E., Linares, D., Sakamoto, T., Gallego-Torres, D., Rueda Ruiz, J. L., Ortega-Huertas, M., and Perez Claros, J. A. (2008), Detrital input, productivity fluctuations, and water mass circulation in the westernmost Mediterranean Sea since the Last Glacial Maximum, *Geochemistry, Geophysics, Geosystems*, 9, Q11U02.

Jirikowic, J. L., and Damon, P. E. (1994), The medieval solar activity maximum, *Climatic Change*, 26(2), 309-316.

Jones, M. D., Roberts, C. N., Leng, M. J., and Türkes, M. (2006), A high-resolution late Holocene lake isotope record from Turkey and links to North Atlantic and monsoon climate, *Geology*, 34(5), 361-364.

Jones, P. D., Osborn, T. J., and Briffa, K. R. (2001), The evolution of climate over the Last Millennium, *Science*, 292(5517), 662-667.

Jones, P. D., and Mann, M. E. (2004), Climate over past millennia, *Reviews of Geophysics*, 42(2), RG2002.

Jones, P. D., Briffa, K. R., Osborn, T. J., Lough, J. M., van Ommen, T. D., Vinther, B. M., Luterbacher, J., Wahl, E. R., Zwiers, F. W., Mann, M. E., Schmidt, G. A., Ammann, C. M., Buckley, B. M., Cobb, K. M., Esper, J., Goosse, H., Graham, N., Jansen, E., Kiefer, T., Kull, C., Küttel, M., Mosley-Thompson, E., Overpeck, J. T., Riedwyl, N., Schulz, M., Tudhope, A. W., Villalba, R., Wanner, H., Wolff, E., and Xoplaki, E. (2009), High-resolution palaeoclimatology of the last millennium: a review of current status and future prospects, *The Holocene*, 19(1), 3-49.

Karl, T. R., Melillo, J. M., and Peterson, T. C. (2009), *Global Climate Change Impacts in the United States*, Cambridge University Press.

Kim, J.-H., Schouten, S., Hopmans, E. C., Donner, B., and Sinninghe Damsté, J. S. (2008), Global sediment core-top calibration of the TEX_{86} paleothermometer in the ocean, *Geochimica et Cosmochimica Acta*, 72(4), 1154-1173.

Kim, J.-H., van der Meer, J., Schouten, S., Helmke, P., Willmott, V., Sangiorgi, F., Koç, N., Hopmans, E. C., and Damsté, J. S. S. (2010), New indices and calibrations derived from the distribution of crenarchaeal isoprenoid tetraether lipids: Implications for past sea surface temperature reconstructions, *Geochimica et Cosmochimica Acta*, 74(16), 4639-4654.

Kisch, H. J. (1991), Illite crystallinity: recommendations on sample preparation, X-ray diffraction settings, and interlaboratory samples, *Journal of Metamorphic Geology*, 9(6), 665-670.

Knippertz, P., Christoph, M., and Speth, P. (2003), Long-term precipitation variability in Morocco and the link to the large-scale circulation in recent and future climates, *Meteorology and Atmospheric Physics*, 83(1), 67-88.

Kolla, V., Biscaye, P. E., and Hanley, A. F. (1979), Distribution of quartz in late Quaternary Atlantic sediments in relation to climate, *Quaternary Research*, 11(2), 261-277.

Lamb, H. H. (1965), The early medieval warm epoch and its sequel, *Palaeogeography, Palaeoclimatology, Palaeoecology*, 1, 13-37.

Lea, D. W. (2003), Elemental and isotopic proxies of past ocean temperatures, in *Treatise on Geochemistry*, edited by D. H. Heinrich and K. T. Karl, pp. 365-390, Pergamon, Oxford.

Leider, A., Hinrichs, K.-U., Mollenhauer, G., and Versteegh, G. J. M. (2010), Core-top calibration of the lipid-based and TEX_{86} temperature proxies on the southern Italian shelf (SW Adriatic Sea, Gulf of Taranto), *Earth and Planetary Science Letters*, 300(1-2), 112-124.

Levin, I., and Kromer, B. (2004), The tropospheric (CO_2)-C-14 level in mid-latitudes of the Northern Hemisphere (1959-2003), *Radiocarbon*, 46(3), 1261-1272.

Levin, I., Hammer, S., Kromer, B., and Meinhardt, F. (2008), Radiocarbon observations in atmospheric CO_2: Determining fossil fuel CO_2 over Europe using Jungfraujoch observations as background, *Science of the Total Environment*, 391(2-3), 211-216.

Lindner, M., Maroschek, M., Netherer, S., Kremer, A., Barbati, A., Garcia-Gonzalo, J., Seidl, R., Delzon, S., Corona, P., Kolström, M., Lexer, M. J., and Marchetti, M. (2010), Climate change impacts, adaptive capacity, and vulnerability of European forest ecosystems, *Forest Ecology and Management*, 259(4), 698-709.

Lionello, P., Malanotte-Rizzoli, P., Boscolo, R., Alpert, P., Artale, V., Li, L., Luterbacher, J., May, W., Trigo, R., Tsimplis, M., Ulbrich, U., and Xoplaki, E. (2006), The Mediterranean climate: An overview of the main characteristics and issues, in *Mediterranean Climate Variability* edited by P. Lionello, P. Malanotte-Rizzoli and R. Boscolo, pp. 1-26, Elsevier, Amsterdam.

Long, E., Macdonald, D., Smith, S., and Calder, F. (1995), Incidence of adverse biological effects within ranges of chemical concentrations in marine and estuarine sediments, *Environmental Management*, 19(1), 81-97.

Macklin, M. G., Benito, G., Gregory, K. J., Johnstone, E., Lewin, J., Michczynska, D. J., Soja, R., Starkel, L., and Thorndycraft, V. R. (2006), Past hydrological events reflected in the Holocene fluvial record of Europe, *CATENA*,

66(1-2), 145-154.

Magny, M., Guiot, J., and Schoellammer, P. (2001), Quantitative reconstruction of Younger Dryas to Mid-Holocene paleoclimates at Le Locle, Swiss Jura, using pollen and lake-level data, *Quaternary Research*, 56(2), 170-180.

Magny, M., Miramont, C., and Sivan, O. (2002), Assessment of the impact of climate and anthropogenic factors on Holocene Mediterranean vegetation in Europe on the basis of palaeohydrological records, *Palaeogeography, Palaeoclimatology, Palaeoecology*, 186(1-2), 47-59.

Magny, M. (2004), Holocene climate variability as reflected by mid-European lake-level fluctuations and its probable impact on prehistoric human settlements, *Quaternary International*, 113(1), 65-79.

Mangini, A., Jung, M., and Laukenmann, S. (2001), What do we learn from peaks of uranium and of manganese in deep sea sediments?, *Marine Geology*, 177(1-2), 63-78.

Mangini, A., Blumbach, P., Verdes, P., Spötl, C., Scholz, D., Machel, H., and Mahon, S. (2007), Combined records from a stalagmite from Barbados and from lake sediments in Haiti reveal variable seasonality in the Caribbean between 6.7 and 3 ka BP, *Quaternary Science Reviews*, 26(9-10), 1332-1343.

Mann, M. E., Bradley, R. S., and Hughes, M. K. (1999), Northern hemisphere temperatures during the past millennium: Inferences, uncertainties, and limitations, *Geophysical Research Letters*, 26(6), 759-762.

Mann, M. E., Zhang, Z., Hughes, M. K., Bradley, R. S., Miller, S. K., Rutherford, S., and Ni, F. (2008), Proxy-based reconstructions of hemispheric and global surface temperature variations over the past two millennia, *Proceedings of the National Academy of Sciences*, 105(36), 13252-13257.

Mann, M. E., Zhang, Z., Rutherford, S., Bradley, R. S., Hughes, M. K., Shindell, D., Ammann, C., Faluvegi, G., and Ni, F. (2009), Global Signatures and Dynamical Origins of the Little Ice Age and Medieval Climate Anomaly, *Science*, 326(5957), 1256-1260.

Marchal, O., Cacho, I., Stocker, T. F., Grimalt, J. O., Calvo, E., Martrat, B., Shackleton, N., Vautravers, M., Cortijo, E., van Kreveld, S., Andersson, C., Koç, N., Chapman, M., Sbaffi, L., Duplessy, J.-C., Sarnthein, M., Turon, J.-L., Duprat, J., and Jansen, E. (2002), Apparent long-term cooling of the sea surface in the northeast Atlantic and Mediterranean during the Holocene, *Quaternary Science Reviews*, 21(4-6), 455-483.

Martín-Puertas, C., Valero-Garcés, B. L., Mata, M. P., González-Sampériz, P., Bao, R., Moreno, A., and Stefanova, V. (2008), Arid and humid phases in southern Spain during the last 4000 years: The Zoñar Lake record, Córdoba, *Holocene*, 18(6), 907-921.

Martín-Puertas, C., Jiménez-Espejo, F., Martínez-Ruiz, F., Nieto-Moreno, V., Rodrigo, M., Mata, M. P., and Valero-Garcés, B. L. (2010), Late Holocene climate variability in the southwestern Mediterranean region: an integrated marine and terrestrial geochemical approach, *Climate of the Past*, 6, 807-816.

Martín-Puertas, C., Valero-Garcés, B., Mata,

M., Moreno, A., Giralt, S., Martínez-Ruiz, F., and Jiménez-Espejo, F. (2011), Geochemical processes in a Mediterranean Lake: a high-resolution study of the last 4,000 years in Zoñar Lake, southern Spain, *Journal of Paleolimnology*, 46(3), 405-421.

Martin, J. D. (2004), *Using XPowder: A software Package for Powder X-Ray Diffraction Analysis*, 105 pp., Spain.

Martínez-Ruiz, F., Kastner, M., Paytan, A., Ortega-Huertas, M., and Bernasconi, S. M. (2000), Geochemical evidence for enhanced productivity during S1 sapropel deposition in the eastern Mediterranean, *Paleoceanography*, 15(2), 200-209.

Martínez-Ruiz, F., Paytan, A., Kastner, M., González-Donoso, J. M., Linares, D., Bernasconi, S. M., and Jiménez-Espejo, F. J. (2003), A comparative study of the geochemical and mineralogical characteristics of the S1 sapropel in the western and eastern Mediterranean, *Palaeogeography, Palaeoclimatology, Palaeoecology*, 190, 23-37.

Martrat, B., Grimalt, J. O., López-Martínez, C., Cacho, I., Sierro, F. J., Flores, J. A., Zahn, R., Canals, M., Curtis, J. H., and Hodell, D. A. (2004), Abrupt temperature changes in the Western Mediterranean over the past 250,000 years, *Science*, 306(5702), 1762-1765.

Martrat, B., Grimalt, J. O., Shackleton, N. J., de Abreu, L., Hutterli, M. A., and Stocker, T. F. (2007), Four climate cycles of recurring deep and surface water destabilizations on the Iberian margin, *Science*, 317(5837), 502-507.

Masqué, P., Fabres, J., Canals, M., Sánchez-Cabeza, J. A., Sánchez-Vidal, A., Cacho, I., Calafat, A. M., and Bruach, J. M. (2003), Accumulation rates of major constituents of hemipelagic sediments in the deep Alboran Sea: a centennial perspective of sedimentary dynamics, *Marine Geology*, 193(3-4), 207-233.

Masson, V., Vimeux, F., Jouzel, J., Morgan, V., Delmotte, M., Ciais, P., Hammer, C., Johnsen, S., Lipenkov, V. Y., Mosley-Thompson, E., Petit, J.-R., Steig, E. J., Stievenard, M., and Vaikmae, R. (2000), Holocene climate variability in Antarctica based on 11 ice-core isotopic records, *Quaternary Research*, 54(3), 348-358.

Mayewski, P. A., Meeker, L. D., Twickler, M. S., Whitlow, S., Yang, Q., Lyons, W. B., and Prentice, M. (1997), Major features and forcing of high-latitude northern hemisphere atmospheric circulation using a 110,000-year-long glaciochemical series, *Journal of Geophysical Research*, 102(C12), 26345-26366.

Mayewski, P. A., Rohling, E. E., Curt Stager, J., Karlén, W., Maasch, K. A., David Meeker, L., Meyerson, E. A., Gasse, F., van Kreveld, S., Holmgren, K., Lee-Thorp, J., Rosqvist, G., Rack, F., Staubwasser, M., Schneider, R. R., and Steig, E. J. (2004), Holocene climate variability, *Quaternary Research*, 62(3), 243-255.

McCave, I. N., Manighetti, B., and Robinson, S. G. (1995), Sortable silt and fine sediment size/composition slicing: parameters for palaeocurrent speed and palaeoceanography, *Paleoceanography*, 10(3), 593-610.

McCave, I. N., and Hall, I. R. (2006), Size sorting in marine muds: Processes, pitfalls, and prospects for paleoflow-speed proxies, *Geochemistry, Geophysics, Geosystems*, 7, Q10N05.

McDermott, F., Mattey, D. P., and Hawkesworth, C. (2001), Centennial-scale Holocene climate variability revealed by a high-resolution speleothem $\delta^{18}O$ record from SW Ireland, *Science*, 294(5545), 1328-1331.

McDonough, W. F., and Sun, S. S. (1995), The composition of the Earth, *Chemical Geology*, 120(3-4), 223-253.

McLennan, S. M. (1989), Rare earth elements in sedimentary rocks; influence of provenance and sedimentary processes, *Reviews in Mineralogy and Geochemistry*, 21(1), 169-200.

McManus, J., Berelson, W. M., Klinkhammer, G. P., Hammond, D. E., and Holm, C. (2005), Authigenic uranium: Relationship to oxygen penetration depth and organic carbon rain, *Geochimica et Cosmochimica Acta*, 69(1), 95-108.

MEDAR (2002), *MEDATLAS/2002 Database. Mediterranean and Black Sea Database of Temperature Salinity and Bio-chemical Parameters. Climatological Atlas*, edited, Institut Français de Recherche pour L'Exploitation de la Mer, (IFREMER) (4 Cdroms).

Meeker, L. D., and Mayewski, P. A. (2002), A 1400-year high-resolution record of atmospheric circulation over the North Atlantic and Asia, *The Holocene*, 12(3), 257-266.

Melki, T., Kallel, N., Jorissen, F. J., Guichard, F., Dennielou, B., Berné, S., Labeyrie, L., and Fontugne, M. (2009), Abrupt climate change, sea surface salinity and paleoproductivity in the western Mediterranean Sea (Gulf of Lion) during the last 28 kyr, *Palaeogeography, Palaeoclimatology, Palaeoecology*, 279(1-2), 96-113.

Millot, C. (1999), Circulation in the Western Mediterranean Sea, *Journal of Marine Systems*, 20(1-4), 423-442.

Millot, C. (2008), Short-term variability of the Mediterranean in- and out-flows, *Geophysical Research Letters*, 35(15).

Moberg, A., Sonechkin, D. M., Holmgren, K., Datsenko, N. M., and Karlen, W. (2005), Highly variable Northern Hemisphere temperatures reconstructed from low- and high-resolution proxy data, *Nature*, 433(7026), 613-617.

Morellón, M., Valero-Garcés, B., González-Sampériz, P., Vegas-Vilarrúbia, T., Rubio, E., Rieradevall, M., Delgado-Huertas, A., Mata, P., Romero, O., Engstrom, D. R., López-Vicente, M., Navas, A., and Soto, J. (2011), Climate changes and human activities recorded in the sediments of Lake Estanya (NE Spain) during the Medieval Warm Period and Little Ice Age, *Journal of Paleolimnology*, 46(3), 423-452.

Moreno, A., Cacho, I., Canals, M., Prins, M. A., Sánchez-Goñi, M.-F., Grimalt, J. O., and Weltje, G. J. (2002), Saharan dust transport and high-latitude glacial climatic variability: The Alboran Sea record, *Quaternary Research*, 58(3), 318-328.

Moreno, A., Cacho, I., Canals, M., Grimalt, J. O., and Sánchez-Vidal, A. (2004), Millennial-scale variability in the productivity signal from the Alboran Sea record, Western Mediterranean Sea, *Palaeogeography, Palaeoclimatology, Palaeoecology*, 211(3-4), 205-219.

Moreno, A., Cacho, I., Canals, M., Grimalt, J. O., Sánchez-Goñi, M. F., Shackleton, N., and Sierro, F. J. (2005), Links between marine and atmospheric processes oscillating on a millennial time-scale. A multi-proxy study of the last 50,000 yr from the Alboran Sea (Western Mediterranean Sea), *Quaternary Science Reviews*, 24(14-15), 1623-1636.

Moreno, A., Valero-Garcés, B. L., González-Sampériz, P., and Rico, M. (2008), Flood response to rainfall variability during the last 2,000 years inferred from the Taravilla Lake record (Central Iberian Range, Spain), *Journal of Paleolimnology*, 40(3), 943-961.

Moreno, A., Pérez, A., Frigola, J., Nieto-Moreno, V., Rodrigo-Gámiz, M., González-Sampériz, P., Morellón, M., Martín-Puertas, C., Corella, J. P., Belmonte, A., Sancho, C., Cacho, I., Herrera, G., Canals, M., Jiménez-Espejo, F., Martínez Ruiz, F., Vegas, T., and and Valero-Garcés, B. L. (2012), The Medieval Climate Anomaly in the IP reconstructed from a compilation of marine and lake records, *Quaternary Science Reviews* (accepted).

Moulin, C., Lambert, C. E., Dulac, F., and Dayan, U. (1997), Control of atmospheric export of dust from North Africa by the North Atlantic Oscillation, *Nature*, 387(6634), 691-694.

Müller, P. J., Kirst, G., Ruhland, G., von Storch, I., and Rosell-Melé, A. (1998), Calibration of the alkenone paleotemperature index $U_{37}^{K'}$ based on core-tops from the eastern South Atlantic and the global ocean (60°N-60°S), *Geochimica et Cosmochimica Acta*, 62(10), 1757-1772.

Murray, A. E., Preston, C. M., Massana, R., Taylor, L. T., Blakis, A., Wu, K., and DeLong, E. F. (1998), Seasonal and spatial variability of bacterial and archaeal assemblages in the coastal waters near Anvers Island, Antarctica, *Applied and Environmental Microbiology*, 64(7), 2585-2595.

Murray, A. E., Blakis, A., Massana, R., Strawzewski, S., Passow, U., Alldredge, A., and DeLong, E. F. (1999), A time series assessment of planktonic archaeal variability in the Santa Barbara Channel, *Aquatic Microbial Ecology*, 20(2), 129-145.

Naranjo, C., García Lafuente, J., Sánchez Garrido, J. C., Sánchez Román, A., and Delgado Cabello, J. (2011), The Western Alboran Gyre helps ventilate the Western Mediterranean Deep Water through Gibraltar, *Deep Sea Research Part I: Oceanographic Research Papers (in press)*.

National Research Council. (2006), *Surface Temperature Reconstructions for the Last 2,000 Years*, The National Academies Press, Washington, DC.

Newman, L., Wanner, H., and Kiefer, T. (2009), Towards a global synthesis of the climate of the last two millennia, *PAGES News*, 17, 130-131.

Nieto-Moreno, V., Martínez-Ruiz, F., Giralt, S., Jiménez-Espejo, F., Gallego-Torres, D., Rodrigo-Gámiz, M., García-Orellana, J., Ortega-Huertas, M., and de Lange, G. J. (2011), Tracking climate variability in the western Mediterranean during the Late Holocene: a multiproxy approach, *Climate of the Past*, 7, 1395-1414.

Nieto-Moreno, V., Martínez-Ruiz, F., Willmott, V., García-Orellana, J., Masqué, P., and Sinninghe Damsté, J. S. (2012), Climate conditions in the westernmost Mediterranean over the last two millenia: a biomarker approach, *Organic Geochemistry* (accepted).

Nijenhuis, I. A., Becker, J., and De Lange, G. J. (2001), Geochemistry of coeval marine sediments in Mediterranean ODP cores and a land section: implications for sapropel formation models, *Palaeogeography, Palaeoclimatology, Palaeoecology*, 165(1-2), 97-112.

Nittrouer, C. A., DeMaster, D. J., McKee, B. A., Cutshall, N. H., and Larsen, I. L. (1984), The effect of sediment mixing on Pb-210 accumulation rates for the Washington continental shelf, *Marine Geology*, 54(3-4), 201-221.

NOAA (1999), *Sediment quality guidelines developed for the National Status and Trends Program*, available at http://ccma.nos.noaa.gov/publications/sqg.pdf.

O'Brien, S. R., Mayewski, P. A., Meeker, L. D., Meese, D. A., Twickler, M. S., and Whitlow, S. I. (1995), Complexity of Holocene climate as reconstructed from a Greenland ice core, *Science*, 270(5244), 1962-1964.

Oksanen, J., Kindt, R., Legendre, P., O'Hara, B., Simpson, G.L., Solymos, P., Stevens, M. H. H., and Wagner, H. (2009), *Vegan: Community Ecology Package*, available at http://cran.r-project.org/web/packages/vegan/index.html, R package version 1.15-4.

Overpeck, J. T., Meehl, G. A., Bony, S., and Easterling, D. R. (2011), Climate data challenges in the 21st century, *Science*, 331(6018), 700-702.

PAGES news (2011), *Medieval Climate Anomaly*, vol. 19, nº1.

Pérez-Folgado, M., Sierro, F. J., Flores, J. A., Cacho, I., Grimalt, J. O., Zahn, R., and Shackleton, N. (2003), Western Mediterranean planktonic foraminifera events and millennial climatic variability during the last 70 kyr, *Marine Micropaleontology*, 48(1-2), 49-70.

Pérez-Folgado, M., Sierro, F. J., Flores, J. A., Grimalt, J. O., and Zahn, R. (2004), Paleoclimatic variations in foraminifera assemblages from the Alboran Sea (Western Mediterranean) during the last 150 ka in ODP Site 977, *Marine Geology*, 212(1-4), 113-131.

Perkins, H., Kinder, T., and Violette, P. L. (1990), The Atlantic inflow in the Western Alboran Sea, *Journal of Physical Oceanography*, 20(2), 242-263.

Pitcher, A., Wuchter, C., Siedenberg, K., Schouten, S., and Sinninghe Damsté, J. S. (2011), Crenarchaeol tracks winter blooms of ammonia-oxidizing *Thaumarchaeota* in the coastal North Sea, *Limnology and Oceanography*, 56, 2308–2318.

Pla, S., and Catalan, J. (2005), Chrysophyte cysts from lake sediments reveal the submillennial winter/spring climate variability in the northwestern Mediterranean region throughout the Holocene, *Climate Dynamics*, 24(2), 263-278.

Poynter, J., and Eglinton, G. (1990), Molecular composition of three sediments from Hole 717C: the Bengal Fan, in *Proceedings of Ocean Drilling Program, Scientific Results, 166*, edited by J.

R. Cochran, Stow, D.A.V., et al., pp. 155-161, College Station, TX (Ocean Drilling Program).

Pozo-Vázquez, D., Gámiz-Fortis, S. R., Tovar-Pescador, J., Esteban-Parra, M. J., and Castro-Díez, Y. (2005), El Niño-Southern oscillation events and associated European winter precipitation anomalies, *International Journal of Climatology*, 25(1), 17-31.

Prahl, F. G., and Wakeham, S. G. (1987), Calibration of unsaturation patterns in long-chain ketone compositions for palaeotemperature assessment, *Nature*, 330(6146), 367-369.

Price, N. B., Calvert, S. E., and Jones, P. G. W. (1970), Distribution of iodine and bromine in sediments of Southwestern Barents-Sea, *Journal of Marine Research*, 28(1), 22-&.

Proctor, C. J., Baker, A., Barnes, W. L., and Gilmour, M. A. (2000), A thousand year speleothem proxy record of North Atlantic climate from Scotland, *Climate Dynamics*, 16(10), 815-820.

Proctor, C., Baker, A., and Barnes, W. (2002), A three thousand year record of North Atlantic climate, *Climate Dynamics*, 19(5), 449-454.

Rampen, S. W., Schouten, S., Wakeham, S. G., and Sinninghe Damsté, J. S. (2007), Seasonal and spatial variation in the sources and fluxes of long chain diols and mid-chain hydroxy methyl alkanoates in the Arabian Sea, *Organic Geochemistry*, 38(2), 165-179.

Rampen, S. W., Schouten, S., Koning, E., Brummer, G.-J. A., and Sinninghe Damsté, J. S. (2008), A 90 kyr upwelling record from the northwestern Indian Ocean using a novel long-chain diol index, *Earth and Planetary Science Letters*, 276(1-2), 207-213.

Rayner, N. A., Parker, D. E., Horton, E. B., Folland, C. K., Alexander, L. V., Rowell, D. P., Kent, E. C., and Kaplan, A. (2003), Global analyses of sea surface temperature, sea ice, and night marine air temperature since the late nineteenth century, *Journal of Geophysical Research*, 108(D14), 4407.

Reimer, P. J., Brown, T. A., and Reimer, R. W. (2004), Discussion: Reporting and calibration of post-bomb C-14 data, *Radiocarbon*, 46(3), 1299-1304.

Reimer, P. J., Baillie, M. G. L., Bard, E., Bayliss, A., Beck, J. W., Blackwell, P. G., Ramsey, C. B., Buck, C. E., Burr, G. S., Edwards, R. L., Friedrich, M., Grootes, P. M., Guilderson, T. P., Hajdas, I., Heaton, T. J., Hogg, A. G., Hughen, K. A., Kaiser, K. F., Kromer, B., McCormac, F. G., Manning, S. W., Reimer, R. W., Richards, D. A., Southon, J. R., Talamo, S., Turney, C. S. M., van der Plicht, J., and Weyhenmeye, C. E. (2009), INTCAL09 and MARINE09 Radiocarbon age calibration curve, 0-50000 years cal BP, *Radiocarbon*, 51(4), 1111-1150.

Rieley, G., Collister, J. W., Stern, B., and Eglinton, G. (1993), Gas chromatography/ isotope ratio mass spectrometry of leaf wax *n*-alkalines from plants of differing carbon dioxide metabolisms, *Rapid Communications in Mass Spectrometry*, 7(6), 488-491.

Rimbu, N., Lohmann, G., Kim, J. H., Arz, H. W., and Schneider, R. (2003), Arctic/North Atlantic Oscillation signature in Holocene sea surface temperature trends as obtained from

alkenone data, *Geophysical Research Letters*, 30(6), 1280.

Rimbu, N., Lohmann, G., Lorenz, S. J., Kim, J. H., and Schneider, R. R. (2004), Holocene climate variability as derived from alkenone sea surface temperature and coupled ocean-atmosphere model experiments, *Climate Dynamics*, 23(2), 215-227.

Roberts, N., Moreno, A., Valero-Garcés, B. L., Corella, J. P., Jones, M., Allcock, S., Woodbridge, J., Morellón, M., Luterbacher, J., Xoplaki, E., and Türkeş, M. (2011), Palaeolimnological evidence for an east–west climate see-saw in the Mediterranean since AD 900, *Global and Planetary Change (in press)*.

Rodó, X., Baert, E., and Comín, F. A. (1997), Variations in seasonal rainfall in Southern Europe during the present century: relationships with the North Atlantic Oscillation and the El Niño-Southern Oscillation, *Climate Dynamics*, 13(4), 275-284.

Rodrigo, F. S., Esteban-Parra, M. J., Pozo-Vázquez, D., and Castro-Díez, Y. (1999), A 500-year precipitation record in Southern Spain, *International Journal of Climatology*, 19(11), 1233-1253.

Rodrigo, F. S., and Trigo, R. M. (2007), Trends in daily rainfall in the Iberian Peninsula from 1951 to 2002, *International Journal of Climatology*, 27(4), 513-529.

Rogerson, M., Cacho, I., Jiménez-Espejo, F., Reguera, M. I., Sierro, F. J., Martínez-Ruiz, F., Frigola, J., and Canals, M. (2008), A dynamic explanation for the origin of the western Mediterranean organic-rich layers, *Geochemistry, Geophysics, Geosystems*, 9.

Rogerson, M., Colmenero-Hidalgo, E., Levine, R. C., Rohling, E. J., Voelker, A. H. L., Bigg, G. R., Schönfeld, J., Cacho, I., Sierro, F. J., Löwemark, L., Reguera, M. I., de Abreu, L., and Garrick, K. (2010), Enhanced Mediterranean-Atlantic exchange during Atlantic freshening phases, *Geochemistry, Geophysics, Geosystems*, 11(8), Q08013.

Rohling, E. J., Hayes, A., Mayewski, P. A., and and Kucera, M. (2009), Holocene climate variability in the Eastern Mediterranean, and the end of the Bronze Age, in *Forces of Transformation: The End of the Bronze Age in the Mediterranean*, edited by C. Bachhuber and R. G. Roberts, pp. 2-5, BANEA Publication Series 1, Oxbow Books, Oxford.

Rosell-Melé, A., and McClymont, E. L. (2007), Biomarkers as paleoceanographic proxies, in *Proxies in Late Cenozoic Paleoceanography*, edited by C. Hillaire-Marcel and A. De Vernal, pp. 441-490, Elsevier, Amsterdam, The Netherlands.

Sánchez-Cabeza, J., Masqué, P., and Ani-Ragolta, I. (1998), ^{210}Pb and ^{210}Po analysis in sediments and soils by microwave acid digestion, *Journal of Radioanalytical and Nuclear Chemistry*, 227(1), 19-22.

Sánchez-Goñi, M. F., Cacho, I., Turon, J. L., Guiot, J., Sierro, F. J., Peypouquet, J. P., Grimalt, J. O., and Shackleton, N. J. (2002), Synchroneity between marine and terrestrial responses to millennial scale climatic variability during the last glacial period in the Mediterranean region, *Climate Dynamics*, 19(1), 95-105.

Santoleri, R., Böhm, E., and Schiano, M. E. (1994), The sea surface temperature of the western Mediterranean Sea: Historical satellite thermal data, in *Seasonal and Interannual Variability of the Western Mediterranean Sea*, edited by P. E. La Violette, pp. 155-176, American Geophysical Union, Washington.

Sarhan, T., García Lafuente, J., Vargas, M., Vargas, J. M., and Plaza, F. (2000), Upwelling mechanisms in the northwestern Alboran Sea, *Journal of Marine Systems*, 23(4), 317-331.

Schefuß, E., Ratmeyer, V., Stuut, J.-B. W., Jansen, J. H. F., and Sinninghe Damsté, J. S. (2003), Carbon isotope analyses of *n*-alkanes in dust from the lower atmosphere over the central eastern Atlantic, *Geochimica et Cosmochimica Acta*, 67(10), 1757-1767.

Schefuß, E., Schouten, S., and Schneider, R. R. (2005), Climatic controls on central African hydrology during the past 20,000 years, *Nature*, 437(7061), 1003-1006.

Schouten, S., Klein Breteler, W. C. M., Blokker, P., Schogt, N., Rijpstra, W. I. C., Grice, K., Baas, M., and Sinninghe Damsté, J. S. (1998), Biosynthetic effects on the stable carbon isotopic compositions of algal lipids: implications for deciphering the carbon isotopic biomarker record, *Geochimica et Cosmochimica Acta*, 62(8), 1397-1406.

Schouten, S., Hoefs, M. J. L., and Sinninghe Damsté, J. S. (2000), A molecular and stable carbon isotopic study of lipids in late Quaternary sediments from the Arabian Sea, *Organic Geochemistry*, 31(6), 509-521.

Schouten, S., Hopmans, E. C., Schefuß, E., and Sinninghe Damsté, J. S. (2002), Distributional variations in marine crenarchaeotal membrane lipids: a new tool for reconstructing ancient sea water temperatures?, *Earth and Planetary Science Letters*, 204(1-2), 265-274.

Schouten, S., Huguet, C., Hopmans, E. C., Kienhuis, M. V. M., and Sinninghe Damsté, J. S. (2007), Analytical methodology for TEX_{86} paleothermometry by high-performance liquid chromatography/atmospheric pressure chemical ionization-mass spectrometry, *Analytical Chemistry*, 79(7), 2940-2944.

Seager, R., Graham, N., Herweijer, C., Gordon, A. L., Kushnir, Y., and Cook, E. (2007), Blueprints for Medieval hydroclimate, *Quaternary Science Reviews*, 26(19-21), 2322-2336.

Serrano, F., González-Donoso, J. M., Palmqvist, P., Guerra-Merchán, A., Linares, D., and Pérez-Claros, J. A. (2007), Estimating Pliocene sea-surface temperatures in the Mediterranean: An approach based on the modern analogs technique, *Palaeogeography, Palaeoclimatology, Palaeoecology*, 243(1-2), 174-188.

Shackleton, N. J. (1974), Attainment of isotopic equilibrium between ocean water and the benthonic foraminifera genus Uvigerina: isotopic changes in the ocean during the last glacial, in *Les Méthodes Quantitatives d'étude des Variations du Climat au Cours du Pléistocène. Colloques Internationaux du CNRS*, edited by J. Labeyrie, pp. 203–210, CNRS, Paris, Gif/Yvette.

Shindell, D. T., Schmidt, G. A., Mann, M. E., Rind, D., and Waple, A. (2001), Solar forcing of regional climate change during the Maunder Minimum, *Science*, 294(5549), 2149-2152.

Siegenthaler, U., Stocker, T. F., Monnin, E., Lüthi, D., Schwander, J., Stauffer, B., Raynaud, D., Barnola, J.-M., Fischer, H., Masson-Delmotte, V., and Jouzel, J. (2005), Stable carbon cycle-climate relationship during the Late Pleistocene, *Science*, 310(5752), 1313-1317.

Sierro, F. J., Hodell, D. A., Curtis, J. H., Flores, J. A., Reguera, I., Colmenero-Hidalgo, E., Bárcena, M. A., Grimalt, J. O., Cacho, I., Frigola, J., and Canals, M. (2005), Impact of iceberg melting on Mediterranean thermohaline circulation during Heinrich events, *Paleoceanography*, 20, PA2019.

Sinninghe Damsté, J. S., Rampen, S., Irene, W., Rijpstra, C., Abbas, B., Muyzer, G., and Schouten, S. (2003), A diatomaceous origin for long-chain diols and mid-chain hydroxy methyl alkanoates widely occurring in quaternary marine sediments: indicators for high-nutrient conditions, *Geochimica et Cosmochimica Acta*, 67(7), 1339-1348.

Solomon, S., Qin, D., Manning, M., Chen, Z., Marquis, M., Averyt, K. B., Tignor, M., and Miller, H. L. (2007), *Climate Change 2007: The Physical Science Basis. Contribution of Working Group I to the Fourth Assessment Report of the Intergovernmental Panel on Climate Change*, 996 pp., Cambridge University Press, Cambridge, United Kingdom and New York, NY, USA.

Solomon, A., Goddard, L., Kumar, A., Carton, J., Deser, C., Fukumori, I., Greene, A. M., Hegerl, G., Kirtman, B., Kushnir, Y., Newman, M., Smith, D., Vimont, D., Delworth, T., Meehl, G. A., and Stockdale, T. (2010), Distinguishing the roles of natural and anthropogenically forced decadal climate variability, *Bulletin of the American Meteorological Society*, 92(2), 141-156.

Sousa, P. M., Trigo, R. M., Aizpurua, P., Nieto, R., Gimeno, L., and García-Herrera, R. (2011), Trends and extremes of drought indices throughout the 20th century in the Mediterranean, *Natural Hazards and Earth System Science*, 11(1), 33-51.

Spang, A., Hatzenpichler, R., Brochier-Armanet, C., Rattei, T., Tischler, P., Spieck, E., Streit, W., Stahl, D. A., Wagner, M., and Schleper, C. (2010), Distinct gene set in two different lineages of ammonia-oxidizing archaea supports the phylum *Thaumarchaeota*, *Trends in Microbiology*, 18(8), 331-340.

Stein, R., Hefter, J., Grützner, J., Voelker, A., and Naafs, B. D. A. (2009), Variability of surface water characteristics and Heinrich-like events in the Pleistocene midlatitude North Atlantic Ocean: Biomarker and XRD records from IODP Site U1313 (MIS 16-9), *Paleoceanography*, 24, PA2203.

Steinhilber, F., Beer, J., and Fröhlich, C. (2009), Total solar irradiance during the Holocene, *Geophysical Research Letters*, 36(19), L19704.

Stine, S. (1994), Extreme and persistent drought in California and Patagonia during mediaeval time, *Nature*, 369(6481), 546-549.

Stuiver, M., and Reimer, P. J. (1993), Extended C-14 database and revised Calib 3.0 C-14 age calibration program, *Radiocarbon*, 35(1), 215-230.

Sumner, G., Homar, V., and Ramis, C. (2001), Precipitation seasonality in eastern and

southern coastal Spain, *International Journal of Climatology*, 21(2), 219-247.

ten Haven, H. L., de Leeuw, J. W., Schenck, P. A., and Klaver, G. T. (1988), Geochemistry of Mediterranean sediments. Bromine/organic carbon and uranium/organic carbon ratios as indicators for different sources of input and post-depositional oxidation, respectively, *Organic Geochemistry*, 13(1-3), 255-261.

Thomson, J., Mercone, D., de Lange, G. J., and van Santvoort, P. J. M. (1999), Review of recent advances in the interpretation of eastern Mediterranean sapropel S1 from geochemical evidence, *Marine Geology*, 153(1-4), 77-89.

Tierney, J. E., Mayes, M. T., Meyer, N., Johnson, C., Swarzenski, P. W., Cohen, A. S., and Russell, J. M. (2010), Late-twentieth-century warming in Lake Tanganyika unprecedented since AD 500, *Nature Geosciences*, 3(6), 422-425.

Trenberth, K. E., Jones, P. D., Ambenje, P., Bojariu, R., Easterling, D., Tank, A. K., Parker, D., Rahimzadeh, F., Renwick, J. A., Rusticucci, M., Soden, B., and Zhai, P. (2007), Observations: Surface and atmospheric climate change, in *Climate Change 2007: The Physical Science Basis. Contribution of Working Group I to the Fourth Assessment Report of the Intergovernmental Panel on Climate Change*, edited by S. Solomon, D. Qin, M. Manning, Z. Chen, M. Marquis, K.B. Averyt, M. Tignor and H.L. Miller Cambridge University Press, United Kingdom and New York, NY, USA.

Tribovillard, N., Algeo, T. J., Lyons, T., and Riboulleau, A. (2006), Trace metals as paleoredox and paleoproductivity proxies: An update, *Chemical Geology*, 232(1-2), 12-32.

Trigo, R. M., Osborn, T. J., and Corte-Real, J. M. (2002), The North Atlantic Oscillation influence on Europe: climate impacts and associated physical mechanisms, *Climate Research*, 20(1), 9-17.

Trigo, R. M., Pozo-Vázquez, D., Osborn, T. J., Castro-Díez, Y., Gámiz-Fortis, S., and Esteban-Parra, M. J. (2004), North Atlantic oscillation influence on precipitation, river flow and water resources in the Iberian Peninsula, *International Journal of Climatology*, 24(8), 925-944.

Trouet, V., Esper, J., Graham, N. E., Baker, A., Scourse, J. D., and Frank, D. C. (2009), Persistent positive North Atlantic Oscillation mode dominated the Medieval Climate Anomaly, *Science*, 324(5923), 78-80.

Trouet, V., Scourse, J. D., and Raible, C. C. (2011), North Atlantic storminess and Atlantic Meridional Overturning Circulation during the last Millennium: Reconciling contradictory proxy records of NAO variability, *Global and Planetary Change (in press)*.

Turney, C. S. M., and Palmer, J. G. (2007), Does the El Niño-Southern Oscillation control the interhemispheric radiocarbon offset?, *Quaternary Research*, 67(1), 174-180.

Usoskin, I. G., Solanki, S. K., Schüssler, M., Mursula, K., and Alanko, K. (2003), Millennium-scale sunspot number reconstruction: Evidence for an unusually active sun since the 1940s, *Physical Review Letters*, 91(21), 211101.

Van der Weijden, C. H. (2002), Pitfalls of normalization of marine geochemical data using a common divisor, *Marine Geology*, 184(3-

4), 167-187.

van Geel, B., Buurman, J., and Waterbolk, H. T. (1996), Archaeological and palaeoecological indications of an abrupt climate change in The Netherlands, and evidence for climatological teleconnections around 2650 BP, *Journal of Quaternary Science*, 11(6), 451-460.

van Geel, B., Raspopov, O. M., Renssen, H., van der Plicht, J., Dergachev, V. A., and Meijer, H. A. J. (1999), The role of solar forcing upon climate change, *Quaternary Science Reviews*, 18(3), 331-338.

Vargas-Yáñez, M., Jesús García, M., Salat, J., García-Martínez, M. C., Pascual, J., and Moya, F. (2008), Warming trends and decadal variability in the Western Mediterranean shelf, *Global and Planetary Change*, 63(2-3), 177-184.

Versteegh, G. J. M., Bosch, H. J., and De Leeuw, J. W. (1997), Potential palaeoenvironmental information of C_{24} to C_{36} mid-chain diols, keto-ols and mid-chain hydroxy fatty acids; a critical review, *Organic Geochemistry*, 27(1-2), 1-13.

Voelker, A. H. L., Lebreiro, S. M., Schönfeld, J., Cacho, I., Erlenkeuser, H., and Abrantes, F. (2006), Mediterranean outflow strengthening during northern hemisphere coolings: A salt source for the glacial Atlantic?, *Earth and Planetary Science Letters*, 245(1-2), 39-55.

Wahl, E. R., Anderson, D. M., Bauer, B. A., Buckner, R., Gille, E. P., Gross, W. S., Hartman, M., and Shah, A. (2010), An archive of high-resolution temperature reconstructions over the past 2+ millennia, *Geochemistry, Geophysics, Geosystems*, 11(1), Q01001.

Wanner, H., Bronnimann, S., Casty, C., Gyalistras, D., Luterbacher, J., Schmutz, C., Stephenson, D. B., and Xoplaki, E. (2001), North Atlantic Oscillation - Concepts and studies, *Surveys in Geophysics*, 22(4), 321-382.

Wanner, H., Beer, J., Bütikofer, J., Crowley, T. J., Cubasch, U., Flückiger, J., Goosse, H., Grosjean, M., Joos, F., Kaplan, J. O., Küttel, M., Müller, S. A., Prentice, I. C., Solomina, O., Stocker, T. F., Tarasov, P., Wagner, M., and Widmann, M. (2008), Mid- to Late Holocene climate change: an overview, *Quaternary Science Reviews*, 27(19-20), 1791-1828.

Wehausen, R., and Brumsack, H. J. (1999), Cyclic variations in the chemical composition of eastern Mediterranean Pliocene sediments: a key for understanding sapropel formation, *Marine Geology*, 153(1-4), 161-176.

Weijers, J. W. H., Schouten, S., Spaargaren, O. C., and Sinninghe Damsté, J. S. (2006), Occurrence and distribution of tetraether membrane lipids in soils: Implications for the use of the TEX_{86} proxy and the BIT index, *Organic Geochemistry*, 37(12), 1680-1693.

Weldeab, S., Siebel, W., Wehausen, R., Emeis, K.-C., Schmiedl, G., and Hemleben, C. (2003), Late Pleistocene sedimentation in the Western Mediterranean Sea: implications for productivity changes and climatic conditions in the catchment areas, *Palaeogeography, Palaeoclimatology, Palaeoecology*, 190(0), 121-137.

Willard, D. A., Bernhardt, C. E., Korejwo, D. A., and Meyers, S. R. (2005), Impact of millennial-scale Holocene climate variability on eastern North American terrestrial ecosystems:

pollen-based climatic reconstruction, *Global and Planetary Change*, 47(1), 17-35.

Wuchter, C., Schouten, S., Coolen, M. J. L., and Sinninghe Damsté, J. S. (2004), Temperature-dependent variation in the distribution of tetraether membrane lipids of marine Crenarchaeota: Implications for TEX_{86} paleothermometry, *Paleoceanography*, 19(4), PA4028.

Wuchter, C., Schouten, S., Wakeham, S. G., and Sinninghe Damsté, J. S. (2005), Temporal and spatial variation in tetraether membrane lipids of marine Crenarchaeota in particulate organic matter: Implications for TEX_{86} paleothermometry, *Paleoceanography*, 20(3), PA3013.

Wuchter, C., Abbas, B., Coolen, M. J. L., Herfort, L., Van Bleijswijk, J., Timmers, P., Strous, M., Teira, E., Herndl, G. J., Middelburg, J. J., Schouten, S., and Damsté, J. S. S. (2006), Archaeal nitrification in the ocean, *Proceedings of the National Academy of Sciences*, 103(33), 12317-12322.

Zhao, M., Eglinton, G., Haslett, S. K., Jordan, R. W., Sarnthein, M., and Zhang, Z. (2000), Marine and terrestrial biomarker records for the last 35,000 years at ODP site 658C off NW Africa, *Organic Geochemistry*, 31(9), 919-930.

Ziegler, M., Jilbert, T., de Lange, G. J., Lourens, L. J., and Reichart, G.-J. (2008), Bromine counts from XRF scanning as an estimate of the marine organic carbon content of sediment cores, *Geochemistry, Geophysics, Geosystems*, 9(5), Q05009.

Appendix I

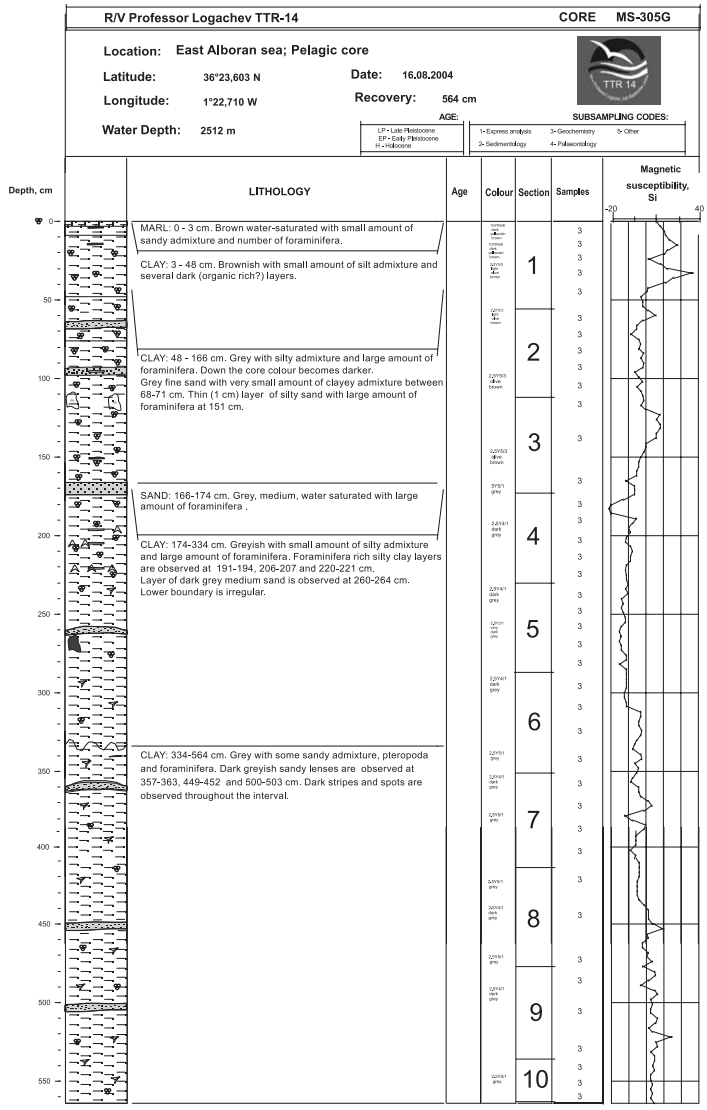

1. Core log TTR-14-MS-305G

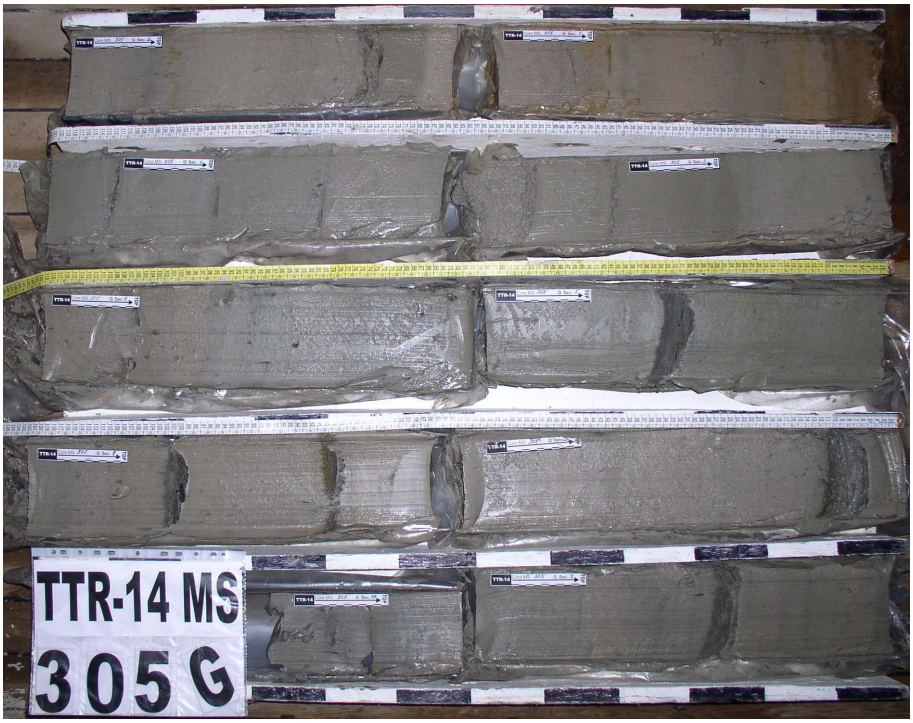

2. Core 305G photo

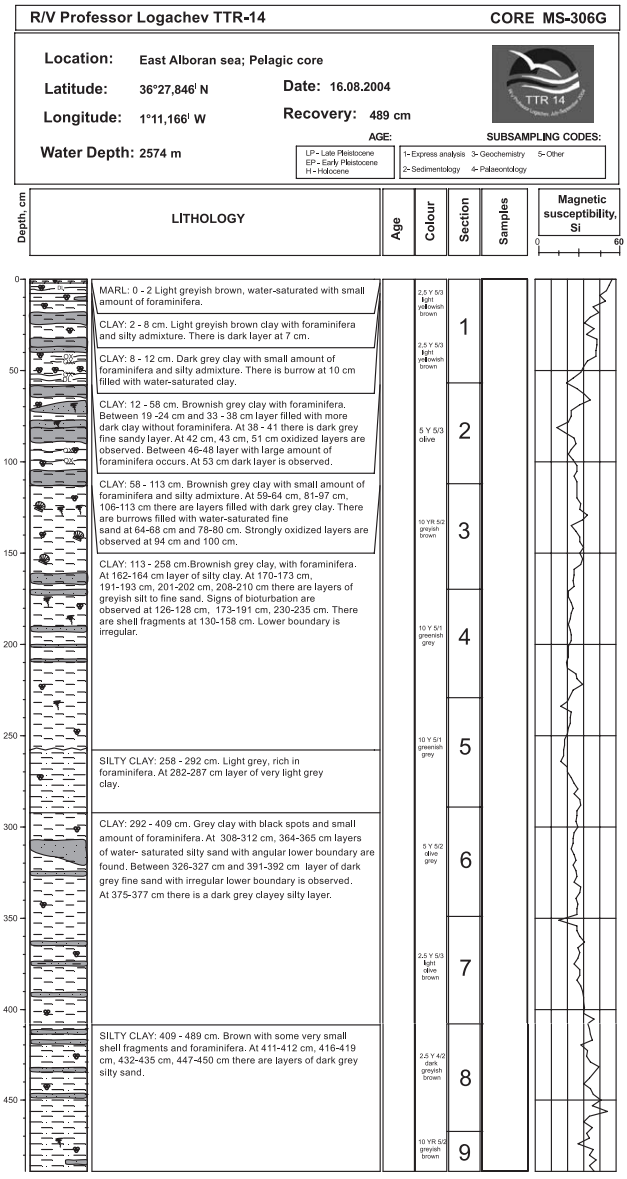

3. Core log TTR-14-MS-306G

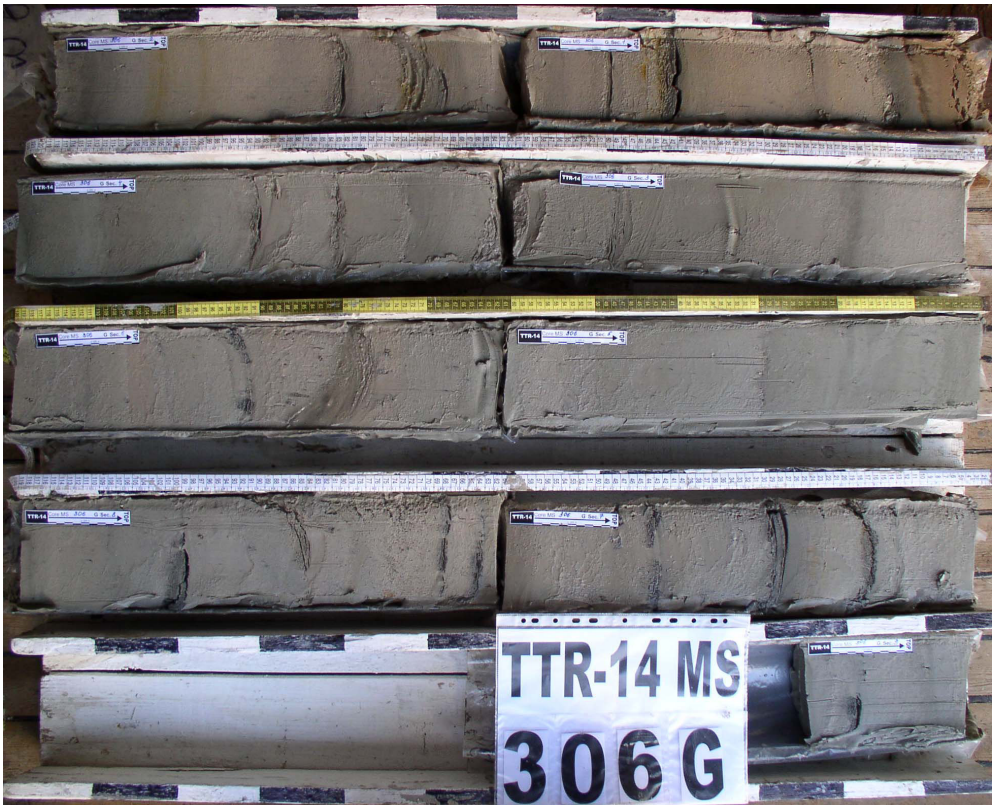

4. Core 306G photo

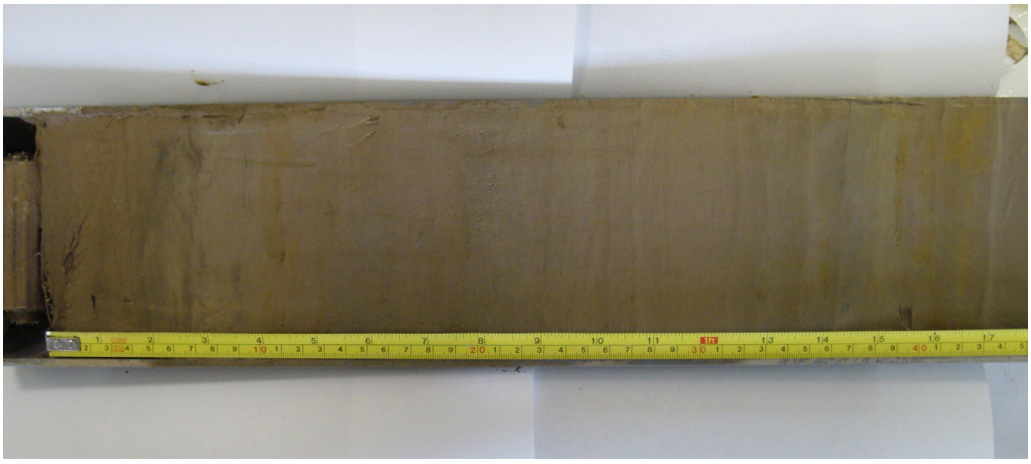

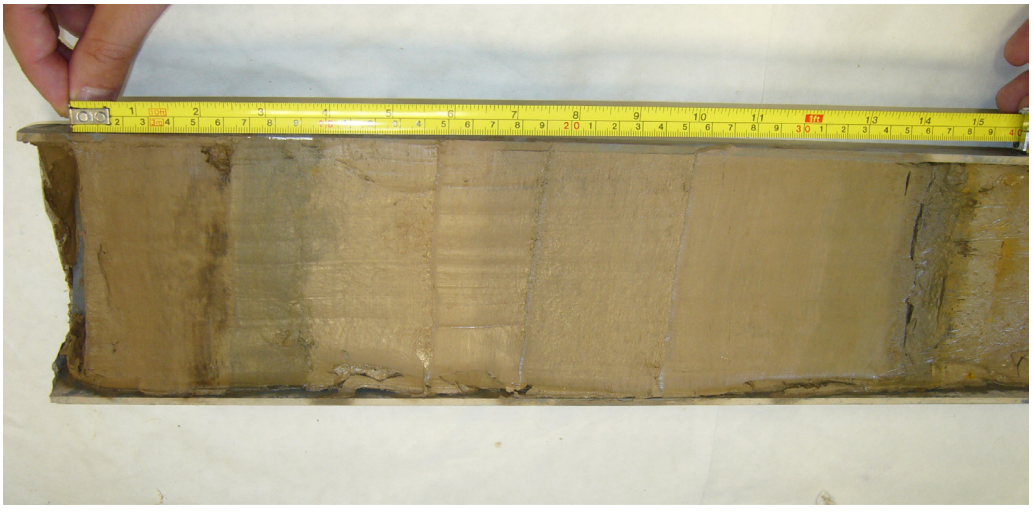

5. Detail of the studied sections in core 305G (top) and 306G (bottom)

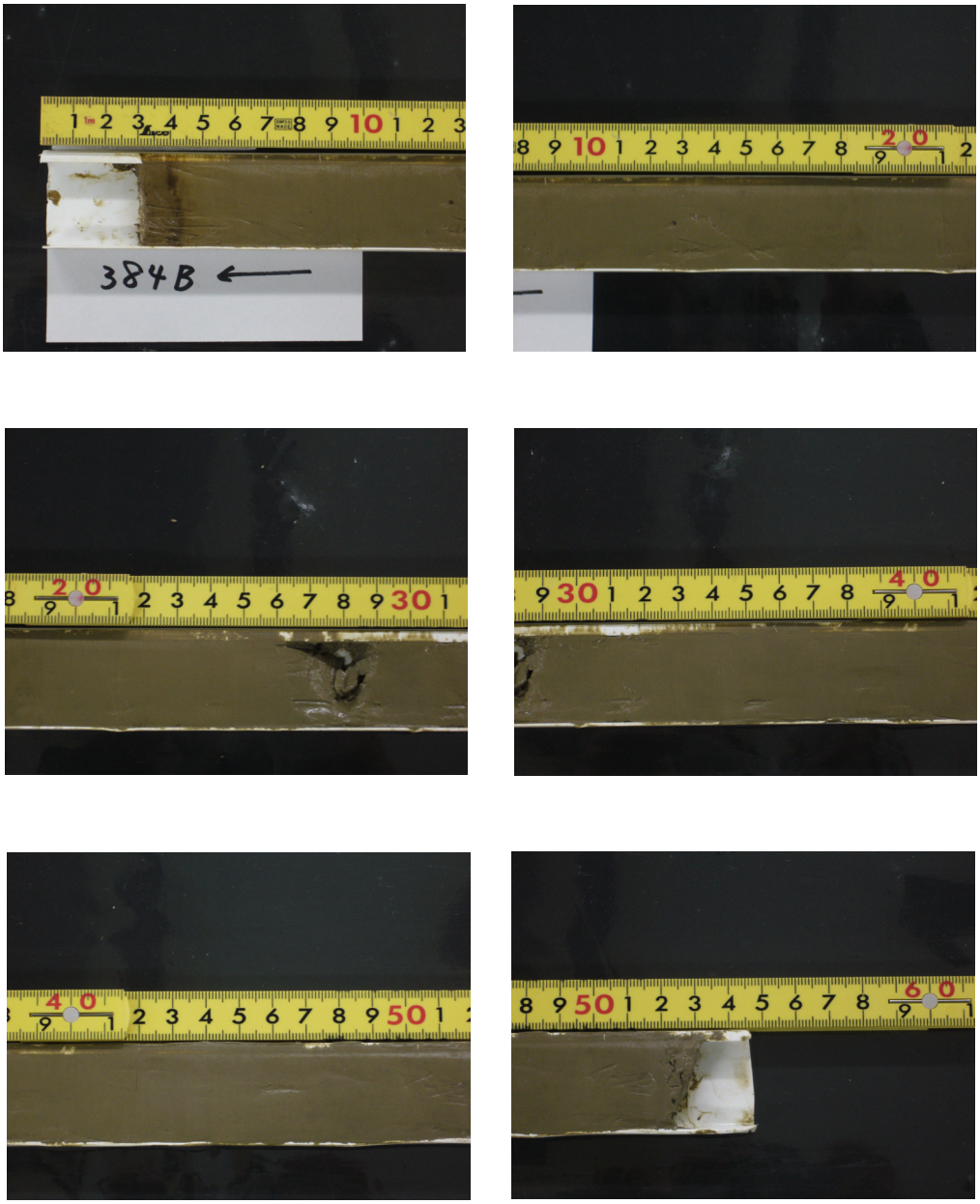

6. U-channel section for box-core 384B

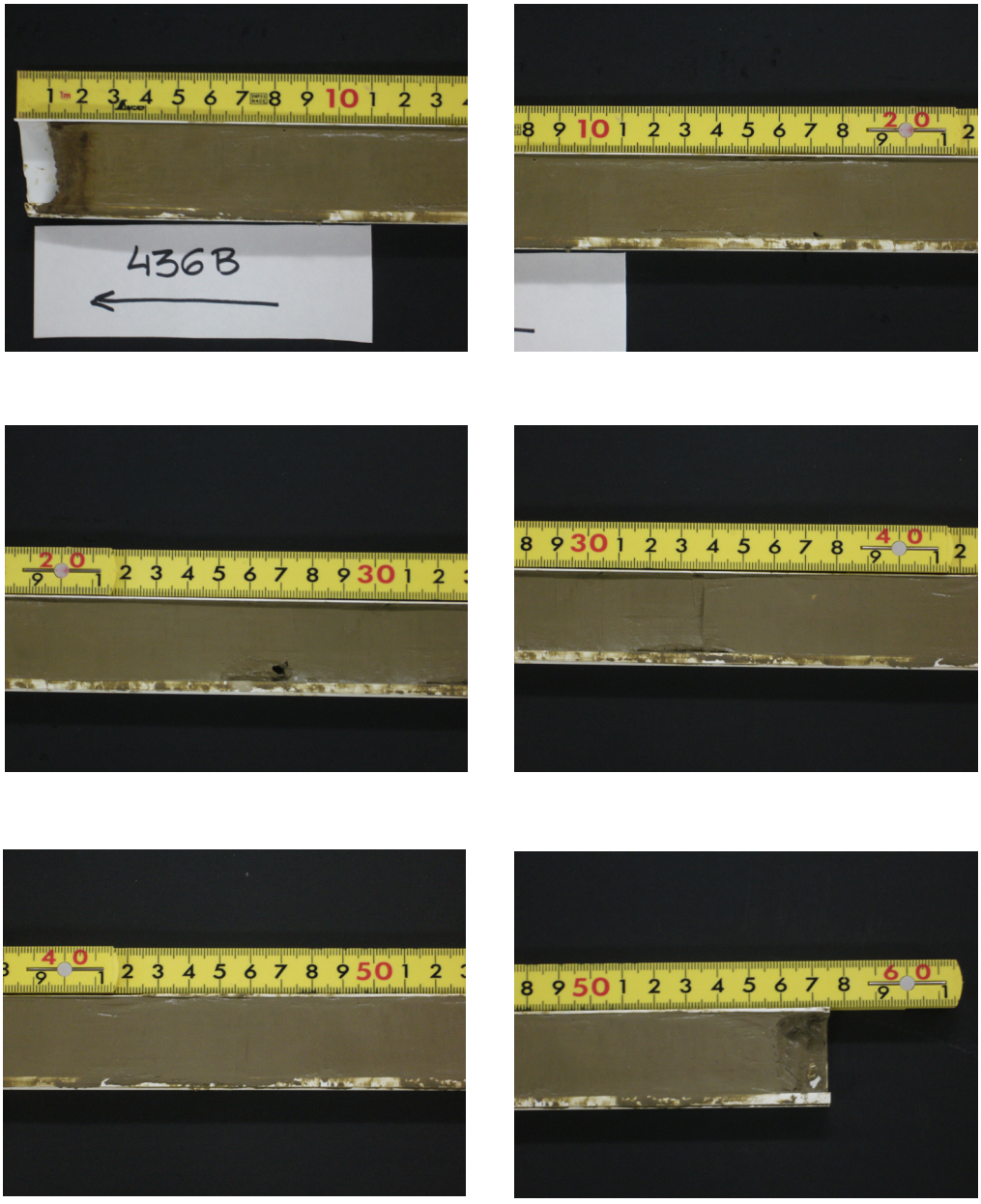

7. U-channel section for box-core 436B

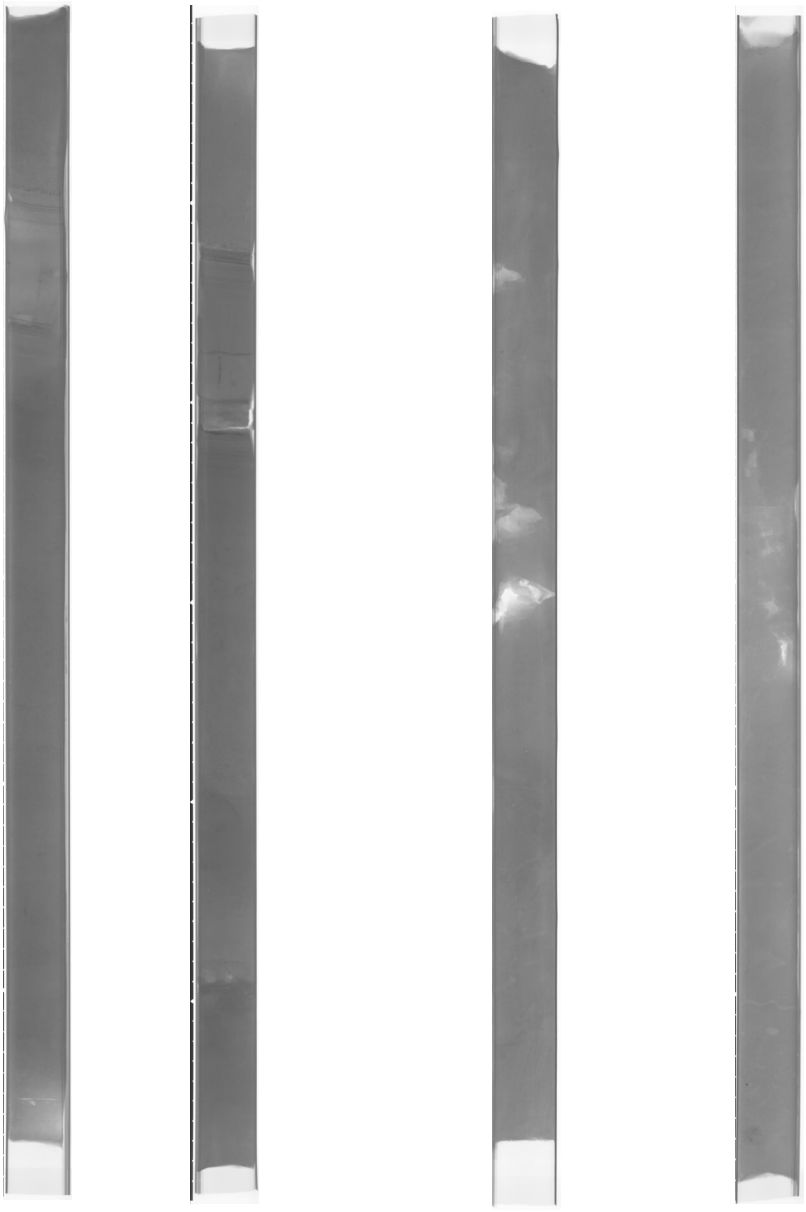

8. X-ray images of the studied cores (from left to the right): core 305G, 306G, 384B, 436B

Appendix II

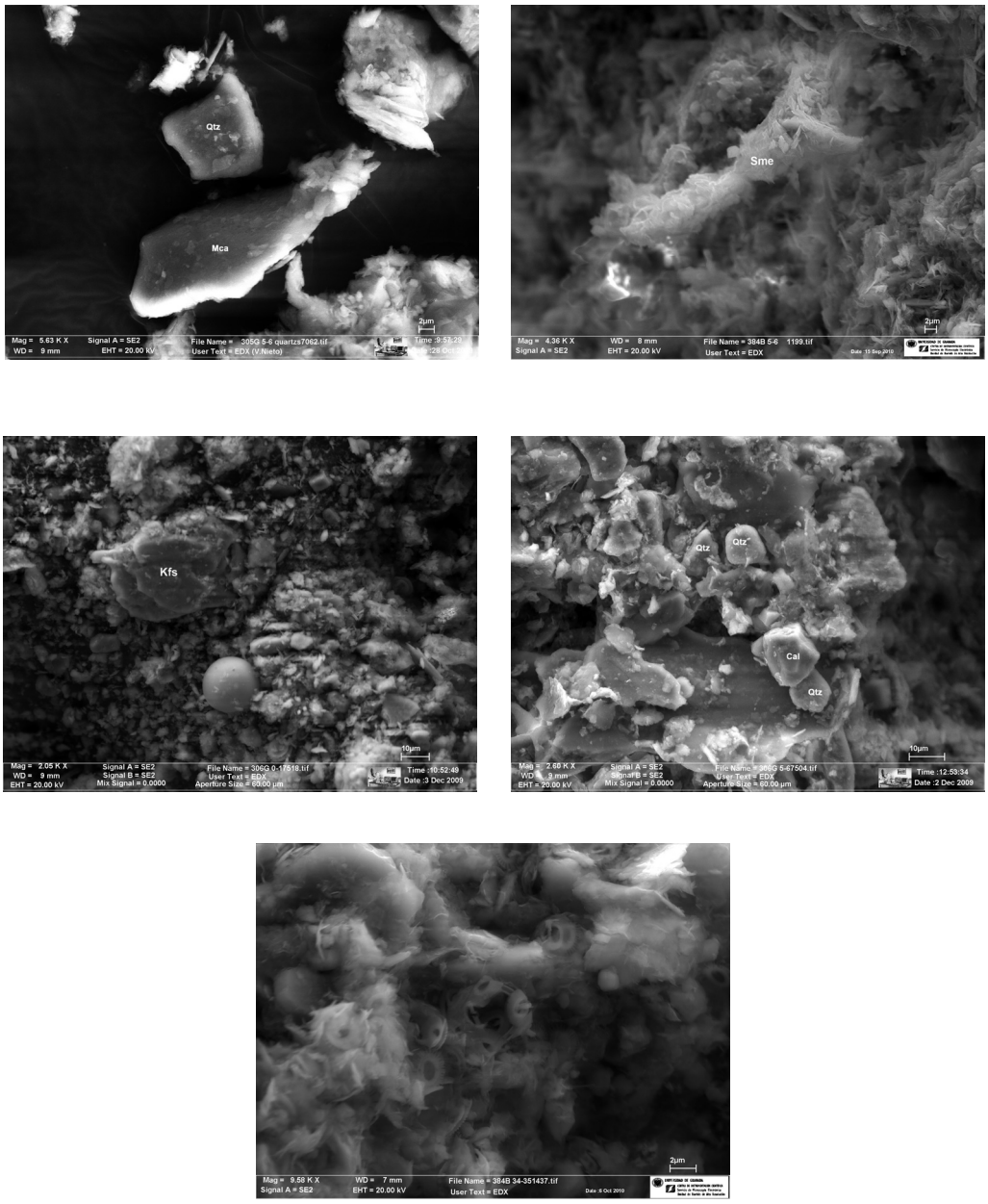

1. Mineral composition of the studied sediments: clay minerals, quartz, calcite/forams and accesory minerals such as feldspars

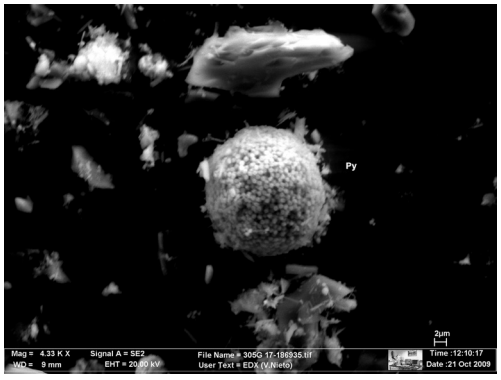

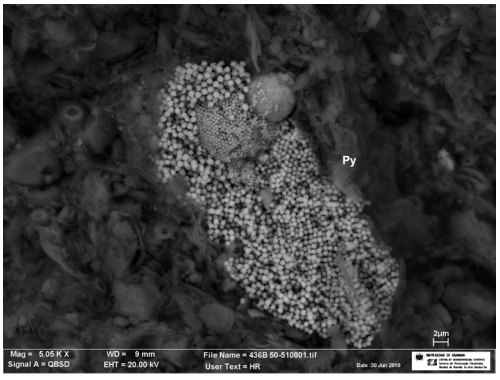

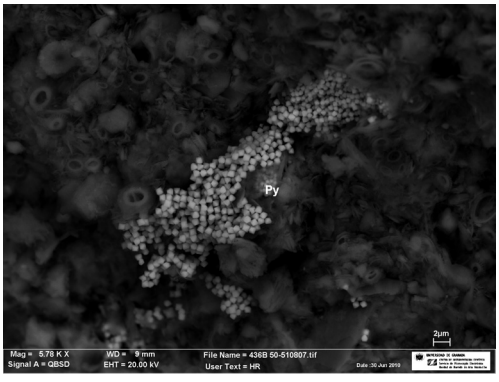

2. Accesory minerals of the studied sediemnts such as zircon and pyrite framboids

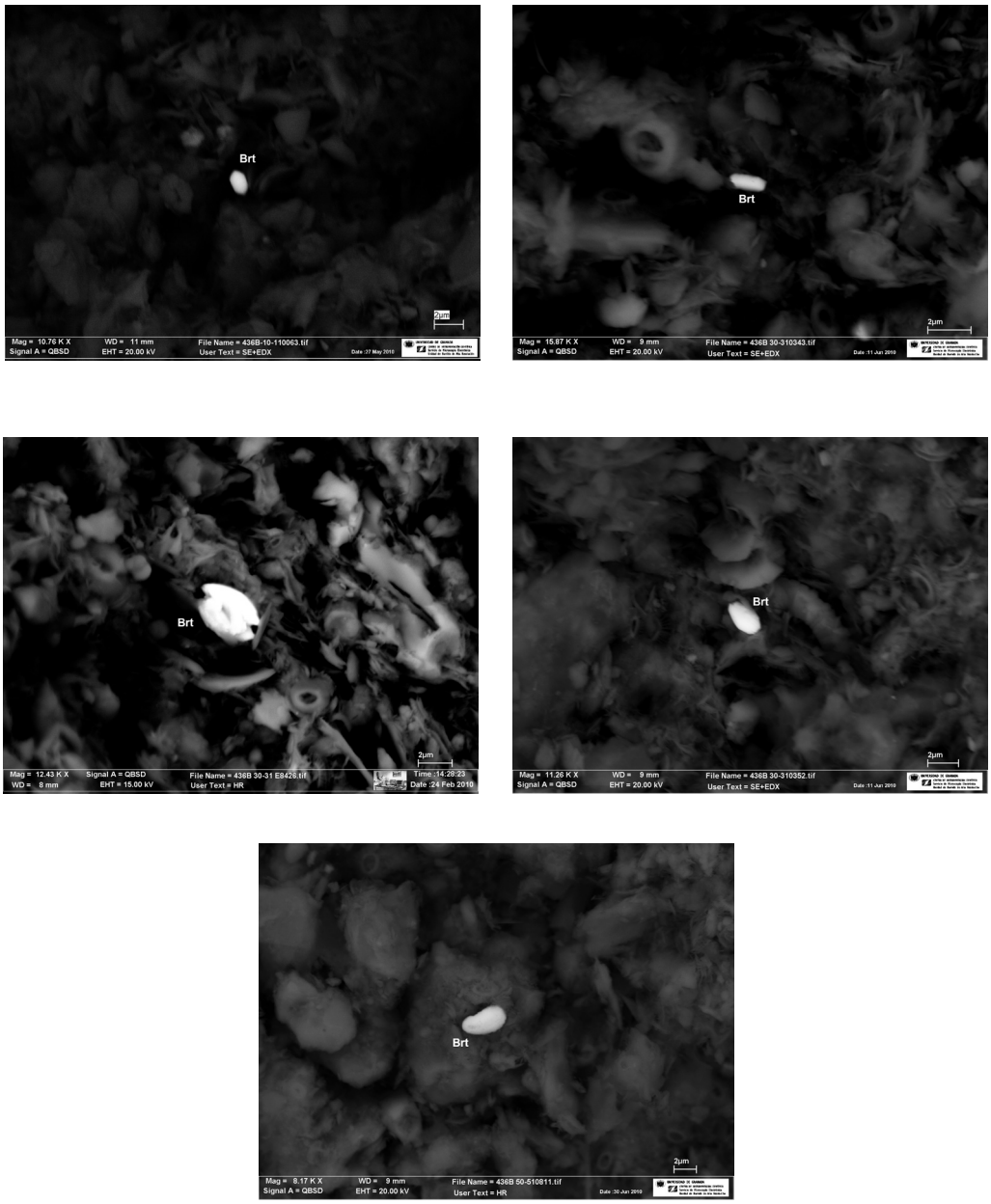

3. Authigenic and detrital barite of the studied sediments from Ba-rich intervals

Appendix III

	Si	Al(IV)	Al(VI)	Mg	Fe	Σoct	K	Ca	Na	Int.cha.
305G 14-15										
	3.40	0.60	1.68	0.26	0.21	2.15	0.33	0.02	0.11	0.48
	3.37	0.63	1.75	0.18	0.16	2.09	0.30	0.02	0.25	0.59
305G 24-25										
	3.45	0.55	1.64	0.35	0.19	2.18	0.14	0.05	0.14	0.38
	3.61	0.39	1.79	0.16	0.10	2.05	0.05	0.05	0.23	0.38
305G 29-30										
	3.60	0.40	1.70	0.24	0.26	2.20	0.21	0.02	0.05	0.30
	3.53	0.47	1.72	0.59	0.34	2.65	0.32	0.02	0.14	0.50
305G 34-35										
	3.20	0.80	1.78	0.27	0.20	2.25	0.25	0.00	0.30	0.55
	3.71	0.29	1.61	0.33	0.19	2.13	0.33	0.04	0.00	0.41
305G 39-40										
	3.41	0.59	2.00	0.10	0.12	2.22	0.00	0.00	0.00	0.00
	3.47	0.53	2.02	0.14	0.00	2.16	0.19	0.00	0.00	0.19
306G 0-1										
	3.38	0.62	1.81	0.26	0.12	2.19	0.12	0.09	0.00	0.30
	3.64	0.36	1.67	0.19	0.19	2.05	0.19	0.09	0.00	0.37
306G 9-10										
	3.46	0.54	1.65	0.28	0.23	2.16	0.14	0.12	0.00	0.38
	3.86	0.14	1.71	0.24	0.17	2.12	0.03	0.00	0.00	0.03
306G 19-20										
	3.48	0.52	1.60	0.38	0.21	2.19	0.24	0.03	0.00	0.30
	3.67	0.33	1.73	0.24	0.17	2.14	0.05	0.02	0.00	0.09
306G 29-30										
	3.29	0.71	1.77	0.26	0.21	2.24	0.23	0.03	0.00	0.29
	3.38	0.62	1.81	0.21	0.16	2.18	0.19	0.03	0.00	0.25
306G 34-35										
	3.59	0.41	1.68	0.26	0.16	2.10	0.28	0.00	0.16	0.44
	3.35	0.65	1.69	0.23	0.18	2.10	0.23	0.00	0.39	0.62

1. Smectite composition identified by HR-TEM in analyzed sediments (Al-rich beidellites of detrital origin)

Appendix IV

1.- Other peer reviewed publications – JCR (SCI) – indexed journal papers.

• Moreno, A., Pérez, A., Frigola, J., **Nieto-Moreno, V.**, Rodrigo-Gámiz, M., González-Sampériz, P., Morellón, M., Martín-Puertas, C., Corella, J. P., Belmonte, A., Sancho, C., Cacho, I., Herrera, G., Canals, M., Jiménez-Espejo, F., Martínez Ruiz, F., Vegas, T. and Valero-Garcés, B. L., 2012. The Medieval Climate Anomaly in the Iberian Peninsula reconstructed from a compilation of marine and lake records. Quaternary Science Reviews (accepted). Impact Factor: 4.657.

• Rodrigo-Gámiz, M., Martínez-Ruiz, F., Jiménez-Espejo, F.J., Gallego-Torres, D., **Nieto-Moreno, V.**, Ariztegui, D., and Romero, O., 2011. Impact of climate variability in the western Mediterranean during the last 20,000 years: oceanic and atmospheric responses. Quaternary Science Reviews, 30 (15-16): 2018-2034. doi:10.1016/j.quascirev.2011.05.011. Impact Factor: 4.245.

• Martín-Puertas, C., Jiménez-Espejo, F., Martínez-Ruiz, F., **Nieto-Moreno, V.**, Rodrigo, M., Mata, M.P., and Valero-Garcés, B.L., 2010. Late Holocene climate variability in the southwestern Mediterranean region: an integrated marine and terrestrial geochemical approach. Climate of the Past, 6(6): 807-816. doi: 10.5194/cp-6-807-2010. Impact Factor: 3.826.

2.- Other peer reviewed publications - in non JCR(SCI) indexed journals.

• Rodrigo-Gámiz M., Martínez-Ruiz F., Jiménez-Espejo F. J., **Nieto-Moreno V.**, and Gallego-Torres D., 2008. Caracterización del aporte eólico en el Mediterráneo Occidental: registro de la respuesta atmosférica a la variabilidad climática. MACLA, 9, 207-208.

• **Nieto-Moreno V.**, Martínez-Ruiz F., Jiménez-Espejo F.J., Gallego-Torres D., Romero, O., and Ortega-Huertas M., 2007. Indicadores mineralógicos y geoquímicos de variabilidad climática: calibración y registro sedimentario reciente del Mediterráneo Occidental. MACLA, 7, 52.